

VISCOPLASTICITY AND DAMAGE MECHANICS MODELS FOR
RATE-DEPENDENT MATERIALS AND THEIR APPLICATION TO ICE

by

Dong Ho Choi

B.S., Civil Engineering, Hanyang University (1984)

M.S., Civil Engineering, Hanyang University (1987)

M.S., Civil Engineering, Georgia Institute of Technology (1987)

Submitted to the Department of Civil and Environmental Engineering
in Partial Fulfillment of the Requirements for the Degree of

Doctor of Philosophy

at the

MASSACHUSETTS INSTITUTE OF TECHNOLOGY

November 1996

[February 1997]

©Massachusetts Institute of Technology 1996. All rights reserved.

Author _____
Department of Civil and Environmental Engineering
November 8, 1996

Certified by _____
Jerome J. Connor
Professor of Civil and Environmental Engineering
Thesis Supervisor

Accepted by _____
Professor Joseph M. Sussman
Chairman, Departmental Committee on Graduate Studies

MASSACHUSETTS INSTITUTE
OF TECHNOLOGY

JAN 29 1997

VISCOPLASTICITY AND DAMAGE MECHANICS MODELS FOR RATE-DEPENDENT MATERIALS AND THEIR APPLICATION TO ICE

by

Dong Ho Choi

Submitted to the Department of Civil and Environmental Engineering
on November 8, 1996, in partial fulfillment of the requirements for the degree of
Doctor of Philosophy in Computational Structural Mechanics

ABSTRACT

The objective of this work is to develop a physically-based constitutive model for rate-dependent materials based on the underlying deformation mechanisms and microstructural properties. The inelastic deformation of polycrystalline ice is highly non-linear and depends on loading rate and temperature, as well as on the granular microstructure. These phenomena are attributed to several processes such as intergranular processes, movement and production of dislocations within grains, the creep anisotropy of ice single crystals, and damage accumulation due to microcracking. In particular, the following is considered in this thesis: the viscoplastic behavior of single crystal ice; the relaxation process of polycrystalline ice; the viscoplastic and damage-enhanced viscoplastic behavior of polycrystalline ice.

In the first section, a constitutive creep model for single crystal ice based on experimental results and on the multiplication process of mobile dislocations is developed. In this model, the primary mechanism is considered to be the dislocation motion on the basal planes of single crystal ice due to strong creep anisotropy. The preferred crystallographic orientation and temperature of single crystal ice are incorporated in describing both the elastic and the inelastic deformations.

The second section presents a model of anelastic response in polycrystalline ice under cyclic loading. This model is developed on the basis of a linear relationship between anelastic strain and stress, and the distribution of relaxation times which can be measured from loss compliance. This study examines the influence of frequency and amplitude of cyclic loading on low anelastic strains.

The third section develops a constitutive model of transient creep in orthotropic polycrystalline ice. The primary mechanisms controlling transient creep are considered to be the motion and production of dislocations within grains and the creep anisotropy of constituent crystals. In this model, the internal stresses, kinematic back stress and isotropic drag stress, are introduced to describe various states of the microstructure of the material. Major features of the model include the hardening and recovery processes in the evolution equations of the internal stresses.

In the fourth section, a multi-axial damage-enhanced creep model for orthotropic polycrystalline ice is presented. This model has been developed in the framework of continuum mechanics using the concept of internal state variables. The proposed evolution equations of internal state variables describe the changing substructure due to the movement and the generation of dislocations and the accumulation of damage due to microcracking. Material and damage anisotropy are formulated to describe the importance of the directional nature of material behavior. The model predictions are in good agreement with experimental data.

Thesis Supervisor: Dr. Jerome J. Connor

Title: Professor of Civil and Environmental Engineering

TO MY PARENTS

Acknowledgements

I would like to express my sincere gratitude to Professor J. J. Connor, who has served as my thesis supervisor. Prof. Connor's constructive suggestions, criticism and encouragement during the course of this study are highly appreciated. I am also grateful to Doctor S. Shyam Sunder, Professor A. S. Argon and Professor C. K. Y. Leung for taking the time to serve on my thesis committee and for their expert guidance and invaluable discussions. Especially, I express my appreciation to Prof. Argon for his enlightening suggestions and helpful discussions regarding behavior of materials. Special thanks are offered to Dr. Shyam Sunder and Prof. Connor for their guidance and financial support, without which my work would not have been possible.

Additionally, I would like to extend my gratitude to my friends and colleagues, who have offered fruitful suggestions during this work. Doctor Alex A. Elvin, a long-time friend during my MIT academic life, is especially acknowledged for his stimulating arguments and criticism on this topic; Professor Mao S. Wu deserves my appreciation for his explanation of his transient creep model in the early stages of my research; Professor Kywang M. Lee, Professor Hong C. Im, Dr. Jinkoo Kim, Thanakorn Pheeraphan and Niell G. Elvin have been academic friends at MIT; Doctor D. Cole of CRREL is thanked for providing his experimental data and accompanying sincere discussion regarding the relaxation process.

In 1992, the U.S. Navy initiated an accelerated research program, called the Sea Ice Mechanics Initiative, to bridge different fracture properties of ice at various scales and to develop physically based constitutive and fracture models for corresponding deformations and fracture processes. Dr. Shyam Sunder initiated an ice mechanics research project at MIT under the title, Physically-based Constitutive Modeling of Ice. As a part of this research program, my work has been supported in part by the Office of Naval Research (Grant No. N00014-92-J-1208) and in the early years by an industrial consortium consisting of ARCO, CONOCO, EXXON, and TEXACO through the MIT Center for Scientific Excellence in Offshore Engineering. Their financial support is greatly appreciated.

I would also like to extend my sincere thanks to the professors of the Department of Civil Engineering, Hanyang University; especially Prof. Dong-Il Chang and Prof. Byung-Wan Cho, who have offered constant encouragement during these past years. My study of fracture mechanics under Prof. Chang provided a foundation in my academic life.

Finally, I would like to give my sincere thanks to my parents, my brother and his wife, and my sisters for their love, consistent support and endless encouragement. Their constant love and sacrifices over the years have made it possible for me to complete my studies in the United States. I married Eunjoo Woo during my course of study. Our marriage has given me joy and stability in an otherwise difficult student life. I am truly appreciative of my wife and her parents for all their love and support. This thesis is dedicated to my parents, without whom this work would not have been possible.

Contents

Abstract	2
Acknowledgements	4
Contents	5
List of Figures	10
List of Tables	14
1 INTRODUCTION AND OBJECTIVES	15
1.1 Introduction	15
1.2 Problem Statement and Research Objectives	18
1.3 Research Approach and Organization of Thesis	19
References	23
Figures	26
2 BACKGROUND IN ICE ENGINEERING	27
2.1 Introduction	27
2.2 Ice Loads on Offshore Structures	28
2.3 Multiple-scale Processes	30
2.3.1 Structural-scale Processes	30

2.3.2	Laboratory-scale Processes	31
	References	35
	Figures	38
3	A CONSTITUTIVE CREEP MODEL FOR SINGLE CRYSTAL ICE	47
3.1	Introduction	48
3.2	Constitutive Model of Single Crystal Ice	49
3.2.1	Uniaxial Model	51
3.2.2	Biaxial Model	53
3.3	Model Predictions	57
3.3.1	Model Parameters	57
3.3.2	Parametric Studies	58
3.3.3	Model Comparison with Experimental Data	60
3.4	Conclusions	61
	References	65
	Figures	68
4	RELAXATION PROCESS IN POLYCRYSTALLINE ICE UNDER CYCLIC LOADING	84
4.1	Introduction	85
4.2	Background	86
4.2.1	Anelasticity	87
4.2.2	Internal Friction	88
4.3	Formulation of Constitutive Model	89
4.3.1	Constitutive Equations	89
4.3.2	Distribution of Relaxation Times	92
4.4	Model Predictions	93

4.4.1	Model Parameters	93
4.4.2	Model Predictions	94
4.5	Conclusions	94
	References	96
	Figures	99
5	A MULTIAXIAL CREEP MODEL, PART I: TRANSIENT CREEP	104
5.1	Introduction	105
5.2	Background	107
5.2.1	Behavior of Polycrystalline Ice	107
5.2.2	Flow Equation	108
5.2.3	Evolution Equations	111
5.2.3.1	Internal Stress	111
5.2.3.2	Evolution Equations	112
5.3	Development of a Constitutive Model	115
5.3.1	Material Anisotropy	115
5.3.1.1	Single Crystal Ice	116
5.3.1.2	Columnar-grained S2 Polycrystalline Ice	118
5.3.1.3	Equiaxed-granular Polycrystalline Ice	120
5.3.2	Inelastic Flow	122
5.3.2.1	Inelastic strain rate	122
5.3.2.2	Evolution equations of internal stresses	125
5.3.2.3	Summary of model equations	127
5.4	Model Formulation with Dimensionless Variables	130
5.5	Model Predictions and Experimental Validation	132
5.5.1	Model Parameters	132

5.5.2	Model Predictions with Normalized Creep Data	134
5.6	Conclusions	137
5.7	Appendix A	140
5.8	Appendix B	141
	References	149
	Figures	154
6	A MULTIAXIAL CREEP MODEL, PART II: DAMAGE-ENHANCED CREEP	163
6.1	Introduction	164
6.2	Background	165
6.3	Formulation of Constitutive Model	168
6.3.1	Inelastic Flow	168
6.3.2	Damage-enhanced Inelastic Flow	170
6.3.2.1	Effect of Microcracks on Creep	171
6.3.2.2	Formulation of Damage-enhanced Inelastic Flow	172
6.3.2.3	Microcrack Density	174
6.3.2.4	Microcrack Evolution	176
6.3.2.5	Microcrack Nucleation	177
6.3.3	Summary of Damage-enhanced Creep Model	178
6.4	Model Parameters and Predictions	181
6.4.1	Parameters	181
6.4.2	Model Comparisons	182
6.5	Conclusions	183
	References	186
	Figures	191

7 CONCLUSIONS AND FUTURE RESEARCH	196
7.1 Summary of Present Work	196
7.2 Future Work	199
References	202

List of Figures

1-1	Physically-based constitutive modeling of ice.	26
2-1	Principal types of Arctic structures: (a) upward-breaking conical structure; (b) conical structure surrounded by grounded rubber pile; (c) conical structure with accreted ice rubble; (d) downward-breaking conical structure, floating but moored; (e) conical structure with ice jammed against it; (f) vertical-walled structure; (g) caisson-retained island with grounded rubber pile; (h) grounded spray-ice island (Sanderson, 1988).	38
2-2	A pressure-area curve for ice. Peak indentation pressure P/Dh is plotted against gross contact area Dh . The average stress required to fail a large area of ice is much lower than that required to fail a small area of ice. These data are raw and have not been in any way corrected for temperature or salinity. (Sanderson, 1988).	39
2-3	Failure mode map as a function of indentation rate and aspect ratio: D=ductile, D-B=ductile-to-brittle transition, and B=brittle (Sanderson, 1988).	40
2-4	Schematic of principal failure mechanisms: (a) creep; (b) radial cracking; (c) buckling; (d) circumferential cracking; (e) spalling; and (f) crushing (Sanderson, 1988).	41
2-5	(a) Local frame of single crystal ice; (b) Reference global frame ($x_1-x_2-x_3$) and local frame ($x_1'-x_2'-x_3'$).	42
2-6	Schematic of polycrystalline ice types: (a) equiaxed-granular ice; (b) columnar-grained S-1 ice; (c) columnar-grained S-2 ice; and (d) columnar-grained S-3 ice.	43
2-7	Behaviors of single ice crystal and polycrystalline ice.	44
2-8	Deformation mode map showing regions of purely ductile and purely brittle behavior as well as the ductile-to-brittle transition in both compression and tension (Wu, 1990).	45

2-9	Multiaxial tests. (a) Geometry: under most test conditions, both axial stress and confining pressure is compressive. (b) Plots of stress difference, axial stress minus confining pressure, at various axial strain rates as a function of confining pressure. Microcracking occurs in the shaded zone, but outside it, creep behavior is independent of confining pressure (data of Jones (1982); figures from Jordaan (1986) and Sanderson (1988)).	46
3-1	Typical stress-strain curves of single crystal ice oriented for basal glide under various levels of constant strain rate.	68
3-2	An S2 polycrystalline ice.	69
3-3	Notation for basal plane orientation in the x1-x2 plane.	70
3-4	Notation for biaxial loading in the x1-x2 plane.	71
3-5	Effect of the stress exponent n on the stress-strain behavior.	72
3-6	Effect of the initial dislocation density ρ_o on the stress-strain behavior. . . .	73
3-7	Effect of the rate of dislocation multiplication α on the stress-strain behavior. . . .	74
3-8	Effect of the inelastic strain exponent m on the stress-strain behavior.	75
3-9	Effect of Young's modulus E on the stress-strain behavior.	76
3-10	Effect of the c-axis orientation θ on the stress-strain behavior.	77
3-11	Effect of temperature T on the stress-strain behavior.	78
3-12	Comparison of experimental and predicted stress-strain curves for constant strain rates at $T = -10^\circ C$	79
3-13	Predicted dislocation density vs. strain for constant strain rates at $T = -10^\circ C$	80
3-14	Comparison of experimental and predicted strain-time responses for constant stresses at $T = -10^\circ C$	81
3-15	Predicted dislocation density vs. strain for constant applied stresses at $T = -10^\circ C$	82
3-16	Variation of the dynamic Young's modulus, $S_{g,22}^{-1}$, with c-axis orientation.	83
4-1	Dynamic compliance as a function of frequency at $T = -10^\circ C$: (a) the storage compliance, $J_1(\omega)$; (b) the loss compliance, $J_2(\omega)$	99

4-2	Stress-strain responses of polycrystalline ice (with a mean grain size of 5.1 <i>mm</i>) subjected to 0.1 <i>Hz</i> sinusoidal stress at $-10^{\circ}C$; experimental data of Cole (1990) and model predictions. Plots are translated along the strain axis for clarity.	100
4-3	Stress-strain responses of polycrystalline ice (with a mean grain size of 1.5 <i>mm</i>) under various cyclic stress levels and frequencies at $-10^{\circ}C$; experimental data of Cole (1990) and model predictions. Plots are translated along the strain axis for clarity.	101
4-4	Stress-strain responses of polycrystalline ice (with a mean grain size of 5.0 <i>mm</i>) under various cyclic stress levels and frequencies at $-10^{\circ}C$; experimental data of Cole (1990) and model predictions. Plots are translated along the strain axis for clarity.	102
4-5	Stress-strain responses of polycrystalline ice (with a mean grain size of 2.5 <i>mm</i>) under various cyclic frequencies and 1 <i>MPa</i> stress at $-10^{\circ}C$; experimental data of Cole (1990) and model predictions. Plots are translated along the strain axis for clarity.	103
5-1	(a) Local frame of single crystal ice; (b) Reference global frame ($x_1-x_2-x_3$) and local frame ($x_1'-x_2'-x_3'$).	154
5-2	Columnar-grained S2 polycrystalline ice containing single crystals with random in-plane <i>c</i> -axes.	155
5-3	Equiaxed-granular polycrystalline ice containing single crystals with random <i>c</i> -axes.	156
5-4	Dimensionless strain rate plotted against dimensionless time, from the data of Jacka (1984) (reproduced from Ashby and Duval, 1985). Predictions of (i) the proposed model, (ii) Shyam Sunder and Wu (1990), (iii) Le Gac and Duval (1980), and (iv) Sinha (1978) as modified by Ashby and Duval (1985) are plotted.	157
5-5	Dimensionless strain plotted against dimensionless time, from the data of Jacka (1984) (reproduced from Ashby and Duval, 1985). Predictions of (i) the proposed model, (ii) Shyam Sunder and Wu (1990), (iii) Le Gac and Duval (1980), and (iv) Sinha (1978) as modified by Ashby and Duval (1985) are plotted.	158
5-6	Dimensionless strain rate plotted against dimensionless strain, from the data of Jacka (1984) (reproduced from Ashby and Duval, 1985). Predictions of (i) the proposed model, (ii) Shyam Sunder and Wu (1990), (iii) Le Gac and Duval (1980), and (iv) Sinha (1978) as modified by Ashby and Duval (1985) are plotted.	159

5-7	Dimensionless strain rate versus dimensionless time. Model response is plotted with the data of Mellor and Cole (1982) under constant stress.	160
5-8	Dimensionless strain versus dimensionless time. Model response is plotted with the data of Mellor and Cole (1982) under constant stress.	161
5-9	Dimensionless strain rate versus dimensionless strain. Model response is plotted with the data of Mellor and Cole (1982) under constant stress.	162
6-1	Typical stress-strain curves of polycrystalline ice under various levels of constant strain rate.	191
6-2	S2 polycrystalline ice containing crystals with random in-plane c-axes.	192
6-3	Equiaxed-granular polycrystalline ice containing crystals with random c-axes.	193
6-4	Stress-strain curve under constant strain-rate: the model prediction is compared with the data of Jordaan and McKenna (1991).	194
6-5	Stress-strain curves under constant strain-rates. The model prediction is compared with the data of Mellor and Cole (1982).	195

List of Tables

5.1	Summary of the multiaxial creep model	129
5.2	Summary of the isotropic one-dimensional creep model	130
5.3	Summary of model parameters	136
6.1	Summary of the multiaxial damage-enhanced creep model	179
6.2	Summary of the isotropic one-dimensional damage-enhanced creep model . .	180
6.3	Summary of model parameters	182

Chapter 1

INTRODUCTION AND OBJECTIVES

1.1 Introduction

The discovery of oil and gas in the Arctic has stimulated the design of large offshore structures. Accurate estimation of ice forces on these structures became necessary for safe and economical design. In a typical ice-structure interaction problem, the strain rates in an ice plate vary spatially and temporally by several orders of magnitude so that a realistic analysis must consider both creep with damage and purely brittle elastic damage. In order to develop rational theories for predicting ice loads at structural-scale and using ice as a structural material, laboratory-scale testings under controlled conditions are essential not only to identify the physical mechanisms of ice under various loading conditions but also to develop constitutive theories for the deformation processes of ice.

In most engineering problems, ice exists at homologous temperatures exceeding 0.9. At these high temperatures, the creep of ice cannot be completely suppressed even at relatively high loading rates in the brittle deformation domain. Experimental studies on the creep behavior of ice have been carried out since the 1950's. Glaciological considerations provided much of the initial motivation for this research. The increasing military and economic interests in the northern Arctic resulted in continuing experimental efforts to define the creep and strength behavior of sea ice. The effects of stress, temperature, microstructure, and chemical impurities on the inelastic deformation of ice have been extensively examined

both in the laboratory and in the field.

Even though substantial progress has been made in the past years with regard to physics and mechanical properties of ice from experiments, the constitutive modeling of ice is a difficult task due to highly rate-dependent phenomena, which include creep, microcracking, and failure. Generally, the deformation and progressive failure of ice is governed by three primary mechanisms: flow, distributed cracking, and localized cracking. In particular, ice may display purely ductile, purely brittle, or combined behaviors, which depend greatly on the temperature and loading conditions. For example, when ice is loaded under low strain rates or low stresses, viscoplasticity theory for the primary mechanism associated with flow is appropriate. However, when high strain rates or high stresses are applied to ice, it fails due to the nucleation and propagation of microcracks. For this purely brittle behavior, fracture mechanics is the primary mechanism associated with localized cracking which has to be modeled to capture the failure strength. During ductile-to-brittle transition, where ice is subjected to intermediate strain rates and stresses, damage mechanics associated with distributed cracking combined with viscoplasticity theory is appropriate. Such deformations are accompanied by the formation and stable growth of microcracks under compressive loading. There is a difference between tensile and compressive fracture: in tension a few microcracks nucleate and propagate unstably causing failure while in compression many microcracks nucleate and extend stably until they interact either causing final failure or enhancing creep by increasing the number of microcracks.

Both the elastic and inelastic behaviors of ice are of great importance in a broad range of ice mechanics problems. Many investigators have studied the inelastic deformation of ice. Many constant stress tests or constant strain-rate tests and studies of deformation mechanisms have characterized the ice behavior during the last several decades (e.g., Glen, 1955; Brill and Camp, 1961; Barnes et al., 1971; Weertman, 1973; Goodman et al., 1981; Mellor and Cole, 1982; Duval et al., 1983; Jacka, 1984). Most studies of creep in polycrystalline ice have emphasized the stress dependence of steady-state creep rate under constant stress test, which follow empirically the power-law creep. Recent work focuses largely on transient creep of freshwater ice, since engineering applications invariably involve complex thermal and mechanical histories.

Many constitutive models (e.g., Michael, 1978; Sinha, 1978; Ting and Shyam Sunder,

1985; Ashby and Duval, 1985; Shyam Sunder and Wu, 1989a,b) have been developed for the viscoelastic and viscoplastic behaviors of ice. Michel (1978) suggested a model based on easy slips on basal planes with grain boundary sliding to accommodate total deformation of polycrystalline ice. Sinha (1978) proposed a phenomenological viscoelasticity model based on the mechanism of grain boundary sliding responsible for transient creep. In Sinha's model, an exponent in relaxation time is used to account for the distribution of relaxation time implicitly. The approaches taken by Liiboutry and Duval (1985), Ashby and Duval (1985), and Shyam Sunder and Wu (1989a,b) incorporate the deformation mechanisms in their models. The central idea is the creep anisotropy, which exists in the hexagonal ice crystals. Ashby and Duval (1985) developed a model based on two types of systems in which creep occurs along the basal (easy) systems with loading, then relaxes as stress transfers from the basal to the non-basal (hard) systems. This relaxation or redistribution of stress generates directional elastic internal stress or back stress, which reverses creep upon unloading. Shyam Sunder and Wu (1989a,b) developed a transient creep model using internal state variables, which describe the changing microstructures. To describe better both primary creep and the response to increments and decrements of the applied load, Meyssonier and Goubert (1994) suggested a model based on a decomposition of the viscoplastic strain into two components, which account separately for the kinematic and the isotropic hardenings. However, these models discussed above are proposed primarily to describe strain-hardening behavior in transient creep, without consideration of effects of microcracks.

More recently, in order to incorporate the effect of microcracks, several approaches have been taken to describe damage processes (Sinha, 1988; Choi and Karr, 1989; McKenna et al., 1989; Schapery, 1991; Jordaan and McKenna, 1991; Zhan et al., 1994). Generally, the formation of microcracks will influence the mechanical behavior of material by reducing the elastic constants, enhancing inelastic strain, and producing macrocrack. To quantify the effect of elastic damage due to microcracks, Wu and Shyam Sunder (1992), Wu and Niu (1995) performed a theoretical analysis of crack nucleation in isotropic polycrystalline ice using the mechanism of elastic anisotropy of the constituent single crystals. Although most of these models may be useful in particular loading conditions such as a constant strain rate at a given temperature, none of them really represent the overall deformations of ice.

1.2 Problem Statement and Research Objectives

The objective of this thesis is to develop a physically-based constitutive model suitable for computational simulations to explain and predict the macroscopic behavior of polycrystalline ice. The development of a physically-based constitutive theory that strongly depends upon fundamental knowledge of the underlying mechanisms, which governs physical and mechanical behavior of ice under various loading histories, would ultimately improve the use of ice as a structural material.

Figure 1-1 illustrates the mechanisms related to macroscopic phenomena at different scales such as crystal-scale, laboratory-scale, and structural-scale. At crystal-scale, the motion and the multiplication process of mobile dislocations are responsible for the inelastic deformation.

At laboratory-scale, many deformation mechanisms operate at microstructural scale to induce flow and damage responses due to microcracking. These deformation mechanisms highly depend on loading rate, temperature, and ice types (e.g., freshwater and sea ice). Flow is attributed to the glide and the climb of dislocations, and to creep anisotropy due to the hexagonal structure of ice. Damage due to microcracking is caused by several mechanisms such as dislocation pile-up, grain boundary sliding, and elastic anisotropy. The local internal stresses induced by these mechanisms nucleate many stable microcracks under compression. In tension, a few microcracks lead to unstable cracks and the failure of the specimen. In this study, the aim is to develop physically-based uniaxial and multiaxial models, which are highly rate- and temperature-dependent, to describe the flow and damage,

At structural-scale, engineers are greatly interested in estimating ice forces against structures (e.g., offshore structures, ships, bridge piers, harbor structures, and submarines). Many failure mechanisms (e.g., creeping, cracking, crushing, bending, buckling, thermal cracking), which greatly influence the ice forces, depend on the loading velocity of ice plate, the aspect ratio between the thickness of ice plate and the width of structures, and the shape of the structures. The other application of ice mechanics is the use of ice as a structural material (e.g., ice roads, parking lots, and airplane runways).

The effect of microcracks on the elastic properties has been studied by many people since the early 1970's. In these studies, the elastic constants, such as modulus and Poisson

ratio, are estimated in terms of a parameter, the so-called crack density. However, the effect of microcracks on the creep properties is less known. The relative importance of the effects of microcracks on the elastic and inelastic deformations may depend on the material and operating conditions. For example, when concrete is loaded at room temperature after curing for a month, microcracks will influence the elastic deformation more than the inelastic deformation. However, studies have reported that the inelastic deformation in ice is highly enhanced by microcracks, whereas microcracks almost do not affect the elastic deformation.

This study incorporates the effects of microcracks on the inelastic deformation for the development of a damage-enhanced creep model. The model can describe strain softening after a peak stress under constant strain-rate loading. Damage accumulation due to rate-sensitive microcracking is considered to be the cause of tertiary creep and strain softening.

A constitutive transient creep model has been developed for freshwater polycrystalline ice by Shyam Sunder and Wu (1989a,b). The generalization of this model and the evolution equations associated with the activity of dislocations and microcracking are required to reflect additional features in ice behavior under various loading histories and test temperatures. With the objective of developing a constitutive model for the analysis of the ice-structure interaction problem, the following tasks are identified: (i) the development of physically-based constitutive equations in the framework of continuum mechanics using the concept of internal state variables and (ii) the development of the evolution equations of internal state variables that describe the changing substructure and accumulation of damage due to microcracking.

1.3 Research Approach and Organization of Thesis

The principal objective of this thesis is to develop constitutive equations to describe inelastic deformation of highly rate-dependent solids, especially ice, based on the underlying deformation mechanisms.

A physically-based constitutive theory is developed in the framework of continuum mechanics using the concept of internal state variables. This work includes the identification of underlying physical mechanisms of deformation under various loading histories. The gen-

eral approach being followed to develop the proposed model consists of three steps: (a) the mathematical formulation of a constitutive model based on internal state variables describing the evolution of the material substructures; (b) the development of robust methods for determining material parameters and functions; and (c) the validation of the constitutive model against available experimental data through numerical simulation.

In the constitutive model, we will consider freshwater polycrystalline ice, with mean grain sizes between 1 and 10 *mm* of single-phase ice of hexagonal structure at temperature between -10 and -50°C (above $0.80 T_M$), and strain rates between 10^{-7} and 10^{-3} s^{-1} . Within the ductile and the ductile-to-brittle regimes, deformation is governed by dislocation movements and microcracking in grains and at grain boundaries. In particular, we compare the developed model with the following experimental data: constant stress tests and constant strain rate tests, and tensile-compressive cyclic loading tests.

This thesis is organized in the following way. In Chapter 2, background in ice mechanics and current understanding of the mechanical properties of ice are discussed.

Chapter 3 describes a constitutive creep model for single ice crystal, which exhibits highly rate- and temperature-dependent behavior and a strong dependence on the basal-plane orientation. In this model, the inelastic deformation is attributed to the multiplication process of mobile dislocations on the basal planes due to strong creep anisotropy. Material properties used in the model are the dislocation velocity and the changing dislocation density based on experimental data. The proposed uniaxial creep model is extended to a biaxial model by allowing inelastic deformation only along the basal planes. This chapter includes parametric studies to understand better the dependence of macroscopic stress-strain curves on microstructural parameters. The chapter also compares the model predictions with experimental data.

Chapter 4 discusses the relaxation process of polycrystalline ice under cyclic loading. In polycrystalline ice, unlike in single ice crystal, the strong creep anisotropy and intergranular processes generate an internal stress field, which activates dislocation sources. The internal stresses and their distributions affect the mechanical properties of ice through the microstructure and its variation due to time-dependent relaxations. The study of its temperature-dependent or frequency-dependent internal friction spectra proves the existence of the distributed relaxations. Since the internal friction is produced from anelastic strain due to

dislocation movements or grain boundary sliding under cyclic stress (Cole, 1995; Tatibouet et al., 1986), the distribution of relaxation times from the internal friction measurements is considered for the relatively low anelastic strain. This chapter describes a constitutive model of anelastic creep model in polycrystalline ice under cyclic loading. This anelastic model is developed on the basis of the linear relationship between anelastic strain and stress and the distribution of relaxation times. Numerical results and experimental data of reversed direct-stress are compared.

Chapter 5 develops a ductile constitutive model of polycrystalline ice using internal variables and their relations with the underlying physical mechanisms of deformation. The constitutive theory is formulated based upon the dominant dislocation-based deformation mechanism. The dislocations in the crystals provide obstacles for mobile dislocations, which lead to work hardening. As the strain rate decreases during transient creep in constant stress tests, or the flow stress increases in constant strain rate tests, polycrystalline solids exhibit work hardening, which can be explained by an increase in the dislocation density with increasing strain. The decrease of work hardening rate is attributed to recovery processes due to the rearrangement and annihilation of dislocations during deformation. The transient behavior results from competing work hardening and recovery processes due to production, rearrangement and annihilation of dislocations. In the limit of steady-state deformation a balance between strain hardening and recovery processes is reached. Major features of this model include recovery functions in addition to internal back stress and isotropic stress, which are introduced to simulate transient creep during loading. The model predictions are then compared with experimental data (Jacka, 1984; Mellor and Cole, 1982).

Chapter 6 describes a multi-axial constitutive damage-enhanced creep model for orthotropic polycrystalline ice. This chapter evaluates highly rate- and temperature-dependent mechanical behavior based on the movement and generation of dislocations and microcracking. Experimental results under constant stresses and constant strain rates show the occurrence of microcracking, which enhances the inelastic deformation. This study incorporates the effects of microcracks on the inelastic deformation for the development of a damage-enhanced creep model. The model can describe strain softening after a peak stress under constant strain-rate loading. Damage accumulation due to rate-sensitive microcracking is considered as a cause of tertiary creep and strain softening. This chapter formulates the inelastic material anisotropy and the damage-enhanced material anisotropy to describe the

directional nature of material damage. The model predictions are compared with experimental results.

Finally, Chapter 7 summarizes the findings. It discusses conclusions and suggests possible future research.

References

- [1] Ashby, M. F. and Duval, P. (1985). The creep polycrystalline ice. *Cold Regions Science and Technology*, Vol. 11, No.3, pp. 285-300.
- [2] Barnes, P., Tabor, D. and Walker, J.C.F. (1971). The friction and creep of polycrystalline ice. *Proc. Royal soc. London, ser. A*, 324, pp. 127-155.
- [3] Brill, R. and Camp, P.R. (1961). Properties of ice. U.S. Army Snow, Ice and Permafrost Research Establishment, *Research Report 68*, 48p.
- [4] Choi, K. and Karr, D.G. (1989). A damage mechanics model for uniaxial creep and cyclic loading of polycrystalline ice. *Proc. 8th Int. Conf. Offshore Mech. and Arctic Eng.*, ASME, Vol. 4, pp. 75-82.
- [5] Cole, D.M. (1990). Reversed direct stress testing of ice: Initial experiment results and analysis. *Cold Regions Science and Technology*, Vol. 18, No.3, pp. 303-321.
- [6] Cole, D.M. (1995). A model for the anelastic straining of saline ice subjected to cyclic loading. *Philosophical Magazine*, In press.
- [7] Derradji-Aouat, A., Sinha, N. K. and Evgin, E. (1993). Experimental study of the behavior of columnar grained ice subjected to cyclic loading. *Proc. 12th Int. Conf. Offshore Mech. and Arctic Eng.*, Vol. 1, pp. 21-28.
- [8] Duval, P., Ashby, M.F. and Anderman, I. (1983). Rate-controlling processes in the creep of polycrystalline ice. *The Journal of Physical Chemistry*, Vol. 87, No. 21, pp. 4066-4074.
- [9] Glen, J.W. (1955). The creep of polycrystalline ice. *Proc. Royal Soc. London, Ser. A*, 288(1175), pp. 519-538.
- [10] Goodman, D.J., Frost, H.J. and Ashby, M.F. (1981). The plasticity of polycrystalline ice. *Philosophical Magazine A*, 43(3), pp. 665-695.
- [11] Gottstein, G. and Argon, A.S. (1987). Dislocation theory of steady state deformation and its approach in creep and dynamic tests. *Acta Metallurgica*, 35(6), pp. 1261-1271.
- [12] Hobbs, P.V. (1974). *Ice Physics*. Clarendon Press, Oxford.
- [13] Jacka, T.H. (1984). The time and strain required for development of minimum strain rates. *Cold Regions Science and Technology*, Vol. 8, pp. 261-268.
- [14] Jordaan, I.J. and McKenna, R.F. (1991). Processes of deformation and fracture of ice in compression. *Proc. IUTAM/IAHR Symp. on Ice-Structure Interaction*, Jones, S.J., McKenna, R.F., Tillotson, J. and Jordaan, I.J. (Ed.), Springer-Verlag, pp. 283-309.
- [15] Llibouty, L. and Duval, P. (1985). Various isotropic and anisotropic ices found in glaciers and polar ice caps and their corresponding rheologies. *Annales Geophysicae*, Vol. 3, pp. 207-224.

- [16] McKenna, R.F., Meyssonier, J. and Jordaan, I.J. (1989). Peak pressures from a damage model for ice compression. *Proc. 8th Int. Conf. Offshore Mech. and Arctic Eng.*, The Hague, The Netherlands, Vol. IV, pp. 67-73.
- [17] Mellor, M. and Cole, D. (1981). Cyclic loading and fatigue in ice. *Cold Regions Science and Technology*, Vol. 4, pp. 41-53.
- [18] Mellor M. and Cole, D. (1982). Deformation and failure of ice under constant stress or constant strain rate. *Cold Regions Science and Technology*, Vol. 5, pp. 201-219.
- [19] Meyssonier, J. and Goubert, A. (1994). Transient creep of polycrystalline ice under uniaxial compression: an assessment of internal state variable models. *Annals of Glaciology*, Vol. 19, pp. 55-62.
- [20] Michel, B. (1978). The strength of polycrystalline ice. *Canadian Journal of Civil Engineering*, Vol. 5, No. 3, pp. 285-300.
- [21] Schapery, R.A. (1991). Models for the deformation behavior of viscoelastic media with distributed damage and their applicability to ice. *Proc. IUTAM/IAHR Symp. on Ice-Structure Interaction*, Jones, S.J., McKenna, R.F., Tillotson, J. and Jordaan, I.J. (Ed.), Springer-Verlag, pp. 191-230.
- [22] Sinha, N.K. (1978). Rheology of columnar-grained ice. *Experimental Mechanics*, Vol. 18, No. 12, pp. 464-470.
- [23] Sinha, N.K. (1988). Crack enhanced creep in polycrystalline material: strain rate sensitive strength and deformation of ice. *Journal of Mater. Sci.*, Vol. 23, pp. 4415-4428.
- [24] Shyam Sunder, S. and Wu, M.S. (1989a). A differential flow model for polycrystalline ice. *Cold Regions Science and Technology*, Vol. 16, No. 1, pp. 45-62.
- [25] Shyam Sunder, S. and Wu, M.S. (1989b). A multiaxial differential model of flow in orthotropic polycrystalline ice. *Cold Regions Science and Technology*, Vol. 16, No. 2, pp. 223-235.
- [26] Tatibouet, J., Perez, J. and Vassoille, R. (1987). Study of grain boundaries in ice by internal friction measurement. *Journal of Physique*, Colloque C1, No 12, 48, C1-197 to C1-203.
- [27] Ting, S.-K. and Shyam Sunder, S. (1985). Constitutive modeling of sea ice with applications to indentation problems. *MIT SCEOE Research Report No. 3*.
- [28] Weertman, J. (1973). Creep of Ice. *Physics and Chemistry of Ice*, Whalley, E., Jones, S.J. and Gold, L.W. (Editors), pp. 320-337.
- [29] Wu, M.S. and Niu, J. (1995). Micromechanical prediction of the compressive failure of ice, Part I: Model development. *Mechanics of Materials*, Vol. 20, pp. 9-32.

- [30] Wu, M.S. and Shyam Sunder, S. (1992). Elastic anisotropy and micro-damage processes in polycrystalline ice, Part I: Theoretical formulation. *International Journal of Fracture*, Vol. 55, pp. 223-243.
- [31] Zhan, C., and Evgin, E. and Sinha, N.K. (1994). A three dimensional anisotropic constitutive model for ductile behavior of columnar grained ice. *Cold Regions Science and Technology*, Vol. 22, pp. 269-284.

PHYSICALLY-BASED CONSTITUTIVE MODELING OF ICE

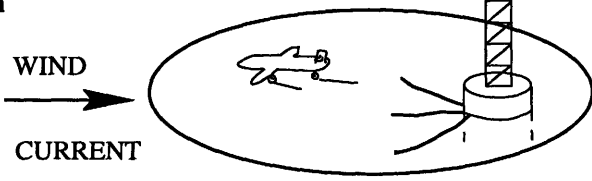
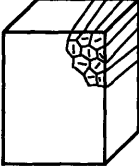
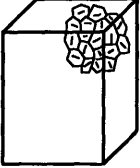

SCALE	SCIENTIFIC APPROACH	MECHANISMS	PHENOMENA
STRUCTURAL-SCALE	<p>100 m</p> <div style="border: 1px solid black; padding: 5px; margin: 5px 0;"> COMPUTATIONAL ALGORITHMS & MODEL <ul style="list-style-type: none"> • Ice Forces (Ice-Structure Interactions) • Ice Deflections (Use of Ice as Structural Material) </div> <p>10 m</p> <div style="text-align: center;">  <p>WIND CURRENT</p> </div> <p>1 m</p>	<p>Elastic Buckling</p> <p>Creep Buckling</p> <p>Creeping</p> <p>Radial & Circumferential Cracking</p> <p>Spalling</p> <p>Crushing</p> <p>Flexural Failure</p>	<p>Scale-dependent Failure Modes</p> <p>Rate-dependent Failure Modes</p>
LABORATORY-SCALE	<div style="border: 1px solid black; padding: 5px; margin: 5px 0;"> PHYSICALLY-BASED CONSTITUTIVE MODEL: <ul style="list-style-type: none"> • Uniaxial & Multiaxial Flow and Damage Model • Rate, Temperature, Ice type dependent Model • Fracture Model </div> <p>10 cm</p> <div style="display: flex; justify-content: space-around; align-items: center;"> <div style="text-align: center;">  <p>Columnar-grained ice</p> </div> <div style="text-align: center;">  <p>Equiaxed granular ice</p> </div> </div> <p>1 cm</p>	<p>Dislocations Glide & Climb</p> <p>Creep Anisotropy</p> <p>Dislocation Pile-up</p> <p>Grain Boundary Sliding</p> <p>Elastic Anisotropy</p> <p>Microcracking</p>	<p>Flow</p> <p>Damage</p> <p>Failure</p>
CRYSTALS	<div style="text-align: center;">  <p>1 Grain</p> </div> <p>1 mm</p>	<p>Dislocations Glides & Multiplication</p>	<p>Flow</p>

Figure 1-1: Physically-based constitutive modeling of ice.

Chapter 2

BACKGROUND IN ICE ENGINEERING

This chapter discusses issues and current understanding in ice engineering, the physical deformations and fracture processes in polycrystalline ice at different scales. In addition, a brief review of the mechanical properties of ice is given.

2.1 Introduction

For centuries, the ice cover challenged mariners attempting polar navigation. For a long time, engineers have been challenged by the problems of constructing bridges across ice-covered waters. To achieve a scientific understanding of ice interaction with man-made structures, experimental programs on creep and fracture behavior of ice have been carried out since the 1950's. Broadly speaking, research in ice engineering may be classified into six major areas:

1. Ice loads on structures (e.g., offshore, ship, bridge and harbor structures);
2. Use of ice as a structural material (e.g., ice roads and bridges, ice barriers for protecting offshore structures);
3. Ice penetration by structures (e.g., submarines, missiles, conical structures);
4. Ice adhesion on structures (e.g., highways, bridges, aircrafts, ships, offshore and hydraulic structures, and electrical/communications network);

5. Geophysics of ice movement (e.g., glacier flow, dynamics of icebergs and sea ice); and
6. Soil mechanics (e.g., frozen soil, permafrost engineering).

The following chapters are primarily focused on the first two areas, although the understanding and theories that have been developed are general and relevant to most of the areas above. Significant progress has been made in sea ice mechanics in the last 30 years. A significant number of problems remain unresolved in order to ensure sound engineering and cost-effective solutions. Recently, the U.S. Navy Office of Naval Research has initiated a research program, named the Sea Ice Mechanics Initiative, to bridge the different fracture properties at various scales and to develop physically-based constitutive and fracture models for the corresponding deformations and fracture processes (Proceedings SIM and AMW, 1995). In the following sections, a brief overview of engineering practices in estimating ice loads and the current understanding of physical processes at different scales is described briefly.

2.2 Ice Loads on Offshore Structures

For the purposes of calculation of design loads for offshore structures, it is convenient to divide ice-loading scenarios in two broad categories: static and dynamic. The loading state is static if ice exists in stationary contact with a structure and then experiences an increasing load applied to it by natural driving forces such as current and wind. The loading state is dynamic if an ice feature is not initially in contact with a structure, but arrives and strikes it with appreciable velocity. In addition, ice loads is also significantly affected by the shape of the structure and the resulting failure modes. For instance, ice will fail in bending on conical structures, in crushing on narrow vertical structures, and sometimes in mixed mode failures against wide structures. The ability to predict ice loads requires that these failure modes be understood and predicted as a function of both ice feature geometry (size and thickness), ice type and structure shape and stiffness. The load magnitudes are also a function of ice strength and size of failure zones, as well as other factors such as friction and clearing processes. The ice strength is greatly affected by ice temperature, salinity and loading rate. Inertia effects may be important in dynamic loading. The maximum size or thickness of these ice features is an important factor in designing structures.

A classical ice force problem is that of ice sheets interacting with a vertically-faced indenter. Figure 2-1 shows these interactions for both cylindrical structures and conical structures when they are surrounded by a variety of ice features including continuous ice sheet, ice ridges contained in ice floes, discrete ice floes, ice rubble features, icebergs and extreme features such as ice inlands.

The use of lower ice loads is important in lowering the costs of offshore platforms for oil and gas development in ice covered regions. The structures must be designed for two levels of loading. The total integrated force on the structure, the *global force*, governs the overall structural geometry and foundation design, while the actual distribution of force on segments of the structure, the *local pressure*, dictates the design of local framing and wall thickness. Experimental data on local pressures, on the other hand, vary by a factor of up to 100 for a given indentation area of contact.

Figure 2-2 shows a pressure-area curve which plots the local peak pressure P/Dh as a function of contact area, i.e., the product of structural diameter D and ice thickness h , shows a strong scale effect. The data set covers a wide variety of ice types (freshwater S2 ice, first-year and multi-year sea ice) and a wide variety of test conditions (laboratory experiments, *in situ* jacking tests, measurements on various structures, and full-scale interactions with islands). All data are raw and have not been corrected for temperature or salinity. Local pressures at failure measured under small-scale laboratory conditions are more than 100 times larger than those measured during full-scale interaction. The general trend in this Figure is that the average stress required to fail a large area of ice is much lower than that required to fail a small volume of ice.

Laboratory-scale ice specimens exhibit the local pressures that can exceed 6 MPa whereas the pressures measured from structural-scale interactions can be as small as 1 MPa . Ice-structure interactions (first-year sea ice) at structural-scales indicate that average ice failure pressures are generally less than 1 MPa , an order of magnitude lower than that predicted by laboratory-scale compressive strength tests. In order to increase the understanding of ice-structure interaction phenomenon and to better predict ice forces, additional research on the fundamental properties of laboratory-scale ice is required.

At this point, there is no rational model based on a physical mechanism that explains this phenomenon. Therefore, predictions of ice forces are mostly based on empirical relationships

and simplified analytical procedures. These issues and current practices are addressed in details (e.g., Sanderson, 1988; Blanchet, 1990; Croasdale, 1988). Currently, two standards for the design of offshore platforms in ice are used. These are the American Petroleum Institute Recommended Practice (API RP2N) “Planning, Designing and Constructing Fixed Offshore Structures and Pipelines for Arctic Conditions” and the Canadian Standards Association Standard (CAN/CSA-471-92) “General Requirements, Design Criteria, the Environment, and Loads”.

2.3 Multiple-scale Processes

2.3.1 Structural-scale Processes

Figure 2-3 shows schematically *failure mode map* of ice as a function of two parameters; indentation rate, defined as the ratio of ice sheet velocity to the indenter diameter, and aspect ratio, defined as the ratio of indenter diameter to ice sheet thickness. The limiting ice loads and the associated modes of failure of the ice sheet during indentation depend principally on the values of these two parameters. In particular, failure occurs as a result of buckling, creeping, cracking, spalling, and crushing. A schematic of the individual failure modes (mechanisms) is given in Fig. 2-4.

As shown in Fig. 2-3, creep is the dominant mode of failure when ice movements are slow, while purely brittle behavior dominates failure when ice movement is fast. Cracking may be either localized or distributed. Localized cracks are typically long but few in number; they are responsible for large-scale fractures in the form of radial, circumferential, and spalled cracks. Distributed cracks are, on the other hand, typically short but extremely large in number; they are responsible for small-scale fractures, also so-called damage, in the form of crushed or pulverized ice.

Ice loads generally reach a maximum at indentation rates which defines the transition from ductile to brittle behavior. As the failure map indicates, the ductile-to-brittle transition is characterized by the simultaneous occurrence of multiple failure modes. Due to difficulties in analyzing multiple failure modes simultaneously, the separate analysis of the ductile and

purely brittle indentation problems has been undertaken in the literature.

2.3.2 Laboratory-scale Processes

Ice formed from sea-water, or sea ice, is the material of prime interest in the design of offshore structures. However, one of the remarkable properties of ice is that it effectively rejects almost all impurities as it crystallizes. Consequently the solid ice phase in sea ice is very pure, although pockets of salt-water are interspersed in the matrix of pure ice. If we allow for the presence of such brine pockets, studies generally find that the mechanical behaviors of sea ice and freshwater polycrystalline ice are very similar. Thus a primary focus on the mechanical behavior of freshwater polycrystalline ice is acceptable. With the understanding of pure ice, we can model sea ice by accounting for brine pockets.

Ice forms from liquid water and preserves some of the geometric features of the water molecules. The geometric configuration of single crystal ice is presented in Fig. 2-5. The arrangement of molecules in individual crystals (or grains) of terrestrial ice is hexagonal in structure. The plane parallel to the layer structure is known as the basal plane. The direction perpendicular to the basal plane is known as the *c*-axis of the crystal. The elastic and creep properties of single crystal ice are different in different directions, i.e., they display anisotropic material behavior.

In nature, ice forms in a variety of ways that depend on growth processes and thermal and mechanical histories. A classification system for freshwater river and lake ice on the basis of its genesis, structure and texture was given by Michel and Ramseier (1971). Because this thesis considers granular and columnar-grained (T-type, S-type) polycrystalline ice, a brief identification of these two types of ice is given.

Granular ice (snow ice or consolidated slush ice) is a conglomerate of randomly-oriented grains, also known as equiaxed or randomly-oriented polycrystalline ice (Fig. 2-6(a)). Columnar grained ice, on the other hand, is an arrangement of ice crystals whose *c*-axes preferentially lie in a plane. In columnar-grained S-1 ice (Fig. 2-6(b)), the *c*-axes of the crystals are in the vertical plane (perpendicular to the water surface); in columnar-grained S-2 ice (Fig. 2-6(c)), the *c*-axes of the crystals are randomly oriented in the horizontal plane (plane parallel to the water surface); in columnar-grained S-3 ice (Fig. 2-6(d)), the preferred orientation of

c-axes of the crystals are in the horizontal plane (parallel to the water surface).

The macroscopic fabric of an ice sheet made up of randomly-oriented granular crystals is isotropic even though the individual crystals are anisotropic. On the other hand, an ice sheet made up of columnar crystals may be anisotropic. This polycrystal anisotropy, also called fabric anisotropy, is a layered transversely isotropic material, where the material behavior in the plane of the ice sheet is isotropic but is different from that perpendicular to the ice sheet. The elastic and creep behaviors of polycrystalline ice depend on the microstructure of the ice.

Figure 2-7 illustrates the behavior of single crystal ice and polycrystalline ice. Since polycrystalline ice is made up of single ice crystals, its behavior is affected by the properties of individual crystals. However, significantly different responses between single ice crystals and polycrystalline ice are reported (Weertman, 1973; Hobbs, 1974; Duval et al., 1983). These differences may be due to such processes as intergranular processes (i.e., sliding and interlocking), the distribution of crystallographic orientation of individual single crystals, alterations of dislocation densities within crystals, and damage accumulation due to microcracking.

Among the important distinctions between single ice crystal and polycrystalline ice behaviors are that single ice crystal oriented for slip on the basal planes exhibits an increasing strain rate during primary creep, whereas polycrystalline ice exhibits a decreasing strain rate. The creep of the basal plane proceeds at a much faster rate than that of polycrystalline ice. In the stress-strain curves under various strain rates, in single crystals oriented for slip on the basal planes, the stress rises to an upper yield point with increasing strain, and decreases to a constant lower yield point, and then gives no evidence of strain hardening, while in polycrystalline ice both strain hardening and strain softening phenomena are observed.

In single ice crystals without microcracks, the deformation of atomic bonds and the multiplication process of mobile dislocations are responsible for the elastic and inelastic deformations, respectively. Under different loading cases, the yield-drop of stress-strain curves under constant strain rates and the accelerating responses under static loading are observed.

The deformation of polycrystalline ice is much more complicated than that of single ice crystals. Atomic bond deformation induces the elastic deformation. The corresponding

stress-strain curve is a straight line. The motion and generation of dislocations are generally responsible for ductile responses such as strain hardening. This plastic behavior has been studied in metals by many mechanicians.

At least five independent slip systems are necessary for accommodating large plastic deformation without microcracks. Most of FCC and BCC metals have them. However, fewer than five independent slip systems in ice induce non-uniform strain when the ice specimen is loaded. As a result, microcracking occurs. The mechanisms for microcracking depend mainly on the loading rate, temperature, and ice type. Because of a variety of ice features and ice conditions encountered as well as highly rate- and temperature-dependent properties of ice, analytical constitutive modeling of ice is more complex.

During a constant stress test (the so-called creep test), polycrystalline ice undergoes time-dependent deformation. An immediate elastic strain is followed by a stage of decreasing rate of strain, called *transient* or *primary creep*. This, in turn, is followed by stages of relatively constant strain-rate called *secondary creep* and an increasing strain-rate called *tertiary creep*, and then final failure.

Under a constant rate of deformation or constant strain-rate test, polycrystalline ice displays a varying stress as it is deformed. When stress is plotted versus strain, the behavior shows a strong dependence on the applied strain rate and is highly rate-sensitive. At lower strain rates where the behavior is ductile, the stress monotonically increases up to a maximum or steady-state value with increasing strain and the material is said to display *strain-hardening* behavior. At very high strain-rates where the behavior is brittle, the stress increases almost linearly with strain up to the point of failure as is the case for linear elastic materials. However at intermediate strain rates corresponding to the ductile-to-brittle transition, the stress first increases to a maximum and then decreases with increasing strain; the material displays negligible strain-hardening behavior followed by *strain-softening* behavior.

The *deformation mode map* (Fig. 2-8) plots the applied stress against the minimum strain-rate from tests both in compression and in tension. The behavior of polycrystalline ice in compression and in tension are similar at very low strain rates but become different as strain rate is increased. At the intermediate and high strain rates, compressive failure occurs due to distributed cracking or damage, while in tension the failure is governed by unstable crack propagation. In the purely brittle region, the compressive strength is greater than

the tensile strength by a factor greater than three. The importance of the ductile-to-brittle transition in predicting design loads stems from the fact that the failure stress in compression reaches its maximum value in this region.

In reality, loads are imposed simultaneously in more than one direction. The resulting multi-axial state of stress significantly influences material behavior. Jones (1982) reported the effects of triaxial loading on the behavior of polycrystalline ice, when a cylindrical ice sample is subjected simultaneously to an axial compressive load and a lateral confining pressure which is proportional to the axial stress (Fig. 2-9). At low strain-rates where the behavior is ductile, and the strength is small, the responses are insensitive to variations in the confining pressure. At higher strain rates where brittle behavior is initiated, the strength increases substantially with confining pressure up to a certain value since the formation of distributed microcracks is suppressed.

Theoretical models which seek to capture the laboratory-scale deformation and failure behavior of materials are known as *constitutive models*. In the simplest form, such models are *empirical* and rely on mathematical expressions to fit the experimental data. On the other hand, phenomenological models are based on the mathematical formalisms of solid mechanics that ensure consistency with well-established physical laws such as those of thermodynamics. These types of models, particularly those founded on classical plasticity theory, have been successfully used in many engineering applications. Recently-proposed *micromechanical models* are established based on the direct incorporation of microstructure, such as inclusions, microcracks, shapes and sizes of constituents. The approach taken in this thesis is to formulate *physically-based but phenomenological models*, which depend on the fundamental knowledge of the underlying mechanisms governing mechanical behavior in the microstructure.

References

- [1] Ahmad S. and Whitworth, R. W. (1988). Dislocation motion in ice: a study by synchrotron X-ray topography. *Philosophical Magazine A*, Vol. 57, No. 5, pp. 749-766.
- [2] Alexander, H. and Haasen, J. R. (1968). Dislocations and plastic flow in the diamond structure. *Solid State Physics*. Vol. 22, F. Seitz, D. Turnbull, and H. Ehrenreich (Editors), Academic Press, New York, pp. 27-158.
- [3] API RP2N (1994). American Petroleum Institute Recommended Practice 2N. *Planning, Designing and Constructing Fixed Offshore Structures and Pipelines for Arctic Conditions*. Draft 1994. API Dallas.
- [4] Ashby, M. F. and Duval, P. (1985). The creep polycrystalline ice. *Cold Regions Science and Technology*, Vol. 11, No.3, pp. 285-300.
- [5] Barnes, P., Tabor, D. and Walker, J.C.F. (1971). The friction and creep of polycrystalline ice. *Proc. Royal soc. London A*, 324, pp. 127-155.
- [6] Blanchet, D. (1990). Ice Design Criteria for Wide Structures. *Canadian Geotechnical Journal*, Vol. 27, No. 6, pp. 701-725.
- [7] Canadian Standards Association (1992). *General Requirements, Design Criteria, the Environment, and Loads* (CAN/CSA-471-92). CSA, Rexdale, Ontario, Canada.
- [8] Cole, D.M. (1986). Effect of grain size on the internal fracturing of polycrystalline ice. U.S. Army Corps of Eng., Cold Reg. Res. Eng. Lab., Report 86-5.
- [9] Croasdale, K.R. (1988). Ice forces: current practices. *Proc. 7th Int. Conf. on Offshore Mechanics and Arctic Engineering*, Huston, Texas, Vol. 4, pp. 133-151.
- [10] Duval, P., Ashby, M.F. and Anderman, I. (1983). Rate-controlling processes in the creep of polycrystalline ice. *The Journal of Physical Chemistry*, Vol. 87, No. 21, pp. 4066-4074.
- [11] Fukuda, A. and Higashi, A. (1973). Dynamical behavior of dislocations in ice crystals. *Crystal Lattice Defects*, Vol. 4, pp. 203-210.
- [12] Glen, J.W. (1955). The creep of polycrystalline ice. *Proc. Royal Soc. London, Ser. A*, 288(1175), pp. 519-538.
- [13] Gold, L.W. (1977). Engineering properties of fresh-water ice. *Journal of Glaciology*, Vol. 19, No. 81, pp. 197-212.
- [14] Goodman, D.J., Frost, H.J. and Ashby, M.F. (1981). The plasticity of polycrystalline ice. *Philosophical Magazine A*, Vol. 43, No. 3, pp. 665-695.
- [15] Higashi, A., Koinuma, S. and Mae, S. (1964). Plastic yielding in ice single crystals. *Japanese Journal of Applied Physics*, Vol. 3, No. 10, pp. 610-616.

- [16] Higashi, A. (1968). Mechanisms of plastic deformation in ice single crystals, *Physics of Snow and Ice*, pp. 227-289.
- [17] Johnston, W.G. (1962). Yield points and delay times in single crystals. *J. Appl. Phys.*, Vol. 33, No. 9, pp. 2716-2730.
- [18] Jones, S.J. and Glen, J.W. (1969). The mechanical properties of single crystals of pure ice. *Journal of Glaciology*, Vol. 8, No. 54, pp. 463-473.
- [19] Jordaan, I.J. (1986). Numerical and finite element technique in calculation of ice-structure interaction. In *IAHR 86*, Vol. 2, pp. 405-440.
- [20] Liiboutry, L. and Duval, P. (1985). Various isotropic and anisotropic ices found in glaciers and polar ice caps and their corresponding rheologies. *Annales Geophysicae*, 3(2), pp. 207-224.
- [21] Liu, F., Baker, I. and Dudley, M. (1993). Dynamic observation of dislocation generation of grain boundaries in ice. *Philosophical Magazine A*, Vol. 67, No. 5, pp. 1261-1276.
- [22] Mellor M. and Cole, D. (1982). Deformation and failure of ice under constant stress or constant strain rate. *Cold Regions Science and Technology*, Vol. 5, pp. 201-219.
- [23] Meyssonier, J. and Duval, P. (1989). Creep behavior of damaged ice under uniaxial compression: a preliminary study. *Proceedings of the 10th Int. Conf. on Port and Ocean Eng. under Arctic Conditions*, Lula, Sweden, Vol. 1, pp. 225-234.
- [24] Michel, B. (1978). A mechanical model of creep of polycrystalline ice. *Can. Geotech. J.*, Vol. 15, pp. 155-170.
- [25] Muguruma, J. and Higashi, A. (1963). Non-basal glide bands in ice crystals, *Nature*, May 11, No. 4880, pp. 573.
- [26] Palmer, A.C., et al. (1983). Fracture and its role in determining ice forces on offshore structures. *Annals of Glaciology*, Vol. 4, pp. 216-221.
- [27] Proceedings of the Sea Ice Mechanics and Arctic Modeling Workshop, April 25-28 1995, Anchorage, Alaska, Organized by Northwest Research Associates, Inc., Bellevue, WA.
- [28] Readey, D.W. and Kingery, W.D. (1964). Plastic deformation of single crystal ice. *Acta Metall.*, Vol. 12, No. 2, pp. 171-178.
- [29] Sanderson, T.J.O. (1988). *Ice Mechanics, Risk to Offshore Structures*. Graham and Trotman, London.
- [30] Shearwood, C. and Whitworth, R.W. (1991). The velocity of dislocations in ice. *Philosophical Magazine A*, Vol. 64, No. 2, pp. 289-302.
- [31] Shyam Sunder, S. and Wu, M.S. (1990). On the constitutive modeling of transient creep in polycrystalline ice. *Cold Regions Science and Technology*, Vol. 18, pp. 267-294.

- [32] Sinha, N.K. (1978). Observations of basal dislocations in ice by etching and replicating. *J. Glaciol.*, Vol. 21, No. 85, pp 385-395.
- [33] Sinha, N.K. (1979). Grain-boundary sliding in polycrystalline materials. *Philosophical Magazine A*, Vol. 40, No. 6, pp. 825-842.
- [34] Weertman, J. (1973). Creep of Ice. *Physics and Chemistry of Ice*,
- [35] Whalley, E., Jones, S.J. and Gold, L.W. (Editors), pp. 320-337.
- [36] Wei, Y. and Dempsey, J.P. (1994). The motion of non-basal dislocations in ice crystals. *Philosophical Magazine A*, Vol. 69, No. 1, pp. 1-10.
- [37] Wu, M.S. (1990). Physically-based constitutive models for transient creep and damage in polycrystalline ice. Ph.D. thesis, MIT, 1990.

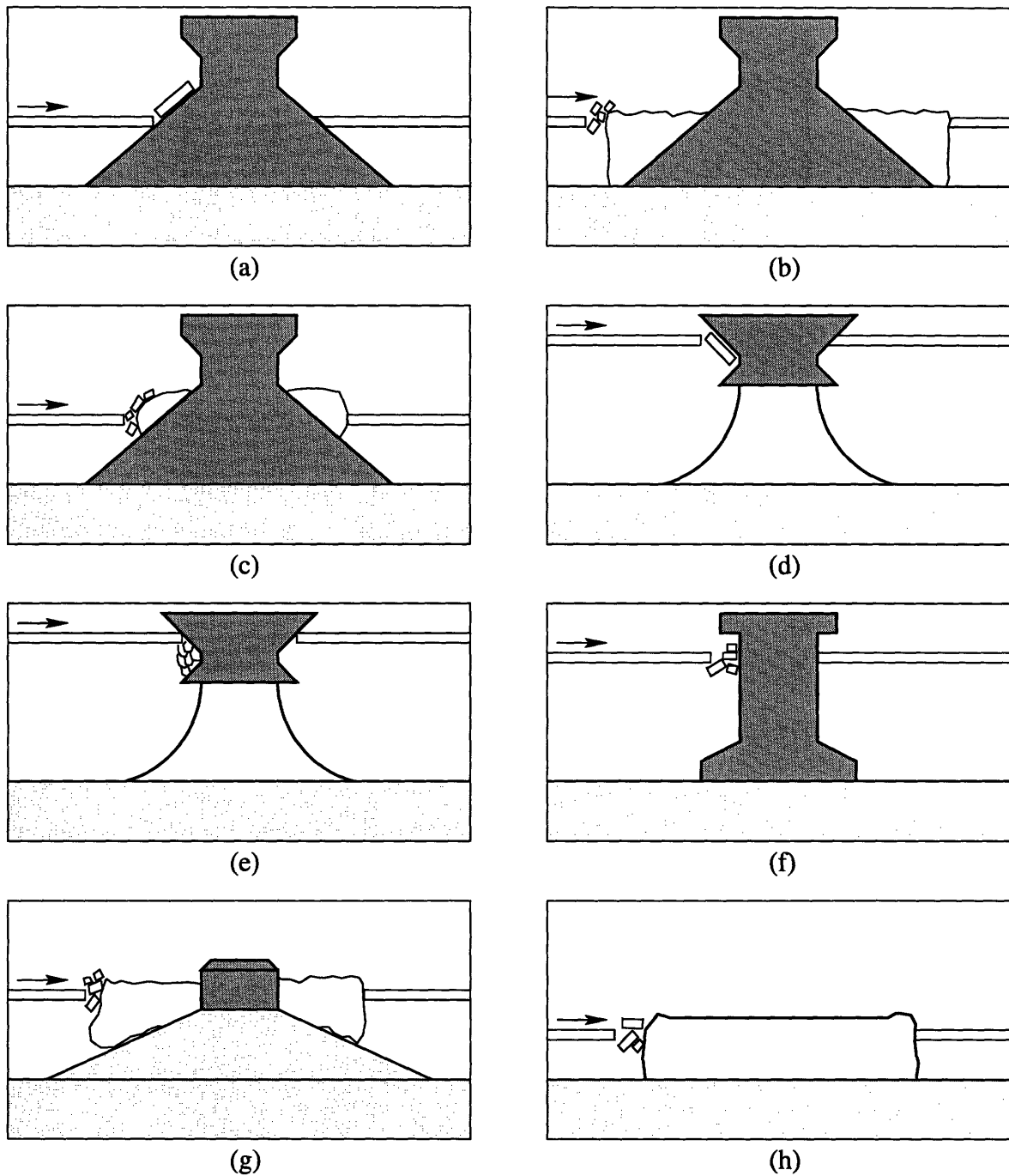


Figure 2-1: Principal types of Arctic structures: (a) upward-breaking conical structure; (b) conical structure surrounded by grounded rubber pile; (c) conical structure with accreted ice rubble; (d) downward-breaking conical structure, floating but moored; (e) conical structure with ice jammed against it; (f) vertical-walled structure; (g) caisson-retained island with grounded rubber pile; (h) grounded spray-ice island (Sanderson, 1988).

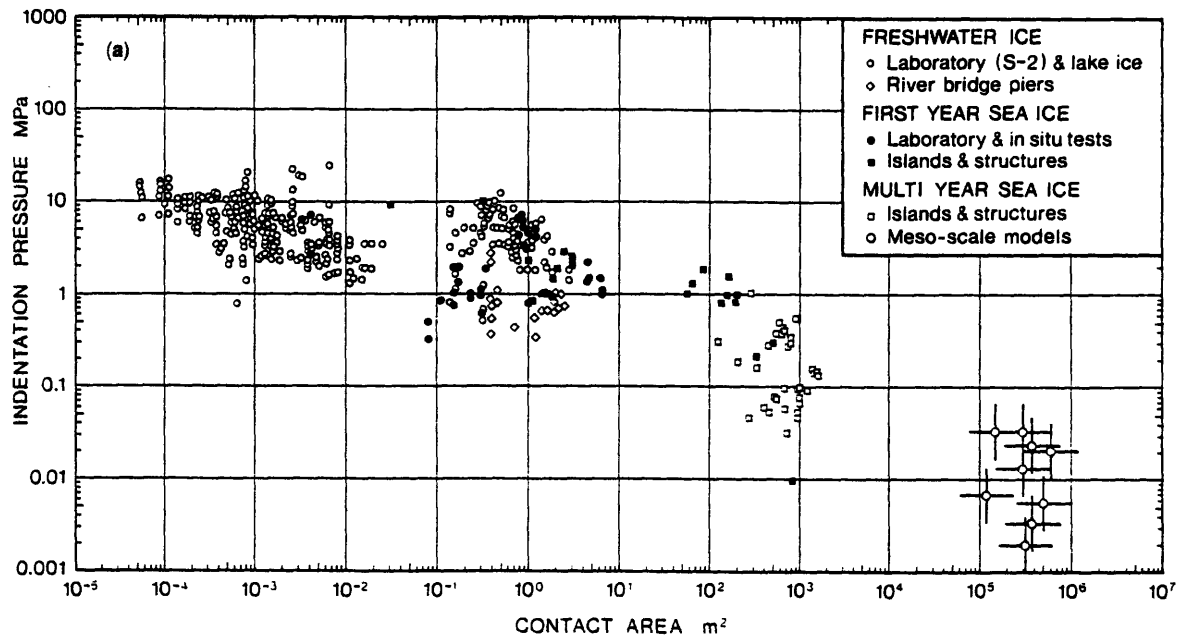


Figure 2-2: A pressure-area curve for ice. Peak indentation pressure P/Dh is plotted against gross contact area Dh . The average stress required to fail a large area of ice is much lower than that required to fail a small area of ice. These data are raw and have not been in any way corrected for temperature or salinity. (Sanderson, 1988).

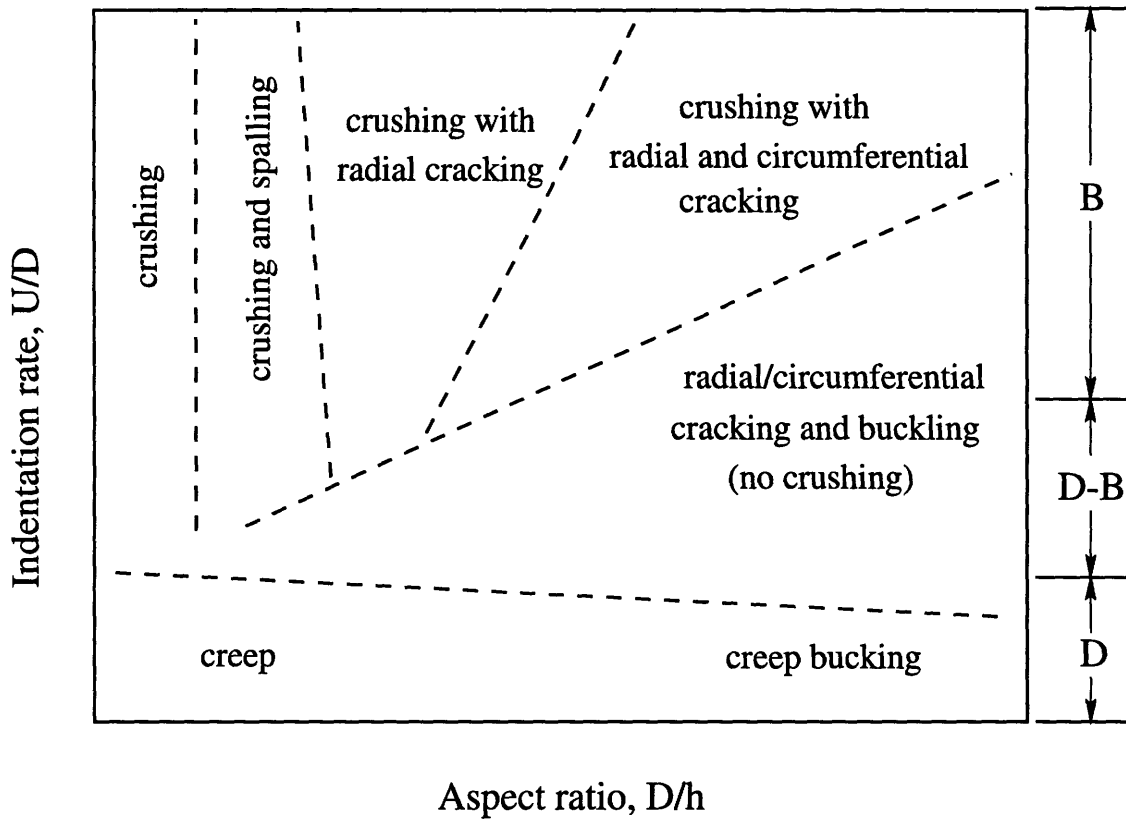
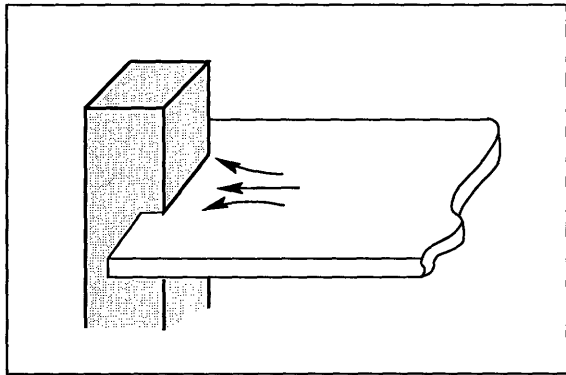
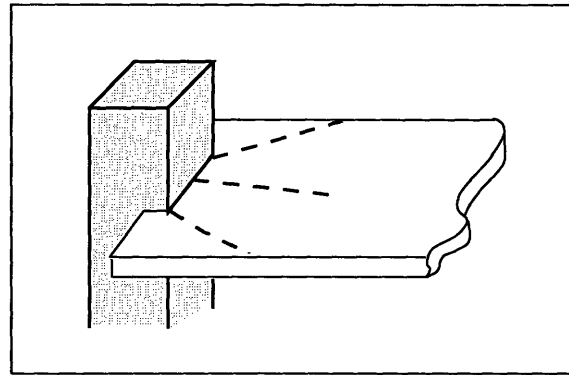


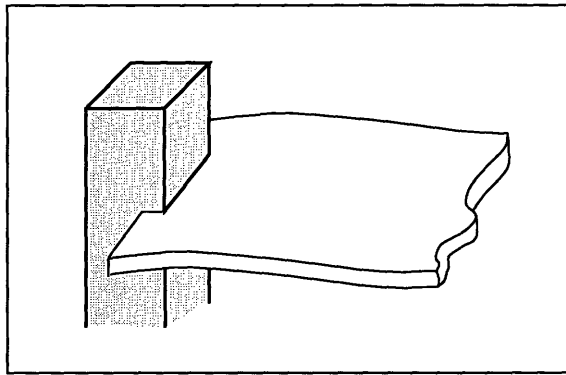
Figure 2-3: Failure mode map as a function of indentation rate and aspect ratio: D=ductile, D-B=ductile-to-brittle transition, and B=brittle (Sanderson, 1988).



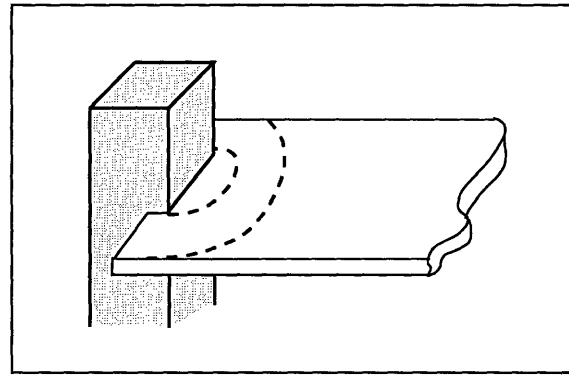
(a)



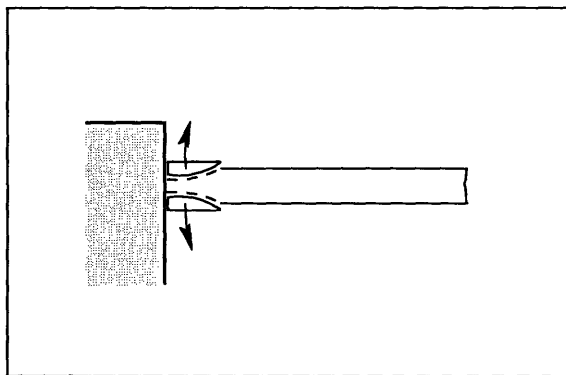
(b)



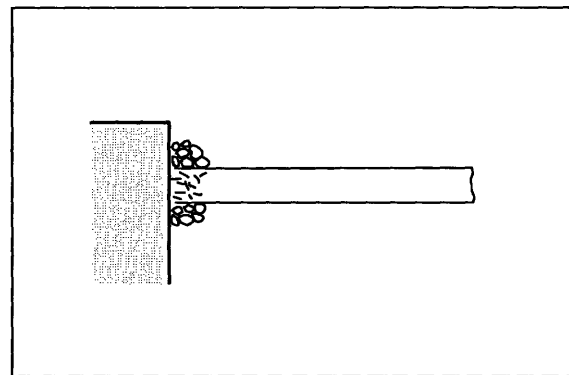
(c)



(d)



(e)



(f)

Figure 2-4: Schematic of principal failure mechanisms: (a) creep; (b) radial cracking; (c) buckling; (d) circumferential cracking; (e) spalling; and (f) crushing (Sanderson, 1988).

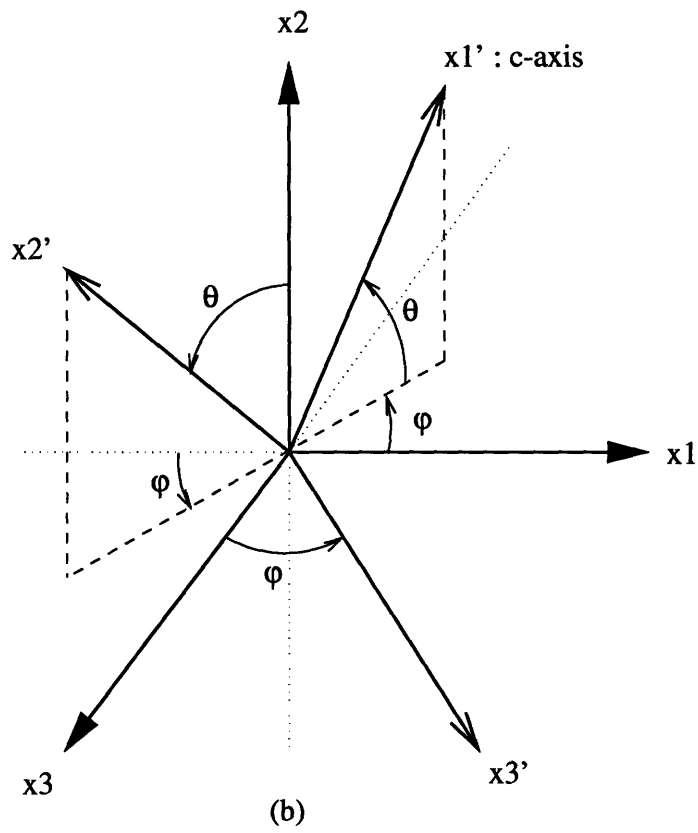
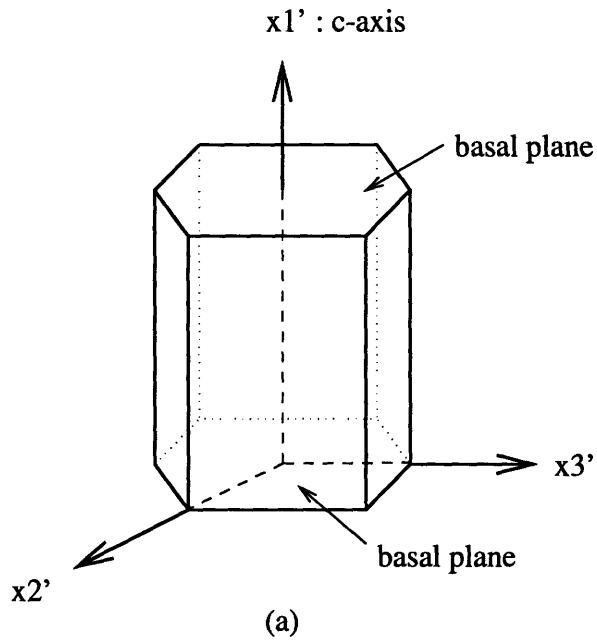


Figure 2-5: (a) Local frame of single crystal ice; (b) Reference global frame $(x_1-x_2-x_3)$ and local frame $(x_1'-x_2'-x_3')$.

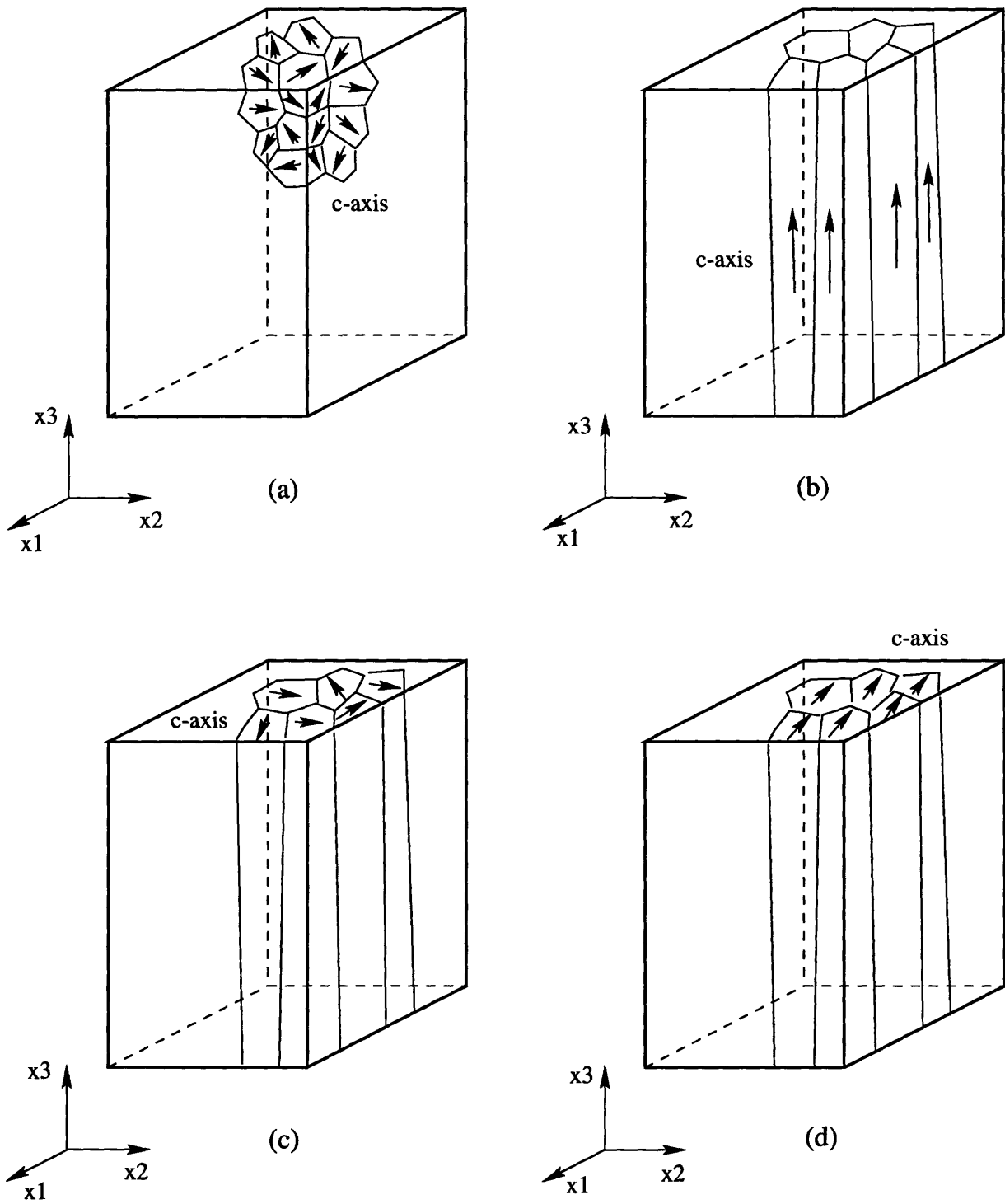


Figure 2-6: Schematic of polycrystalline ice types: (a) equiaxed-granular ice; (b) columnar-grained S-1 ice; (c) columnar-grained S-2 ice; and (d) columnar-grained S-3 ice.

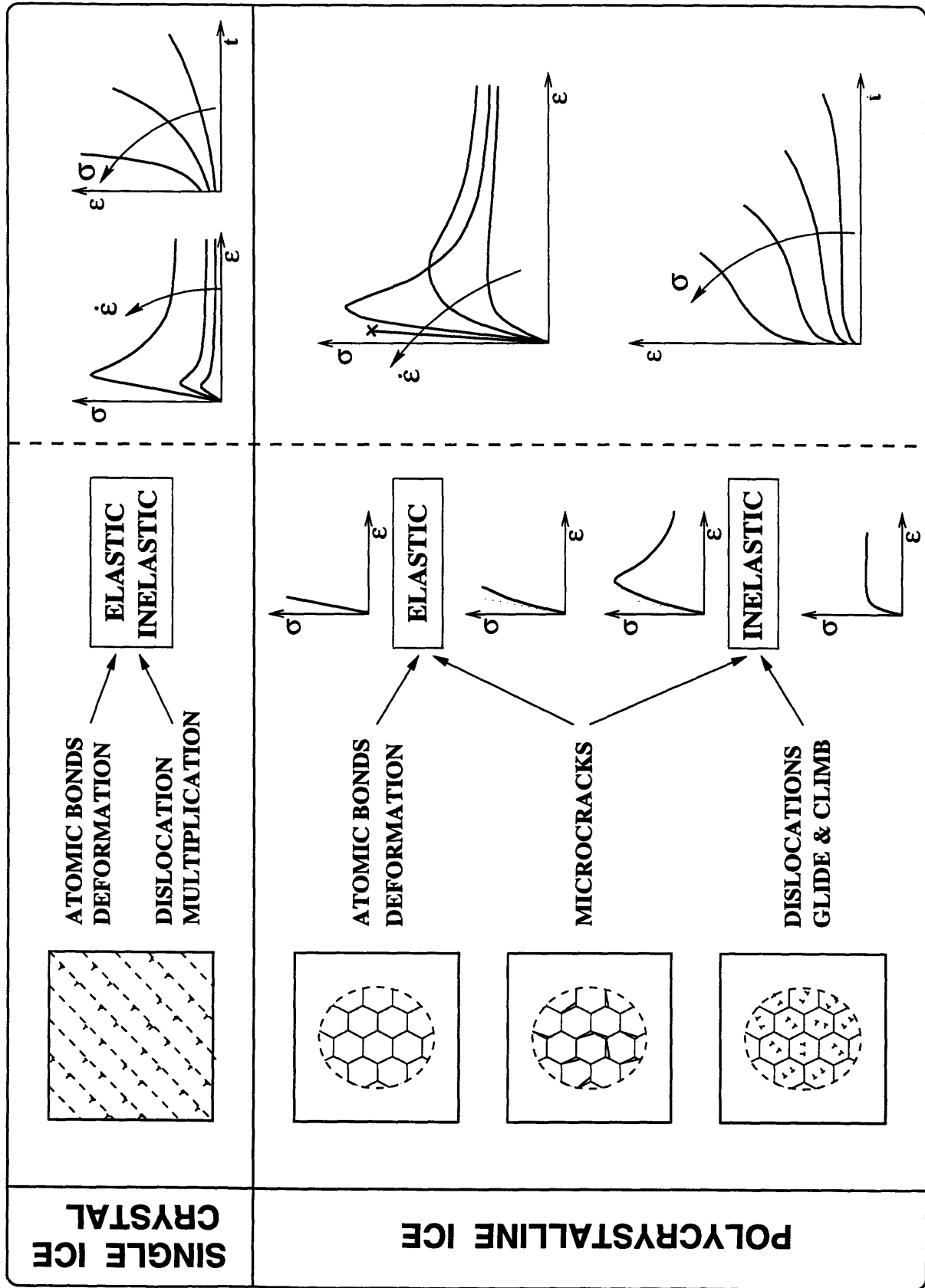


Figure 2-7: Behaviors of single ice crystal and polycrystalline ice.

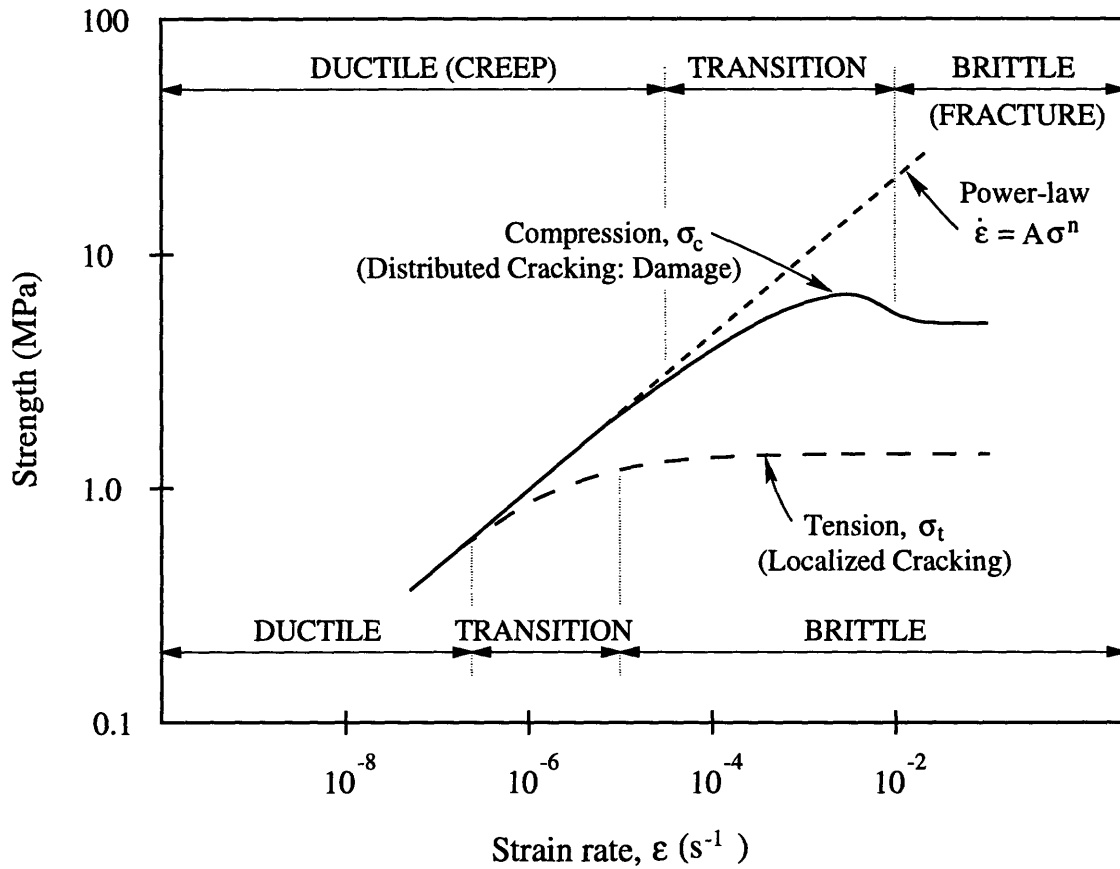


Figure 2-8: Deformation mode map showing regions of purely ductile and purely brittle behavior as well as the ductile-to-brittle transition in both compression and tension (Wu, 1990).

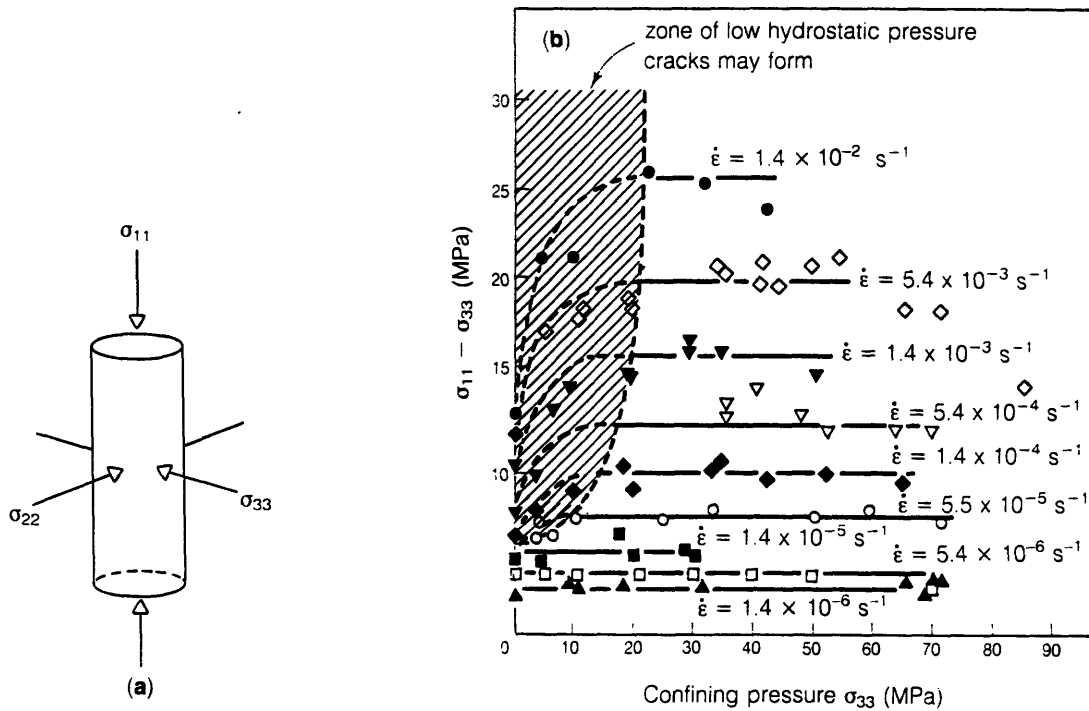


Figure 2-9: Multiaxial tests. (a) Geometry: under most test conditions, both axial stress and confining pressure is compressive. (b) Plots of stress difference, axial stress minus confining pressure, at various axial strain rates as a function of confining pressure. Microcracking occurs in the shaded zone, but outside it, creep behavior is independent of confining pressure (data of Jones (1982); figures from Jordaan (1986) and Sanderson (1988)).

Chapter 3

A CONSTITUTIVE CREEP MODEL FOR SINGLE CRYSTAL ICE

Abstract

A constitutive creep model for single crystal ice has been formulated based on the experimental results and the mechanism of the multiplication process of mobile dislocations. In this model, the primary mechanism is considered to be the dislocation motion on the basal planes of single crystal ice due to strong creep anisotropy. The preferred crystallographic orientation and temperature of single crystal ice are incorporated in describing both the elastic and the inelastic deformations in the creep model. Material properties used in the model are the dislocation velocity and the changing dislocation density of single crystal ice based on experimental data. The proposed uniaxial creep model is extended to a biaxial model by allowing inelastic deformation only along the basal planes. Parametric studies are performed to better understand the dependence of macroscopic stress-strain curves on microstructural parameters. The results show strong influence of the loading rate and stress level. Comparison of the model predictions with experimental data shows excellent agreement over a range of strain rates.

3.1 Introduction

The inelastic deformation of polycrystalline ice is highly non-linear and depends on the loading rate and temperature, as well as on the granular microstructure. Since polycrystalline ice is made up of individual single ice crystals, the behavior is affected by the properties of individual crystals. However, differences in response between single crystal ice and polycrystalline ice are reported (Weertman, 1973; Hobbs, 1974; Duval et al., 1983). These differences may be due to certain processes such as intergranular effects (e.g., sliding and interlocking of grain boundaries), the distribution of crystallographic orientation of individual single crystals, alterations of dislocation densities within grains, and damage accumulation due to microcracking. In order to establish better understanding of the behavior of polycrystalline ice, this paper studies the effect of dislocation densities within crystals on the macroscopic stress-strain response for single crystal ice.

Many papers concerned with the mechanical properties of single crystals of pure and sea ice have been published (e.g., Steinemann, 1954; Griggs and Coles, 1954; Readey and Kingery, 1964; Higashi et al., 1964; Higashi, 1968; Jones and Glen, 1969; Doyon and Michel, 1991; Brown and Kawamura, 1991; Hu et al., 1996). These studies show experimental results of the inelastic behavior for various levels of constant strain rate, constant stress, and temperature. Typical stress-strain curves of single crystal ice oriented for basal glide and subjected to constant strain rates are shown in Figure 3-1; the stress rises to an upper yield point with increasing strain and then decreases to a constant lower yield point.

The occurrence of upper and lower yield points is exhibited by materials such as LiF, Ge and Si. An explanation for this phenomenon was first provided by Johnston (1962), and discussed later in the review article by Alexander and Haasen (1968). The underlying mechanism is designated as the multiplication process of mobile dislocations, and is attributed to two factors: (i) an increase in the mobile dislocation density with deformation and (ii) the dependence of the average dislocation velocity on stress. Based on observations of the yield behavior of single crystal ice oriented for basal glide and subjected to a constant strain rate, a mathematical description for the multiplication process has been attempted by Higashi (1968), Jones and Glen (1969), and Michel (1978). However, their models describe the behavior of single crystal ice only for particular loading conditions such as a constant strain rate at a given temperature.

In the present study, we develop a more comprehensive formulation for the inelastic deformation of single crystal ice under various loading conditions and temperatures. Material properties used in the proposed model are measurable microstructural parameters such as the dislocation velocity and the changing dislocation density of single crystal ice. This model accounts for rate- and temperature-dependence and for the dependence on basal plane orientation relative to the applied loading direction. The extension of the uniaxial model to a biaxial model is achieved by considering the hexagonal anisotropy of ice crystal structure. The model developed in this study can be used to analyze the complex deformation of polycrystalline ice, e.g., finite element simulation of non-homogeneous, inelastic deformation in polycrystalline ice modeled as a collection of individual single crystals with different basal plane orientations.

The organization of this paper is as follows. In Section 3-2, the formulation of a constitutive creep model for uniaxial behavior of single crystal ice is described based on the experimental observations and modified multiplication process of mobile dislocations. The model is also extended to the biaxial case. Section 3-3 contains the results of parametric studies performed to establish a better understanding of the dependence of macroscopic stress-strain curves on microstructural parameters. In addition, predicted stress-strain curves based on a particular set of parameter values are compared with available experimental data. Lastly, conclusions are discussed in Section 3-4.

3.2 Constitutive Model of Single Crystal Ice

We consider a columnar-grained ice for which the c-axis orientation of the individual single crystals is randomly distributed in the plane normal to the axis of the column. Michel and Ramseier (1971) classified this ice as S2 ice. Figure 3-2 illustrates the structure of S2 ice for the case where the column axis coincides with the x_3 direction. The c-axis lies in the x_1 - x_2 plane, and the ice is considered to be isotropic in this plane. As previously discussed, the mechanical properties of polycrystalline ice are affected by the constituent single crystals. These constituent single crystals exhibit high rate- and temperature-dependence and strong dependence of basal plane orientation to the applied loading. In this section, a mathematical formulation of the inelastic deformation of single crystal ice is presented based on the

experimental observations and modified multiplication theory of mobile dislocations. The proposed uniaxial creep model is further extended to the biaxial case.

The multiplication process of mobile dislocations in a single crystal ice involves the following stages. In the initial unloaded state, the density of mobile dislocations is low. When a constant strain rate is imposed, in the initial loading stage where the change of dislocation density is small, the stress rises linearly at small strains. As strain increases, the inelastic strain becomes dominant, resulting from more dislocations created. As a result, their average velocity decreases. The stress, which is related to the dislocation velocity and is required to maintain a constant strain rate, decreases after the yield point where the dislocation multiplication is most intense. When a sufficient number of mobile dislocations are present, the decreasing stress due to increasing dislocation density is balanced by work hardening, and the stress remains essentially constant as the strain is increased further.

For a single crystal ice without microcracks, inelastic deformation is primarily due to the motion of dislocations through the crystal. The direct observation of dislocation motion on the basal and non-basal planes, such as the prismatic and pyramidal planes, is made by the etch pit method (Muguruma and Higashi, 1963; Sinha, 1978; Wei and Dempsey, 1994), by X-ray diffraction topographs (Fukuda and Higashi, 1973), and synchrotron X-ray topography (Ahmad and Whitworth, 1988; Shearwood and Whitworth, 1991). Experimental observations of dislocations (Higashi, 1968; Fukuda and Higashi, 1973) show that single crystal ice deforms primarily by easy glide in the basal planes, even though the motion of dislocations is observed also on the non-basal planes. This behavior is known as strong creep anisotropy and is explained by the fact that the shear resistance to slip on the non-basal planes is almost 60 times higher than that on the basal plane (Duval et al., 1983).

The stress-strain curves for single crystal ice oriented for basal glide show the large yield drop without visible microcracks, and the amount of the drop increases with increasing strain rate and with decreasing temperature. To simulate this phenomenon, we focus our attention on the dislocation motion on the basal plane.

3.2.1 Uniaxial Model

Consider single crystal ice with the preferred c-axis orientation for dislocation motion as shown in Fig. 3-3. The shear stress τ on the basal plane due to the applied stress σ can be written in terms of a function of χ , the angle between the applied stress and the c-axis orientation,

$$\tau = \sigma S \quad (3.1)$$

where the Schmid's orientation factor, S , is defined as $S = \sin \chi \cos \chi$. The kinetic law of dislocation glide is expressed with Orowan's equation (Orowan, 1940)

$$\dot{\gamma}^c = b\rho\nu \quad (3.2)$$

where $\dot{\gamma}^c$ is the inelastic shear strain rate, b is the magnitude of Burgers vector, ρ is the average density of mobile dislocations, and ν is the average velocity of dislocations.

It has been suggested by Johnston and Gilman (1959) and Johnston (1962) that the dislocation velocity in LiF is a function of stress and temperature. In a study of plastic deformation of Si and Ge single crystals, Patel and Chaudhuri (1966) measured the stress and temperature dependence of dislocation velocity. Fukuda and Higashi (1973) measured with X-ray diffraction topographs the velocity of individual dislocations in single crystal ice subjected to various stresses. The velocities of both the basal and non-basal dislocations have been found to depend on stress and temperature (Ahmad and Whitworth, 1988; Shearwood and Whitworth, 1991). These experimental studies suggest that the dislocation velocity on the basal plane is described by a combination of the Arrhenius exponential function for temperature and a power law for stress:

$$\nu = \nu_o \exp\left(-\frac{Q}{RT}\right) \left(\frac{\tau_{eff}}{\sigma_o}\right)^{n1} \quad (3.3)$$

where ν_o is a pre-exponential constant with dimensions of velocity, Q is the activation energy, R is the universal gas constant, T is the absolute temperature in degrees Kelvin, $n1$ is the stress exponent, σ_o is the reference flow stress, and τ_{eff} is the effective shear stress defined as the difference between the shear stress τ and the internal back stress τ_i . It is noted that the internal back stress on the basal planes opposing glide due to lattice friction is negligible, since the flow stress for slip on the basal planes of an ice crystals is very low and dislocations

on the basal planes can move at shear stresses lower than 0.01 *MPa* (Duval et al., 1991; Wei and Dempsey, 1994).

It is difficult to determine directly the relationship between ρ and γ^c from experiments. Dislocation multiplication occurs if the stress on a dislocation along a glide plane exceeds the Orowan stress given by various scholars (e.g., Ashby, 1969):

$$\tau_o = \frac{2\mu b}{\lambda} \quad (3.4)$$

where μ is the shear modulus and λ is an internal length-scale. As Johnston and Gilman (1959) observed that dislocation multiplication rate increases with the mean dislocation velocity, the rate of production of dislocations is expressed by, among others, Gittus (1975); Amodeo and Ghoniem (1990):

$$\dot{\rho} = \frac{\rho v}{\lambda}. \quad (3.5)$$

Substituting Eq. (3.5) into Eq. (3.2) results in a linear dependence of ρ on γ^c . The linear relationship between the dislocation density and the inelastic strain has been considered in LiF single crystals (Johnston, 1962) and in ice single crystals (Highasi, 1968; Jones and Glen, 1969; Michel, 1978). For constant stress tests on Ge, Berner and Alexander (1967) showed that the dislocation density increases with inelastic strain and applied stress. No direct measurement on ice single crystals has been published yet concerning the dependence of the dislocation density on inelastic strain and applied stress. In this study, the following relation based on the multiplication process of mobile dislocations is assumed for the average dislocation density

$$\rho = \{\rho_o + \alpha(\gamma^c)^m\} \left(\frac{\tau}{\sigma_o}\right)^{n2} \quad (3.6)$$

where ρ_o is the initial dislocation density, α is the rate of dislocation multiplication that may be highly dependent on temperature, m is the inelastic strain exponent, and $n2$ is the stress exponent.

Substitution of Eqs (3.3) and (3.6) into Eq. (3.2) results in

$$\dot{\gamma}^c = H \{\rho_o + \alpha(\gamma^c)^m\} \left(\frac{\tau}{\sigma_o}\right)^n \quad (3.7)$$

where $n = (n1 + n2)$ is the stress exponent and H is defined as

$$H = b\nu_o \exp\left(-\frac{Q}{RT}\right). \quad (3.8)$$

Using Eqs (3.1) and (3.7), the transformation of the inelastic shear strain rate on the basal plane to the global axis parallel to the loading direction leads to

$$\dot{\epsilon}^c = \dot{\gamma}^c S = H \left\{ \rho_o + \alpha \left(\frac{\epsilon^c}{S} \right)^m \right\} S^{n+1} \left(\frac{\sigma}{\sigma_o} \right)^n. \quad (3.9)$$

If the elastic deformation of the ice crystal is included, the uniaxial elastic strain rate may be written as

$$\dot{\epsilon}^e = \frac{\dot{\sigma}}{E} \quad (3.10)$$

where Young's modulus E is equal to $1/S_{g,22}$, and \mathbf{S}_g is the elastic compliance matrix of single crystal ice referred to the global frame (see Appendix A). Combining the elastic and inelastic strain rates, the total strain rate is written as

$$\dot{\epsilon} = \dot{\epsilon}^e + \dot{\epsilon}^c = \frac{\dot{\sigma}}{E} + H \left\{ \rho_o + \alpha \left(\frac{\epsilon^c}{S} \right)^m \right\} S^{n+1} \left(\frac{\sigma}{\sigma_o} \right)^n. \quad (3.11)$$

The expression for the time rate of change of stress, $\dot{\sigma}$, is obtained from Eq. (3.11), and has the form

$$\dot{\sigma} = E \left[\dot{\epsilon} - H \left\{ \rho_o + \alpha \left(\frac{\epsilon^c}{S} \right)^m \right\} S^{n+1} \left(\frac{\sigma}{\sigma_o} \right)^n \right]. \quad (3.12)$$

3.2.2 Biaxial Model

The multi-axial macroscopic deformation of polycrystalline solids can be presented in terms of glide rates on all active slip systems, as has been established by many authors (e.g., Kocks, 1970; Hutchinson, 1970; Nemat-Nasser and Hori, 1987; deBotton and Ponte Castañeda, 1995). The plastic deformation of polycrystalline ice involves an interaction between slip systems such as basal and non-basal deformations; the rate of plastic deformation is controlled by non-basal systems (Duval et al., 1983; Wei and Dempsey, 1994; Liu et al., 1993). Therefore, all slip systems need to be considered in order to describe polycrystalline ice behavior. The aim of this paper, however, is to describe the deformation of single crystal ice oriented for basal glide that deforms primarily by the glide in the basal planes. Even if

the non-basal deformation is included in a biaxial model, the contribution from non-basal deformation would be minimal due to strong creep anisotropy which causes easy glide on the basal plane.

We consider single crystal ice with the preferred orientation of basal planes under biaxial stresses located in the global frame (x1-x2). The angle between a c-axis and the global x1-direction is denoted by θ as shown in Fig. 3-4. The following contracted Voigt notation is used instead of tensor notation, and the vector form of the strain and stress components is written respectively as $\boldsymbol{\epsilon} = [\epsilon_{11} \ \epsilon_{22} \ \epsilon_{12}]^T$ and $\boldsymbol{\sigma} = [\sigma_{11} \ \sigma_{22} \ \sigma_{12}]^T$, where superscript T denotes the transpose operation.

The total strain rate vector is given by

$$\dot{\boldsymbol{\epsilon}} = \dot{\boldsymbol{\epsilon}}^e + \dot{\boldsymbol{\epsilon}}^c \quad (3.13)$$

where $\dot{\boldsymbol{\epsilon}}^e$ and $\dot{\boldsymbol{\epsilon}}^c$ are the elastic and inelastic strain rate vectors of single crystal ice, respectively. The elastic strain rate vector is written as

$$\dot{\boldsymbol{\epsilon}}^e = \mathbf{S}_g \dot{\boldsymbol{\sigma}} \quad (3.14)$$

where \mathbf{S}_g is the compliance matrix of single crystal ice (see Appendix A) and $\dot{\boldsymbol{\sigma}}$ is the stress rate vector in the global frame.

The stress transformation law expressed in matrix notation has the form

$$\boldsymbol{\sigma}' = \mathbf{T} \boldsymbol{\sigma} \quad (3.15)$$

where $\boldsymbol{\sigma}'$ is the stress vector in the local frame (x1'-x2'), and \mathbf{T} is a 2-dimensional transformation matrix,

$$\mathbf{T} = \begin{bmatrix} c^2 & s^2 & 2cs \\ s^2 & c^2 & -2cs \\ -cs & cs & c^2 - s^2 \end{bmatrix} \quad (3.16)$$

and $c = \cos \theta$ and $s = \sin \theta$. Substituting Eq. (3.16) into Eq. (3.15) results in

$$\begin{Bmatrix} \sigma'_{11} \\ \sigma'_{22} \\ \sigma'_{12} \end{Bmatrix} = \begin{bmatrix} c^2 \sigma_{11} + s^2 \sigma_{22} + 2cs \sigma_{12} \\ s^2 \sigma_{11} + c^2 \sigma_{22} - 2cs \sigma_{12} \\ -cs \sigma_{11} + cs \sigma_{22} + (c^2 - s^2) \sigma_{12} \end{bmatrix}. \quad (3.17)$$

Since dislocation movement is allowed only along the basal planes in this model, the basal shear stress component σ'_{12} is solely responsible for the inelastic strain. Using Eq. (3.3), the dislocation velocity on the basal plane can be written as

$$\nu = \nu_o \exp\left(-\frac{Q}{RT}\right) \left|\frac{\sigma'_{12}}{\sigma_o}\right|^{n1} \quad (3.18)$$

where $|\sigma'_{12}|$ denotes the absolute value of σ'_{12} . Also, using Eq. (3.6), the average density of mobile dislocations is given by

$$\rho = \left\{ \rho_o + \alpha |\dot{\gamma}'_{12}|^m \right\} \left|\frac{\sigma'_{12}}{\sigma_o}\right|^{n2} \quad (3.19)$$

where $\dot{\gamma}'_{12}$ is the inelastic shear strain in the basal plane. We use the absolute values for $\dot{\gamma}'_{12}$ and σ'_{12} in Eq. (3.19) in order to eliminate the influence of the direction of the slip on the generation of mobile dislocation density. The basal shear strain rate $\dot{\gamma}'_{12}$ due to σ'_{12} is obtained by combining Eqs (3.2), (3.18) and (3.19)

$$\dot{\gamma}'_{12} = 2\dot{\epsilon}'_{12} = H \left\{ \rho_o + \alpha |\dot{\gamma}'_{12}|^m \right\} \left|\frac{\sigma'_{12}}{\sigma_o}\right|^n \text{sgn}(\sigma'_{12}). \quad (3.20)$$

The sense of the strain rate is determined by the sign of σ'_{12} . The other components of inelastic strain rate vector due to σ'_{12} are zero ($\dot{\epsilon}'_{11} = \dot{\epsilon}'_{22} = 0$).

The inelastic strain rate vector in the global directions (x1-x2) is determined with the following transformation law

$$\dot{\epsilon}^c = \mathbf{T}(-\theta) \dot{\epsilon}'^c. \quad (3.21)$$

Expanding Eq. (3.21) leads to

$$\begin{pmatrix} \dot{\epsilon}_{11}^c \\ \dot{\epsilon}_{22}^c \\ \dot{\epsilon}_{12}^c \end{pmatrix} = \begin{pmatrix} -2cs \dot{\epsilon}_{12}^c \\ 2cs \dot{\epsilon}_{12}^c \\ (c^2 - s^2) \dot{\epsilon}_{12}^c \end{pmatrix}. \quad (3.22)$$

Noting Eqs (3.17) and (3.20), one can write Eq. (3.22) as

$$\begin{pmatrix} \dot{\epsilon}_{11}^c \\ \dot{\epsilon}_{22}^c \\ \dot{\epsilon}_{12}^c \end{pmatrix} = H \begin{pmatrix} -cs \left\{ \rho_o + \alpha \left| \frac{\epsilon_{11}^c}{-cs} \right|^m \right\} \\ cs \left\{ \rho_o + \alpha \left| \frac{\epsilon_{22}^c}{cs} \right|^m \right\} \\ \frac{1}{2}(c^2 - s^2) \left\{ \rho_o + \alpha \left| \frac{2\epsilon_{12}^c}{c^2 - s^2} \right|^m \right\} \end{pmatrix} \left| \frac{\sigma'_{12}}{\sigma_o} \right|^n \text{sgn}(\sigma'_{12}) \quad (3.23)$$

where

$$\sigma'_{12} = -cs \sigma_{11} + cs \sigma_{22} + (c^2 - s^2) \sigma_{12}. \quad (3.24)$$

To verify Eq. (3.23), two special loading conditions are considered. Firstly, when single crystal ice with arbitrary angle θ is subjected to a compressive stress σ_{22} only, the inelastic strain rate component in the x2-direction is obtained from Eq. (3.23) as

$$\dot{\epsilon}_{22}^c = -H \left\{ \rho_o + \alpha \left| \frac{\epsilon_{22}^c}{cs} \right|^m \right\} cs \left| \frac{cs \sigma_{22}}{\sigma_o} \right|^n \quad (3.25)$$

which is the same as Eq. (3.9). The minus sign denotes the compressive state. Secondly, when single crystal ice with $\theta = 90^\circ$ ($c = 0, s = 1$) is subjected to a shear stress σ_{12} only, the inelastic shear strain rate component is obtained as

$$\dot{\gamma}_{12}^c = 2\dot{\epsilon}_{12}^c = H \left\{ \rho_o + \alpha \left| \frac{\gamma_{12}^c}{2} \right|^m \right\} \left| \frac{\sigma_{12}}{\sigma_o} \right|^n \quad (3.26)$$

and the normal strain components are zero ($\dot{\epsilon}_{11}^c = \dot{\epsilon}_{22}^c = 0$).

3.3 Model Predictions

3.3.1 Model Parameters

The parameters used in the proposed model may be estimated from experimental measurements (Fukuda and Higashi, 1973; Jones and Glen, 1969). The measured activation energy for easy glide on the basal plane lies between about 39 and 68 kJ/mol depending on temperature (Readey and Kingery, 1964; Jones and Glen, 1969) and impurities (Nakamura and Jones, 1973). The fact that the activation energy for creep in ice is similar to those for dielectric relaxation and self-diffusion in ice suggests that the velocity of dislocations is controlled by the diffusive motion of hydrogen atoms and the movement of Bjerrum defects (Hobbs, 1974). In this study, 63 kJ/mol ($=0.65 \text{ eV}$) is used for the activation energy. The value of the universal gas constant R is equal to $8.314 \text{ J mol}^{-1}\text{K}^{-1}$. The magnitude of Burgers vector was calculated by Hondoh and Higashi (1983) in the course of considering grain boundary dislocations in bicrystals of ice. Here, we use $b = 0.6a$, where a is the lattice parameter of ice. At -10°C , $a = 4.52 \times 10^{-10} \text{ m}$ so that $b = 2.71 \times 10^{-10} \text{ m}$.

In Glen's power law relationship between the applied stress and the minimum strain rate, the value of the stress exponent varies with both stress and temperature, ranging from 1.3 to 4.0 for single crystal ice (Jones and Glen, 1969; Nakamura and Jones, 1973; Hobbs, 1974; Nakamura, 1978) and from 2.5 to 4.2 for polycrystalline ice (see e.g., Kamb, 1961; Weertman, 1973). Duval et al. (1983) collected data for basal glide in single crystals of ice at -10°C , and showed that the stress exponent n is close to 2.

The responses of single crystal ice, as in polycrystalline ice, show considerable scatter even under the same loading conditions, such as the same temperature and loading rate. This scatter increases if ice specimens are made by different researchers. The authors believe that the scatter comes from different microstructure and impurity contents, which highly depend on experimental procedures. Parametric studies on the stress exponent n , the initial dislocation density ρ_0 , the rate of dislocation multiplication α , and the inelastic strain exponent m , Young's modulus E , the c -axis orientation θ , and temperature T are performed in the following section to establish the influence of these parameters on the macroscopic stress-strain curves, since some of these parameters vary with ice and are difficult to de-

termine accurately by experiments. This simulation is performed at $T = -10^{\circ}C$. Unless otherwise noted, the chosen values for the parameters are: $b = 2.71 \times 10^{-10} \text{ m}$; $\nu_o = 2.17 \times 10^7 \text{ m s}^{-1}$; $Q = 63 \text{ kJ/mol}$; $E = 8500 \text{ MPa}$; $\sigma_o = 1 \text{ MPa}$; $\theta = 45^{\circ}$; $n = 2$; $m = 2/3$; $\rho_o = 3.2 \times 10^{10} \text{ m}^{-2}$; $\alpha = 4.1 \times 10^{12} \text{ m}^{-2}$.

The stress-time history corresponding to a specified applied strain rate is generated by numerically integrating Eq. (3.12) using the fourth-order Runge-Kutta algorithm for the first four time steps and the Adams-Moulton algorithm for the remaining time steps.

3.3.2 Parametric Studies

Effect of the stress exponent, n

The calculated stress-strain curves are shown in Fig 3-5 for the values of the stress exponent $n = 1.5, 2.0, 2.5,$ and 3.0 for an applied strain rate of $5 \times 10^{-4} \text{ s}^{-1}$. The fact that the stress-strain curves for the basal glide in single crystal ice showed the large yield drop was explained by the theory for a no work-hardening material, which has small value of the exponent n of stress dependence of the strain rate. The amount of yield drop associated with the dislocation multiplication varies significantly with the stress exponent. The results show that the smaller the stress exponent, the larger the yield drop.

Effect of the initial dislocation density, ρ_o

The single crystal ice has the initial mobile dislocations on the basal planes. Even though observations are made using various methods (etch pits, X-ray diffraction topographs and synchrotron X-ray topography), it is difficult to determine accurately the initial dislocation density. The estimated initial dislocation densities were 10^7 m^{-2} in LiF (Johnston, 1962), $5.0 \times 10^9 \text{ m}^{-2}$ (Jones and Glen, 1969) and $9.5 \times 10^{10} \text{ m}^{-2}$ (Doyon and Michel, 1991) in their single crystals of ice. To see the effect of the initial dislocation density, the stress-strain curves under an applied strain rate of $5 \times 10^{-4} \text{ s}^{-1}$ are shown in Fig. 3-6 for various initial dislocation density from $\rho_o = 5 \times 10^8$ to $\rho_o = 5 \times 10^{11} \text{ m}^{-2}$. The results show that a smaller value of the initial dislocation density results in higher yield stress and larger yield drop.

Effect of the rate of dislocation multiplication, α

The density of mobile dislocations on the basal planes increases as the inelastic strain increases. Johnston (1962) determined $\alpha = 10^{13} m^{-2}$ from experimental results on LiF. However, direct measurement of the change of dislocation density is not made in single crystal ice. To see the effect of the rate of dislocation multiplication, the calculated stress-strain curves under an applied strain rate of $5 \times 10^{-4} s^{-1}$ are shown in Fig. 3-7 for the values of $\alpha = 1 \times 10^{12}, 5 \times 10^{12}, 1 \times 10^{13},$ and $5 \times 10^{13} m^{-2}$. As the rate of dislocation multiplication is smaller, the transition from the upper yield point to a plateau is slower.

Effect of the inelastic strain exponent, m

The calculated stress-strain curves are shown in Fig. 3-8 for the values of $m = 1.0, 3/4, 2/3,$ and $1/2$ for an applied strain rate of $5 \times 10^{-4} s^{-1}$. This value governs the shape of the change of the dislocation density with increasing inelastic strain. The figure shows that the plateau after the upper yield occurs at the smaller strains with smaller values of the exponent m .

Effect of Young's modulus, E

The effects of Young's modulus are shown in Fig. 3-9. The Young's modulus is varied from $E = 9500 MPa$ to $3500 MPa$ for an applied strain rate of $5 \times 10^{-4} s^{-1}$. This simulation shows that Young's modulus has affected the initial slope of the stress-strain curves, but has little effect on the overall stress-strain curves.

Effect of the c-axis orientation, θ

The calculated stress-strain curves are shown in Fig. 3-10 for the values of $\theta = 30^\circ, 35^\circ, 40^\circ, 45^\circ$ for an applied strain rate of $5 \times 10^{-4} s^{-1}$. This calculated results show that as the c-axis orientation is close to 45° , the lower stress is obtained. It is noteworthy that the responses are equal for $\theta = 30^\circ$ and $60^\circ, \theta = 35^\circ$ and $55^\circ,$ and $\theta = 40^\circ$ and 50° .

Effect of temperature, T

Figure 3-11 shows the effects of temperature. The ice temperature varies from $T = -5^\circ C$

to -20°C for an applied strain rate of $5 \times 10^{-4} \text{ s}^{-1}$. Both the upper and lower yield stresses increase with decreasing temperature.

3.3.3 Model Comparison with Experimental Data

Weertman (1973) presented the results of Ramseier (1972) in the form of compressive stress-strain curves of single crystal ice at -10°C and various strain rates. The specimen axis makes an angle of 45° with the c-axis of the crystal. Figure 3-12 compares the responses of the current model with the experiments of single crystal ice (Ramseier, 1972). For the best fit, the following parameter set is chosen:

$$b = 2.71 \times 10^{-10} \text{ m}; \quad \nu_o = 2.17 \times 10^7 \text{ m s}^{-1}; \quad Q = 63 \text{ kJ/mol};$$

$$E = 4500 \text{ MPa}; \quad \sigma_o = 1 \text{ MPa}; \quad \theta = 45^{\circ};$$

$$n = 2; \quad m = 2/3; \quad \rho_o = 3.2 \times 10^{10} \text{ m}^{-2}; \quad \alpha = 4.1 \times 10^{12} \text{ m}^{-2}.$$

Considering the existence of scatter in natural materials like ice, the comparison between the model prediction and the data shows very good agreement for the range of the applied strain rates. It is noted, however, that 4500 MPa is used for the apparent Young's modulus instead of the dynamic Young's modulus (close to 8500 MPa), to fit better the initial slope of the stress-strain curves of data.

Higashi et al. (1964) reported experimental results on the stress-strain relations of single ice crystals. One of the characteristic features of the curves is that the slope of the initial linear portion is a function of strain rate as well as temperature. This is quite unique since the stress-strain curves of LiF and Ge also show the same large yield drop, and indicate little dependence of the initial slopes of these curves on the applied strain rate. In polycrystalline ice, the rate-dependence of the apparent Young's modulus has been attributed to relative movement between grains in the grain boundary region (Gold, 1977). Traetteberg et al. (1975) showed that the time-dependent elastic modulus and the initial response of ice could be described by the time-dependence of the relaxation time and by anelastic theory (Nowick and Berry, 1972). This phenomenon in single crystal ice may be attributed to an anelastic relaxation process, possibly involving some thermally activated rearrangement of dislocations.

The dependence of the initial slope on strain rate suggests that anelastic relaxation may be considered, in addition to plastic deformation due to dislocation multiplication. Anelastic relaxation has been discussed by Schoeck (1956) and Eshelby (1961) for viscoelastic materials, and by Weertman (1963), Higashi et al. (1964), and Hu et al. (1996) for ice crystals. No constitutive theory exists yet to describe both anelastic relaxation and plastic deformation. In this study, the anelastic relaxation is taken into account by using an apparent Young's modulus. This choice affects the initial slope of the stress-strain curve but has little effect on the overall stress-strain curve.

Figure 3-13 shows the corresponding calculated dislocation densities for various strain rates with $n_2 = 1$ in Eq. (3.6). This result shows that the multiplication process of mobile dislocations is enhanced with increasing strain rate. The trends and calculated values of the dislocation densities are reasonable when compared with the data.

In Fig. 3-14, the strain response under constant stresses of 1 *MPa* and 0.455 *MPa* at -10°C is plotted against the data of Griggs and Coles (1954). Good correspondence is achieved between the model prediction and the data. The corresponding calculated dislocation densities for constant stresses are shown in Fig. 3-15. This result shows that the change of dislocation densities significantly depends on the stress levels. In constant stress tests on Ge, Berner and Alexander (1967) have shown that the dislocation density reached for any given strain depends greatly on the applied stress: the larger the applied stress, the higher the dislocation multiplication.

3.4 Conclusions

A constitutive creep model for single crystal ice has been formulated based on experimental results and the mechanism of the multiplication process of mobile dislocations. The model predictions are in good agreement with available experimental data of single crystal ice, which is highly sensitive to changes in strain rate, stress, and temperature.

Based on the assumption that the dislocation motion on the basal plane is the dominant mechanism for single crystal ice due to strong creep anisotropy, this work studies the effect of dislocation densities within crystals on the macroscopic response. Material properties used

in the proposed model were the dislocation velocity and the changing dislocation density of single crystal ice based on experimental data. The model incorporates crystallographic basal orientation of single crystal ice and temperature. The uniaxial creep model was extended to biaxial loading. Parametric studies were performed to establish better understanding of the dependence of macroscopic stress-strain curves on microstructural parameters. The model results show strong dependence on the loading rate and stress level. The predicted stress-strain curve for the applied strain rate shows an upper and lower yielding. The strain-time response under constant applied stress exhibits softening behavior.

The constitutive relations developed in this study provide an essential starting point for analyzing the complex deformation of polycrystalline ice. In this case, other aspects, such as interactions of slip systems, intergranular effects and damage accumulation due to microcracking, need to be incorporated in order to obtain a robust numerical capability.

Appendix A

Elastic Constants of Single Crystal Ice

Gammon et al. (1983) have determined the dynamic elastic constants of single crystal ice at $T = -16^\circ\text{C}$ using the method of Brillouin spectroscopy. The complete six-by-six compliance matrix of single crystal ice in the local frame is

$$\mathbf{S}'_g = \begin{bmatrix} 0.8441 & -0.2316 & -0.2316 & & & \\ & 1.0318 & -0.4287 & & 0 & \\ & & 1.0318 & & & \\ & & & 2.9210 & & \\ & \text{sym.} & & & 3.3179 & \\ & & & & & 3.3179 \end{bmatrix} 10^{-1} \text{ GPa}^{-1} \quad (\text{A1})$$

where the local frame $x_2'-x_3'$ is the plane of transverse isotropy; the c-axis lies along the x_1' direction ($\theta = 0^\circ$). It is noted that there are five independent constants due to the hexagonal crystal structure of ice.

The above elastic constants are mildly temperature-dependent. The following empirical relationship for the compliance matrix at temperature T was proposed by Gammon et al. (1983)

$$\mathbf{S}'_g(T) = \mathbf{S}'_g(T_o) \frac{1 - \delta T_o}{1 - \delta T} \quad (\text{A2})$$

where $\delta = 1.418 \times 10^{-3} \text{ }^\circ\text{C}^{-1}$, and $\mathbf{S}'_g(T_o)$ is the known compliance matrix at a specific temperature ($T_o = -16^\circ\text{C}$), and all temperatures are measured in $^\circ\text{C}$. It is noted that between 0°C and -20°C the variation in dynamic constants of single crystal ice is practically negligible.

Under plane strain conditions ($\epsilon_{33} = 0$) with x_1 - x_2 being the plane of interest, the complete six-by-six compliance matrix reduces to three-by-three matrix as (see Savin, 1961)

$$S'_{g,ij} = \left(S'_{g,ij} - \frac{S'_{g,i3} S'_{g,3j}}{S'_{g,33}} \right)_f \quad (\text{A3})$$

where $i, j = 1, 2, 6$ and the subscript f emphasize that the components of the complete

six-by-six matrix should be used. The plane strain compliance matrix using Eq. (A3) is given as

$$\mathbf{S}'_g(\theta = 0^\circ) = \begin{bmatrix} 0.7921 & -0.3278 & 0 \\ -0.3278 & 0.8537 & 0 \\ 0 & 0 & 3.3179 \end{bmatrix} 10^{-1} \text{ GPa}^{-1}. \quad (\text{A4})$$

Under plane stress conditions ($\sigma_{33} = 0$) with x1-x2 being the plane of interest, the complete six-by-six compliance matrix reduces to three-by-three matrix as

$$\mathbf{S}'_g(\theta = 0^\circ) = \begin{bmatrix} 0.8441 & -0.2316 & 0 \\ -0.2316 & 1.0318 & 0 \\ 0 & 0 & 3.3179 \end{bmatrix} 10^{-1} \text{ GPa}^{-1}. \quad (\text{A5})$$

The compliance matrix \mathbf{S}_g of single crystal ice in the global reference frame (x1-x2) is written as

$$\mathbf{S}_g = \mathbf{T}^T \mathbf{S}'_g \mathbf{T} \quad (\text{A6})$$

where \mathbf{S}'_g denotes the compliance matrix of single crystal ice in a local frame (x1'-x2') and the 2-dimensional transformation matrix \mathbf{T} is given in Eq. (3.16). Finally, the compliance matrices for plane strain and plane stress (e.g., the c-axis orientation of $\theta = 45^\circ$) are given respectively as

$$\mathbf{S}_g(\theta = 45^\circ) = \begin{bmatrix} 1.0770 & -0.5819 & 0 \\ -0.5819 & 1.0770 & 0 \\ 0 & 0 & 2.3014 \end{bmatrix} 10^{-1} \text{ GPa}^{-1} \quad (\text{A7})$$

and

$$\mathbf{S}_g(\theta = 45^\circ) = \begin{bmatrix} 1.1826 & -0.4763 & 0 \\ -0.4763 & 1.1826 & 0 \\ 0 & 0 & 2.3391 \end{bmatrix} 10^{-1} \text{ GPa}^{-1}. \quad (\text{A8})$$

The variation of the dynamic Young's modulus, $S_{g,22}^{-1}$, with orientation of c-axis is shown in Fig. 3-16. Results are plotted for both plane strain and plane stress.

References

- [1] Ahmad, S. and R. W. Whitworth (1988). Dislocation motion in ice: a study by synchrotron X-ray topography, *Philosophical Magazine A* 57, 749.
- [2] Alexander, H. and J. R. Haasen (1968). Dislocations and plastic flow in the diamond structure, *Solid State Physics* 22, pp. 27-158, F. Seitz, D. Turnbull, and H. Ehrenreich (Editors), Academic Press, New York.
- [3] Amodeo, R.J. and N.M. Ghoniem (1990). Dislocation dynamics I. A proposed methodology for deformation micromechanics, *Phys. Rev. B* 41, 6958.
- [4] Ashby, M.F. (1969). On the Orowan stress, *Physics of Strength and Plasticity*, A.S. Argon (Ed.), MIT Press, Cambridge, pp. 113-131.
- [5] Berner, K. and H. Alexander (1967). Dislocation density and local slip in germanium single crystals, (In German), *Acta Metall.* 15, 933.
- [6] Brown, R.L. and T. Kawamura (1991). A preliminary comparison of the properties of pure ice and sea ice single crystals, *Cold Regions Science and Technology* 19, 275.
- [7] deBotton, G. and P. Ponte Castañeda (1995). Variational estimates for the creep behaviour of polycrystals, *Proc. Roy. Soc. London A* 448, 121.
- [8] Doyon, B. and B. Michel (1991). Creep of mono- and bicrystals of ice, *The 11th Int. Conf. on Port and Ocean Eng. under Arctic Conditions*, Vol. 1, pp. 486-500, September 24-28, St. John's, Canada.
- [9] Duval, P., M.F. Ashby, and I. Anderman (1983). Rate-controlling processes in the creep of polycrystalline ice, *The Journal of Physical Chemistry* 87, 4066.
- [10] Duval, P., P. Kalifa, and J. Meyssonier (1991). Creep constitutive equations for polycrystalline ice and effect of microcracking, *Proc. IUTAM/IAHR Symp. on Ice-Structure Interaction*, Jones, S.J., McKenna, R.F., Tillotson, J. and Jordaan, I.J. (Ed.), Springer-Verlag, pp. 55-67.
- [11] Eshelby, J.D. (1961). Dislocations in visco-elastic materials, *Philosophical Magazine A* 6, 953.
- [12] Fukuda, A. and A. Higashi (1973). Dynamical behavior of dislocations in ice crystals, *Crystal Lattice Defects* 4, 203.
- [13] Gammon, P.H., H. Kieffe, M.J. Clouter, and W.W. Denner (1983). Elastic constants of artificial and natural ice samples by Brillouin spectroscopy, *Journal of Glaciology* 29, 433.
- [14] Gittus, J. (1975). *Creep, Viscoelasticity and Creep Fracture in Solids*, Applied Science Publishers.

- [15] Gold, L.W. (1977). Engineering properties of fresh-water ice, *Journal of Glaciology* 19, 197.
- [16] Griggs, D.T. and N.E. Coles (1954). Creep of single crystals of ice, *U.S. Army Snow, Ice and Permafrost Research Establishment*, SIPRE Report 11.
- [17] Higashi, A. (1968). Mechanical properties of ice single crystals, *Proc. Int. Symp. on Physics of Ice*, pp. 197-212, N. Riehl, B. Bullemer, and H. Engelhardt (Editors), Munich, Germany, September 9-14.
- [18] Higashi, A., S. Koinuma, and S. Mae (1964). Plastic yielding in ice single crystals, *Japanese Journal of Applied Physics* 3, 610.
- [19] Hobbs, P.V. (1974). *Ice Physics*, Clarendon Press, Oxford.
- [20] Hondoh, T. and A. Higashi (1983). Generation and absorption of dislocations at large-angle grain boundaries in deformed ice crystals, *Journal of Physical Chemistry* 87, 4044.
- [21] Hu, X., F. Liu, I. Baker and D. Black (1996). The effect of X-radiation on the plastic deformation of ice, *Philosophical Magazine A* 73, 1355.
- [22] Hutchinson, J.W. (1970). Elastic-plastic behavior of polycrystalline metals and composites, *Proc. Roy. Soc. London A* 319, 247.
- [23] Johnston, W.G. (1962). Yield points and delay times in single crystals, *J. Applied Physics* 33, 2716.
- [24] Johnston, W.G. and J.J. Gilman (1959). Dislocation velocities, dislocation densities, and plastic flow in Lithium Fluoride crystals, *J. Applied Physics* 30, 129.
- [25] Jones, S.J. and J.W. Glen (1969). The mechanical properties of single crystals of pure ice, *Journal of Glaciology* 8, 463.
- [26] Kamb, W.B. (1961). The glide direction in ice, *Journal of Glaciology* 3, 1097.
- [27] Kocks, U.F. (1970). The relation between polycrystal deformation and single-crystal deformation, *Metall. Trans.* 1, 1121.
- [28] Michel, B. (1978). A mechanical model of creep of polycrystalline ice, *Canadian Geotech. J.* 15, 155.
- [29] Michel, B. and R.O. Ramseier (1971). Classification of river and lake ice, *Can. Geotech. J.* 8, 36.
- [30] Muguruma, J. and A. Higashi (1963). Non-basal glide bands in ice crystals, *Nature*, May 11, No. 4880, p. 573.
- [31] Nakamura, T. (1978). Mechanical properties of impure ice single crystals at high temperatures, *4th Proceedings IAHR Symposium on Ice Problems*, Part I, pp. 275-291.

- [32] Nakamura, T. and S.J. Jones (1973). Mechanical properties of impure ice crystals, *Physics and Chemistry of Ice*, Whalley, E., Jones, S.J. and Gold, L.W. (Editors), pp. 365-369.
- [33] Nemat-Nasser, S. and M. Hori (1987). Void collapse and void growth in crystalline solids, *J. Appl. Phys.* 62, 2746.
- [34] Norwick, A.S. and B.S. Berry (1972). *Anelastic relaxation in crystalline solids*, Academic Press, New York, 677p.
- [35] Orowan, E. (1940). Problems of plastic gliding, *Proc. Phys. Soc.* 52, 8.
- [36] Patel, J.R. and A.R. Chaudhuri (1966). Charged impurity effects on the deformation of dislocation-free Germanium, *Phys. Rev.* 143, 601.
- [37] Ramseier, R.O. (1972). *Ph.D. Thesis*. Laval University, Canada.
- [38] Readey, D.W. and W.D. Kingery (1964). Plastic deformation of single crystal ice, *Acta Metall.* 12, 171.
- [39] Savin, G.N. (1961). *Stress concentrations around holes*, Pergamon Press, Oxford.
- [40] Schoeck, G. (1956). Moving dislocations and solute atoms, *Phys. Rev.* 102, 1458.
- [41] Shearwood, C. and R.W. Whitworth (1991). The velocity of dislocations in ice, *Philosophical Magazine A* 64, 289.
- [42] Sinha, N.K. (1978). Observations of basal dislocations in ice by etching and replicating, *Journal of Glaciology* 21, 385.
- [43] Steinemann, S. (1954). Results of preliminary experiments on the plasticity of ice crystals, *Journal of Glaciology* 2, 404.
- [44] Traetteberg, A., L.W. Gold, and R. Frederking (1975). The strain rate and temperature dependence of Young's modulus of ice, *Proc. IAHR Third Int. Symp. on Ice Problems*, Frankenstein, G.E. (Ed.), pp. 479-486.
- [45] Weertman, J. (1963). The Eshelby-Schoeck viscous dislocation damping mechanism applied to the steady-state creep of ice, *Ice and Snow*, Kingery, W.D. (Ed.), MIT Press, Cambridge, pp. 28-33.
- [46] Weertman, J. (1973). Creep of Ice, *Physics and Chemistry of Ice*, Whalley, E., Jones, S.J. and Gold, L.W. (Editors), pp. 320-337.
- [47] Wei, Y. and J.P. Dempsey (1994). The motion of non-basal dislocations in ice crystals, *Philosophical Magazine A* 69, 1.
- [48] Wu, M.S. (1990). Physically-based constitutive models for transient creep and damage in polycrystalline ice, *Ph.D. Thesis*, Massachusetts Institute of Technology, USA.

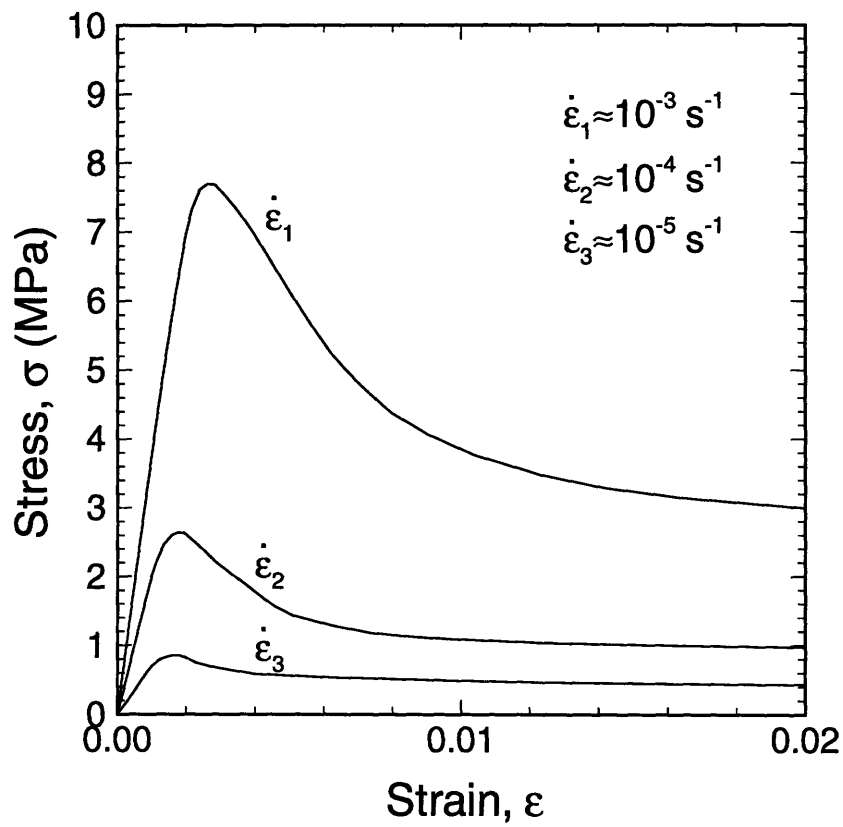


Figure 3-1: Typical stress-strain curves of single crystal ice oriented for basal glide under various levels of constant strain rate.

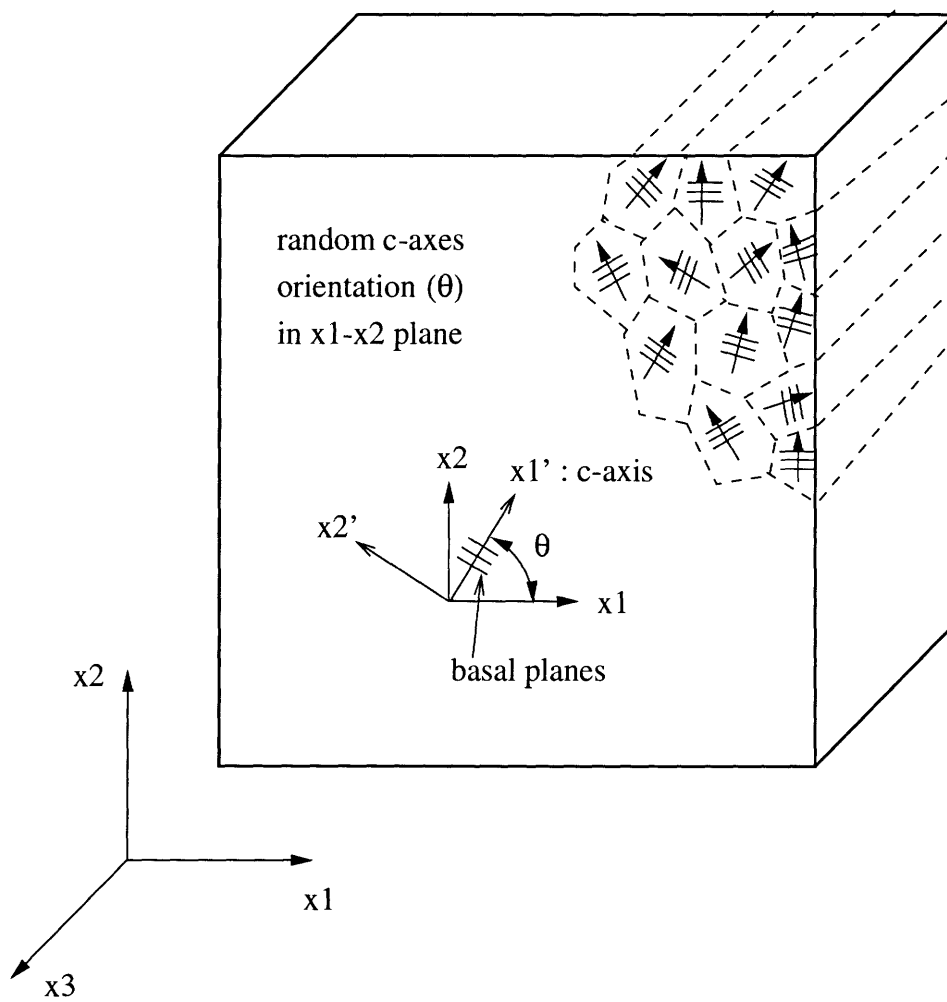


Figure 3-2: An S2 polycrystalline ice.

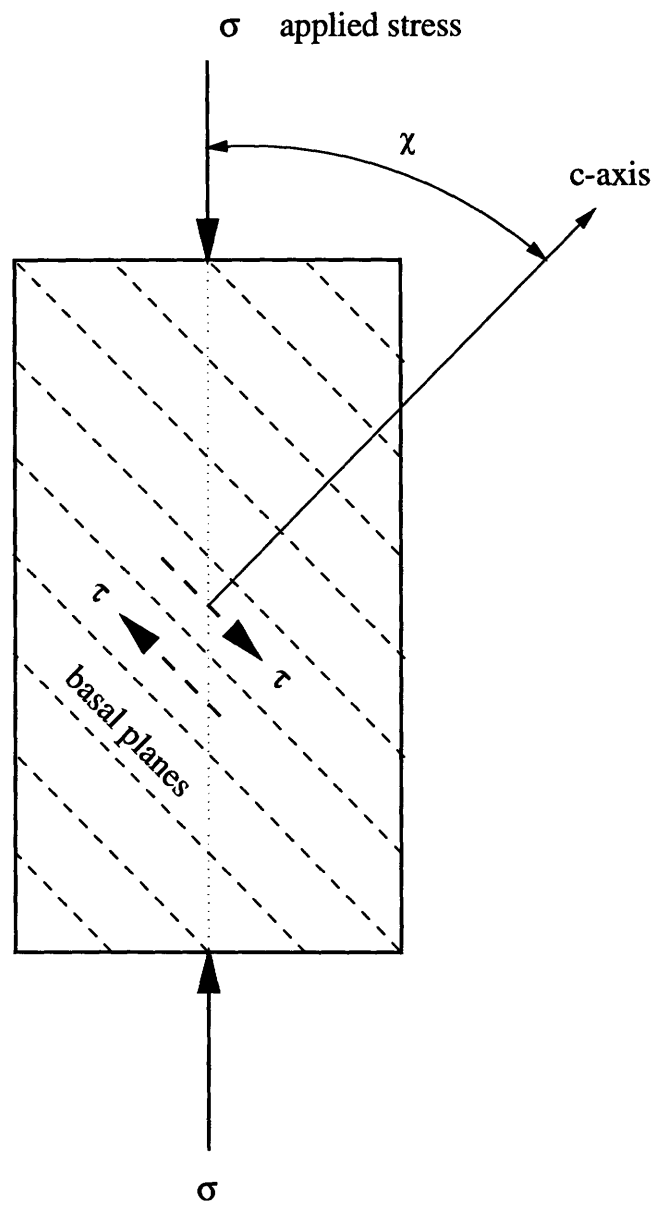


Figure 3-3: Notation for basal plane orientation in the x_1 - x_2 plane.

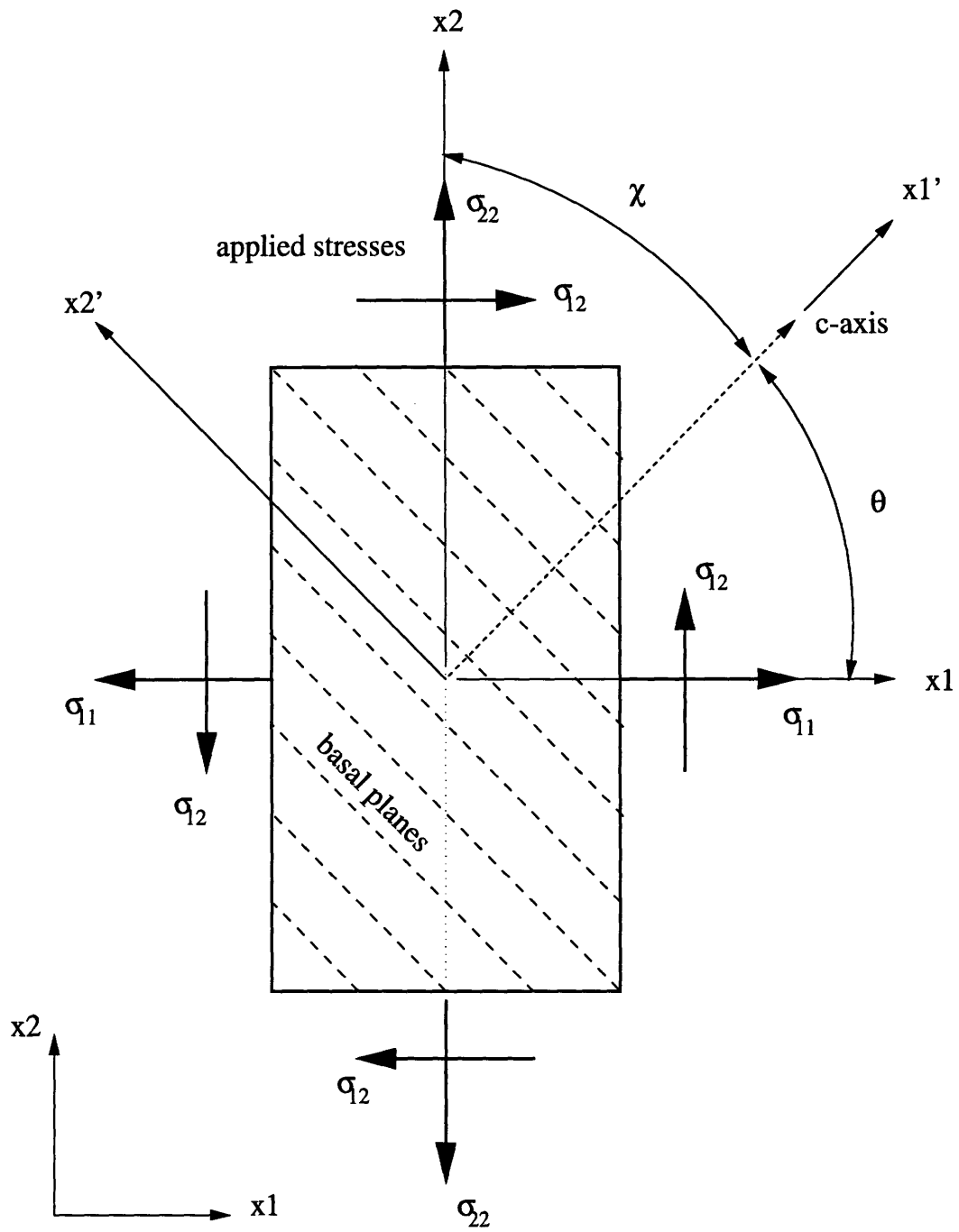


Figure 3-4: Notation for biaxial loading in the x_1 - x_2 plane.

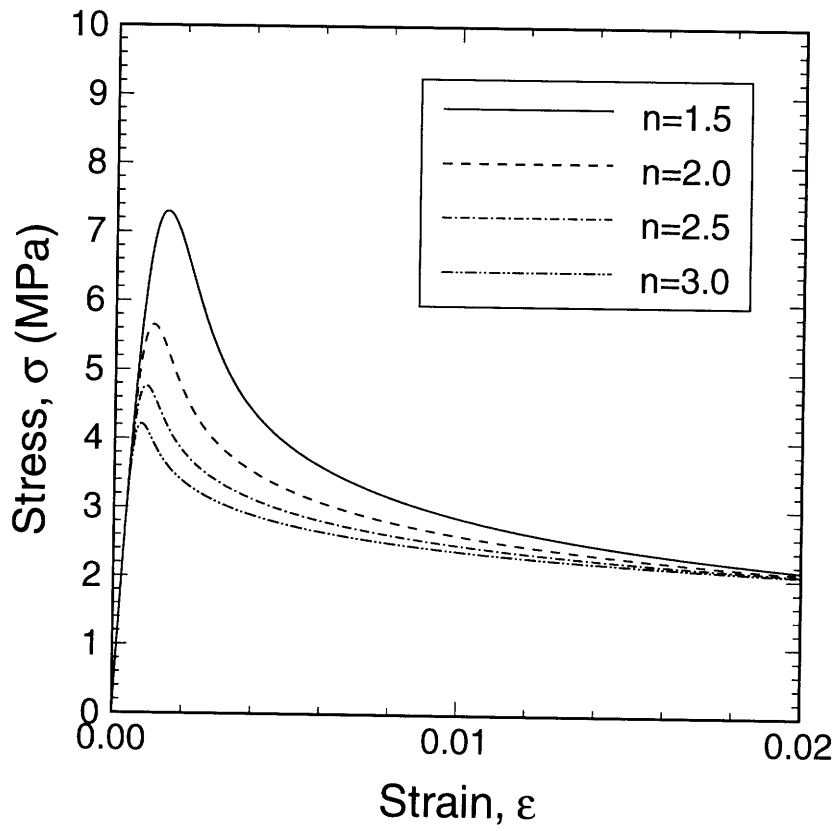


Figure 3-5: Effect of the stress exponent n on the stress-strain behavior.

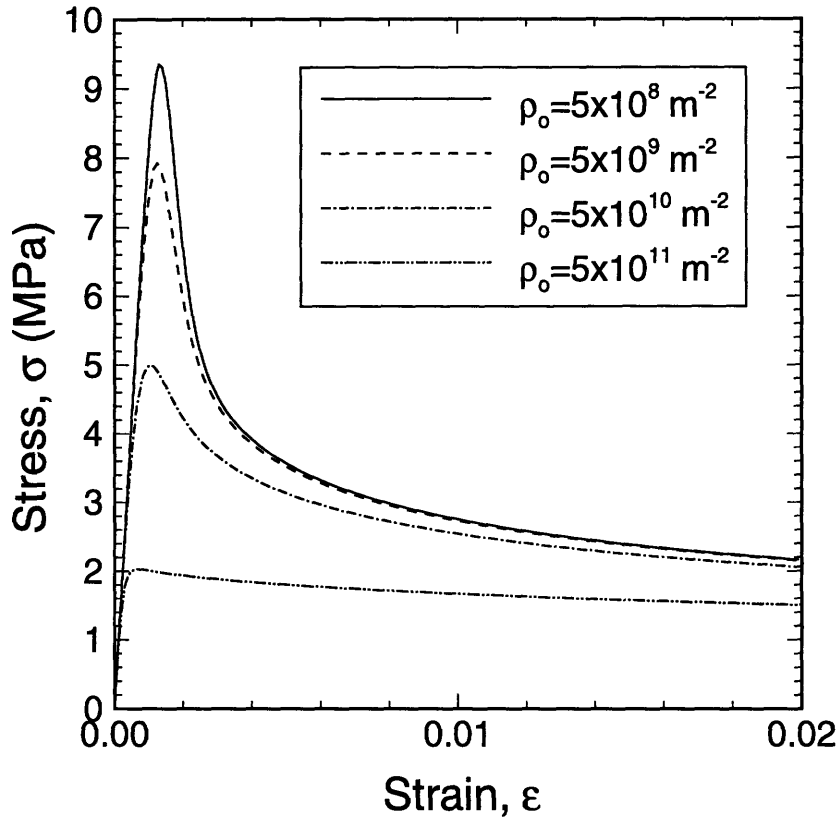


Figure 3-6: Effect of the initial dislocation density ρ_0 on the stress-strain behavior.

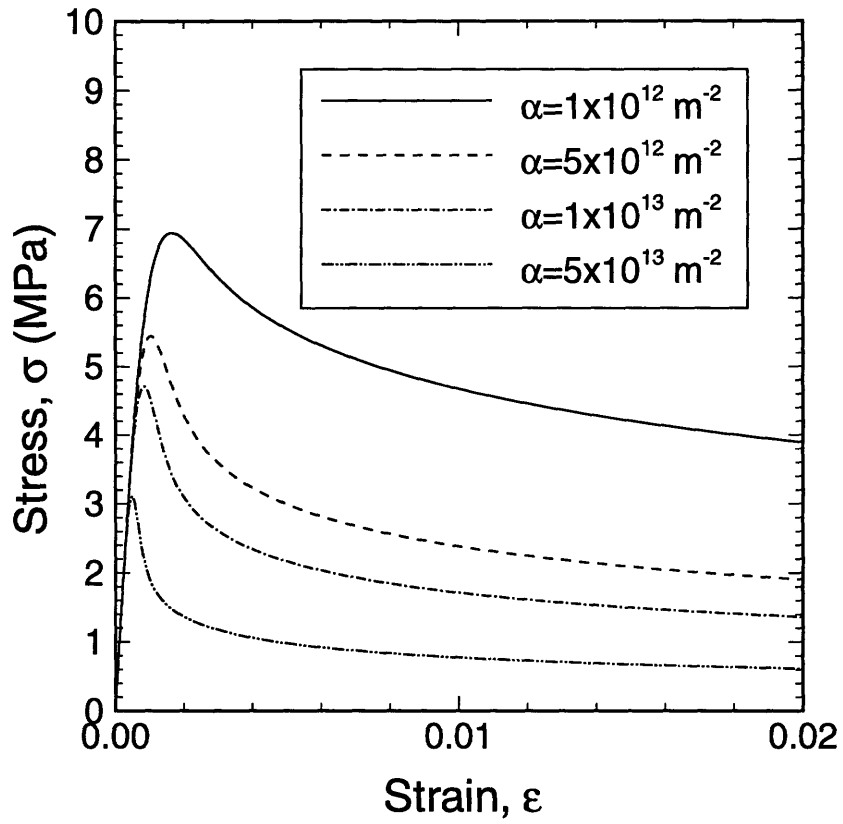


Figure 3-7: Effect of the rate of dislocation multiplication α on the stress-strain behavior.

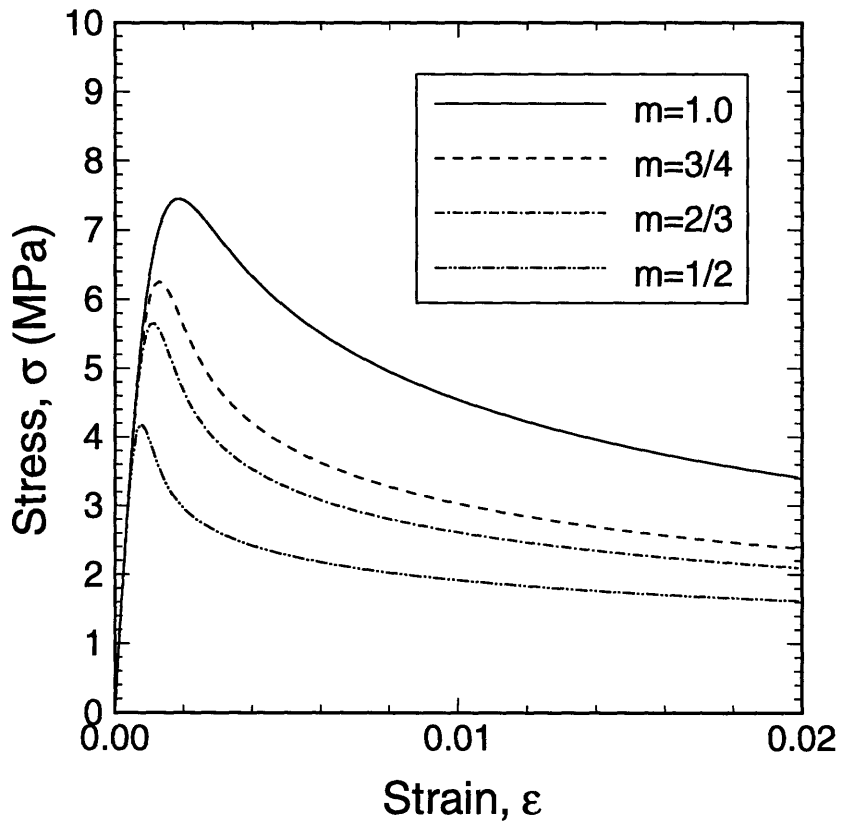


Figure 3-8: Effect of the inelastic strain exponent m on the stress-strain behavior.

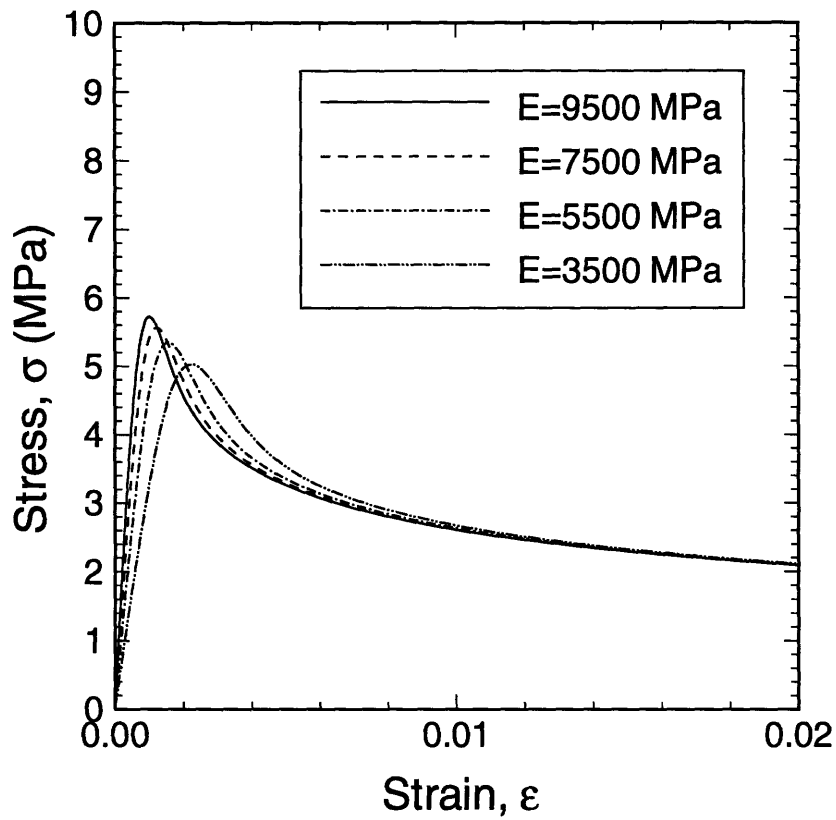


Figure 3-9: Effect of Young's modulus E on the stress-strain behavior.

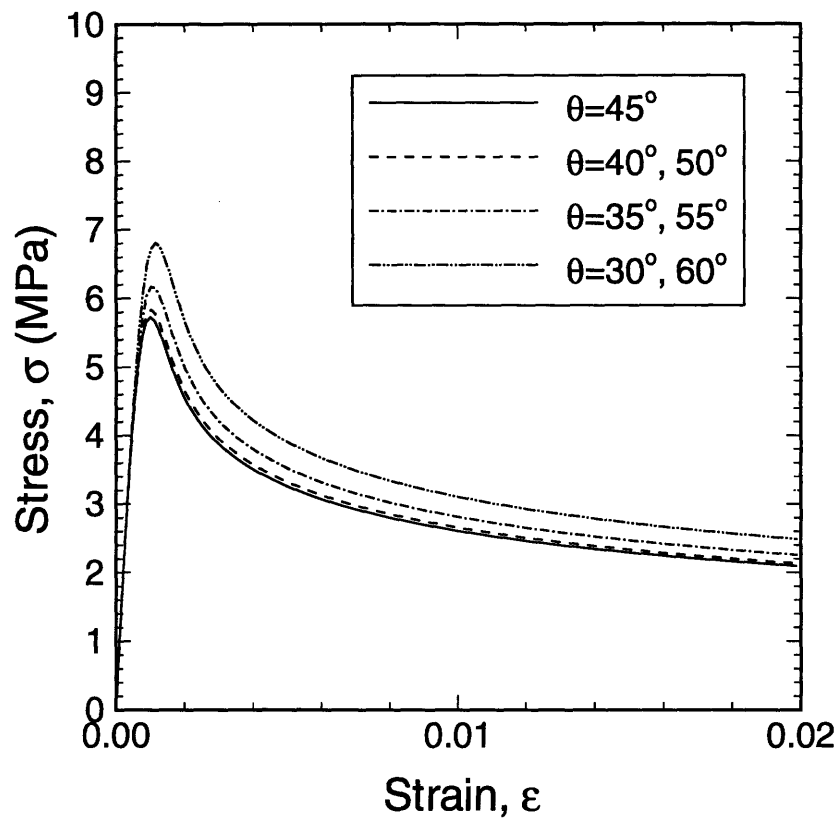


Figure 3-10: Effect of the c-axis orientation θ on the stress-strain behavior.

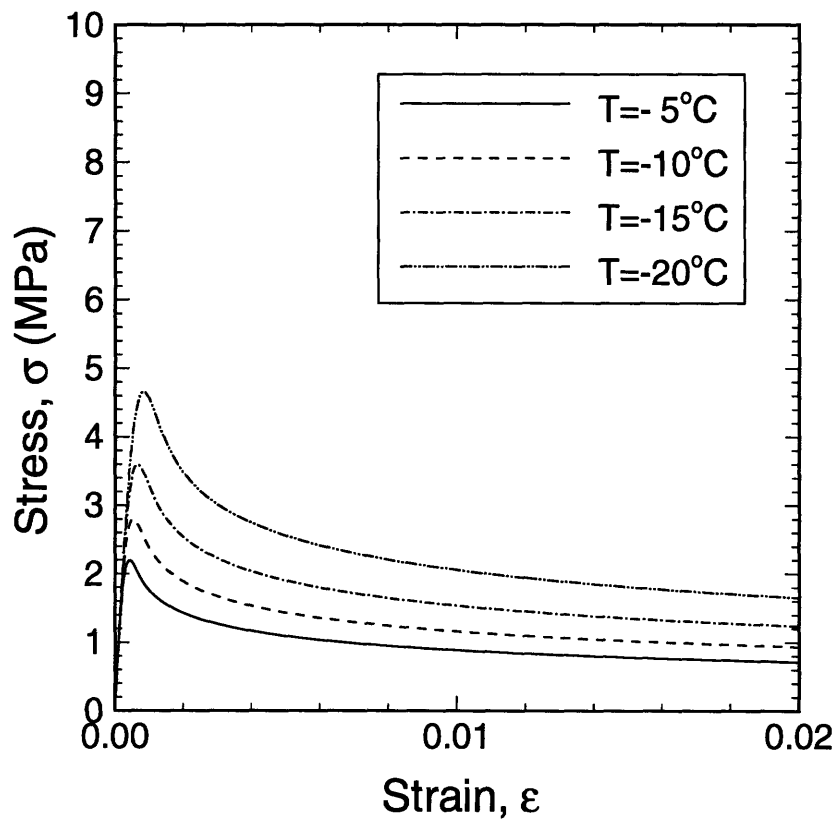


Figure 3-11: Effect of temperature T on the stress-strain behavior.

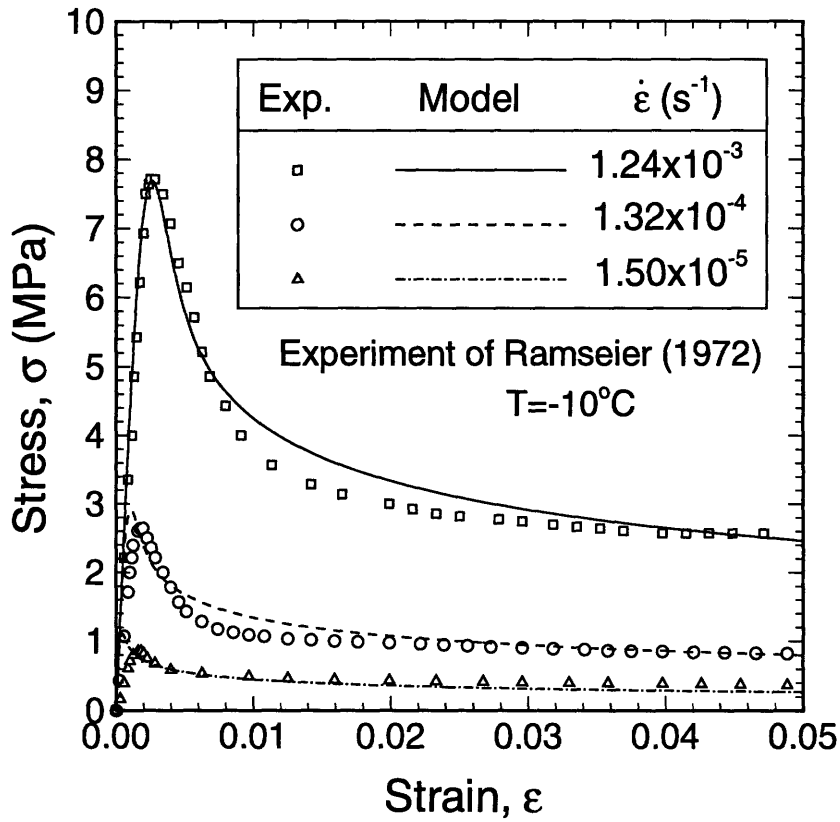


Figure 3-12: Comparison of experimental and predicted stress-strain curves for constant strain rates at $T = -10^{\circ}C$

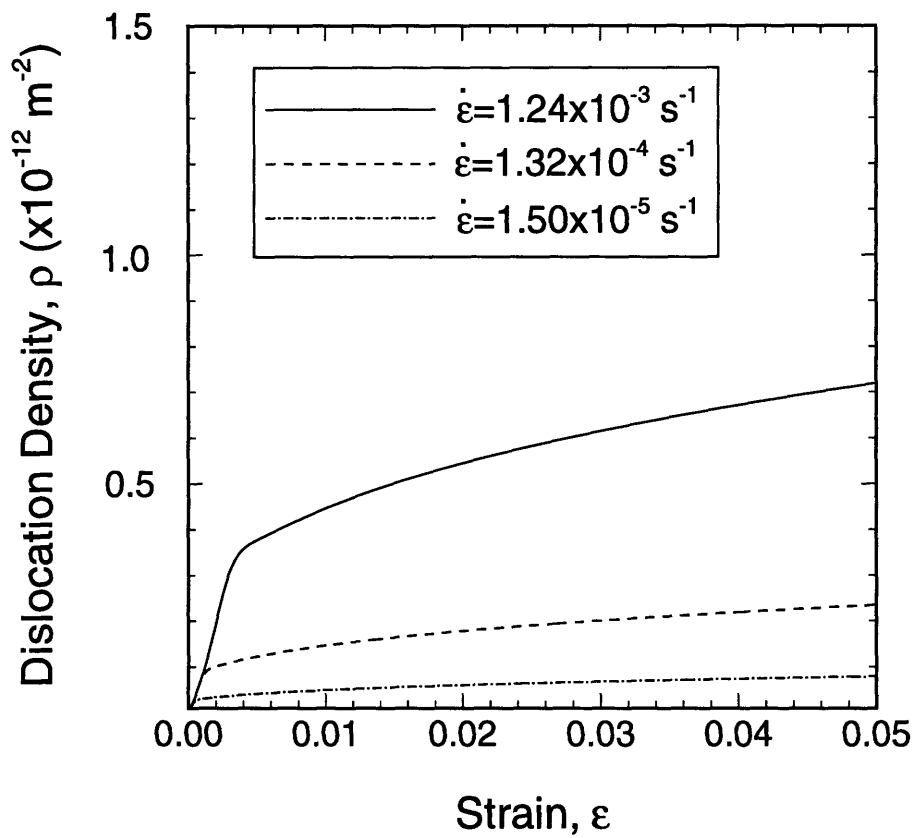


Figure 3-13: Predicted dislocation density vs. strain for constant strain rates at $T = -10^{\circ}\text{C}$.

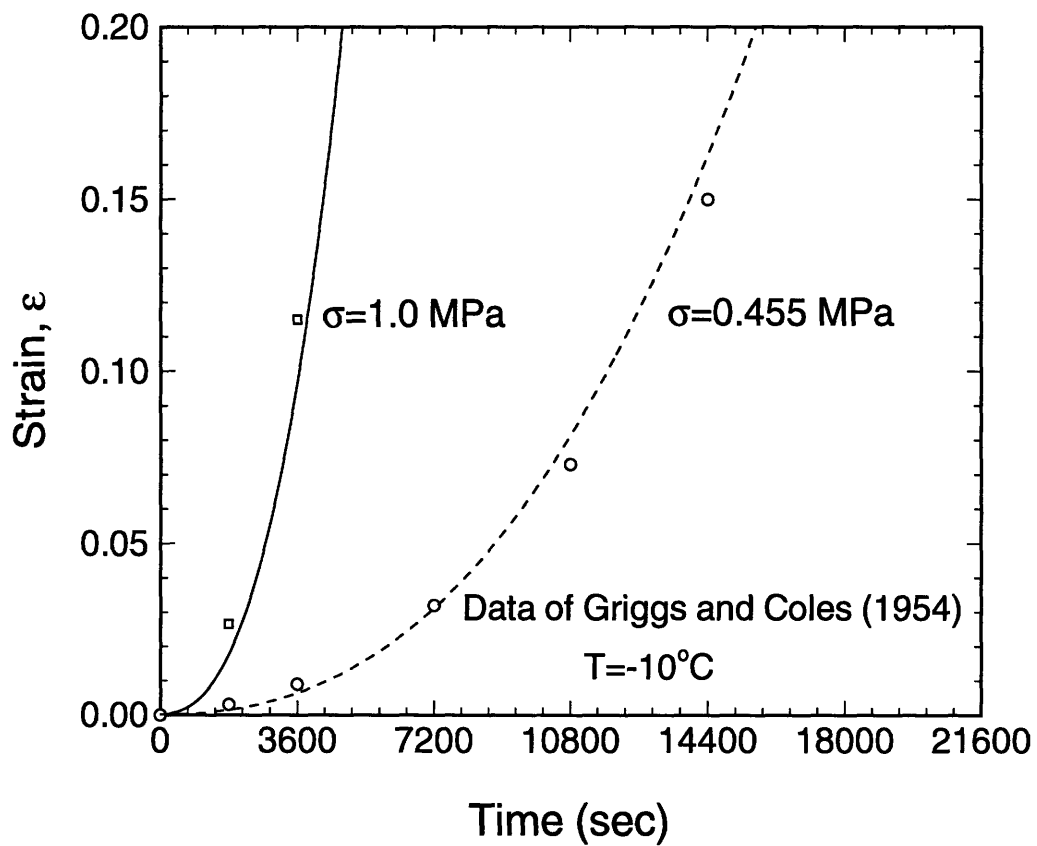


Figure 3-14: Comparison of experimental and predicted strain-time responses for constant stresses at $T = -10^{\circ}C$.

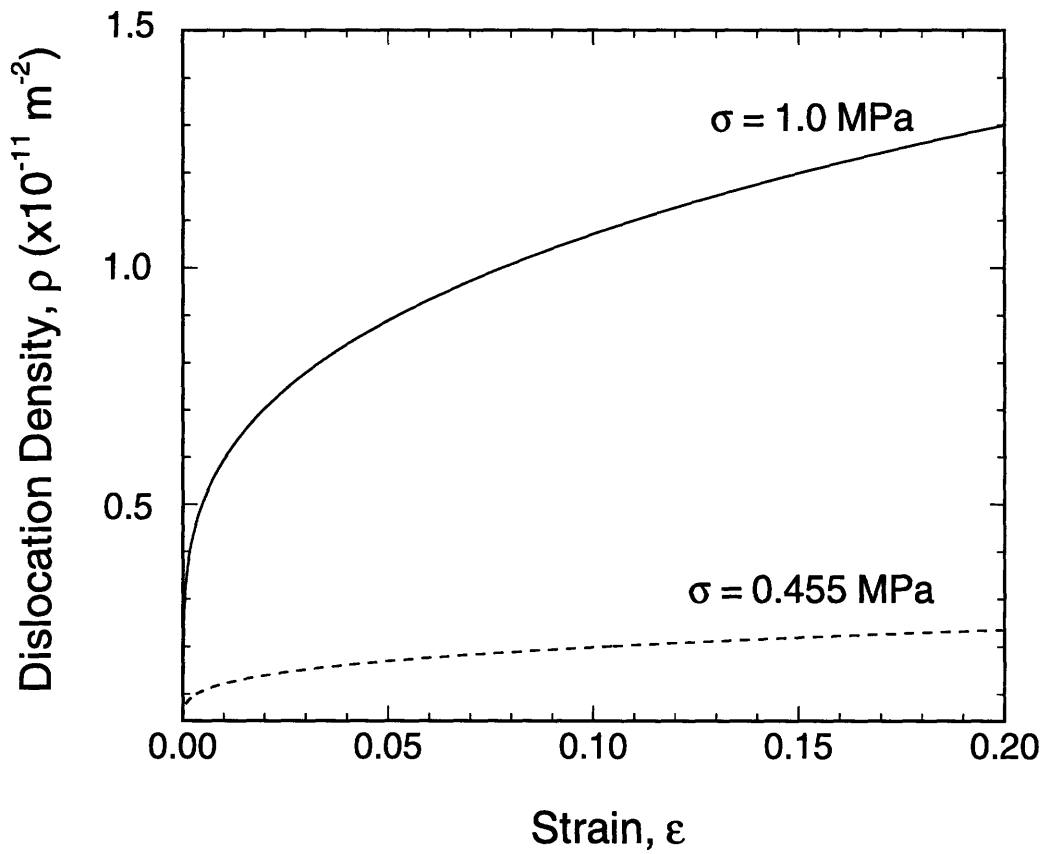


Figure 3-15: Predicted dislocation density vs. strain for constant applied stresses at $T = -10^\circ\text{C}$.

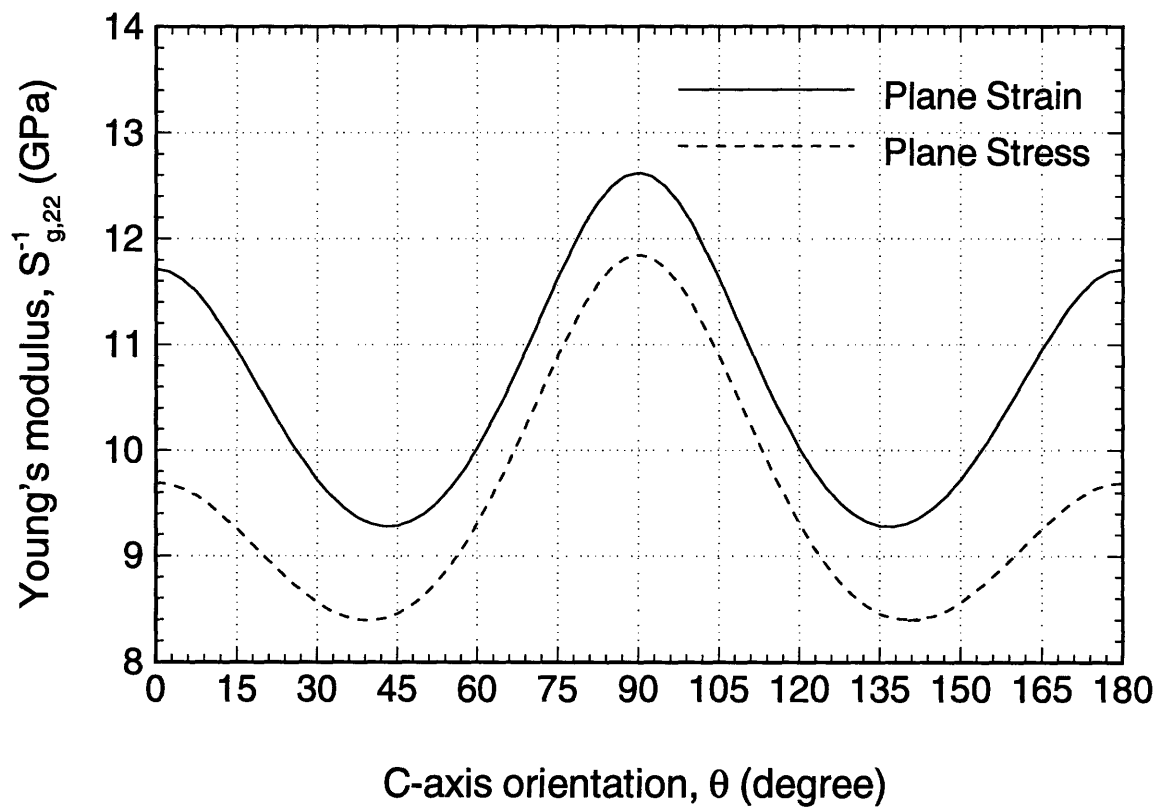


Figure 3-16: Variation of the dynamic Young's modulus, $S_{g,22}^{-1}$, with c-axis orientation.

Chapter 4

RELAXATION PROCESS IN POLYCRYSTALLINE ICE UNDER CYCLIC LOADING

Abstract

During ice-structure interaction in the ductile-to-brittle transition, ice is subjected to a non-monotonic vibratory loading, as parts of the ice sheet fail over time. In order to simulate this vibratory loading, it is necessary to understand the behavior of ice when it is subjected to loading and unloading cycles. Experimental data on the cyclic behavior of ice has been reported under reversed direct-stress conditions, but no constitutive theory exists as yet to describe this phenomenon based on the underlying microstructural mechanism.

This chapter describes a model of anelastic response in polycrystalline ice under cyclic loading. The model is developed here on the basis of the linear relationship between anelastic strain and stress, and the distribution of relaxation times which can be measured from loss compliance. The model predictions are compared with cyclic experimental data (Cole, 1990) that span a range of stress amplitudes (0.6 - 1.4 *MPa*) and frequencies (1 - 10^{-3} *Hz*) at -10°C . The resulting model is capable of describing the anelastic response of polycrystalline ice under cyclic loading.

4.1 Introduction

The study of the cyclic behavior of ice is of interest for several reasons: natural ice suffers cyclic loading through wave or tidal action, and when ice is used for structural purposes the loading may be repetitive (Nixon and Smith, 1987). When ice is subjected to cyclic loading, designers may need to take into account the fatigue behavior of natural ice which happens during sea ice breakup or the flexure of a floating ice plate.

Experimental data on the cyclic behavior of ice have been published under cyclic loading in uniaxial compression and reversed direct-stress (Mellor and Cole, 1981; Nixon and Smith, 1984, 1987; Cole, 1990, 1995; Derradji-Aouat et al., 1993). No constitutive equation, however, exists to describe cyclic behavior based on the underlying microstructural mechanisms. Cole (1995) measured energy loss which occurs during cyclic loading as a result of two distinct relaxation processes: (i) the glide of basal dislocations and (ii) grain boundary sliding. In the test range of frequencies ($1 - 10^{-3} \text{ Hz}$) and temperatures ($-10 - -50^\circ\text{C}$), Cole (1995) found that the dislocation-based mechanism dominates over grain boundary relaxation. The relaxation associated with grain boundary sliding, however, explains the anelasticity observed at higher frequencies and lower temperatures.

The purpose of this chapter is to propose a model for the anelastic response of polycrystalline ice based on a dislocation-based mechanism that is dominant in a range of stress amplitudes ($0.6 - 1.4 \text{ MPa}$) and frequencies ($1 - 10^{-3} \text{ Hz}$) at -10°C . This study examines the influence of frequency and amplitude of cyclic loading on low anelastic strains (less than 10^{-3}).

The organization of the chapter is as follows. Section 4-2 supplies background information on the behavior of ice under constant stress, with a discussion of cyclic loading. In Section 4-3, a mathematical formulation for the modelling of anelastic response of polycrystalline ice is presented. In particular, the frequency-dependent anelastic relaxation that produces energy loss is taken into account by a distribution of relaxation times. Section 4-4 contains model parameters and corresponding model predictions. These predictions are compared with the available experimental data (Cole, 1990). Lastly, conclusions are drawn in Section 4-5.

4.2 Background

Ice mostly exists above $0.8 T_M$, where T_M is the melting temperature. The mechanical behavior of crystalline solids at such high temperatures is controlled by thermally activated rate processes. Thus, the behavior of ice is very sensitive to rate and temperature variations.

Freshwater polycrystalline ice consists of single crystals. Typical grain sizes are between 1 and 10 *mm*. For inelastic deformation without microcracks, polycrystalline ice needs to satisfy certain conditions such as strain compatibility in the grain boundaries. It is also known that polycrystalline ice is affected greatly by the microstructure (e.g., grain size and structure of grains). At low loading rates, mechanisms responsible for inelastic strain are mainly dislocation movement in transgranular matrix and the grain boundary sliding process, which is the relative motion between adjacent grains.

Many constant stress and constant strain-rate tests, and studies of deformation mechanisms, have characterized the behavior of ice over the last several decades (e.g., Glen, 1955; Barnes et al., 1971; Weertman, 1973; Goodman et al., 1981; Duval et al., 1983). Most studies of ice have emphasized the stress dependence of the steady-state creep rate under constant stress, which follows empirically the power-law creep.

In the past two decades, many constitutive equations have been developed to model ductile behavior of ice (e.g., Sinha, 1978; Michel, 1978; LeGac and Duval, 1980; Ashby and Duval, 1985; Shyam Sunder and Wu, 1989a,b). Many of these constitutive equations have been formulated for transient creep under uniaxial constant stress and constant strain rate. The first tests and studies on the deformation behavior and fatigue failure of ice under cyclic loading were conducted by Mellor and Cole (1981). These investigators performed compressive stress-controlled cyclic loading tests on granular freshwater polycrystalline ice. Later, Cole (1990) presented experimental results of reversed direct-stress on granular freshwater polycrystalline ice to examine the effects of frequency, temperature, and stress-amplitude on internal friction and hysteresis loops.

4.2.1 Anelasticity

Ice exhibits a significant amount of anelastic strain during loading and time-dependent recoverable strain during unloading (Duval, 1976,1978; Cole, 1991). Processes such as dislocation movement on basal planes or grain boundary sliding give rise to anelastic strain that produces relaxation processes observed during cyclic loading.

The glide motion of dislocations is controlled by proton rearrangement, which is a unique characteristic of ice (Goodman et al., 1981). The origin of the anelasticity in ice is a stress-induced reorientation of the hydrogen atoms about the oxygen atoms. Dislocations move forward under applied stress and glide back toward their original positions upon removal of the stress.

Sinha (1979) postulates that the contribution of anelastic strain to total strain is a linear stress dependence based on the process of grain boundary sliding. According to Duval et al. (1991), the strain from grain boundary sliding underestimates the relatively high levels of anelastic strain observed in ice. Since grain boundary sliding alone cannot account for the large anelastic strain in ice, dislocation movement within grains has large effects under monotonic constant stress loading (Duval et al., 1991; Cole, 1991).

As the stress level and temperature increases or frequency decreases, Cole (1991) observed that anelastic strain becomes a nonlinear function of stress. However, at relatively low anelastic strain observed under cyclic loading, the bow-out motion of pinned dislocations on the basal planes produces anelastic strain approximately proportional to stress. Generally, as strain or stress levels increase, the dislocation breakaway process and an increase in dislocation density result in nonlinear stress dependence of anelastic strain.

It is noted that anelastic strain is often ignored in metal plasticity because anelastic strain at low temperatures is small compared to total strain. However, in ice, during the cyclic deformation where strain amplitudes are small, the anelastic contribution is too large to neglect. The changes observed in the strain amplitude during cyclic loading could be due to the changes in anelastic response rather than in plastic response.

According to Cole (1995), the substructure developed during cyclic loading differs considerably from that developed under monotonic constant stress loading. The total strain

during cyclic loading is relatively small, less than 10^{-3} , compared to that, on the order of 10^{-2} , at the minimum strain rate under constant stress tests. Cole (1995) observed in his ice specimens that the density of dislocations contributing to anelastic strain remains constant during cyclic loading.

Under cyclic loading, polycrystalline ice, which has a limited number of slip systems and very low stacking fault energy, does not exhibit the characteristics of fatigue behavior that are shown by ductile materials which have more slip systems or a high stacking fault energy. Thus, polycrystalline ice exhibits less susceptibility to fatigue damage due to the difficulty of cross-slip (Cole, 1991).

4.2.2 Internal Friction

When the material is subjected to alternate tension and compression, the strain lags behind the applied stress. A hysteresis loop during alternate cyclic stress gives rise to energy loss. The area of the hysteresis loop is the amount of energy that is dissipated. The study of energy loss during cyclic loading gives insight to the underlying micromechanical mechanisms. There are a number of ways in which to examine the loss mechanisms, including the calculation of internal friction, storage and loss compliance and changes in the elastic modulus.

There are many processes that can cause internal friction, corresponding to a phase lag between the applied stress and the resulting strain. The origin of internal friction effects varies greatly from material to material. The study of internal friction or loss compliance in ice (Cole, 1995) helps us to understand the following effects: the movement of dislocations on the basal planes and the relative motion of grains at grain boundaries. Internal friction can be closely associated with relaxation effects through the variation of the elastic moduli. Each process has a characteristic time of relaxation, and this corresponds to a peak on the curve relating internal friction with frequency of loading. Since the relaxation times vary with temperature, it is possible to vary the temperature while the frequency remains constant.

The internal friction in polycrystalline ice is studied from the view of anelastic strain associated with dislocation movement within grains (Tatibouet et al., 1986; Cole, 1995) or grain boundary sliding (Tatibouet et al., 1987). The dislocation velocity can also be predicted from internal friction measurements (Fukuda et al., 1987). In the study of internal friction

on single crystals of ice at high temperature, Tatibouet et al., (1986) explains the frequency dependence of cyclic stress by the distribution in the restoring forces, which is induced by the line tension of dislocations pinned between quasi-immobile segments of the dislocation network.

4.3 Formulation of Constitutive Model

4.3.1 Constitutive Equations

Since polycrystalline ice is a rate-dependent material, the total strain rate $\dot{\epsilon}$ is given by

$$\dot{\epsilon} = \dot{\epsilon}^e + \dot{\epsilon}^c \quad (4.1)$$

where $\dot{\epsilon}^e$ and $\dot{\epsilon}^c$ are the elastic and anelastic strain rates, respectively. The elastic strain rate is written as

$$\dot{\epsilon}^e = \frac{\dot{\sigma}}{E} \quad (4.2)$$

where σ is the applied stress and E is Young's modulus. The anelastic strain rate due to dislocation movement is expressed by Orowan's equation (Orowan, 1940)

$$\dot{\epsilon}^c = \phi b \rho \nu \quad (4.3)$$

where ϕ is a geometrical factor taking into account the orientation of the slip systems, b is the magnitude of Burgers vector, ρ is the average density of mobile dislocations, and ν is the average velocity of dislocations.

The dislocation element moves a distance x when the applied force $b\sigma$ exceeds the potential resistance $\partial\Delta F/\partial x$. The driving force, the difference between the applied force and potential resistance, is balanced by the inertia force $m\ddot{x}$ and the drag force $\eta\dot{x}$. Therefore, the most general equation of motion of a unit length of dislocation is mathematically described as (Kocks et al., 1975)

$$m \frac{d^2x}{dt^2} + \eta \frac{dx}{dt} + \frac{\partial\Delta F}{\partial x} - b\sigma = 0 \quad (4.4)$$

where m is the dislocation mass per unit length and the temperature-dependent drag coef-

efficient η is given by

$$\eta = \eta_0 \exp\left(\frac{Q}{RT}\right) \quad (4.5)$$

where η_0 is a constant, Q is the activation energy, R is the universal gas constant, and T is the absolute temperature in degrees Kelvin.

For our range of interest, the inertia force can be ignored. In this case, Eq. (4.4) reduces to

$$\eta \dot{x} = b\sigma - \frac{\partial \Delta F}{\partial x} . \quad (4.6)$$

Note that \dot{x} is the average velocity of dislocations. For a small displacement, one assumes that the potential resistance is proportional to dislocation movement:

$$\frac{\partial \Delta F}{\partial x} = Kx \quad (4.7)$$

where K is an average internal resisting stress to the motion of dislocation. Therefore, in Eq. (4.6), we postulate that the velocity of dislocation at small strains is linearly dependent on the applied stress.

As Cole (1995) observed in his experiments for saline ice under cyclic loading, the density of dislocations contributing to anelastic strain remains constant. Therefore, Eq. (4.3) becomes

$$\epsilon^c = \phi b \rho x . \quad (4.8)$$

Using Eq. (4.8), substitution of Eqs (4.6) and (4.7) into Eq. (4.3) results in

$$\dot{\epsilon}^c = \left(\frac{\sigma - A_1 E \epsilon^c}{B} \right) \quad (4.9)$$

where $A_1 E$ and B are defined as

$$A_1 E = \frac{K}{\phi b^2 \rho} \quad (4.10)$$

$$B = \frac{\eta}{\phi b^2 \rho} . \quad (4.11)$$

According to Eq. (4.1), the total strain rate is written as

$$\dot{\epsilon} = \dot{\epsilon}^e + \dot{\epsilon}^c = \frac{\dot{\sigma}}{E} + \left(\frac{\sigma - A_1 E \epsilon^c}{B} \right) . \quad (4.12)$$

The variable B is considered to correspond to a mean spacing of barriers of the same strength throughout the specimen. However, in reality a distribution of barrier spacings and strengths is expected.

The solutions of Eq. (4.12) for applied constant stress σ_o and sinusoidal stress $\sigma_o \sin \omega t$ are given by

$$\epsilon = \frac{\sigma_o}{E} + \frac{\sigma_o}{A_1 E} \left\{ 1 - \exp\left(-\frac{t}{\tau}\right) \right\} \quad \text{for } \sigma = \sigma_o \quad (4.13)$$

$$\epsilon = \sigma_o J_2(\omega) \exp\left(-\frac{t}{\tau}\right) + \sigma_o \{ J_1(\omega) \sin \omega t - J_2(\omega) \cos \omega t \} \quad \text{for } \sigma = \sigma_o \sin \omega t \quad (4.14)$$

where τ is relaxation time defined as

$$\tau = \frac{B}{A_1 E} = \frac{\eta}{K} \quad (4.15)$$

and the storage compliance $J_1(\omega)$ and the loss compliance $J_2(\omega)$ are written as

$$J_1(\omega) = \frac{1}{E} + \frac{1}{A_1 E} \frac{1}{1 + (\omega\tau)^2} \quad (4.16)$$

$$J_2(\omega) = \frac{1}{A_1 E} \frac{\omega\tau}{1 + (\omega\tau)^2} . \quad (4.17)$$

The first term in Eq. (4.14) determines the transient behavior and the second describes the steady-state response. Equation (4.17) describes a relaxation peak with central frequency determined by the relaxation time τ . Therefore, when the time dependent drag coefficient η is known from independent tests, K can be estimated from the central frequency of the relaxation peak. Such data of the compliance versus frequency was measured by Cole and Durell (1995).

To simulate the behavior of polycrystalline ice under the compressive cyclic stress $\frac{1}{2}\sigma_o(1 - \cos \omega t)$ tested by Mellor and Cole (1981), the solution of Eq. (4.12) is

$$\epsilon = \frac{\sigma_o}{2} \{-J_R + J_1(\omega)\} \exp\left(-\frac{t}{\tau}\right) + \frac{\sigma_o}{2} \{J_R - J_1(\omega) \cos \omega t - J_2(\omega) \sin \omega t\} \quad (4.18)$$

where

$$J_R = \frac{1}{E} \frac{(1 + A_1)}{A_1} . \quad (4.19)$$

4.3.2 Distribution of Relaxation Times

The motion of dislocations is described by using the averaged internal stress and temperature-dependent drag coefficient, which have a considerable statistical variation in their magnitudes related to the variation in basal plane orientations. Experiments show that a dislocation internal friction peak is much broader than that of a single activated process (Weertman, 1973; Cole, 1995). Constitutive equations based on dislocation-based mechanisms need to taken into account the distribution of these physical properties.

Cole (1994) concludes from his experiments that the strength of dislocation relaxation depends on the microstructure, basal plane orientation and frequency. As studied by Cole and Durell (1995), loss compliance versus frequency shows a broad distribution, which serves as proof for the distribution of relaxation times. The distributed relaxation in a given state could also be studied by measuring temperature-dependent or frequency-dependent internal friction spectra.

The relaxation processes can be considered through the distribution of activation energy or frequency factor or both (Nowick and Berry, 1972; Kocks et al., 1975; Argon, 1985). The distribution in frequency factor is a special manifestation of the presence of considerable activation entropies, as is well known in thermally-activated processes governing crystal plasticity by dislocation glide (Kocks et al., 1975)

In the present study, the distribution of relaxation times takes into account the relaxation process. In order to describe adequately the frequency dependence of the anelastic strain, Eqs (4.16) and (4.17) are modified by using distribution function $\Psi(\ln \tau/\tau_m)$ as

$$J_1^d(\omega) = \frac{1}{E} + \frac{1}{A_1 E} \int_{-\infty}^{+\infty} \Psi(\ln \tau/\tau_m) \frac{1}{1 + (\omega\tau)^2} d(\ln \tau/\tau_m) \quad (4.20)$$

$$J_2^d(\omega) = \frac{1}{A_1 E} \int_{-\infty}^{+\infty} \Psi(\ln \tau/\tau_m) \frac{\omega\tau}{1 + (\omega\tau)^2} d(\ln \tau/\tau_m) \quad (4.21)$$

where the distribution function needs to satisfy the condition

$$\int_{-\infty}^{+\infty} \Psi(\ln \tau/\tau_m) d(\ln \tau/\tau_m) = 1 \quad (4.22)$$

and the log-normal distribution is expressed by

$$\Psi(z) = \frac{1}{\beta\sqrt{2\pi}} \exp \left\{ - \left(\frac{z}{\sqrt{2}\beta} \right)^2 \right\} \quad (4.23)$$

after a change of variable, $z = \ln \tau / \tau_m$. In Eq. (4.23), $\ln \tau_m$ is a center of relaxation times and β is a distribution parameter for broadness. Figure 4-1 shows the storage and loss compliances for no distribution and log-normal distribution for a particular β .

Finally, the anelastic responses are obtained from Eqs (4.14) and (4.18) with $J_1^d(w)$ and $J_2^d(w)$ instead of $J_1(w)$ and $J_2(w)$.

4.4 Model Predictions

4.4.1 Model Parameters

The dynamic elastic constants of single crystal ice is determined at $T = -16^\circ C$ using the method of Brillouin spectroscopy by Gammon et al. (1983). The theoretical effective elastic constants of polycrystalline ice can be computed by using various homogenization methods (see Appendix B in Chapter 5). For freshwater polycrystalline ice the value of Young's modulus is approximately 9.3 *GPa*.

The measured activation energy for easy glide on the basal plane lies between about 39 *kJ/mol* (=0.4 *eV*) and 68 *kJ/mol* (=0.7 *eV*) depending on temperature (Jones and Glen, 1969) and impurities (Nakamura and Jones, 1973). The fact that the activation energy for creep in ice is similar to those for dielectric relaxation and self-diffusion in ice suggests that the velocity of dislocations is controlled by diffusive motion of hydrogen atoms and the movement of Bjerrum defects (Hobbs, 1974). In the present study, 53 *kJ/mol* (=0.55 *eV*) is used for the activation energy. The magnitude of Burgers vector was calculated by Hondoh and Higashi (1983). In the present study, we use $b = 0.6a$, where a is the lattice parameter of ice. At $-10^\circ C$, $a = 4.52 \times 10^{-10}$ *m* so that $b = 2.71 \times 10^{-10}$ *m*.

The model parameters related to distributed relaxation are obtained as follows. When the time dependent drag coefficient η is known, K , the center of distribution, and β , the broad-

ness of the distribution, are estimated from Cole and Durell's (1995) plot of loss compliance versus frequency. The following values of the parameters are obtained:

$$E = 9.3 \text{ GPa}; \quad \phi = 1/3; \quad b = 2.71 \times 10^{-10} \text{ m}; \quad \rho = 1.5 \times 10^9 \text{ m}^{-2}; \quad K = 10^{-7} \text{ MPa};$$

$$\eta_0 = 7.05 \times 10^{-16} \text{ MPa sec}; \quad Q = 53 \text{ kJ mol}^{-1}; \quad \beta = 1.40.$$

4.4.2 Model Predictions

Figure 4-2 compares stress-strain responses of polycrystalline ice subjected to 0.1 *Hz* sinusoidal stress at -10°C . Figures 4-3 and 4-4 compare stress-strain responses of polycrystalline ice under various cyclic stress levels (0.6 - 1.2 *MPa*) and frequencies (0.01, 0.1, 1 *Hz*) at -10°C . Considering scatter and data extraction inaccuracies (e.g., Young's modulus and microstructural properties such as dislocation density and grain size), the comparison between the model prediction and the data shows good agreement. It is interesting to note that anelastic strain occurs even at 1 *Hz*. Figure 4-5 compares stress-strain responses of polycrystalline ice under various cyclic frequencies (10^{-3} , 10^{-2} , 10^{-1} , 1 *Hz*) and 1 *MPa* stress at -10°C . The comparisons show good agreement over the range of frequencies. As noted by Cole (1995), variations in the initial dislocation density would strongly influence the anelastic behavior observed at low strains. The variations of initial dislocation density and grain size are not considered in the model.

4.5 Conclusions

A constitutive model for polycrystalline ice subjected to cyclic loading applicable for relatively low anelastic strain, less than 10^{-3} , has been developed. The model predictions are compared with experimental data obtained by Cole (1990). From the various stress levels and frequencies considered, a comparison shows that this model adequately describes the frequency dependence at low strains. The model is based on intracrystalline processes involving dislocations. The motion of dislocations can be described by using the averaged internal stress and temperature-dependent dislocation drag. In polycrystalline ice, however, the distribution of these dislocation properties exists within grains due to a variation in

basal plane orientation. At relatively small anelastic strains, the effect of these distributions is taken into account by the distribution of relaxation times. The proposed model uses log-normal distribution of relaxation times for the measured loss compliance. Evidence for this distribution is provided from the data of Cole and Durell (1995).

The limited experimental data for polycrystalline ice under cyclic loading has restricted attempts to develop unified constitutive equations to describe the behavior of ice under cyclic loading and constant stress loading. In order to develop a comprehensive constitutive model based on a microstructural mechanism, more experimental work focused on the microstructure is required. Finally, a physically-based model can be developed if the physical mechanisms underlying the deformation process are adequately accounted for in the functional form of the constitutive equations.

References

- [1] Argon, A.S. (1985). Inelastic behavior of glassy and partially crystallized metallic alloys. *Proc. 7th Int. Conf. on the Strength of Metals and Alloys*, McQueen, H.J., Bailon, J.-P., Dickson, J.I., Jonas, J.J., and Akben, M.G. (Editors), Montreal, Canada, 12-16 August, pp. 2007-2030.
- [2] Ashby, M. F. and Duval, P. (1985). The creep polycrystalline ice. *Cold Regions Science and Technology*, Vol. 11, No.3, pp. 285-300.
- [3] Barnes, P., Tabor, D. and Walker, J.C.F. (1971). The friction and creep of polycrystalline ice. *Proc. Royal soc. London A*, 324, pp. 127-155.
- [4] Cole, D.M. (1990). Reversed direct stress testing of ice: Initial experiment results and analysis. *Cold Regions Science and Technology*, Vol. 18, No.3, pp. 303-321.
- [5] Cole, D.M. (1991). Anelastic straining in polycrystalline ice. In: *Proceedings of the 6th International Specialty Conference on Cold Regions Engineering*, Edited by D. Sodhi, pp. 504-518, West Lebanon, New Hampshire, 26-28 February.
- [6] Cole, D.M. (1994). The effect of microstructure and temperature on the constitutive behavior of ice at low strains. *IAHR Ice Symposium*, Trondheim, Norway, pp. 1-8.
- [7] Cole, D.M. (1995). A model for the anelastic straining of saline ice subjected to cyclic loading. *Philosophical Magazine*, In press.
- [8] Cole, D.M. and Durell, G.D. (1995). The cyclic loading of saline ice. *Philosophical Magazine*, In press.
- [9] Derradji-Aouat, A., Sinha, N. K. and Evgin, E. (1993). Experimental study of the behavior of columnar grained ice subjected to cyclic loading. *Proc. 12th Int. Conf. Offshore Mech. and Arctic Eng.*, Vol. 1, pp. 21-28.
- [10] Duval, P. (1976). Lois de fluage transitoire ou permanent de la glace polycrystalline pour divers eats de contrainte. *Annales de Geophysique*, Tom. 32, No. 4, pp. 335-350.
- [11] Duval, P. (1978). Anelastic behavior of polycrystalline ice. *Journal of Glaciology*, Vol. 21, No. 85, pp. 621-628.
- [12] Duval, P., Ashby, M.F. and Anderman, I. (1983). Rate-controlling processes in the creep of polycrystalline ice. *The Journal of Physical Chemistry*, Vol. 87, No. 21, pp. 4066-4074.
- [13] Duval, P., Kalifa, P. and Meyssonier, J. (1991). Creep constitutive equations for polycrystalline ice and effect of microcracking. *Proc. IUTAM/IAHR Symp. on Ice-Structure Interaction*, Jones, S.J., McKenna, R.F., Tillotson, J. and Jordaan, I.J. (Ed.), Springer-Verlag, pp. 55-67.

- [14] Gammon, P.H., H. Kiefte, M.J. Clouter, and W.W. Denner (1983), Elastic constants of artificial and natural ice samples by brillouin spectroscopy, *Journal of Glaciology* 29, 433-459.
- [15] Glen, J.W. (1955). The creep of polycrystalline ice. *Proc. Royal Soc. London, Ser. A*, 288(1175), pp. 519-538.
- [16] Goodman, D.J., Frost, H.J. and Ashby, M.F. (1981). The plasticity of polycrystalline ice. *Philosophical Magazine A*, 43(3), pp. 665-695.
- [17] Hobbs, P.V. (1974). *Ice Physics*. Clarendon Press, Oxford.
- [18] Homer, D.R. and Glen, J.W. (1978). The creep activation energies of ice. *Journal of Glaciology*, Vol. 21, No. 85, pp. 429-444.
- [19] Hondoh, T. and Higashi, A. (1983). Generation and absorption of dislocations at large-angle grain boundaries in deformed ice crystals. *Journal of Physical Chemistry*, Vol. 87, No. 21, pp. 4044-4050.
- [20] Jones, S.J. and Glen, J.W. (1969). The mechanical properties of single crystals of pure ice. *Journal of Glaciology*, Vol. 8, No. 54, pp. 463-473.
- [21] Kocks, U.F., Argon, A.S. and Ashby, M.F. (1975). Thermodynamics and kinetics of slip. *Progress in Materials Science*, Vol. 19.
- [22] Le Gac, H. and Duval, P. (1980). Constitutive relations for the nonelastic deformation of polycrystalline ice. *Proceedings of the IUTAM Symposium on the Physics and Mechanics of Ice*, Edited by P. Tryde, Springer, pp. 51-59.
- [23] Mellor M. and Cole, D. (1981). Cyclic loading and fatigue in ice. *Cold Regions Science and Technology*, Vol. 4, pp. 41-53.
- [24] Michel, B. (1978). The strength of polycrystalline ice. *Canadian Journal of Civil Engineering*, Vol. 5, No. 3, pp. 285-300.
- [25] Nakamura, T. and Jones, S.J. (1973). Mechanical properties of impure ice crystals. *Physics and Chemistry of Ice*, Whalley, E., Jones, S.J. and Gold, L.W. (Editors), pp. 365-369.
- [26] Nixon, W.A. and Smith, R.A. (1984). Preliminary results on the fatigue behavior of polycrystalline freshwater ice. *Cold Regions Science and Technology*, Vol. 9, No. 3, pp. 267-269.
- [27] Nixon, W.A. and Smith, R.A. (1987). The fatigue behavior of freshwater ice. *Journal De Physique*, Vol. 48, No. 3, pp. C1-329 to C1-335.
- [28] Norwick, A.S. and Berry, B.S. (1972). *Anelastic relaxation in crystalline solids*, Academic Press, New York, 677p.

- [29] Shyam Sunder, S. and Wu, M.S. (1989a). A differential flow model for polycrystalline ice. *Cold Regions Science and Technology*, Vol. 16, No. 1, pp. 45-62.
- [30] Shyam Sunder, S. and Wu, M.S. (1989b). A multiaxial differential model of flow in orthotropic polycrystalline ice. *Cold Regions Science and Technology*, Vol. 16, No. 2, pp. 223-235.
- [31] Sinha, N.K. (1978). Rheology of columnar-grained ice. *Experimental Mechanics*, Vol. 18, No. 12, pp. 464-470.
- [32] Sinha, N.K. (1979). Grain-boundary sliding in polycrystalline materials. *Philosophical Magazine A*, Vol. 40, No. 6, pp. 825-842.
- [33] Tatibouet, J., Perez, J. and Vassoille, R. (1986). High-temperature internal friction and dislocations in ice Ih. *Journal of Physique*, Vol. 47, No. 1, pp. 51-60.
- [34] Tatibouet, J., Perez, J. and Vassoille, R. (1987). Study of grain boundaries in ice by internal friction measurement. *Journal of Physique*, Colloque C1, No 12, 48, C1-197 to C1-203.
- [35] Weertman, J. (1973). Creep of Ice. Whalley, E., Jones, S.J. and Gold, L.W. (Editors), *Physics and Chemistry of Ice*, pp. 320-337.

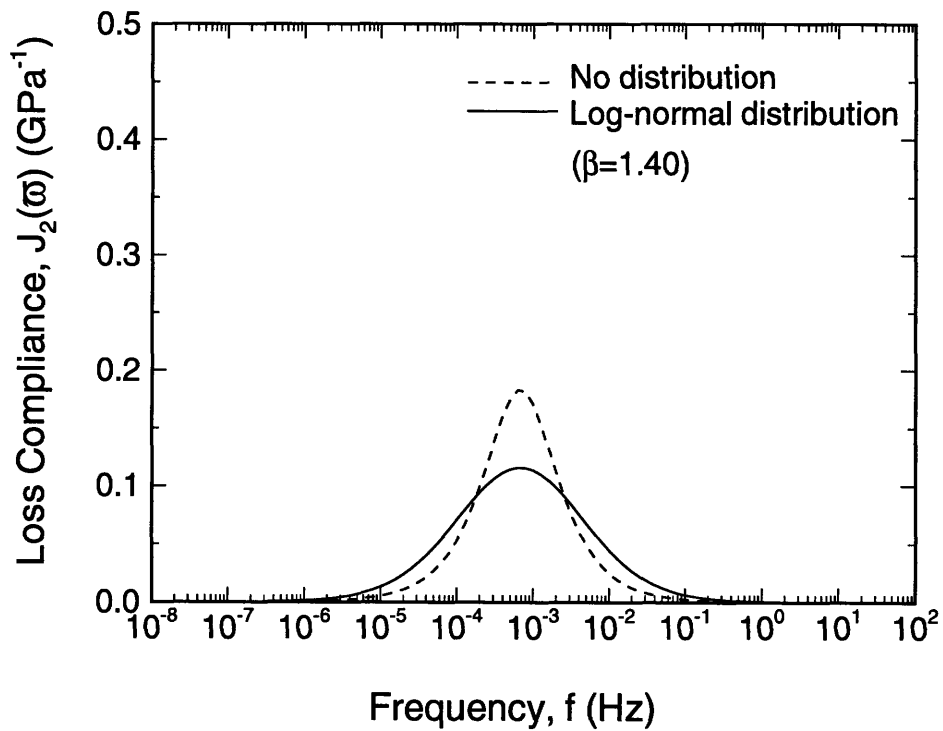
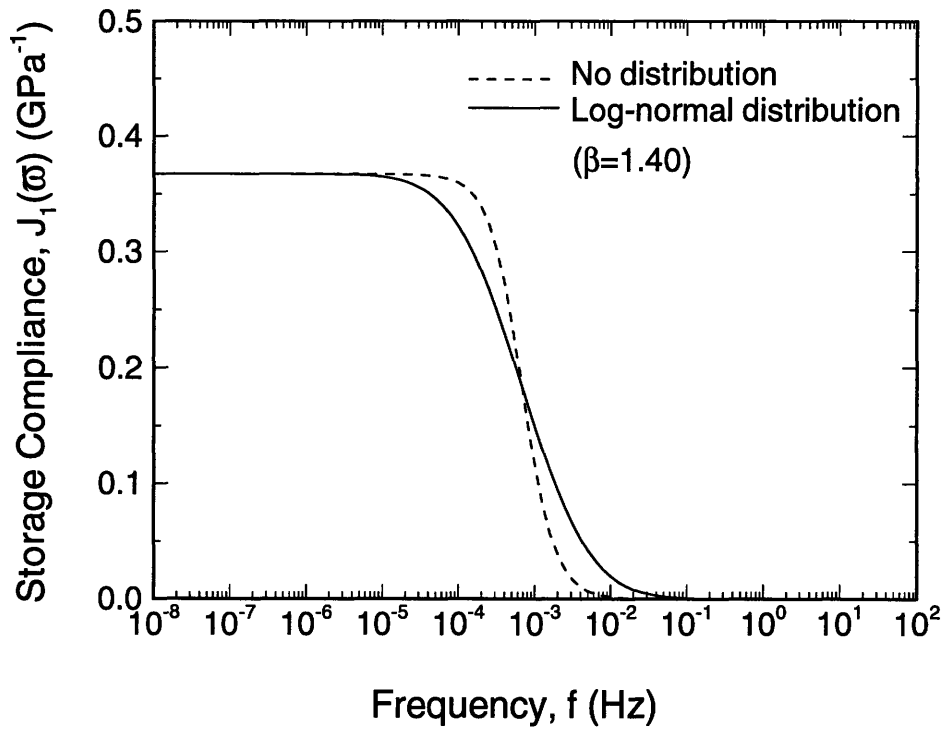


Figure 4-1: Dynamic compliance as a function of frequency at $T = -10^\circ\text{C}$: (a) the storage compliance, $J_1(\omega)$; (b) the loss compliance, $J_2(\omega)$.

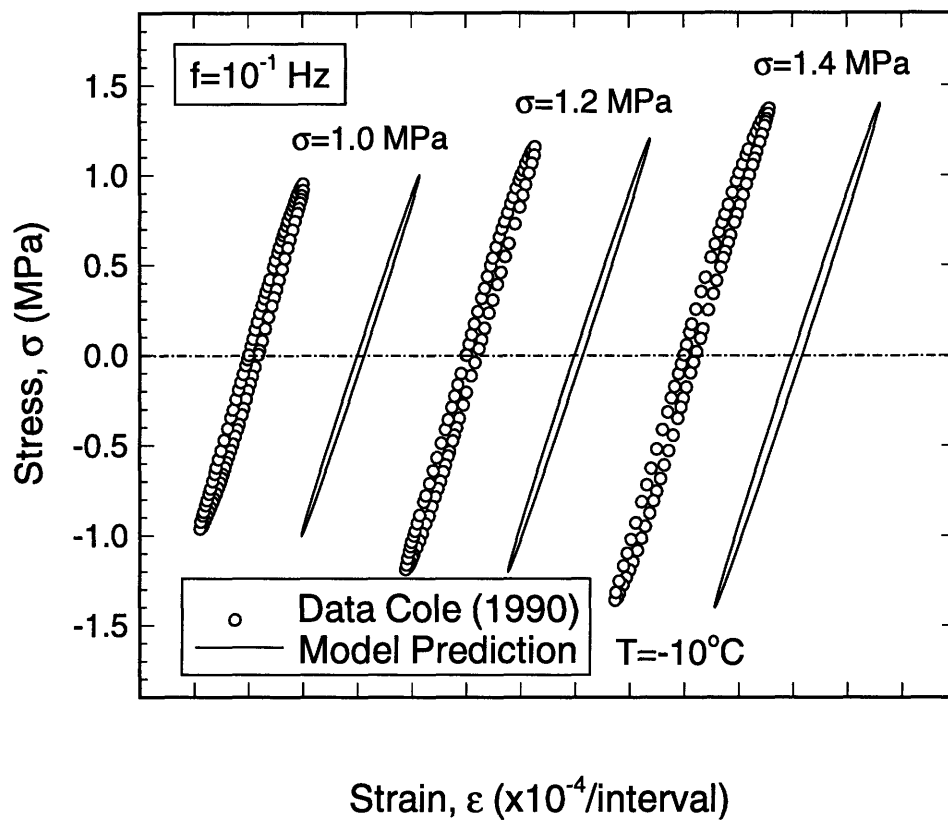


Figure 4-2: Stress-strain responses of polycrystalline ice (with a mean grain size of 5.1 mm) subjected to 0.1 Hz sinusoidal stress at -10°C ; experimental data of Cole (1990) and model predictions. Plots are translated along the strain axis for clarity.

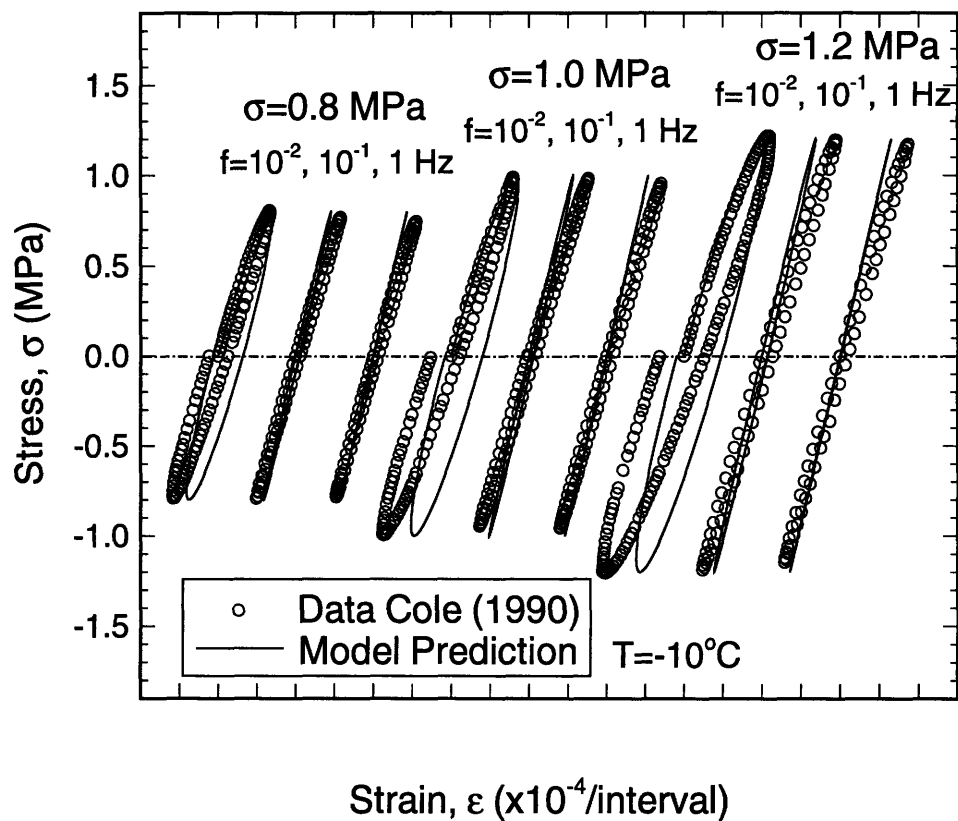


Figure 4-3: Stress-strain responses of polycrystalline ice (with a mean grain size of 1.5 mm) under various cyclic stress levels and frequencies at -10°C ; experimental data of Cole (1990) and model predictions. Plots are translated along the strain axis for clarity.

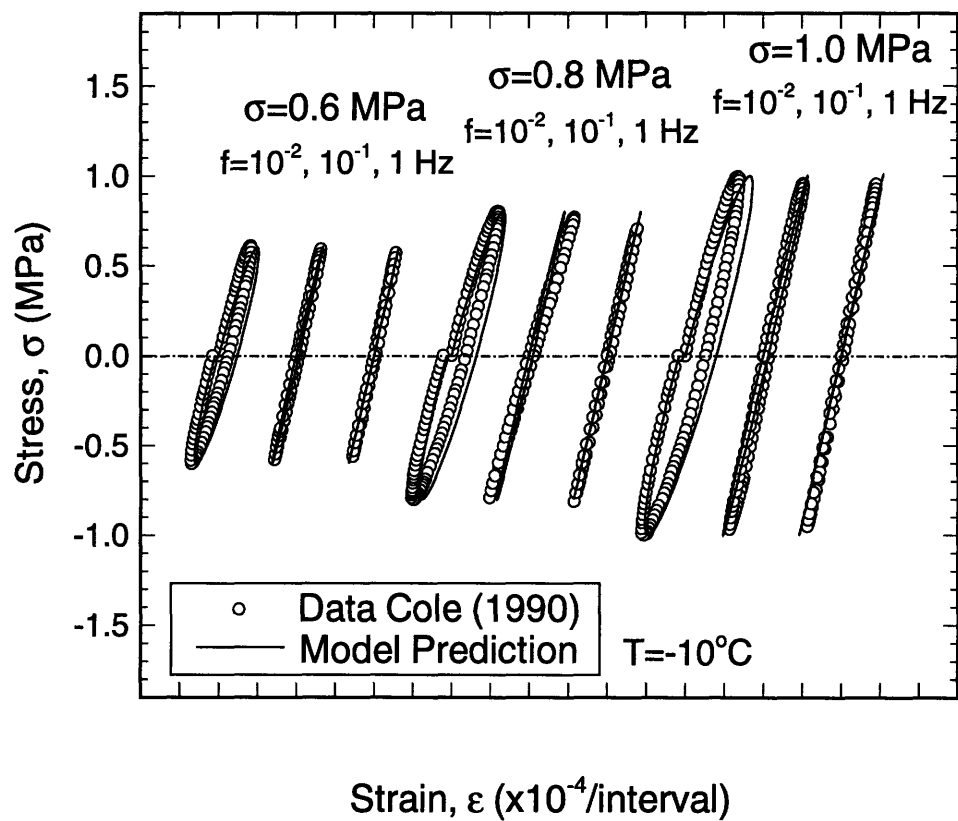


Figure 4-4: Stress-strain responses of polycrystalline ice (with a mean grain size of 5.0 mm) under various cyclic stress levels and frequencies at -10°C ; experimental data of Cole (1990) and model predictions. Plots are translated along the strain axis for clarity.

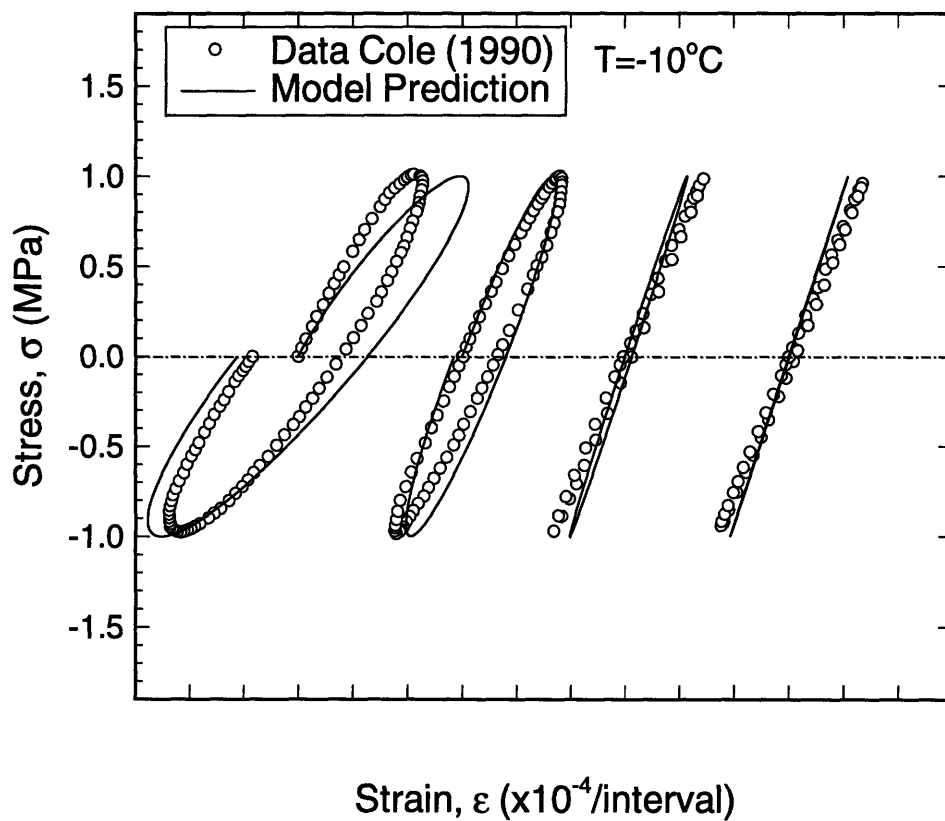


Figure 4-5: Stress-strain responses of polycrystalline ice (with a mean grain size of 2.5 mm) under various cyclic frequencies and 1 MPa stress at -10°C ; experimental data of Cole (1990) and model predictions. Plots are translated along the strain axis for clarity.

Chapter 5

A MULTIAXIAL CREEP MODEL, PART I: TRANSIENT CREEP

Abstract

This chapter describes a constitutive model of transient creep in orthotropic polycrystalline ice. In this study, the primary mechanisms controlling the macroscopic behavior are considered to be the motion and production of dislocations within grains and an interaction between basal and non-basal slip systems within constituent single crystals. Average equivalent stresses for single crystal ice and polycrystalline ice are defined. In particular, the equivalent stress for polycrystalline ice is obtained by averaging equivalent stresses for all single crystals in a representative volume. A specific form of dissipation potential, which incorporates internal stresses, is proposed for inelastic flow. The internal stresses, kinematic back stress and isotropic drag stress, describe various states of the microstructure in the material. Major features of the model include the hardening and recovery processes within evolution equations of the internal stresses. The proposed model satisfies the non-dimensional requirements of Ashby and Duval (1985) for strain, strain rate and time, and predicts the experimentally observed relationship between them with a fixed set of material parameters.

5.1 Introduction

In most engineering problems, polycrystalline ice exists at homologous temperatures exceeding $0.9T_M$. At these high temperatures, the creep of polycrystalline ice cannot be completely suppressed even at relatively high loading rates. Many constant stress or constant strain-rate tests and studies of deformation mechanisms have characterized polycrystalline ice behavior during the last several decades (e.g., Glen, 1955; Barnes et al., 1971; Weertman, 1973; Goodman et al., 1981; Mellor and Cole, 1982; Duval et al., 1983; Jacka, 1984). Most of these studies have emphasized the stress dependence of the steady-state creep rate under constant stress following the empirical power-law creep.

Both the elastic and inelastic behavior of polycrystalline ice are of great importance in a broad range of ice engineering problems. Several investigators have studied the transient creep of ice, since engineering applications invariably involve complex thermal and mechanical histories. Michel (1978) suggests a model based on easy slip on the basal plane and accompanying grain boundary sliding to accommodate total deformation. Sinha (1978, 1979) describes a phenomenological viscoelasticity model based on the mechanism of grain boundary sliding responsible for transient creep. In Sinha's model, the exponent in relaxation time is used to account implicitly for the distribution of relaxation time. Schapery (1991) has extended a non-linear viscoelastic model for composite materials to polycrystalline ice. His approach uses a stress function, instead of stress, in the integral representation of strain.

Constitutive models for polycrystalline ice based on internal state variables have been developed for monotonic constant stress loading (Le Gac and Duval 1980; Ashby and Duval, 1985; Shyam Sunder and Wu, 1989a, 1990; Meyssonier and Goubert, 1994). These internal state variables are used to describe phenomenologically various states of intracrystalline processes associated with dislocation activities. Internal state variables have been used in constitutive models for metallic materials (Miller, 1976; Hart, 1976; Chaboche, 1977; Anand, 1982), for rock materials (Aubertin et al., 1991), and for polymers (Boyce et al., 1988). Ashby and Duval (1985) develop a model based on two types of systems in which creep occurs in the basal (easy) systems on loading, then relaxes as stress transfers from the basal to the non-basal (hard) systems. This relaxation or redistribution of stress generates directional internal stress or back stress, which allows for the recovery of a fraction of transient creep upon unloading. Shyam Sunder and Wu (1989b) have proposed a multiaxial model for

transient creep based on the theory of internal state variables, which describe the change of microstructure of the material during deformation. In their model, the inelastic strain rate is decomposed into transient and viscous strain rates. To describe better both transient creep and the response to increments and decrements of applied load, Meyssonier and Goubert (1994) have proposed a model based on a decomposition of viscoplastic strain into two components, which account separately for the kinematic and isotropic hardenings.

The present study presents a multiaxial model of transient creep in orthotropic polycrystalline ice. The most significant aspect of the proposed model is the formulation of kinematic equations which are firmly based on physical processes that reflect salient microstructural aspects. In this study, the primary mechanism is considered to be the motion and production of dislocations and the creep anisotropy of single crystal ice. Major features of the model include the hardening and recovery processes within evolution functions of kinematic back stress and of isotropic drag stress. The evolution equations of these internal stresses satisfy the non-dimensional requirements of Ashby and Duval (1985) for transient creep.

This chapter is organized as follows. In Section 5-2, a brief discussion for the behavior of polycrystalline ice is presented. In addition, Section 5-2 also presents the flow equation of inelastic deformation for polycrystalline ice and the physical interpretation of internal stresses and their corresponding evolution equations, which describe various states of the microstructure of the material. Section 5-3 develops mathematical formulations for transient creep of anisotropic and isotropic polycrystalline ice based on the creep anisotropy of single crystal ice. Also in Section 5-3, average equivalent stresses for single crystal ice and polycrystalline ice are defined. In particular, the equivalent stress for polycrystalline ice is obtained by averaging equivalent stresses for all single crystals in a representative volume. A specific form of dissipation potential, which incorporates internal stresses, is proposed for inelastic flow. A particular form for evolution equations of internal stresses, kinematic back stress and isotropic drag stress, is proposed. A summary of model equations is given in Tables 5.1 and 5.2. In Section 5-4, the dimensionless variables for strain, strain rate, time, back stress and isotropic drag stress are used to express the dimensionless creep strain rate and the dimensionless evolution equations of the internal stresses. The dimensionless model shows a unique relationship between dimensionless variables and is independent of applied stress and temperature. Section 5-5 contains model parameters, normalization of available data under constant stress and the predictions of the model.

5.2 Background

5.2.1 Behavior of Polycrystalline Ice

The mechanical behavior of crystalline solids at high temperatures is controlled by thermally-activated rate processes. Thus, the behavior of polycrystalline ice is very sensitive to rate and temperature variations. Generally, the time-dependent inelastic deformation, so-called creep, is divided into three regimes under constant stress tests. The first regime, called transient or primary creep, shows the decrease in strain rate. The second regime, called steady-state or secondary creep, shows a constant strain rate. The third regime, called tertiary creep, shows an increase in strain rate. In polycrystalline ice, the region of increasing strain rate in a constant stress test arises at higher stress levels due to microcracking-induced damage and at lower stress levels due to the recrystallization process (Duval et al., 1983; Jacka and Budd, 1991).

The effects of microcracks on the creep have been incorporated phenomenologically in constitutive models (e.g., Sinha, 1988; Choi and Karr, 1989; Zhan et al., 1994). A more comprehensive study of these effects is presented in Chapter 6. Dynamic recrystallization is known to occur in polycrystalline ice after a critical strain, which can be approximately 1 % strain under low stress. This recrystallization can induce the development of a preferred c-axis orientation, and then accelerate the strain rate or decrease the flow strength (Duval et al., 1983). This phenomenon has not been fully understood physically, and therefore is not discussed in this thesis.

The strain rates from the diffusional creep mechanism are much smaller than those observed from a range of tests related to engineering applications. This observation suggests that the deformation of polycrystalline ice without microcracks is controlled by several processes, such as the motion and production of dislocations on slip planes within grains, and grain boundary sliding. The resistance to shear on the basal plane is at least 60 times less than that on the non-basal planes, such as prismatic and pyramidal planes, at -10°C (Duval et al., 1983). This great difference in resistance is known as creep anisotropy, which plays a major role in controlling the macroscopic behavior of polycrystalline ice.

Wei and Dempsey (1994) have discussed the plasticity of ice in terms of intersections

between the basal and non-basal dislocations. While the basal deformation of single crystals of ice may be described in terms of dislocation glide along basal planes, the rate of plastic deformation of polycrystalline ice is controlled by the climb process and the motion of the jogged non-basal dislocations. Liu et al. (1993) have studied the interaction of dislocations with grain boundaries in polycrystalline ice using X-ray topography. In their study, the areas near grain boundaries always deform before the grain interiors owing to stress concentrations. The grain boundary sliding is achieved by the rotation of grains and further enhanced when the adjoining crystals undergo slip, and lattice dislocations impinge on grain boundaries. However, since grain boundary sliding alone cannot account for large strains, the slip or climb of dislocations within grains has large effects on inelastic strain.

In this study of transient creep, the primary mechanisms are considered to be the motion and production of dislocations and the creep anisotropy of single crystal ice. The constitutive model consists of two types of kinetics: flow equation, which describes flow at a given structure or state of material; and evolution equations, which describe the rate of the change of microstructure under the influence of strain rate and temperature.

5.2.2 Flow Equation

The rate controlling mechanisms of inelastic deformation for freshwater polycrystalline ice are described by the motion (glide and/or climb) and production of dislocations within grains and on grain boundaries (Kocks et al., 1975). Hence, the inelastic strain rate is described by Orowan's equation (Orowan, 1940)

$$\dot{\epsilon}^c = \phi b \rho_m \nu \quad (5.1)$$

where ϕ is a geometric factor taking into account the orientation of the slip systems, b is the magnitude of Burgers vector, and ρ_m and ν are the average density and the average velocity of mobile dislocations, respectively.

For the rate process of the thermally-activated motion of dislocations, the dislocation velocity is given as

$$\nu = \nu_o \exp\left(-\frac{Q^*(\bar{\sigma})}{RT}\right) \quad (5.2)$$

where ν_o is a frequency factor, $Q^*(\bar{\sigma})$ is the apparent activation energy which is a function of effective stress $\bar{\sigma}$, R is the universal gas constant, and T is the absolute temperature in degrees Kelvin. It is noted that the dislocation velocity increases when the temperature is increased. In statistical mechanics, the net dislocation velocity from the forward and reverse activations over an energy barrier is given by

$$\nu = \nu_{fo} \exp\left(-\frac{Q_f^*(\bar{\sigma})}{RT}\right) - \nu_{ro} \exp\left(-\frac{Q_r^*(\bar{\sigma})}{RT}\right) \quad (5.3)$$

where ν_{fo} and ν_{ro} are constants in the forward and reverse activations, respectively. The apparent activation energies in the forward and reverse activations, Q_f^* and Q_r^* , are considered linearly dependent on effective stress as follows

$$Q_f^* = Q_f - V_f \bar{\sigma} \quad (5.4)$$

$$Q_r^* = Q_r - V_r \bar{\sigma} \quad (5.5)$$

where V_f and V_r are activation volumes for the forward and reverse activations, respectively. Substituting Eqs (5.4) and (5.5) into Eq. (5.3), the net dislocation velocity is given by

$$\nu = \nu_{fo} \exp\left(-\frac{Q_f - V_f \bar{\sigma}}{RT}\right) - \nu_{ro} \exp\left(-\frac{Q_r + V_r \bar{\sigma}}{RT}\right). \quad (5.6)$$

With the assumptions of symmetrical energy barriers for the forward and reverse activations, and a single flow mechanism:

$$V_f = V_r = V; \quad \nu_{fo} = \nu_{ro} = \nu_o/2; \quad Q_f = Q_r = Q \quad (5.7)$$

where Q is the activation energy of the rate-controlling dislocation mechanism, Eq. (5.6) reduces to

$$\nu = \frac{\nu_o}{2} \exp\left(-\frac{Q}{RT}\right) \left\{ \exp\left(\frac{V\bar{\sigma}}{RT}\right) - \exp\left(-\frac{V\bar{\sigma}}{RT}\right) \right\}. \quad (5.8)$$

Hence

$$\nu = \nu_o \exp\left(-\frac{Q}{RT}\right) \sinh \frac{V\bar{\sigma}}{RT}. \quad (5.9)$$

At low stresses, Eq. (5.9) reduces further to

$$\nu = \nu_o \exp\left(-\frac{Q}{RT}\right) \frac{V\bar{\sigma}}{RT}. \quad (5.10)$$

From experiments (Fukuda and Higashi, 1973; Shearwood and Whitworth, 1991), the average dislocation velocity ν at a given temperature is expressed by

$$\nu = C\bar{\sigma} \exp\left(-\frac{Q}{RT}\right) \quad (5.11)$$

where C is a constant. It is noted that Eq. (5.11) is equivalent to Eq. (5.10) at constant temperature.

Introduction of impurities in pure ice (e.g., HF-doped, NaCl-doped, HCL-doped ice) increases dislocation velocity in the crystals (Riley et al., 1978; Shearwood and Whitworth, 1991). HF-doped ice deforms much more easily than pure ice. However, at present a direct effect of doping on the velocity of dislocations is not understood.

The mobile dislocation density ρ_m depends on stress to the second power at minimum strain rate (Weertman, 1983):

$$\rho_m = \left(\frac{\bar{\sigma}}{\mu b}\right)^2. \quad (5.12)$$

Substitution of Eqs (5.1) and (5.11) into (5.12) results in the minimum strain rate

$$\dot{\epsilon}_{min}^c = A \exp\left(-\frac{Q}{RT}\right) \bar{\sigma}^n \quad (5.13)$$

where A is a temperature-independent constant and n is the stress exponent. This power-law creep at minimum strain rate is known as Norton's law, first recognized by Glen (1955), and widely accepted in the ice literature (e.g., Weertman, 1973; Goodman et al., 1981). For creep controlled by dislocation motion, where the inelastic strain rate is proportional to the product of the dislocation density and dislocation velocity, Weertman (1973) describes the third power stress dependence on the minimum strain rate in his microcreep model.

5.2.3 Evolution Equations

5.2.3.1 Internal Stress

The inelastic flow of polycrystalline ice at high temperatures is not related to the applied stress, but rather to the mean effective stress

$$\bar{\sigma} = f(\sigma, \sigma_i) \quad (5.14)$$

where σ is the applied stress and σ_i are the internal stresses. The origin of the concept of an internal stress is based on the observation of a discrepancy between the stress dependence of measured dislocation velocity and the stress dependence of the inelastic strain rate. The existence of the internal stress is verified physically by experimental methods, such as stress- and strain rate-dip tests during constant stress loading and constant strain rate loading, respectively (Duval et al., 1983). The results of these studies suggest that the evolution of the internal stress can be related to the evolution of complex dislocation substructures.

Due to hexagonal crystal structure, the creep anisotropy of single crystal ice is enormous. The strain rate of polycrystalline ice under compressive uniaxial stress is about 1000 times less than that of single crystal ice oriented for easy glide on the basal plane (Glen, 1955; Duval et al., 1983). The great difference in the strain rates of single crystal ice and polycrystalline ice can be accounted for by the fact that easy slip on the basal plane and difficult climb of dislocation on non-basal planes create internal stresses and thus the resolved shear stress on the basal plane of any grain in polycrystalline ice is less than the applied stress. This internal stress gives directional or kinematic hardening, as it opposes further deformation.

In addition to kinematic hardening, polycrystalline ice shows isotropic hardening. As described by Duval et al. (1983), short-range interactions between dislocations on parallel planes (Taylor hardening) or on intersecting planes (Forest hardening), or between moving dislocations and arrays of dislocations during cell walls induce non-directional or isotropic hardening. In the following, the mathematical relation between internal stress and dislocation density describes the evolution equation for isotropic drag stress.

5.2.3.2 Evolution Equations

The physical process that governs the strain rate- and temperature-dependence of inelastic deformation occurs as a result of the movement and production of the thermally-activated dislocations. The dislocations in the crystals provide obstacles for mobile dislocations. As the flow stress increases during the constant strain rate test or the strain rate decreases in transient creep during the constant stress test, polycrystalline solids exhibit work hardening, which can be explained by an increase of the dislocation density with increasing inelastic strain. The decrease of work hardening rate is attributed to recovery processes due to the rearrangement and annihilation of dislocations during deformation. Work hardening and recovery processes caused by cross slip, climb, and subboundary annihilation due to migration can describe the evolution of the dislocation density (Gottstein and Argon, 1987). While the deformation behavior at low temperatures is explained with recovery by cross slip, the steady state at high temperatures is based on recovery by dislocation climb.

The evolution of the average dislocation density ρ is described by the storage ρ^+ of mobile dislocations and the reduction ρ^- of dislocations by various recovery mechanisms:

$$\frac{d\rho}{d\epsilon^c} = \frac{d\rho^+}{d\epsilon^c} + \frac{d\rho^-}{d\epsilon^c} . \quad (5.15)$$

The storage rate of dislocation is given as

$$\frac{d\rho^+}{d\epsilon^c} = \frac{1}{bL} \quad (5.16)$$

where the storage length L is usually taken proportional to a constant C_1 times the average dislocation spacing l (Argon and Bhattacharya, 1987),

$$L = C_1 l = \frac{C_1}{\sqrt{\rho}} . \quad (5.17)$$

Thus, the storage rate of dislocation becomes

$$\frac{d\rho^+}{d\epsilon^c} = \frac{\sqrt{\rho}}{C_1 b} \quad (5.18)$$

which is an athermal buildup of dislocation density. The reduction of the dislocation density by the recovery process, such as cross slip of dislocations, is expressed as (Kocks, 1976; Argon

and Bhattacharya, 1987)

$$\frac{d\rho^-}{d\epsilon^c} = -D_s\rho \quad (5.19)$$

where D_s is a temperature-dependent constant related to a probability of cross slip:

$$D_s = D_{so} \exp\left(-\frac{Q}{RT}\right) \quad (5.20)$$

where D_{so} is a constant. Combining Eqs (5.18) and (5.19), the evolution of the average dislocation density becomes

$$\frac{d\rho}{d\epsilon^c} = \frac{\sqrt{\rho}}{C_1 b} - D_s\rho. \quad (5.21)$$

For the relation between internal stress and dislocation density, the internal stress corresponding to dislocation glide and climb is considered proportional to the square root of the corresponding dislocation density (e.g., Kocks et al., 1975):

$$\sigma_i = \alpha\mu b\sqrt{\rho} \quad (5.22)$$

where α is a constant and μ denotes the shear modulus. At constant temperature and constant strain rate, the hardening rate $d\sigma_i/d\epsilon^c$ is derived from Eqs (5.21) and (5.22) as

$$\frac{d\sigma_i}{d\epsilon^c} = \frac{\alpha}{2C_1}\mu - \frac{D_s}{2}\sigma_i. \quad (5.23)$$

It is noted that a linear dependence of hardening rate on internal stress appears in the presence of only glide-induced dynamic recovery. The evolution of internal stress with respect to time can be expressed by

$$\frac{d\sigma_i}{dt} = \left(\frac{\alpha}{2C_1}\mu - \frac{D_s}{2}\sigma_i\right)\dot{\epsilon}^c \quad (5.24)$$

where the dot denotes time derivative.

At high temperatures, the activation energy for steady-state creep is usually found to be constant and equal to the activation energy for self diffusion (Takeuchi and Argon, 1976). The dominant role of diffusion processes in deformation at high temperatures strongly supports the theory that the recovery process is dominated by climb. The reduction of the dislocation density by the lattice-diffusional recovery process due to the climb of edge dislocations is

written as (Gottstein and Argon, 1987)

$$d\rho^- = -\frac{D_c}{C_2}\rho^2 dt \quad (5.25)$$

where C_2 is a constant, D_c is given by

$$D_c = D_{co} \exp\left(-\frac{Q}{RT}\right) \quad (5.26)$$

and D_{co} is a constant. Combining Eqs (5.21), (5.22), and (5.25), the evolution equation of internal stress, which considers both dynamic and static recoveries in the deformation at high temperatures, can be written as

$$\frac{d\sigma_i}{dt} = \left(\frac{\alpha}{2C_1}\mu - \frac{D_s}{2}\sigma_i\right)\dot{\epsilon}^c - \frac{D_c}{2C_2}\frac{\sigma_i^3}{(\alpha\mu b)^2}. \quad (5.27)$$

If one considers only static recovery, Eq. (5.27) can be written as

$$\frac{d\sigma_i}{dt} = \frac{\alpha}{2C_1}\mu\dot{\epsilon}^c - \frac{D_c}{2C_2}\frac{\sigma_i^3}{(\alpha\mu b)^2}. \quad (5.28)$$

In general, the evolution of internal stress is simplified to

$$\dot{\sigma}_i = h\dot{\epsilon}^c - r \quad (5.29)$$

where the hardening rate, which includes the dynamic recovery term, is

$$h = \frac{d\sigma_i}{d\epsilon^c} = \frac{\alpha}{2C_1}\mu - \frac{D_s}{2}\sigma_i \quad (5.30)$$

and the rate of static recovery is

$$r = \frac{D_c}{2C_2}\frac{\sigma_i^3}{(\alpha\mu b)^2}. \quad (5.31)$$

When transient creep is a result of competing work hardening and recovery processes, a balance between these two processes is reached at steady-state condition. These processes are described in terms of $d\sigma/d\epsilon^c$ versus σ for the constant strain rate test and $d\dot{\epsilon}^c/d\epsilon^c$ versus $\dot{\epsilon}^c$ for the constant stress test. In the study of dynamic behavior of dislocations in polycrystalline ice, Fukuda and Higashi (1973) have observed annihilation of dislocations with two opposite

signs from a dipole or intersections.

In the modeling of transient creep, a logarithmic creep law has been observed in many ductile metals at low temperatures where recovery effects are negligible. At high temperatures, where recovery effects become observable, the transient creep rate is proportional to $t^{-2/3}$, leading to transient creep being proportional to $t^{1/3}$. Mott (1955) and Argon and Bhattacharya (1987) described this transient creep, which is known as Andrede's creep, as closely associated with rapid recovery or climb of dislocations in the work-hardening of metals. The transient strain rate, following Andrede's creep law, has also been observed in polycrystalline ice (Glen, 1955; Duval, 1976).

5.3 Development of a Constitutive Model

A physically-based constitutive model can be achieved if the physical mechanisms underlying the deformation process are adequately reflected in the functional form of the constitutive equations. The evolution of the microstructure of polycrystalline ice during transient creep and a detailed characterization of its relationship to macroscopic deformation are not fully understood. Nevertheless, a model is proposed to provide satisfactory descriptions of transient creep based on the underlying mechanisms.

In the following constitutive model, we will consider freshwater polycrystalline ice, with grain sizes between 1 mm and 10 mm, at temperatures between $-50^{\circ}C$ and $-10^{\circ}C$ (above $0.80 T_M$), and at strain rates between 10^{-7} and $10^{-5} s^{-1}$. Within this ductile regime, deformation is governed by several mechanisms, such as: the movement and production of dislocations, mostly within grains, grain boundary sliding, and the creep anisotropy of single crystal ice.

5.3.1 Material Anisotropy

The deformation of polycrystalline ice is highly non-linear and depends on loading rate and temperature, as well as on the granular microstructure. Since polycrystalline ice is made up of single ice crystals, its behavior is affected by the properties of individual crystals.

This Section describes a mathematical representation of the effect of the crystallographic orientation of single crystals on the elastic and inelastic responses of polycrystalline ice.

Following the contracted Voigt notation, vector notation is used instead of tensor notation. The total strain rate vector $\dot{\epsilon}$ is decomposed as follows

$$\dot{\epsilon} = \dot{\epsilon}^e + \dot{\epsilon}^c \quad (5.32)$$

where $\dot{\epsilon}^e$ and $\dot{\epsilon}^c$ are the elastic and inelastic strain rate “vectors” (in the sense of the contracted Voigt notation), respectively. The elastic strain rate vector is written as

$$\dot{\epsilon}^e = \mathbf{S} \dot{\sigma} \quad (5.33)$$

where $\dot{\sigma}$ is the applied stress vector and \mathbf{S} is the elastic compliance matrix of polycrystalline ice (see Appendix B of Chapter 5). The vector form of the strain and stress components are written as $\epsilon = [\epsilon_{11} \ \epsilon_{22} \ \epsilon_{33} \ \epsilon_{23} \ \epsilon_{13} \ \epsilon_{12}]^T$ and $\sigma = [\sigma_{11} \ \sigma_{22} \ \sigma_{33} \ \sigma_{23} \ \sigma_{13} \ \sigma_{12}]^T$, where superscript T denotes the transpose operation.

5.3.1.1 Single Crystal Ice

Due to hexagonal crystal structure, the creep anisotropy of single crystal ice is enormous (Glen and Perutz, 1954; Steinman, 1954; Higashi, 1968; Duval et al., 1983). Shear resistance on the basal plane is almost 60 times lower than that on the non-basal planes, such as prismatic and pyramidal planes. Therefore, crystals can more easily deform by dislocation glide on the basal planes than on the non-basal planes. The tests done by Higashi (1968) showed that at -19°C and a strain rate of $3 \times 10^{-6} \text{ s}^{-1}$, the peak uniaxial stress for non-basal slip in single crystal ice was between 10 and 20 times higher than the peak stress for basal slip. Slip in the basal plane, however, has been found not to be dependent on any direction (Glen and Perutz, 1954; Kamb, 1961; Hobbs, 1974). A direction perpendicular to the basal plane is known as the c -axis of the crystal. Single crystal ice, therefore, can be considered a transversely isotropic material.

Consider x_1' , x_2' , and x_3' to be the local frame axes of a single crystal with its c -axis parallel to the x_1' axis, as shown in Figure 5-1. The equivalent stress $\hat{\sigma}_e$ for a general

anisotropic material is defined as

$$\hat{\sigma}_e^2 = \frac{3}{c_1 + c_3} \left\{ \frac{c_1}{3}(\sigma'_{11} - \sigma'_{22})^2 + \frac{c_2}{3}(\sigma'_{22} - \sigma'_{33})^2 + \frac{c_3}{3}(\sigma'_{33} - \sigma'_{11})^2 + 2(c_4\sigma'_{23}{}^2 + c_5\sigma'_{13}{}^2 + c_6\sigma'_{12}{}^2) \right\} \quad (5.34)$$

where σ'_{11} , σ'_{22} , σ'_{33} , σ'_{23} , σ'_{13} , and σ'_{12} are stresses in the local frame; c_1 , c_2 , c_3 , c_4 , c_5 , and c_6 are material constants; and the $x1'$ -axis is chosen to be the reference direction so that $\hat{\sigma}_e = \sigma_{11}$ with states of stress $[\sigma_{11} \ 0 \ 0 \ 0 \ 0 \ 0]^T$.

For a transversely isotropic single crystal ice with its c -axis parallel to the $x1'$ axis, Eq. (5.34) is reduced to

$$\hat{\sigma}_e^2 = \frac{3}{2c_1} \left\{ \frac{c_1}{3}(\sigma'_{11} - \sigma'_{22})^2 + \frac{c_2}{3}(\sigma'_{22} - \sigma'_{33})^2 + \frac{c_1}{3}(\sigma'_{33} - \sigma'_{11})^2 + 2(c_4\sigma'_{23}{}^2 + c_6\sigma'_{13}{}^2 + c_6\sigma'_{12}{}^2) \right\} \quad (5.35)$$

where the local frame $x2'$ - $x3'$ is the plane of transverse isotropy. The equivalent stress has to be invariant when the coordinate system rotates around the c -axis. The same equivalent stress for states of stress $[0 \ \sigma \ -\sigma \ 0 \ 0 \ 0]^T$ and $[0 \ 0 \ 0 \ \sigma \ 0 \ 0]^T$ results in the following relationship:

$$c_1 + 2c_2 = 3c_4. \quad (5.36)$$

Therefore, among the four material constants, c_1 , c_2 , c_4 , c_6 , only three of them are independent.

The transformation law between the stresses in the local ($x1'$ - $x2'$ - $x3'$) and global ($x1$ - $x2$ - $x3$) frames has the following form:

$$\boldsymbol{\sigma}' = \mathbf{T}(\theta, \varphi) \boldsymbol{\sigma} \quad (5.37)$$

where $\boldsymbol{\sigma}'$ and $\boldsymbol{\sigma}$ are stress “vectors” (in the sense of the contracted Voigt notation) in the local and global coordinate systems, respectively; the three-dimensional transformation matrix $\mathbf{T}(\theta, \varphi)$ is given by Eq. (5.A5) in Section 5.7 Appendix A.

5.3.1.2 Columnar-grained S2 Polycrystalline Ice

We consider columnar-grained polycrystalline ice for which the c-axis orientation of the single crystals is randomly distributed in the plane normal to the axis of the column. Michel and Ramseier (1971) classified this ice as S2 ice. Figure 5-2 illustrates the structure of S2 ice for the case where the column axis coincides with the x3 direction. The c-axis lies in the x1-x2 plane (i.e., $\varphi = 0$), and the ice is considered isotropic in this plane. S2 ice, therefore, is transversely isotropic.

The equivalent stress for single crystal ice in terms of stresses in the global frame (x1-x2-x3) is obtained by the following stress transformation. The relationship between the stresses in the two frames is given by

$$\boldsymbol{\sigma}' = \mathbf{T}(\theta) \boldsymbol{\sigma} \quad (5.38)$$

where the three-dimensional transformation matrix $\mathbf{T}(\theta)$ is

$$\mathbf{T}(\theta) = \begin{bmatrix} c^2 & s^2 & 0 & 0 & 0 & 2cs \\ s^2 & c^2 & 0 & 0 & 0 & -2cs \\ 0 & 0 & 1 & 0 & 0 & 0 \\ 0 & 0 & 0 & c & -s & 0 \\ 0 & 0 & 0 & s & c & 0 \\ -cs & cs & 0 & 0 & 0 & c^2 - s^2 \end{bmatrix} \quad (5.39)$$

where $c = \cos \theta$ and $s = \sin \theta$, and θ denotes the angle between the c-axis and the global x1-axis (see Fig. 5-2). This transformation applies for the case when $x3'$ coincides with $x3$.

By substituting the stress components of Eq. (5.38) into Eq. (5.35), the equivalent stress for single crystal ice in the global reference frame is obtained as

$$\begin{aligned} \hat{\sigma}_e^2 = & \frac{3}{2c_1} \left\{ \frac{c_1}{3} \left(c^2 \sigma_{11} + s^2 \sigma_{22} + 2cs \sigma_{12} - s^2 \sigma_{11} - c^2 \sigma_{22} + 2cs \sigma_{12} \right)^2 \right. \\ & + \frac{c_2}{3} \left(s^2 \sigma_{11} + c^2 \sigma_{22} - 2cs \sigma_{12} - \sigma_{33} \right)^2 + \frac{c_1}{3} \left(\sigma_{33} - c^2 \sigma_{11} - s^2 \sigma_{22} - 2cs \sigma_{12} \right)^2 \\ & \left. + 2c_4 (c \sigma_{23} - s \sigma_{13})^2 + 2c_6 (s \sigma_{23} + c \sigma_{13})^2 + 2c_6 \left(-cs \sigma_{11} + cs \sigma_{22} + (c^2 - s^2) \sigma_{12} \right)^2 \right\}. \end{aligned} \quad (5.40)$$

The effect of the crystallographic orientation of individual grains on the inelastic response

in polycrystalline ice have been studied (Lile, 1978; Azuma, 1995). Considering that a polycrystalline aggregate is replaced by an equivalent homogeneous body and assuming that the stress field in each individual grain is assumed to be uniform and equal to the macroscopic stress in polycrystalline ice (Voigt, 1889; Sachs, 1928), the equivalent stress of an anisotropic polycrystalline aggregate can be obtained by weighting the equivalent stress at each crystal orientation by the relative frequency of that orientation. This averaging procedure over the representative volume V yields

$$\sigma_{eq}^2 = \int_V \int_0^\pi \hat{\sigma}_e^2(\theta) \Theta(\theta) d\theta dV \quad (5.41)$$

where $\Theta(\theta)$ is the probability density function of the c-axis orientation for the polycrystalline aggregates. The c-axes in S2 ice are uniformly distributed for all θ , ($0 \leq \theta \leq \pi$) and the probability density function of the c-axis becomes

$$\Theta(\theta) = \frac{1}{\pi}. \quad (5.42)$$

The equivalent stress for columnar-grained S2 polycrystalline ice can be obtained by an averaging of the equivalent stresses for all single crystals in a representative volume:

$$\sigma_{eq}^2 = \frac{1}{\pi} \int_0^\pi \hat{\sigma}_e^2(\theta) d\theta. \quad (5.43)$$

The substitution of Eq. (40) into Eq. (5.43) and simplifying the result yields

$$\sigma_{eq}^2 = \frac{3}{\beta} \left\{ \frac{a_1}{3} (\sigma_{11} - \sigma_{22})^2 + \frac{a_2}{3} (\sigma_{22} - \sigma_{33})^2 + \frac{a_2}{3} (\sigma_{33} - \sigma_{11})^2 + 2(a_4 \sigma_{23}^2 + a_4 \sigma_{13}^2 + a_6 \sigma_{12}^2) \right\} \quad (5.44)$$

where the global plane (x1-x2) is the plane of transverse isotropy; with β chosen to be $(a_1 + a_2)$ so that $\sigma_{eq} = \sigma_{11}$ when the stress components are described by the vector $\boldsymbol{\sigma} = [\sigma_{11} \ 0 \ 0 \ 0 \ 0 \ 0]^T$, i.e., the x1-axis is chosen to be a reference direction. Material constants are given in terms of the material constants of a single crystal:

$$\begin{aligned} a_1 &= \frac{3c_1 - c_2 + 6c_6}{8} \\ a_2 &= a_3 = \frac{c_1 + c_2}{2} \end{aligned}$$

$$\begin{aligned}
a_4 &= a_5 = \frac{c_4 + c_6}{2} \\
a_6 &= \frac{5c_1 + c_2 + 6c_6}{12}.
\end{aligned}
\tag{5.45}$$

The equivalent stress has to be invariant when the coordinate system rotates around the x3-axis. Since this invariance gives the same equivalent stress for states of stresses $[\sigma \ -\sigma \ 0 \ 0 \ 0 \ 0]^T$ and $[0 \ 0 \ 0 \ 0 \ 0 \ \sigma]^T$, the following relationship can be obtained:

$$2a_1 + a_2 = 3a_6. \tag{5.46}$$

Therefore, among the four parameters, a_1 , a_2 , a_4 , and a_6 , only three of them are independent. This result is also verified by substituting Eq. (5.45) into Eq. (5.46).

Equation (5.44) may be expressed in compact form:

$$\sigma_{eq}^2 = \frac{3}{\beta} \boldsymbol{\sigma}^T \mathbf{G} \boldsymbol{\sigma} \tag{5.47}$$

where the stress-transformation matrix \mathbf{G} is given by

$$\mathbf{G} = \begin{bmatrix} \frac{(a_1 + a_2)}{3} & -\frac{a_1}{3} & -\frac{a_2}{3} & 0 & 0 & 0 \\ -\frac{a_1}{3} & \frac{(a_1 + a_2)}{3} & -\frac{a_2}{3} & 0 & 0 & 0 \\ -\frac{a_2}{3} & -\frac{a_2}{3} & \frac{2a_2}{3} & 0 & 0 & 0 \\ 0 & 0 & 0 & 2a_4 & 0 & 0 \\ 0 & 0 & 0 & 0 & 2a_4 & 0 \\ 0 & 0 & 0 & 0 & 0 & 2a_6 \end{bmatrix}.
\tag{5.48}$$

5.3.1.3 Equiaxed-granular Polycrystalline Ice

Figure 5-3 shows equiaxed-granular polycrystalline ice in which the c-axis orientation of the constituent single crystals is randomly distributed in the three-dimensional (x1-x2-x3) space. This granular polycrystalline ice, therefore, is considered to be an isotropic material.

The transformation law between the stresses in the local and global frames is given by

$$\boldsymbol{\sigma}' = \mathbf{T}(\theta, \varphi) \boldsymbol{\sigma} \tag{5.49}$$

where $\boldsymbol{\sigma}'$ and $\boldsymbol{\sigma}$ are stress vectors in the local and global coordinate systems, respectively; the three-dimensional transformation matrix, $\mathbf{T}(\theta, \varphi)$, is given by Eq. (5.A5) in Section 5.7 Appendix A. The equivalent stress of single crystal ice in the global reference frame is obtained by substituting the stress components in Eq. (5.49) into Eq. (5.35).

Assuming, as done in columnar-grained S2 ice, that all grains undergo the same uniform stress and a polycrystalline aggregate is replaced by an equivalent representative body, the equivalent stress of an isotropic polycrystalline aggregate can be obtained by weighting the equivalent stress at each crystal orientation by the relative frequency of that orientation over the representative volume V :

$$\sigma_{eq}^2 = \int_V \int_0^\pi \int_{-\pi/2}^{\pi/2} \hat{\sigma}_e^2(\theta, \varphi) \Theta(\theta, \varphi) \cos(\varphi) d\varphi d\theta dV \quad (5.50)$$

where $\Theta(\theta, \varphi)$ is the probability density function of the c-axis orientation for the polycrystalline aggregate. The c-axes in equiaxed-granular polycrystalline ice are uniformly distributed for all θ ($0 \leq \theta \leq \pi$) and all φ ($-\pi/2 \leq \varphi \leq \pi/2$), thus the probability density function of the c-axis becomes

$$\Theta(\theta, \varphi) = \frac{1}{2\pi}. \quad (5.51)$$

The substitution of Eq. (5.51) into Eq. (5.50) results in

$$\sigma_{eq}^2 = \frac{1}{2\pi} \int_0^\pi \int_{-\pi/2}^{\pi/2} \hat{\sigma}_e^2(\theta, \varphi) \cos(\varphi) d\varphi d\theta. \quad (5.52)$$

The substitution of the equivalent stress of single crystal ice in the global reference frame into Eq. (5.52) and simplifying the result yields an averaged equivalent stress for equiaxed-granular polycrystalline ice:

$$\sigma_{eq}^2 = \frac{3}{\beta} \left\{ \frac{a}{3} (\sigma_{11} - \sigma_{22})^2 + \frac{a}{3} (\sigma_{22} - \sigma_{33})^2 + \frac{a}{3} (\sigma_{33} - \sigma_{11})^2 + 2a (\sigma_{23}^2 + \sigma_{13}^2 + \sigma_{12}^2) \right\} \quad (5.53)$$

where β is chosen to be $2a$ and the material constant a is given by

$$a = \frac{5a_1 + 4a_2 + 6a_6}{15}. \quad (5.54)$$

Equation (5.53) may be expressed in matrix notation as

$$\sigma_{eq}^2 = \frac{3}{2} \boldsymbol{\sigma}^T \mathbf{G} \boldsymbol{\sigma} \quad (5.55)$$

where the stress-transformation matrix \mathbf{G} for an isotropic polycrystalline ice is

$$\mathbf{G} = \begin{bmatrix} \frac{2}{3} & -\frac{1}{3} & -\frac{1}{3} & 0 & 0 & 0 \\ -\frac{1}{3} & \frac{2}{3} & -\frac{1}{3} & 0 & 0 & 0 \\ -\frac{1}{3} & -\frac{1}{3} & \frac{2}{3} & 0 & 0 & 0 \\ 0 & 0 & 0 & 2 & 0 & 0 \\ 0 & 0 & 0 & 0 & 2 & 0 \\ 0 & 0 & 0 & 0 & 0 & 2 \end{bmatrix}. \quad (5.56)$$

5.3.2 Inelastic Flow

This section develops a mathematical formulation for highly rate-dependent columnar-grained and equiaxed-granular polycrystalline ice based on the underlying mechanisms for their inelastic behavior. The constitutive equation is written as a function of two internal state variables, \mathbf{X} and B , as well as external variables, such as stress and temperature. The strain rate during transient creep at constant stress and temperature results both from the evolution of back stress \mathbf{X} as the kinematic hardening variable and the evolution of isotropic stress B as the isotropic hardening variable.

The model development assumes that the inelastic deformation is incompressible, with the same behavior in compression and tension. The following formulation assumes the major influence to be only the second invariant of the deviatoric stress tensor.

5.3.2.1 Inelastic strain rate

To derive the relationship between the inelastic strain rate $\dot{\boldsymbol{\epsilon}}^e$ and the stress $\boldsymbol{\sigma}$, the reduced equivalent stress for columnar-grained S2 polycrystalline ice may be expressed in matrix notation as

$$\sigma_{d,eq}^2 = \frac{3}{\beta} \boldsymbol{\sigma}_d^T \mathbf{G} \boldsymbol{\sigma}_d \quad (5.57)$$

where the reduced stress is defined as

$$\boldsymbol{\sigma}_d = \boldsymbol{\sigma} - \mathbf{X} \quad (5.58)$$

and the internal variable \mathbf{X} represents the back stress.

In the rate-dependent context, there is no yield/failure function and an inelastic dissipation function serves in deriving constitutive relations. If inelastic flow in polycrystalline ice *without microcracks* is taken to follow Glen's power law, a scalar-valued dissipation potential $\Phi_o(\boldsymbol{\sigma}, \mathbf{X}, B, T)$ of the Norton-Hoff type can be defined as

$$\Phi_o = \frac{\dot{\epsilon}_o B}{n+1} \left(\frac{\sigma_{d,eq}}{B} \right)^n \quad (5.59)$$

where n is the stress exponent, usually taken as 3 in the experimental literature, the internal variable B represents the isotropic drag stress, and $\dot{\epsilon}_o$ is a temperature-dependent reference strain rate. The effect of temperature on the reference strain rate is represented by an Arrhenius relationship:

$$\dot{\epsilon}_o = A_o \exp\left(-\frac{Q}{RT}\right) \quad (5.60)$$

where A_o is a temperature-independent constant, Q is the activation energy, R is the universal gas constant, and T is temperature in degrees Kelvin.

Normality between $\dot{\epsilon}^c$ and $\boldsymbol{\sigma}$ requires

$$\dot{\epsilon}^c = \frac{\partial \Phi_o}{\partial \boldsymbol{\sigma}_d}. \quad (5.61)$$

The inelastic strain rate is determined by substituting Eq. (5.59) into Eq. (5.61):

$$\dot{\epsilon}^c = \dot{\epsilon}_o \frac{3}{\beta} \left(\frac{\sigma_{d,eq}}{B} \right)^n \frac{\mathbf{G}\boldsymbol{\sigma}_d}{\sigma_{d,eq}}. \quad (5.62)$$

It is worth noting that for the special case of isotropic polycrystalline ice (i.e., a_1 to a_6 equal to 1) with no kinematic hardening, the inelastic strain rate is obtained from Eq. (5.62) as

$$\dot{\epsilon}^c = \dot{\epsilon}_o \frac{3}{2} \left(\frac{\sigma_{eq}}{B} \right)^n \frac{\boldsymbol{\sigma}'}{\sigma_{eq}} \quad (5.63)$$

where the equivalent stress is reduced to the classical von Mises equivalent stress

$$\sigma_{eq} = \left(\frac{3}{2} \boldsymbol{\sigma}' \cdot \boldsymbol{\sigma}' \right)^{1/2} \quad (5.64)$$

and a deviatoric stress $\boldsymbol{\sigma}'$ is defined as

$$\boldsymbol{\sigma}' = \boldsymbol{\sigma} - \sigma_m \mathbf{I}. \quad (5.65)$$

where σ_m is the hydrostatic stress and \mathbf{I} is the identity matrix.

Using the hypothesis of energy equivalence, the relationship between the equivalent stress defined in Eq. (5.57) and an equivalent strain rate measure can be established. The rate of dissipation of energy per unit volume, Φ_o , is given by:

$$\Phi_o = \boldsymbol{\sigma}_d^T \dot{\boldsymbol{\epsilon}}^c. \quad (5.66)$$

Application of the hypothesis then yields:

$$\boldsymbol{\sigma}_d^T \dot{\boldsymbol{\epsilon}}^c = \sigma_{d,eq} \dot{\epsilon}_{eq}^c \quad (5.67)$$

where $\dot{\epsilon}_{eq}^c$ is the equivalent inelastic strain rate. Substituting Eq. (5.62) into Eq. (5.67) and using Eq. (5.57) result in

$$\dot{\epsilon}_{eq}^c = \dot{\epsilon}_o \left(\frac{\sigma_{d,eq}}{B} \right)^n. \quad (5.68)$$

Given Eqs (5.57) and (5.68), the explicit expression for the equivalent inelastic strain rate can be expressed in matrix form as (Shyam Sunder and Wu, 1989b)

$$\dot{\epsilon}_{eq}^c = \frac{\beta}{3} \dot{\boldsymbol{\epsilon}}^{cT} \mathbf{H} \dot{\boldsymbol{\epsilon}}^c \quad (5.69)$$

where the strain-rate transformation matrix \mathbf{H} is given by

$$\mathbf{H} = \begin{bmatrix} \frac{3(a_1 + a_2)a_2^2}{a^{*2}} & \frac{-3a_1a_2^2}{a^{*2}} & \frac{-3a_1a_2^2}{a^{*2}} & 0 & 0 & 0 \\ \frac{-3a_1a_2^2}{a^{*2}} & \frac{3(a_1 + a_2)a_2^2}{a^{*2}} & \frac{-3a_1a_2^2}{a^{*2}} & 0 & 0 & 0 \\ \frac{-3a_1a_2^2}{a^{*2}} & \frac{-3a_1a_2^2}{a^{*2}} & \frac{6a_1^2a_2}{a^{*2}} & 0 & 0 & 0 \\ 0 & 0 & 0 & \frac{1}{2a_4} & 0 & 0 \\ 0 & 0 & 0 & 0 & \frac{1}{2a_4} & 0 \\ 0 & 0 & 0 & 0 & 0 & \frac{1}{2a_6} \end{bmatrix} \quad (5.70)$$

where $a^* = 2a_1a_2 + a_2^2$. Eq. (5.69) reduces to the equivalent strain rate for isotropic materials if the material parameters a_1 to a_6 are equal to 1.

In this section, material or texture anisotropy effects during transient flow are modeled orthotropically by defining equivalent values for the thermodynamic force tensors in a manner analogous to the Hill-criterion of plastic yield (Hill, 1950). The three parameters which are used to describe columnar-grained S2 polycrystalline ice can be estimated from the material constants of single crystal ice.

The proposed model has some similar features with the transient creep model developed by Shyam Sunder and Wu (1989b). These models differ, however, in that the proposed model has an inelastic strain rate whereas Shyam Sunder and Wu's model have two inelastic strain rates in their formulation. In addition, evolution equations of internal stresses in the proposed model are different from those of Shyam Sunder and Wu's model. In the following section, evolution equations for the internal stresses are formulated using strain hardening and recovery processes.

5.3.2.2 Evolution equations of internal stresses

In the previous section, the kinetic equation described the dependence of the inelastic strain rate on applied stress, temperature, and internal stresses. In particular, the macroscopic inelastic strain rate in the incremental form was a function of applied stress, isotropic drag stress was related to isotropic hardening, and internal back stress was related to kinematic hardening. The change in microstructure is described by the evolution equations of these

internal stresses.

The internal state variable used for isotropic hardening is some measure of the current flow stress or level of work hardening used to account for the changes in size of the flow surface in the classical theory of plasticity. The internal state variable for kinematic hardening describes the back stress responsible for the anelastic response. If flow surfaces were defined as surfaces of constant flow rate analogous to yield surfaces, the back stress would be the location of the center of a set of surfaces.

Kinematic back stress, \mathbf{X}

Kinematic hardening is attributed to the directional internal stress caused by the creep anisotropy of single crystal ice, the great difference in resistance to creep between the basal plane and non-basal planes. When ice is unloaded, this internal stress is responsible for large recoverable strain. At small strains, however, the reversible motion of dislocations results in anelastic strain. The anelastic strain depends on the specific motion of the dislocation structure, such as the dislocation bowing-out by pinning at dislocation networks and the dislocation pile-up at strong barriers such as grain boundaries (Cole, 1991). Grain boundary sliding may also affect a significant part of the recoverable transient creep.

It is very important to include back stress in the constitutive model for time-dependent recoverable strain upon unloading and for cyclic behavior. This back stress influences the shapes and stabilizations of cyclic hysteresis loops. For monotonic increasing deformation, the back stress increases from zero, and saturates when the creep strain rate reaches its steady-state value. The increase of the back stress results in kinematic hardening. The Bauschinger effect can be attributed to the interaction of dislocations resulting in the internal back stress field.

The following evolution equation of kinematic back stress \mathbf{X} is proposed

$$\dot{\mathbf{X}} = h_1 E (\dot{\epsilon}^c - r_1 \mathbf{X}^n) \quad (5.71)$$

where E is the isotropic Young's modulus, h_1 is the kinematic hardening constant, and r_1 is the recovery constant.

Isotropic drag stress, B

Since isotropic hardening is a result of the way dislocations interact and trap each other, and thus depends on the statistics of their distributions and motion, the processes contributing to isotropic hardening are dipole formation, Forest hardening, the formation of kink bands of cell boundaries, and combinations of these (Ashby and Duval, 1985). The dislocation density in ice increases in transient creep during constant stress loading; thus the change of deformation resistance represents the isotropic hardening effect of the average dislocation density.

In the case of polycrystalline ice, most of the structural changes of interest during transient creep occur for strains whose magnitude is typically less than 1 %. From the assumption that isotropic hardening is related to dislocation interactions due to the change of the dislocation density, the isotropic variable describes the characteristics of the resistance to inelastic flow.

The following evolution equation of isotropic drag stress B is proposed

$$\dot{B} = \frac{h_2 E}{\sigma_{d,eq}} (B_{sat} - B) |\dot{\epsilon}_{eq}^c| \quad (5.72)$$

where h_2 is the isotropic hardening constant and B_{sat} is the saturated value of B .

5.3.2.3 Summary of model equations

A summary of the multiaxial creep model for transversely isotropic polycrystalline ice is presented in Table 5.1. A summary of the isotropic one-dimensional model is shown in Table 5.2. The governing equations of the model are summarized here for isotropic polycrystalline ice under uniaxial stress σ .

While the initial value of X is zero for an annealed material prior to loading, the initial value of B , i.e. B_o , may represent the annealed state of the material or some level of initial hardening introduced by pre-straining. The internal stresses X and B evolve with strain and time. Steady-state is reached when the inelastic strain rate becomes the minimum strain rate and the evolution rates of internal stresses decay to zero.

By defining the steady-state values of X and B as:

$$X_{sat} = k_1 \sigma \quad (5.73)$$

$$B_{sat} = k_2 B_o , \quad (5.74)$$

the minimum strain rate can be derived by substituting Eqs (5.73) and (5.74) into Eq. (5.88):

$$\dot{\epsilon}_{min}^c = \dot{\epsilon}_o \left(\frac{1 - k_1}{k_2 B_o} \right)^n \sigma^n \quad (5.75)$$

where k_1 and k_2 are dimensionless constants. The minimum strain rate is also defined when both $\dot{X} = 0$ and $\dot{B} = 0$ from Eqs (5.89) and (5.90), respectively, i.e.

$$\dot{\epsilon}_{min}^c = r_1 X_{sat}^n \quad (5.76)$$

$$B = B_{sat} . \quad (5.77)$$

The recovery constant r_1 is obtained by equating Eqs (5.75) to (5.76):

$$r_1 = \dot{\epsilon}_o \left(\frac{1 - k_1}{k_1 k_2 B_o} \right)^n . \quad (5.78)$$

Table 5.1: Summary of the multiaxial creep model

- Total strain rate

$$\dot{\epsilon} = \dot{\epsilon}^e + \dot{\epsilon}^c \quad (5.79)$$

- Elastic strain rate

$$\dot{\epsilon}^e = \mathbf{S} \dot{\sigma} \quad (5.80)$$

- Inelastic strain rate

$$\dot{\epsilon}^c = \dot{\epsilon}_o \frac{3}{\beta} \left(\frac{\sigma_{d,eq}}{B} \right)^n \frac{\mathbf{G} \sigma_d}{\sigma_{d,eq}} \quad (5.81)$$

where $\dot{\epsilon}_o = A_o \exp\left(-\frac{Q}{RT}\right)$; $\sigma_d = \sigma - \mathbf{X}$; $\sigma_{d,eq}^2 = \frac{3}{\beta} \sigma_d^T \mathbf{G} \sigma_d$; $\beta = a_1 + a_2$ (5.82)

$$\mathbf{G} = \begin{bmatrix} \frac{(a_1 + a_2)}{3} & -\frac{a_1}{3} & -\frac{a_2}{3} & 0 & 0 & 0 \\ -\frac{a_1}{3} & \frac{(a_1 + a_2)}{3} & -\frac{a_2}{3} & 0 & 0 & 0 \\ -\frac{a_2}{3} & -\frac{a_2}{3} & \frac{2a_2}{3} & 0 & 0 & 0 \\ 0 & 0 & 0 & 2a_4 & 0 & 0 \\ 0 & 0 & 0 & 0 & 2a_4 & 0 \\ 0 & 0 & 0 & 0 & 0 & 2a_6 \end{bmatrix} \quad (5.83)$$

- Kinematic back stress

$$\dot{\mathbf{X}} = h_1 E (\dot{\epsilon}^c - r_1 \mathbf{X}^n) \quad \text{where} \quad r_1 = \dot{\epsilon}_o \left(\frac{1 - k_1}{k_1 k_2 B_o} \right)^n \quad (5.84)$$

- Isotropic drag stress

$$\dot{B} = \frac{h_2 E}{\sigma_{d,eq}} (B_{sat} - B) |\dot{\epsilon}_{eq}^c| \quad \text{where} \quad B_{sat} = k_2 B_o \quad (5.85)$$

Table 5.2: Summary of the isotropic one-dimensional creep model

- Total strain rate

$$\dot{\epsilon} = \dot{\epsilon}^e + \dot{\epsilon}^c \quad (5.86)$$

- Elastic strain rate

$$\dot{\epsilon}^e = \frac{\dot{\sigma}}{E} \quad (5.87)$$

- Inelastic strain rate

$$\dot{\epsilon}^c = \dot{\epsilon}_o \left(\frac{\sigma - X}{B} \right)^n \quad \text{where} \quad \dot{\epsilon}_o = A_o \exp \left(-\frac{Q}{RT} \right) \quad (5.88)$$

- Kinematic back stress

$$\dot{X} = h_1 E (\dot{\epsilon}^c - r_1 X^n) \quad \text{where} \quad r_1 = \dot{\epsilon}_o \left(\frac{1 - k_1}{k_1 k_2 B_o} \right)^n \quad (5.89)$$

- Isotropic drag stress

$$\dot{B} = \frac{h_2 E}{\sigma - X} (B_{sat} - B) |\dot{\epsilon}^c| \quad \text{where} \quad B_{sat} = k_2 B_o \quad (5.90)$$

5.4 Model Formulation with Dimensionless Variables

For a special case of constant stress loading, Ashby and Duval (1985) have suggested that unique relationships exist between certain dimensionless variables for polycrystalline ice, up to the point where the minimum strain rate occurs. Such relationships are predicted by the proposed model as shown below.

For creep of polycrystalline ice at constant applied stress, Ashby and Duval (1985) have considered the following dimensionless variables for strain, strain rate and time:

$$\tilde{\epsilon} = \frac{\epsilon E}{\sigma} \quad (5.91)$$

$$\tilde{\epsilon} = \frac{\dot{\epsilon}}{\dot{\epsilon}_{min}} \quad (5.92)$$

$$\tilde{t} = \frac{t\dot{\epsilon}_{min}E}{\sigma} . \quad (5.93)$$

The internal stresses in the proposed model are normalized in the following form:

$$\tilde{X} = \frac{X}{\sigma} \quad (5.94)$$

$$\tilde{B} = \frac{B}{B_o} . \quad (5.95)$$

Initial values for dimensionless variables \tilde{X} and \tilde{B} are 0 and 1, respectively. The steady-state values of X and B are defined in Eqs (5.73) and (5.74), and hence their dimensionless steady-state values are k_1 and k_2 , respectively.

By substituting Eqs (5.91)-(5.95) in Eqs (5.88)-(5.90), the following dimensionless strain (creep) rate and evolution equations of the internal variables are obtained:

$$\tilde{\epsilon}^c = \left(\frac{k_2}{1 - k_1} \right)^n \left(\frac{1 - \tilde{X}}{\tilde{B}} \right)^n \quad (5.96)$$

$$\dot{\tilde{X}} = h_1 \left\{ \tilde{\epsilon}^c - \left(\frac{\tilde{X}}{k_1} \right)^n \right\} \quad (5.97)$$

$$\dot{\tilde{B}} = h_2 k_2 \left(\frac{k_2 - \tilde{B}}{1 - \tilde{X}} \right) \tilde{\epsilon}^c . \quad (5.98)$$

As shown in Eqs (5.96)-(5.98), the model predicts an unique relationship between dimensionless variables and is independent of applied stress level and temperature. The dimensionless model predictions with normalized creep data are given in Section 5.5.2.

5.5 Model Predictions and Experimental Validation

5.5.1 Model Parameters

Elastic Parameters

The elastic constants of polycrystalline ice are given in Appendix B of Chapter 5. The dynamic elastic constants of single crystal ice were determined at $T = -16^\circ C$ using the method of Brillouin spectroscopy, by Gammon et al. (1983). The theoretical effective elastic constants of polycrystalline ice can be computed by using various homogenization methods, such as the Ruess and Voigt assumptions (Sinha, 1989; Nanthikesan and Shyam Sunder, 1994), the self-consistent method (Wang and Schapery, 1995), and a computational model (Elvin, 1996).

Creep Parameters

The values of material parameters n , Q , A , B_o , k_1 , k_2 , r_1 , h_1 and h_2 for polycrystalline ice may be determined from isothermal constant stress tests in the following procedure.

The minimum strain (creep) rate for polycrystalline ice at high temperatures is given as a function of stress σ and temperature T :

$$\dot{\epsilon}_{min}^c = A \exp\left(-\frac{Q}{RT}\right) \sigma^n \quad (5.99)$$

where A is a temperature-independent constant, Q is the apparent creep activation energy, R is the universal gas constant equal to $8.314 J mol^{-1} K^{-1}$, T is the temperature in degrees Kelvin, and n is the stress exponent, usually taken as 3 (Glen, 1955; Weertman, 1973). The determination of the creep parameters n , A and Q for columnar-grained freshwater ice, sea ice and equiaxed-granular freshwater ice have been extensively investigated in the ice literature (Gold, 1973; Homer and Glen, 1978; Hooke, 1981; Sinha, 1978; Duval et al., 1983; Weertman, 1983; Sanderson, 1984).

The apparent activation energy can be obtained from Eq. (5.99), when the minimum

creep rate is known at two different temperatures T_1 and T_2 for a given stress σ , as follows:

$$Q = \frac{RT_1T_2}{T_1 - T_2} \ln \left(\frac{\dot{\epsilon}_{min1}^c}{\dot{\epsilon}_{min2}^c} \right) \quad (5.100)$$

where $\dot{\epsilon}_{min1}^c$ and $\dot{\epsilon}_{min2}^c$ are minimum strain rates at temperature T_1 and T_2 , respectively.

Three values of A are determined from three sources for different ice type; the data of Sinha (1978) on columnar-grained S2 freshwater ice, the data compiled by Duval et al. (1983) for isotropic freshwater ice and the data compiled by Sanderson (1984) for columnar-grained freshwater ice and sea ice.

Under a constant stress test, the initial value of B , i.e. B_o , can be estimated from experimental measurement of the initial creep rate by equating the initial creep rate of the model:

$$\dot{\epsilon}_{ini}^c (exp.) = \dot{\epsilon}_o \left(\frac{\sigma}{B_o} \right)^n \quad (5.101)$$

where the initial value of R is zero, the constant A_o may be set to unity without loss of generality.

For a given n , A and B_o , the values of k_1 and k_2 , used in the steady-state values of X and B , may be estimated as follows. The usual way to determine internal stress at a given stress and temperature is to conduct a constant stress test at some base stress, and then impose a stress reduction. The strain response is characterized by an instantaneous elastic strain recovery followed by an incubation period of creep rate and a transient period during which the creep rate decreases. The creep rate achieved just after the stress reduction is the creep rate associated with the new stress, but with the old microstructure. The stress measured at the zero creep rate may be interpolated as the internal back stress at the original base stress and temperature.

The zero creep rate just after a stress reduction $\Delta\sigma$ during steady-state flow under a base stress σ gives the relationship that the reduced stress equals the saturated back stress at the original base stress:

$$\sigma - \Delta\sigma = R_{sat} = k_1\sigma \quad (5.102)$$

from which the value of k_1 may be estimated. The value of k_2 is estimated by equating the

two minimum creep rates, Eqs (5.75) and (5.99):

$$A_o \left(\frac{1 - k_1}{k_2 B_o} \right)^n = A . \quad (5.103)$$

The recovery constant r_1 is given in Eq. (5.78) as:

$$r_1 = \dot{\epsilon}_o \left(\frac{1 - k_1}{k_1 k_2 B_o} \right)^n . \quad (5.104)$$

The parameters h_1 and h_2 govern the rate and amount of kinematic and isotropic hardening, respectively. The values of these parameters are estimated from experimental creep data by an iterative curve-fitting procedure. For highly textured ice associated with a relatively small component of creep strain the value of h_1 is very small. It follows that steady-state will be achieved in a short period of time. On the other hand, for an untextured isotropic polycrystalline ice associated with a relatively large component of creep strain, the value of h_1 is small and it takes much longer to achieve steady-state (Shyam Sunder and Wu, 1990).

The model parameters c_1 , c_2 , and c_6 are used to represent the creep anisotropy of ice single crystals. Without loss of any generality, c_2 can be taken as 1. Thus only two parameters need to be determined from constant stress tests on single crystal ice.

5.5.2 Model Predictions with Normalized Creep Data

Comparison of model predictions with the creep data of Jacka

Ashby and Duval (1985) proposed that under constant applied stress dimensionless variables for strain, strain rate and time that can be used to develop master curves for creep data, which are independent of the loading parameters, such as applied stress level and temperature.

Jacka (1984) has published results of uniaxial compression tests on isotropic (equiaxed-granular) polycrystalline ice with a mean grain size of 1.7 ± 0.2 mm. The samples were tested under constant stresses ranging from 0.1 to 1.5 MPa at the following specific temperatures: -5.0 , -10.6 , -17.7 and $-32.5^\circ C$. Figures 5-4, 5-5 and 5-6 show plots for Jacka's

data (taken from Ashby and Duval, 1985) corresponding to $\tilde{\epsilon}$ versus \tilde{t} , $\tilde{\epsilon}$ versus \tilde{t} and $\tilde{\epsilon}$ versus $\tilde{\epsilon}$, respectively. The predictions of the model are indicated by solid lines with the chosen parameters:

$$n = 3; k_1=0.1; k_2=3.2; h_1=1/70; h_2=1/30.$$

Also shown are the model predictions of Sinha's equation (1978) (modified by Ashby and Duval, 1985) with values of $n=3$, $A=70$, $C''=1.6 \times 10^{-2}$ and of Le Gac and Duval's equation (1980) with values of $n=3$, $h=100 \text{ MPa}$, $h'=600 \text{ MPa}$, $k=0.71$, $k'=0.28$, $hB/\alpha k^3=6.14 \times 10^5$. The predictions of Shyam Sunder and Wu (1989a, 1990) are shown in the same figures using their model parameters, $n=3$, $A=0.0142$, $B_o=0.286$ and $\tilde{H}=0.02$. Both Shyam Sunder and Wu (1989a, 1990) and the proposed model satisfy the non-dimensional requirements and capture the trend of the normalized creep data of Jacka (1984). These models, however, differ in several ways: while the total inelastic rate in Shyam Sunder and Wu's model is the sum of two components, a transient component and a steady-state component, there is only one component, inelastic strain rate, in the proposed model; while evolution equations in Shyam Sunder and Wu's model have constant dynamic recovery terms, those of the proposed model have varying dynamic and static recovery terms, which more closely correspond to the underlying mechanisms.

Comparison of model predictions with the creep data of Mellor and Cole

Using the non-dimensional variables introduced by Ashby and Duval (1985), the constant stress creep data of Mellor and Cole (1982) with a range of stresses (0.8 - 3.8 MPa), and temperature at -5°C are non-dimensionalized. Figures 5-7, 5-8 and 5-9 show plots for the data of Mellor and Cole (1982) corresponding to $\tilde{\epsilon}$ versus \tilde{t} , $\tilde{\epsilon}$ versus \tilde{t} and $\tilde{\epsilon}$ versus $\tilde{\epsilon}$. The predictions of the model are plotted with solid lines with the following parameters:

$$n = 3; k_1=0.25; k_2=1.5; h_1=1/70; h_2=1/15.$$

The normalized data shows considerable scatter in tertiary creep as well as in transient creep. Compared to 0.1 to 1.5 MPa in the experiments of Jacka (1984), higher stress levels in the experiments of Mellor and Cole (1982) caused microcracks in the ice specimens and these microcracks enhance the creep rate during the transient creep. As a result, the minimum strain rate occurs in the range $\tilde{t}=1.0$ to 1.5 in Mellor and Cole's ice, while in Jacka's ice $\tilde{t}=1.5$ to 2.0.

Mellor and Cole (1982) and Lawrence and Cole (1982) have reported that microcracks start to form at a certain strain. As mentioned by Ashby and Duval (1985), the non-dimensional variables are applicable only up to the stage where the minimum strain rate occurs and internal microcracks are not present. The loss of experimental accuracy at small strains, as mentioned by Mellor and Cole (1982), makes it difficult for us to determine the required model parameters.

Even though the model predictions capture the trend of the normalized data up to the transient creep, a more comprehensive creep model, which incorporates the effects of microcracking, needs to be developed. It is also worth noting that the experimental data obtained from a number of ice crystals and polycrystalline ice tested at the same strain rate and temperature are scattered. This is believed to be due to the differences in the initial dislocation density and the non-uniform crystallographic orientations of single crystals in the polycrystalline aggregate. The scatter of available experimental data on polycrystalline ice has made it difficult to develop the constitutive model.

Summary of model parameters

A summary of model parameters is given in Table 5.3.

Table 5.3: Summary of model parameters

Parameters	Jacka (1984) (Granular Ice)	Mellor and Cole (1982) (Granular Ice)
E (MPa)	9000	9000
n	3	3.43
Q (kJ mol ⁻¹)	67	67
A (MPa ⁻³ s ⁻¹)	3.40×10^6	2.23×10^6
A_o (s ⁻¹)	1	1
B_o (MPa)	1.87×10^{-3}	7.92×10^{-3}
k_1	0.1	0.27
k_2	3.2	1.30
h_1	1/70	1/70
h_2	1/30	1/10
r_1 (MPa ⁻³ s ⁻¹)	1.68×10^{-4}	1.73×10^{-5}

5.6 Conclusions

A multiaxial constitutive model of transient creep for orthotropic polycrystalline ice has been developed based on the internal stresses. Since polycrystalline ice is made up of individual single ice crystals, the behavior is affected by the properties of individual crystals. In this study of transient creep, the following processes are considered: the creep anisotropy of single crystal ice, the distribution of crystallographic orientation of individual single crystals and alterations of dislocation densities within grains. The state of microstructure is described by back stress and drag stress. While back stress is introduced for time-dependent recoverable strain due to the creep anisotropy, the drag stress is developed from deformation resistance, accounting for the average dislocation density for non-homogeneous dislocation structures. By using internal stresses and their evolution equations, transient creep of polycrystalline ice has been modeled successfully.

The material anisotropy of polycrystalline ice are formulated by applying the averaging methods to the elastic and inelastic properties of constituent single ice crystals. In particular, effective elastic constants of polycrystalline ice are computed by the Ruess and Voigt averaging assumptions. The equivalent stress for polycrystalline ice is obtained by weighting the equivalent stress at each crystal orientation by the relative frequency of that orientation, based on Voigt (or Sachs) averaging assumption.

Even though the proposed model can describe the viscoplastic responses related to the hardening behavior, results show that the proposed model has difficulty in describing the stress-strain curves of polycrystalline ice, when many microcracks are present. The present analysis suggests that an improvement can be realized by taking into account the damage caused by microcracking. However, the constitutive equations developed in this chapter provide the essential basis for developing an orthotropic damage-enhanced creep model which will be capable of describing the following behaviors of polycrystalline ice: highly rate- and temperature-dependent primary and tertiary creep.

In Chapter 6, a physically-based, damage-enhanced creep model will be developed. The effects of microcracking will be incorporated in the transient creep model. Particular emphasis will be placed on the influence of microcracking on creep. Extensive numerical simulations will be carried out to provide a comparison with experimental data.

Notations

A	temperature-independent constant in the minimum strain rate ($MPa^{-n}s^{-1}$)
A_o	constant in the reference strain rate (s^{-1})
a	material creep constant of isotropic polycrystalline ice
a_i	material creep constants of polycrystalline ice
B	isotropic drag stress (MPa)
\tilde{B}	dimensionless isotropic drag stress
B_o	initial value of B (MPa)
B_{sat}	steady-state value of B (MPa)
C	undamaged elastic stiffness matrix of polycrystalline ice (MPa)
C_g	undamaged elastic stiffness matrix of single crystal ice (MPa)
$C'_{g,ij}$	undamaged elastic stiffness components of single crystal ice (MPa)
c	$\cos \theta$
c_i	material creep constants of single crystal ice
E	isotropic Young's modulus (MPa)
G	stress-transformation tensor
H	kinematic transformation tensor
h	hardening function of internal stress
h_1, h_2	hardening constants of internal stresses X and B
k_1, k_2	dimensionless constants used in X_{sat} and B_{sat}
I	identity matrix
n	stress exponent in power law
Q	activation energy ($kJmol^{-1}$)
Q	orthonormal rotational matrix
R	universal gas constant ($Jmol^{-1}K^{-1}$)
r	recovery function of internal stress
r_1	recovery constant in kinematic hardening variable X ($MPa^{-n}s^{-1}$)
S	undamaged elastic compliance matrix of polycrystalline ice (MPa^{-1})
S_g	undamaged elastic compliance matrix of single crystal ice (MPa^{-1})
$S'_{g,ij}$	undamaged elastic compliance components of single crystal ice (MPa^{-1})
s	$\sin \theta$
T	temperature in degrees Kelvin (K)
T	transformation matrix
t	time (s)
\tilde{t}	dimensionless time
V	activation volume
X, \mathbf{X}	kinematic back stress and tensor (vector) (MPa)
\tilde{X}	dimensionless kinematic back stress
X_{sat}	steady-state value of X (MPa)
$x1, x2, x3$	reference global axes
$x1', x2', x3'$	local axes

α	constant
β	material constant
$\epsilon, \dot{\epsilon}$	total strain and total strain rate (s^{-1})
$\epsilon^e, \dot{\epsilon}^e$	elastic strain and elastic strain rate (s^{-1})
$\epsilon^c, \dot{\epsilon}^c$	inelastic strain and inelastic strain rate (s^{-1})
$\dot{\epsilon}_o$	temperature-dependent reference strain rate (s^{-1})
$\boldsymbol{\epsilon}, \dot{\boldsymbol{\epsilon}}$	total strain and total strain rate tensor (vector) (s^{-1})
$\boldsymbol{\epsilon}^e, \dot{\boldsymbol{\epsilon}}^e$	elastic strain and elastic strain rate tensor (vector) (s^{-1})
$\boldsymbol{\epsilon}^c, \dot{\boldsymbol{\epsilon}}^c$	inelastic strain and inelastic strain rate tensor (vector) (s^{-1})
μ	shear modulus (MPa)
ν	average velocity of mobile dislocations
ρ	average density of dislocations
ρ_m	average density of mobile dislocations
σ	stress (MPa)
$\sigma_{d,eq}$	reduced equivalent stress scalar for polycrystalline ice (MPa)
$\hat{\sigma}_e$	equivalent stress scalar for single crystal ice (MPa)
σ_{eq}	equivalent stress scalar for polycrystalline ice (MPa)
$\bar{\sigma}$	effective stress (MPa)
σ_i	internal stress (MPa)
σ_{ij}	stresses in the global frame (MPa)
σ'_{ij}	stresses in the local frame (MPa)
σ_m	hydrostatic stress (MPa)
$\boldsymbol{\sigma}$	stress tensor (vector) (MPa)
$\boldsymbol{\sigma}_d$	reduced stress tensor (vector) defined as $\boldsymbol{\sigma} - \mathbf{X}$ (MPa)
ϕ	geometrical constant
Φ_o	dissipation potential for undamaged polycrystalline ice
Θ	probability density function of c-axis orientation
θ, φ	c-axis orientation of single crystal ice in the global frame

5.7 Appendix A

Coordinate Transformation

Let (x_1, x_2, x_3) be the reference rectangular Cartesian coordinate system (reference global frame) and (x_1', x_2', x_3') be the local rectangular Cartesian coordinate system (local frame), where x_1' corresponds to the c-axis of single crystal ice (see Fig. 5-1). To relate the global set of axes (x_1, x_2, x_3) with the local set of axes (x_1', x_2', x_3') , two rotation are necessary: first, (x_1, x_2, x_3) is rotated by the angle θ about the x_3 axis: then, the new system is rotated by the angle φ about the x_2 axis. The rotation of a third angle is not necessary, because there is no preferential slip direction along the basal plane.

Considering the direction cosines d_{ij} , angles between the local axes (x_1', x_2', x_3') and the global axes (x_1, x_2, x_3) , is defined as

axes	x_1	x_2	x_3
x_1'	l_1	l_2	l_3
x_2'	m_1	m_2	m_3
x_3'	n_1	n_2	n_3

then, the stress components in the local frame is determined in terms of stresses in the global frame by the relationship

$$\sigma'_{ij} = d_{ik} d_{jl} \sigma_{kl}. \quad (5.A1)$$

To represent the relationship in matrix form, the orthonormal rotation matrix is defined as

$$\mathbf{Q}(\theta, \varphi) = \begin{bmatrix} \cos \theta \cos \varphi & \sin \theta & -\cos \theta \sin \varphi \\ -\sin \theta \cos \varphi & \cos \theta & \sin \theta \sin \varphi \\ \sin \varphi & 0 & \cos \varphi \end{bmatrix}. \quad (5.A2)$$

the relationship between the stresses in the two frames are given by

$$[\sigma'] = \mathbf{Q}(\theta, \varphi) [\sigma] \mathbf{Q}^T(\theta, \varphi) \quad (5.A3)$$

where $[\sigma']$ and $[\sigma]$ are stress tensors respectively in the local and global coordinate systems, and superscript T denotes the transpose operation. By the matrix manipulation, Eq. (5.A3)

can be written as

$$\boldsymbol{\sigma}' = \mathbf{T}(\theta, \varphi) \boldsymbol{\sigma} \quad (5.A4)$$

where the most general three-dimensional transformation matrix, $\mathbf{T}(\theta, \varphi)$, which transfers components in the local frame to the reference frame, is given by

$$\mathbf{T}(\theta, \varphi) = \begin{bmatrix} l_1^2 & l_2^2 & l_3^2 & 2l_2l_3 & 2l_1l_3 & 2l_1l_2 \\ m_1^2 & m_2^2 & m_3^2 & 2m_2m_3 & 2m_1m_3 & 2m_1m_2 \\ n_1^2 & n_2^2 & n_3^2 & 2n_2n_3 & 2n_1n_3 & 2n_1n_2 \\ m_1n_1 & m_2n_2 & m_3n_3 & m_2n_3 + m_3n_2 & m_1n_3 + m_3n_1 & m_1n_2 + m_2n_1 \\ l_1n_1 & l_2n_2 & l_3n_3 & l_2n_3 + l_3n_2 & l_1n_3 + l_3n_1 & l_1n_2 + l_2n_1 \\ l_1m_1 & l_2m_2 & l_3m_3 & l_2m_3 + l_3m_2 & l_1m_3 + l_3m_1 & l_1m_2 + l_2m_1 \end{bmatrix}. \quad (5.A5)$$

5.8 Appendix B

Elastic Constants of Single Ice Crystal

Gammon et al. (1983) have determined the dynamic elastic constants of single crystal ice at $T = -16^\circ\text{C}$ using the method of Brillouin spectroscopy. The complete six-by-six compliance and stiffness matrices of single crystal ice in the local frame are

$$\mathbf{S}'_g = \begin{bmatrix} 0.8441 & -0.2316 & -0.2316 & 0 & 0 & 0 \\ & 1.0318 & -0.4287 & 0 & 0 & 0 \\ & & 1.0318 & 0 & 0 & 0 \\ & & & 2.9210 & 0 & 0 \\ & \text{sym.} & & & 3.3179 & 0 \\ & & & & & 3.3179 \end{bmatrix} 10^{-1} \text{ GPa}^{-1} \quad (5.B1)$$

$$\mathbf{C}'_g = \begin{bmatrix} 15.010 & 5.765 & 5.765 & 0 & 0 & 0 \\ & 13.929 & 7.082 & 0 & 0 & 0 \\ & & 13.929 & 0 & 0 & 0 \\ & & & 3.424 & 0 & 0 \\ & \text{sym.} & & & 3.014 & 0 \\ & & & & & 3.014 \end{bmatrix} \text{ GPa} \quad (5.B2)$$

where the local frame x_2' - x_3' is the plane of transverse isotropy; the c -axis lies in the x_1' direction ($\theta = 0^\circ$). It is noted that there are five independent constants due to the hexagonal crystal structure of ice.

The above elastic constants are mildly temperature-dependent. The following empirical relationship for the compliance and stiffness matrices at temperature T is obtained (Gammon et al., 1983)

$$\mathbf{S}'_g(T) = \mathbf{S}'_g(T_o) \frac{1 - \delta T_o}{1 - \delta T}, \quad \mathbf{C}'_g(T) = \mathbf{C}'_g(T_o) \frac{1 - \delta T}{1 - \delta T_o} \quad (5.B3)$$

where $\delta = 1.418 \times 10^{-3} \text{ } ^\circ\text{C}^{-1}$, and $\mathbf{S}'_g(T_o)$ and $\mathbf{C}'_g(T_o)$ are the known compliance and stiffness matrices at a specific temperature ($T_o = -16^\circ\text{C}$), and all temperatures are measured in $^\circ\text{C}$. It is noted that between 0°C and -20°C the variation in dynamic elastic constants of single crystal ice is practically negligible. Wu (1990) used these elastic properties in his theoretical analysis of the microcracking in polycrystalline ice.

The elastic stress-strain relations for single crystal ice are defined as

$$\dot{\epsilon}^e = \mathbf{S}_g \dot{\sigma}, \quad \dot{\sigma} = \mathbf{C}_g \dot{\epsilon}^e \quad (5.B4)$$

where $\dot{\sigma}$ is the stress rate “vector” (in the sense of the contracted Voigt notation), $\dot{\epsilon}^e$ is the elastic strain rate vector, and \mathbf{S}_g and \mathbf{C}_g are respectively the compliance and stiffness matrices of single crystal ice in the global reference frame. If the global reference frame is not coincide with the local frame for the hexagonal ice crystal, then \mathbf{S}_g and \mathbf{C}_g are given by

$$\mathbf{S}_g = \mathbf{T}^T \mathbf{S}'_g \mathbf{T}, \quad \mathbf{C}_g = \mathbf{T}^{-1} \mathbf{C}'_g \mathbf{T}^{-T} \quad (5.B5)$$

where \mathbf{S}'_g and \mathbf{C}'_g are the compliance and stiffness matrices of single crystal ice in the local frame, the three-dimensional transformation matrix, \mathbf{T} , based on the direction cosines

between the global reference frame and the local frame is given by

$$\mathbf{T} = \begin{bmatrix} c^2 & s^2 & 0 & 0 & 0 & 2cs \\ s^2 & c^2 & 0 & 0 & 0 & -2cs \\ 0 & 0 & 1 & 0 & 0 & 0 \\ 0 & 0 & 0 & c & -s & 0 \\ 0 & 0 & 0 & s & c & 0 \\ -cs & cs & 0 & 0 & 0 & c^2 - s^2 \end{bmatrix} \quad (5.B6)$$

where $c = \cos \theta$ and $s = \sin \theta$, in which θ denotes the angle between a c-axis and global x1-axis (see Fig. 3). This transformation applies for the case where x_3' coincides with x_3 , i.e., there is a rotation of axes in the x1-x2 plane.

Plane strain/Plane stress

Under plane strain conditions ($\epsilon_{33} = 0$) with x1-x2 being the plane of interest, the complete six-by-six compliance matrix reduces to a three-by-three matrix given by (see Savin, 1961)

$$S'_{g,ij} = \left(S'_{g,ij} - \frac{S'_{g,i3} S'_{g,3j}}{S'_{g,33}} \right)_f \quad (5.B7)$$

where $i, j = 1, 2, 6$ and the subscript f emphasize that the components of the complete six-by-six matrix should be used. The plane strain compliance matrix using Eq. (5.B7) is calculated to be

$$\mathbf{S}'_g(\theta = 0^\circ) = \begin{bmatrix} 0.7921 & -0.3278 & 0 \\ -0.3278 & 0.8537 & 0 \\ 0 & 0 & 3.3179 \end{bmatrix} 10^{-1} \text{ GPa}^{-1} \quad (5.B8)$$

and the plane strain stiffness matrix is

$$\mathbf{C}'_g(\theta = 0^\circ) = \begin{bmatrix} 15.010 & 5.765 & 0 \\ 5.765 & 13.929 & 0 \\ 0 & 0 & 3.014 \end{bmatrix} \text{ GPa} . \quad (5.B9)$$

Under plane stress conditions ($\sigma_{33} = 0$) with x1-x2 being the plane of interest, the

complete six-by-six stiffness matrix reduces to a three-by-three matrix given by

$$C'_{g,ij} = \left(C'_{g,ij} - \frac{C'_{g,i3} C'_{g,3j}}{C'_{g,33}} \right)_f \quad (5.B10)$$

where $i, j = 1, 2, 6$ and the subscript f emphasize that the components of the complete six-by-six matrix should be used. The plane stress stiffness matrix using Eq. (5.B10) is

$$C'_g(\theta = 0^\circ) = \begin{bmatrix} 12.624 & 2.834 & 0 \\ 2.834 & 10.328 & 0 \\ 0 & 0 & 3.014 \end{bmatrix} \text{ GPa} \quad (5.B11)$$

and the plane stress compliance matrix is

$$S'_g(\theta = 0^\circ) = \begin{bmatrix} 0.8441 & -0.2316 & 0 \\ -0.2316 & 1.0318 & 0 \\ 0 & 0 & 3.3179 \end{bmatrix} 10^{-1} \text{ GPa}^{-1}. \quad (5.B12)$$

If the global reference frame is not coincide with the local frame for the hexagonal ice crystal, then Eq. (5.B5) is applied with the two-dimensional transformation matrix given by

$$\mathbf{T} = \begin{bmatrix} c^2 & s^2 & 2cs \\ s^2 & c^2 & -2cs \\ -cs & cs & c^2 - s^2 \end{bmatrix}. \quad (5.B13)$$

Effective Elastic Constants of Columnar-grained S2 Polycrystalline Ice

For S2 ice, the c-axis orientation are uniformly distributed between 0 and π radians in the x1-x2 plane. Define θ to be the angle between the c-axis and the global x1-direction (Fig. 5-2). The effective compliance and stiffness can be computed by the Ruess and Voigt assumptions, which involve averaging over all orientation in the plane

$$\mathbf{S} = \frac{1}{\pi} \int_0^\pi \mathbf{S}_g(\theta) d\theta \quad (\text{Ruess}), \quad \mathbf{C} = \frac{1}{\pi} \int_0^\pi \mathbf{C}_g(\theta) d\theta \quad (\text{Voigt}) \quad (5.B14)$$

where $\mathbf{S}_g(\theta)$ and $\mathbf{C}_g(\theta)$ denote the compliance and stiffness of ice single crystals with orientation θ in the global frame and are determined by Eq. (5.B5). The corresponding inverses of

Eq. (5.B14) give the effective elastic stiffness and compliance based on the Ruess and Voigt assumptions.

Substituting Eq. (5.B5) into Eq. (5.B14) yields the following effective compliance for S2 ice using the Ruess assumptions

$$\begin{aligned}
S_{11} &= S_{22} = \frac{1}{8} (3 S'_{g,11} + 3 S'_{g,22} + 2 S'_{g,12} + S'_{g,66}) \\
S_{33} &= S'_{g,22} \\
S_{12} &= S_{21} = \frac{1}{8} (S'_{g,11} + S'_{g,22} + 6 S'_{g,12} - S'_{g,66}) \\
S_{13} &= S_{31} = S_{23} = S_{32} = \frac{1}{2} (S'_{g,12} + S'_{g,23}) \\
S_{44} &= S_{55} = \frac{1}{2} (S'_{g,44} + S'_{g,66}) \\
S_{66} &= 2 (S_{11} - S_{12})
\end{aligned} \tag{5.B15}$$

and the effective stiffness for S2 ice using the Voigt assumptions can be similarly obtained

$$\begin{aligned}
C_{11} &= C_{22} = \frac{1}{8} (3 C'_{g,11} + 3 C'_{g,22} + 2 C'_{g,12} + 4 C'_{g,66}) \\
C_{33} &= C'_{g,22} \\
C_{12} &= C_{21} = \frac{1}{8} (C'_{g,11} + C'_{g,22} + 6 C'_{g,12} - 4 C'_{g,66}) \\
C_{13} &= C_{31} = C_{23} = C_{32} = \frac{1}{2} (C'_{g,12} + C'_{g,23}) \\
C_{44} &= C_{55} = \frac{1}{2} (C'_{g,44} + C'_{g,66}) \\
C_{66} &= \frac{1}{2} (C_{11} - C_{12}).
\end{aligned} \tag{5.B16}$$

It is noted that in both the compliance and stiffness, five independent constants exist, the remaining terms are zero.

The complete six-by-six compliance and stiffness matrices of the columnar-grained S2 ice

at $-16^{\circ}C$ are

$$\mathbf{S} = \begin{bmatrix} 1.0603 & -0.3540 & -0.3302 & 0 & 0 & 0 \\ & 1.0603 & -0.3302 & 0 & 0 & 0 \\ & & 1.0318 & 0 & 0 & 0 \\ & & & 3.1195 & 0 & 0 \\ & \text{sym.} & & & 3.1195 & 0 \\ & & & & & 2.8236 \end{bmatrix} 10^{-1} \text{ GPa}^{-1} \quad (5.B17)$$

$$\mathbf{C} = \begin{bmatrix} 13.800 & 6.434 & 6.424 & 0 & 0 & 0 \\ & 13.800 & 6.424 & 0 & 0 & 0 \\ & & 13.929 & 0 & 0 & 0 \\ & & & 3.219 & 0 & 0 \\ & \text{sym.} & & & 3.219 & 0 \\ & & & & & 4.623 \end{bmatrix} \text{ GPa} \quad (5.B18)$$

where the plane of transverse isotropy is the x1-x2 plane.

Plane strain/Plane stress

Under plane strain conditions ($\epsilon_{33} = 0$) with x1-x2 being the plane of interest, the complete six-by-six compliance matrix reduces to a three-by-three matrix given by

$$S_{ij} = \left(S_{ij} - \frac{S_{i3} S_{3j}}{S_{33}} \right)_f \quad (5.B19)$$

where $i, j = 1, 2, 6$ and the subscript f emphasize that the components of the complete six-by-six matrix should be used. The plane strain compliance matrix using Eq. (5.B19) is

$$\mathbf{S} = \begin{bmatrix} 0.9546 & -0.4597 & 0 \\ -0.4597 & 0.9546 & 0 \\ 0 & 0 & 2.8236 \end{bmatrix} 10^{-1} \text{ GPa}^{-1} \quad (5.B20)$$

and the plane strain stiffness matrix is

$$\mathbf{C} = \begin{bmatrix} 13.800 & 6.434 & 0 \\ 6.434 & 13.800 & 0 \\ 0 & 0 & 4.623 \end{bmatrix} \text{ GPa} . \quad (5.B21)$$

Under plane stress conditions ($\sigma_{33} = 0$) with x1-x2 being the plane of interest, the complete six-by-six stiffness matrix reduces to a three-by-three matrix given by

$$C_{ij} = \left(C_{ij} - \frac{C_{i3}C_{3j}}{C_{33}} \right)_f \quad (5.B22)$$

where $i, j = 1, 2, 6$ and the subscript f emphasize that the components of the complete six-by-six matrix should be used. The plane stress stiffness matrix using Eq. (5.B22) is

$$\mathbf{C} = \begin{bmatrix} 10.837 & 3.471 & 0 \\ 3.471 & 10.837 & 0 \\ 0 & 0 & 4.623 \end{bmatrix} \text{ GPa} \quad (5.B23)$$

and the plane stress compliance matrix is

$$\mathbf{S} = \begin{bmatrix} 1.0603 & -0.3540 & 0 \\ -0.3540 & 1.0603 & 0 \\ 0 & 0 & 2.8236 \end{bmatrix} 10^{-1} \text{ GPa}^{-1}. \quad (5.B24)$$

Effective Elastic Constants of Equiaxed-granular Polycrystalline Ice

The six-by-six elastic compliance matrix of equiaxed-granular (isotropic) polycrystalline ice at -16°C is (Gammon et al. (1983))

$$\mathbf{S} = \begin{bmatrix} 1.0716 & -0.3486 & -0.3486 & 0 & 0 & 0 \\ & 1.0716 & -0.3486 & 0 & 0 & 0 \\ & & 1.0716 & 0 & 0 & 0 \\ & & & 2.8401 & 0 & 0 \\ \text{sym.} & & & & 2.8401 & 0 \\ & & & & & 2.8401 \end{bmatrix} 10^{-1} \text{ GPa}^{-1}. \quad (5.B25)$$

The elastic compliance matrices under plane strain and plane stress conditions are computed to be

$$\mathbf{S} = \begin{bmatrix} 0.9582 & -0.4620 & 0 \\ -0.4620 & 0.9582 & 0 \\ 0 & 0 & 2.8401 \end{bmatrix} 10^{-1} \text{ GPa}^{-1} \quad (5.B26)$$

and

$$\mathbf{S} = \begin{bmatrix} 1.0716 & -0.3486 & 0 \\ -0.3486 & 1.0716 & 0 \\ 0 & 0 & 2.8401 \end{bmatrix} 10^{-1} \text{ GPa}^{-1}. \quad (5.B27)$$

References

- [1] Anand, L. (1982). Constitutive equations for the rate-dependent deformation of metals at elevated temperatures. *Journal of Engineering Materials Technology*, Vol. 104, pp. 12-17.
- [2] Argon, A.S. and Bhattacharya, A. K. (1987). Primary creep in nickel: experiments and theory. *Acta Metall.*, Vol. 35, No. 7, pp. 1499-1514.
- [3] Ashby, M.F. and Duval, P. (1985). The creep polycrystalline ice. *Cold Regions Science and Technology*, Vol. 11, No.3, pp. 285-300.
- [4] Aubertin, M., Gill, D.E. and Ladanyi, B. (1991). A unified viscoplastic model for the inelastic flow of alkali halides. *Mechanics of Materials*, Vol. 11, pp. 63-82.
- [5] Azuma, N. (1995). A flow law for anisotropic polycrystalline ice under uniaxial compressive deformation. *Cold Regions Science and Technology*, Vol. 23, pp. 137-147.
- [6] Barnes, P., Tabor, D. and Walker, J.C.F. (1971). The friction and creep of polycrystalline ice. *Proc. Royal soc. London A*, 324, pp. 127-155.
- [7] Boyce, M.C., Parks, D.M. and Argon, A.S. (1988). Large inelastic deformation of plassy polymers. Part I: Rate dependent constitutive model. *Mechanics and Materials*, Vol. 7, pp. 15-33.
- [8] Chaboche, J.L. (1977). Viscoplastic constitutive equations for the description of cyclic and anisotropic behavior of metals. *Bull. de l'Acad. Polonaise des Sciences, Series, Sc. et Tech.*, Vol. 25, No. 1, pp. 33-42.
- [9] Choi, K. and Karr, D.G. (1989). A damage mechanics model for uniaxial creep and cyclic loading of polycrystalline ice. *Proc. 8th Int. Conf. Offshore Mech. and Arctic Eng.*, ASME, Vol. 4, pp. 75-82.
- [10] Cole, D.M. (1991). Anelastic straining in polycrystalline ice. In: *Proceedings of the 6th International Specialty Conference on Cold Regions Engineering*, Edited by D. Sodhi, pp. 504-518, West Lebanon, New Hampshire, 26-28 February.
- [11] Duval, P. (1976). Lois de fluage transitoire ou permanent de la glace polycrystalline pour divers etats de contrainte. *Annales de Geophysique*, Tom. 32, No. 4, pp. 335-350.
- [12] Duval, P., Ashby, M.F. and Anderman, I. (1983). Rate-controlling processes in the creep of polycrystalline ice. *The Journal of Physical Chemistry*, Vol. 87, No. 21, pp. 4066-4074.
- [13] Elvin, A.A. (1996). Number of grains required to homogenize elastic properties of polycrystalline ice. *Mechanics of Materials*, Vol. 22, pp. 51-64.
- [14] Fukuda, A. and Highasi, A. (1973). Dynamical behavior of dislocations in ice crystals. *Crystal Lattice Defects*, Vol. 4, pp. 203-210.

- [15] Gammon, P.H., Kieft, H., Clouter, M.J. and Denner, W.W. (1983). Elastic constants of artificial and natural ice samples by Brillouin spectroscopy. *Journal of Glaciology*, Vol. 29, pp. 433-459.
- [16] Glen, J.W. (1955). The creep of polycrystalline ice. *Proc. Royal Soc. London, Ser. A*, 288(1175), pp. 519-538.
- [17] Glen, J.W. and Perutz, H. F. (1954). The growth and deformation of ice crystals. *Journal of Glaciology*, Vol. 2, No. 2, pp. 397-403.
- [18] Gold, L.W. (1973). Activation energy for creep of columnar-grained ice. In: *Physics and chemistry of ice*, Eds. E. Whalley, S.J. Jones and L.W. Gold, Ottawa, Royal Society of Canada, pp. 362-364.
- [19] Goodman, D.J., Frost, H.J. and Ashby, M.F. (1981). The plasticity of polycrystalline ice. *Philosophical Magazine A*, 43(3): 665-695.
- [20] Gottstein, G. and Argon, A.S. (1987). Dislocation theory of steady state deformation and its approach in creep and dynamic tests. *Acta Metallurgica*, 35(6), pp. 1261-1271.
- [21] Hart, E.W. (1976). Constitutive relations for the nonelastic deformation of metals. *Journal of Engineering Materials Technology*, Vol. 96, pp. 193-202.
- [22] Higashi, A. (1968). Mechanisms of plastic deformation in ice single crystals. *Physics of Snow and Ice*, pp. 227-289.
- [23] Hill, R. (1950). *The mathematical theory of plasticity*. Oxford Univ. Press, London, 356pp.
- [24] Hobbs, P.V. (1974). *Ice Physics*. Clarendon Press, Oxford.
- [25] Homer, D.R. and Glen, J.W. (1978). The creep activation energies of ice. *Journal of Glaciology*, Vol. 21, No. 85, pp. 429-444.
- [26] Hooke, R.L. (1981). Flow law for polycrystalline ice in glaciers: Comparison of theoretical predictions, laboratory data, and field measurements, *Rev. Geophys. Space Phys.*, Vol. 19, pp. 664-672.
- [27] Jacka, T.H. (1984). The time and strain required for development of minimum strain rates. *Cold Regions Science and Technology*, Vol. 8, pp. 261-268.
- [28] Jacka, T.H. and Budd, W.F. (1991). The use of tertiary creep rates in ice at high strains in compression and shear. *Proc. IUTAM/IAHR Symp. on Ice-Structure Interaction*, Jones, S.J., McKenna, R.F., Tillotson, J. and Jordaan, I.J. (Ed.), Springer-Verlag, pp. 21-35.
- [29] Kamb, W.B. (1961). The glide direction in ice. *Journal of Glaciology*, Vol. 3, pp. 1097-1106.

- [30] Kocks, U.F. (1976). Laws for work-hardening and low-temperature creep. *Journal of Engineering Materials and Technology*, ASME Ser. H 98, pp. 76-85.
- [31] Kocks, U.F., Argon, A.S. and Ashby, M.F. (1975). Thermodynamics and kinetics of slip. *Progress in Materials Science*, Vol. 19.
- [32] Lawrence, W.F.St. and Cole, D.M. (1982). Acoustic emissions from polycrystalline ice. *Cold Regions Science and Technology*, Vol. 5, pp. 183-199.
- [33] Lile, R.C. (1978). The effects of anisotropy on the creep of polycrystalline ice. *Journal of Glaciology*, Vol. 21, pp. 475-484.
- [34] Liu, F., Baker, I., and Dudley, M. (1993). Dynamic observations of dislocation generation at grain boundaries in ice. *Philosophical Magazine A*, Vol. 67, pp. 1261-1276.
- [35] Le Gac, H. and Duval, P. (1980). Constitutive relations for the nonelastic deformation of polycrystalline ice. *Proceedings of the IUTAM Symposium on the Physics and Mechanics of Ice*, Edited by P. Tryde, Springer, pp. 51-59.
- [36] Mellor M. and Cole, D. (1982). Deformation and failure of ice under constant stress or constant strain rate. *Cold Regions Science and Technology*, Vol. 5, pp. 201-219.
- [37] Meyssonier, J. and Goubert, A. (1994). Transient creep of polycrystalline ice under uniaxial compression: an assessment of internal state variable models. *Annals of Glaciology*, Vol. 19, pp. 55-62.
- [38] Michel, B. (1978). The strength of polycrystalline ice. *Canadian Journal of Civil Engineering*, Vol. 5, No. 3, pp. 285-300.
- [39] Michel, B. and R.O. Ramseier (1971). Classification of river and lake ice. *Can. Geotech. J.*, Vol. 8, pp. 36-45.
- [40] Miller, A.K. (1976). An inelastic constitutive model for monotonic, cyclic, and creep deformation: Part I - Equations development and analytical procedures. *Journal of Engineering Materials Technology*, Vol. 96, pp. 97-105.
- [41] Mott, N.F. (1955). A theory of work-hardening of metals II: Flow without slip-lines, recovery and creep. *Philosophical Magazine*, 43, pp. 742-765.
- [42] Nanthikesan, S. and Shyam Sunder, S. (1994). Anisotropic elasticity of polycrystalline ice I_h . *Cold Reg. sci. Technol.*, Vol. 22, pp. 149-169.
- [43] Orowan, E. (1940). Problems of plastic gliding. *Proc. Phys. Soc.*, Vol. 52, pp. 8.
- [44] Riley, N.W., Noll, G., and Glen, J.W. (1978). The creep of NaCl-doped ice monocrystals. *Journal of Glaciology*, Vol. 21, pp. 501-506.
- [45] Sachs, G. (1928). Zur Ableitung einer Fließbedingung. *Zietschrift Verein. Deut. Ing.*, Vol. 72, pp. 734-736.

- [46] Sanderson, T.J.O. (1984). Theoretical and measured ice forces on wide structures. *Proc. 7th Int. Symp. on Ice, IAHR*, Hamburg, West Germany, pp. 151-207.
- [47] Savin, G.N. (1961). *Stress concentrations around holes*. Pergamon Press, Oxford.
- [48] Schapery, R.A. (1991). Models for the deformation behavior of viscoelastic media with distributed damage and their applicability to ice. *Proc. IUTAM/IAHR Symp. on Ice-Structure Interaction*, Jones, S.J., McKenna, R.F., Tillotson, J. and Jordaan, I.J. (Ed.), Springer-Verlag, pp. 191-230.
- [49] Shearwood, C. and Whitworth, R.W. (1991). The velocity of dislocations in ice. *Philosophical Magazine A*, Vol. 64, No. 2, pp. 289-302.
- [50] Shyam Sunder, S. and Wu, M.S. (1989a). A differential flow model for polycrystalline ice. *Cold Regions Science and Technology*, Vol. 16, No. 1, pp. 45-62.
- [51] Shyam Sunder, S. and Wu, M.S. (1989b). A multiaxial differential model of flow in orthotropic polycrystalline ice. *Cold Regions Science and Technology*, Vol. 16, No. 2, pp. 223-235.
- [52] Shyam Sunder, S. and Wu, M.S. (1990). On the constitutive modeling of transient creep in polycrystalline ice. *Cold Regions Science and Technology*, Vol. 18, pp. 267-294.
- [53] Sinha, N.K. (1978). Rheology of columnar-grained ice. *Experimental Mechanics*, Vol. 18, No. 12, pp. 464-470.
- [54] Sinha, N.K. (1979). Grain-boundary sliding in polycrystalline materials. *Philosophical Magazine A*, Vol. 40, No. 6, pp. 825-842.
- [55] Sinha, N.K. (1988). Crack-enhanced creep in polycrystalline material: strain-rate sensitive strength and deformation of ice. *Journal of Materials Science*, Vol. 23, No. 12, pp. 4415-4428.
- [56] Sinha, N.K. (1989). Elasticity of natural types of polycrystalline ice, *Cold Reg. Sci. Technol.*, Vol. 17, pp. 127-135.
- [57] Steinemann, S. (1954). Results of preliminary experiments on the plasticity of ice crystals. *Journal of Glaciology*, Vol. 2, No. 16, pp. 404-413.
- [58] Takeuchi, S. and Argon, A.S. (1976). Steady-state creep of single-phase crystalline matter at high temperature. *Journal of Materials Science*, Vol. 11, pp. 1542-1566.
- [59] Voigt, W. (1889). Ueber die Beziehung zwischen den beiden Elasticitäts-constanten isotroper Körper, *Ann. Phys.*, Vol. 38, pp. 573-587.
- [60] Wang, L. and Schapery, R.A. (1995). Prediction of elastic and viscoelastic properties of anisotropic columnar ice. *Ice Mechanics*, AMD Vol. 207, ASME, pp. 33-47.
- [61] Weertman, J. (1973). Creep of Ice. *Physics and Chemistry of Ice*, Whalley, E., Jones, S.J. and Gold, L.W. (Editors), pp. 320-337.

- [62] Weertman, J. (1983). Creep deformation of ice. *Ann. Rev. Earth Planet. Sci.*, Vol. 11, pp. 215-240.
- [63] Wei, Y. and Dempsey, J.P. (1994). The motion of non-basal dislocations in ice crystals. *Philosophical Magazine A*, Vol. 69, No. 1, pp. 1-10.
- [64] Wu, M.S. (1990). Physically-based constitutive models for transient creep and damage in polycrystalline ice. *Ph.D. Thesis*, Massachusetts Institute of Technology, USA.
- [65] Zhan, C., Evgin, E. and Sinha, N.K. (1994). A three dimensional anisotropic constitutive model for ductile behavior of columnar grained ice. *Cold Regions Science and Technology*, Vol. 22, pp. 269-284.

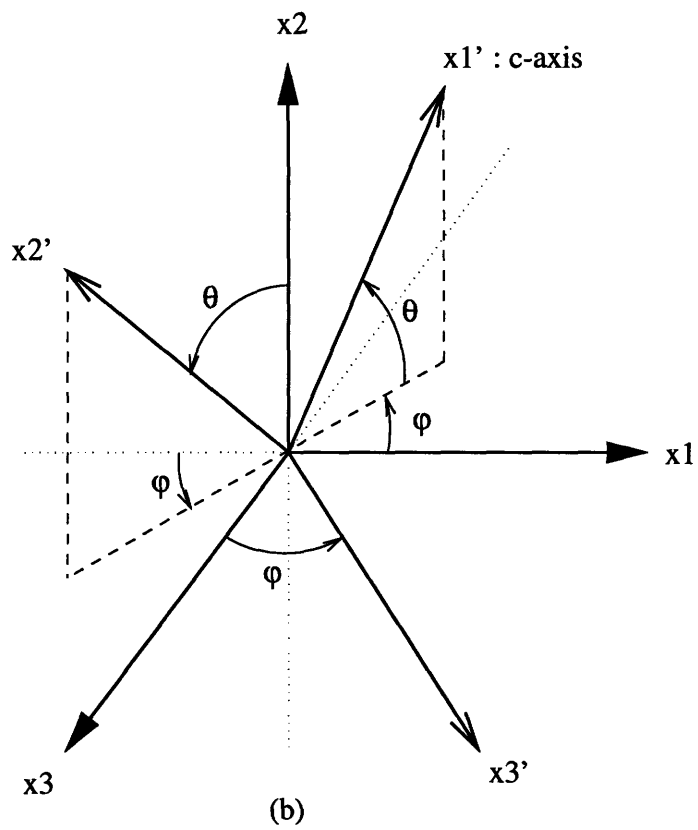
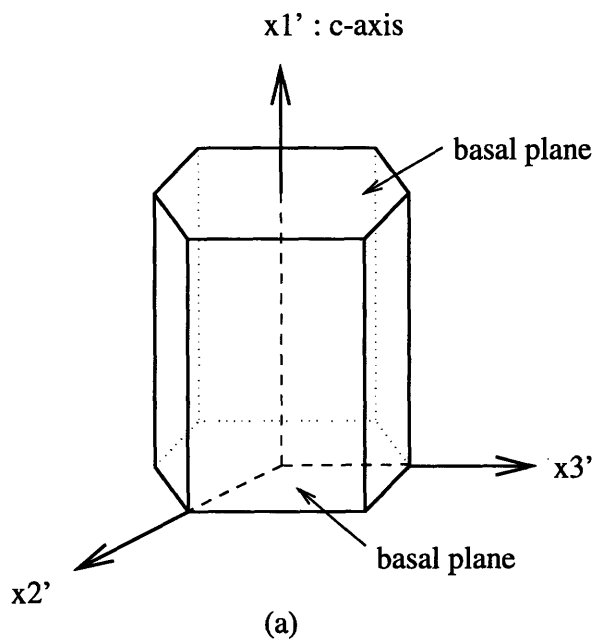


Figure 5-1: (a) Local frame of single crystal ice; (b) Reference global frame (x_1 - x_2 - x_3) and local frame (x_1' - x_2' - x_3').

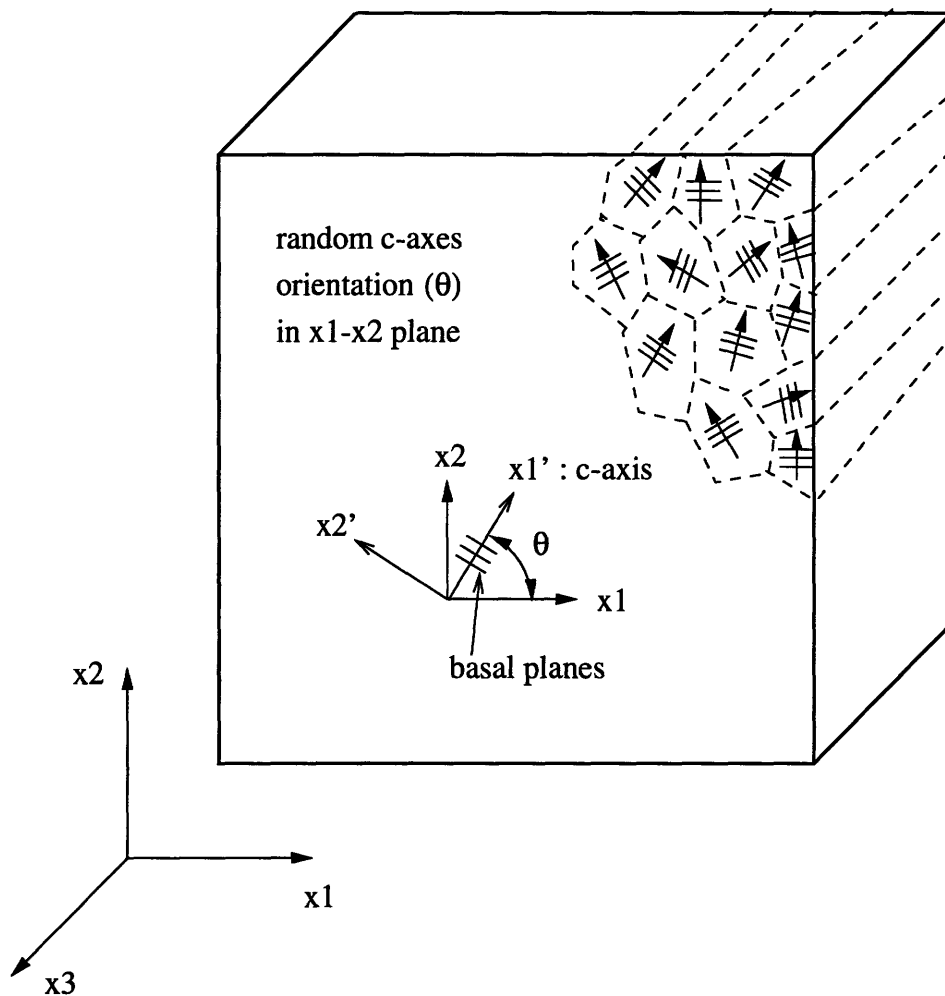


Figure 5-2: Columnar-grained S2 polycrystalline ice containing single crystals with random in-plane c-axes.

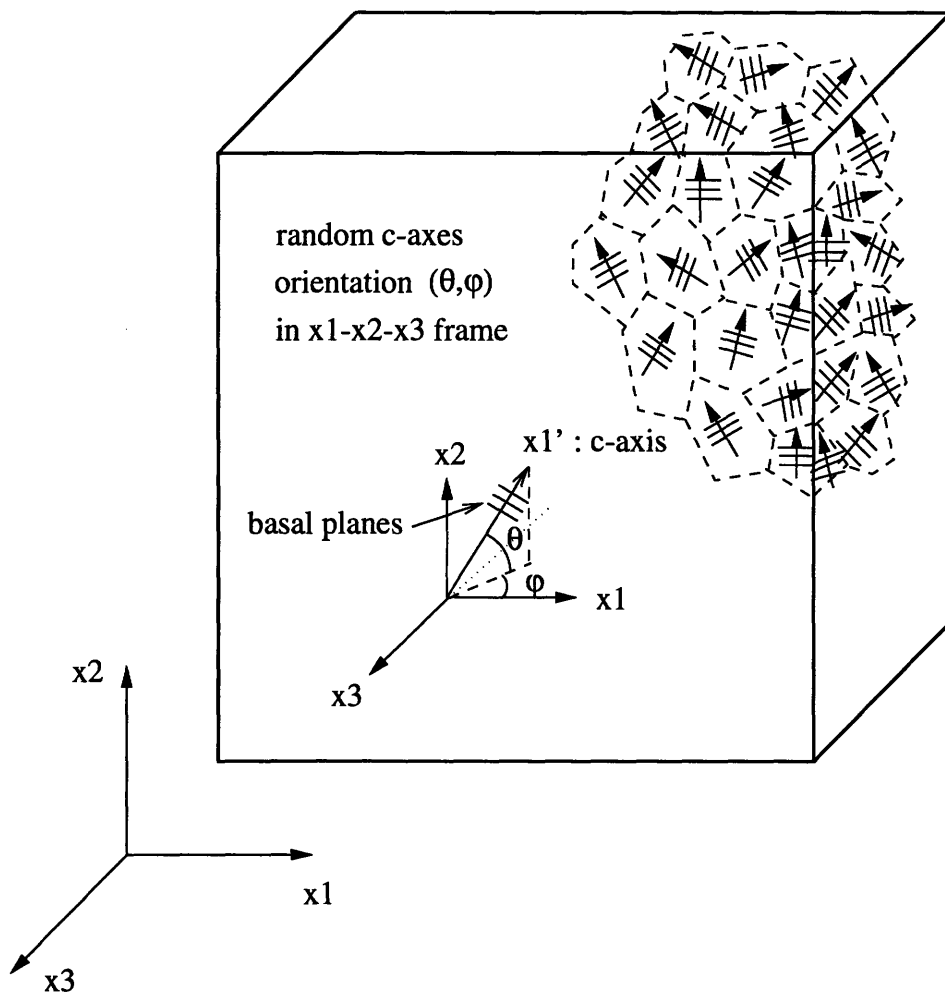


Figure 5-3: Equiaxed-granular polycrystalline ice containing single crystals with random c-axes.

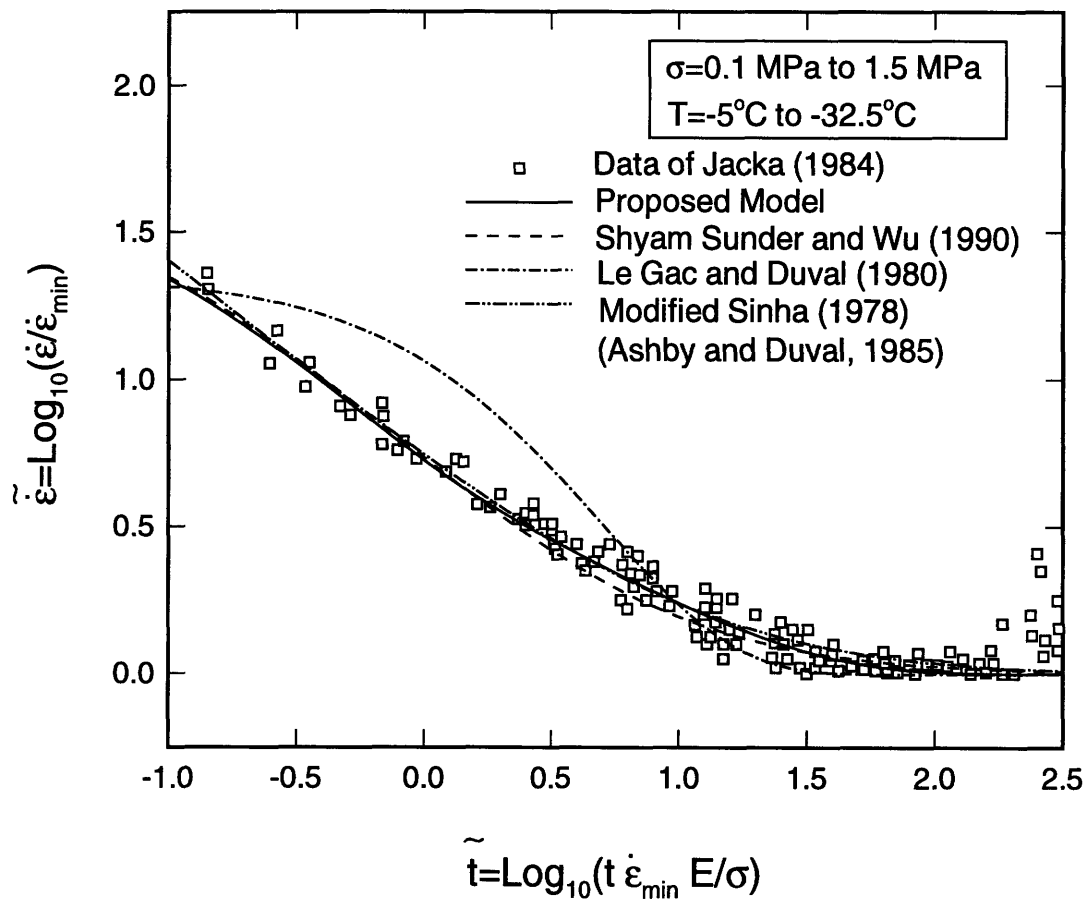


Figure 5-4: Dimensionless strain rate plotted against dimensionless time, from the data of Jacka (1984) (reproduced from Ashby and Duval, 1985). Predictions of (i) the proposed model, (ii) Shyam Sunder and Wu (1990), (iii) Le Gac and Duval (1980), and (iv) Sinha (1978) as modified by Ashby and Duval (1985) are plotted.

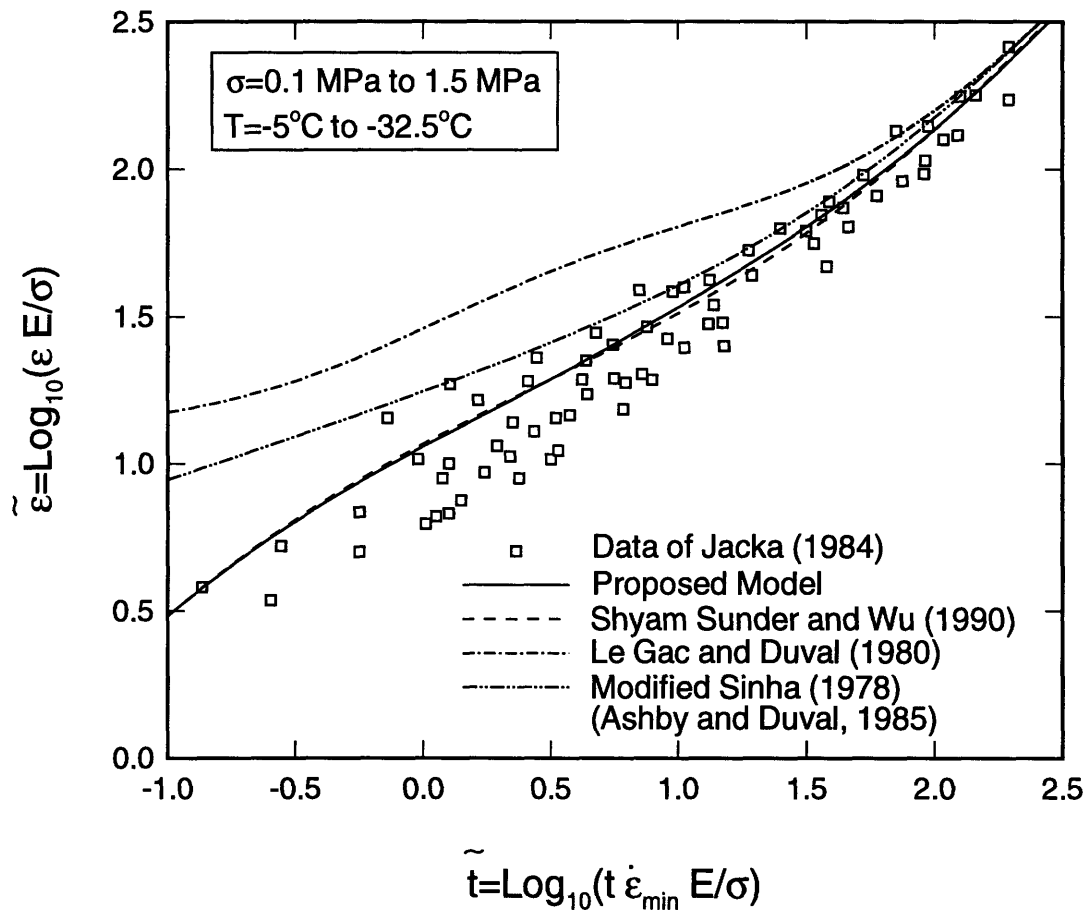


Figure 5-5: Dimensionless strain plotted against dimensionless time, from the data of Jacka (1984) (reproduced from Ashby and Duval, 1985). Predictions of (i) the proposed model, (ii) Shyam Sunder and Wu (1990), (iii) Le Gac and Duval (1980), and (iv) Sinha (1978) as modified by Ashby and Duval (1985) are plotted.

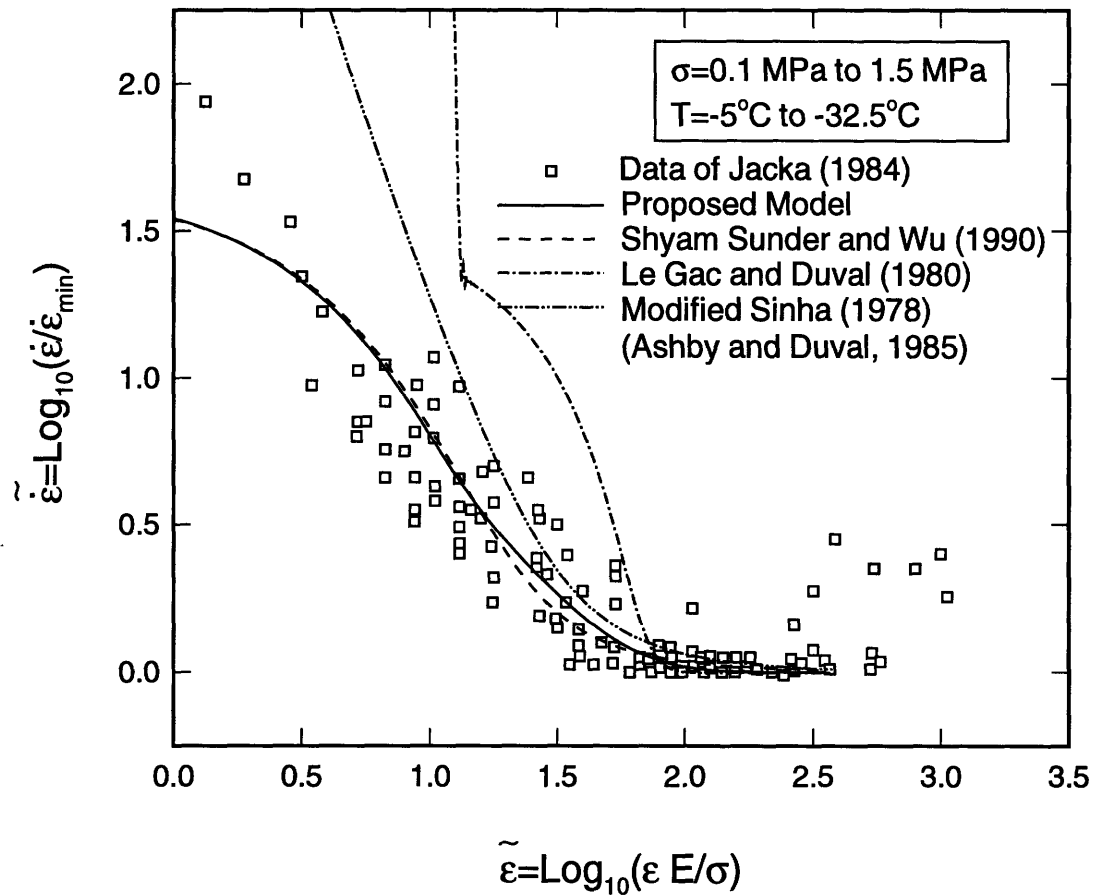


Figure 5-6: Dimensionless strain rate plotted against dimensionless strain, from the data of Jacka (1984) (reproduced from Ashby and Duval, 1985). Predictions of (i) the proposed model, (ii) Shyam Sunder and Wu (1990), (iii) Le Gac and Duval (1980), and (iv) Sinha (1978) as modified by Ashby and Duval (1985) are plotted.

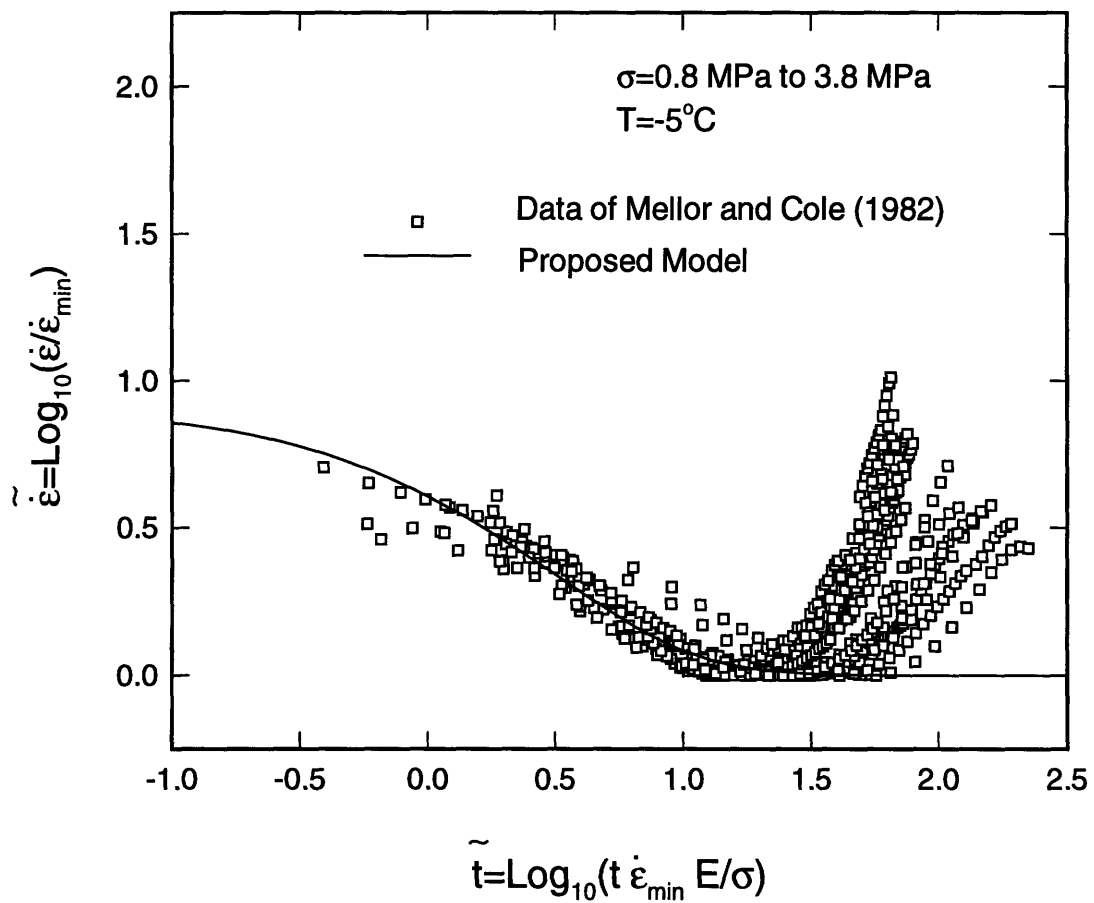


Figure 5-7: Dimensionless strain rate versus dimensionless time. Model response is plotted with the data of Mellor and Cole (1982) under constant stress.

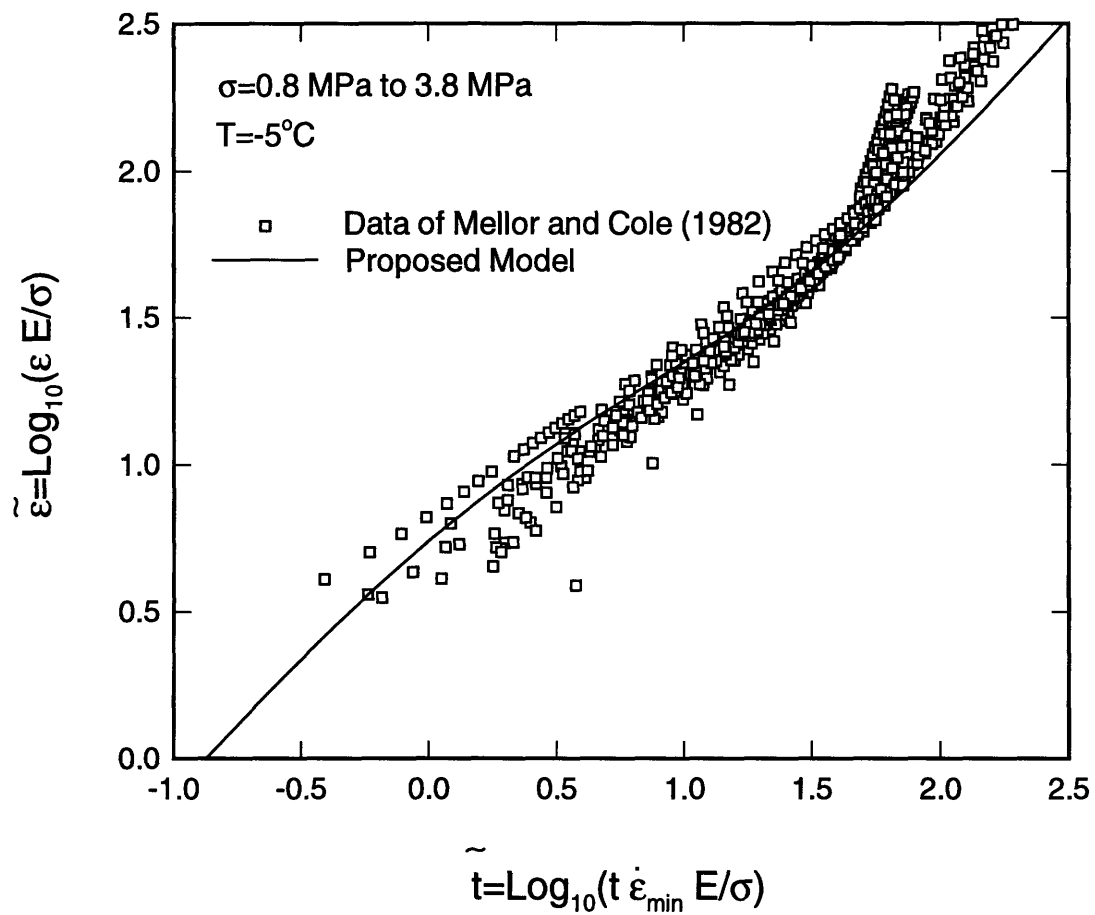


Figure 5-8: Dimensionless strain versus dimensionless time. Model response is plotted with the data of Mellor and Cole (1982) under constant stress.

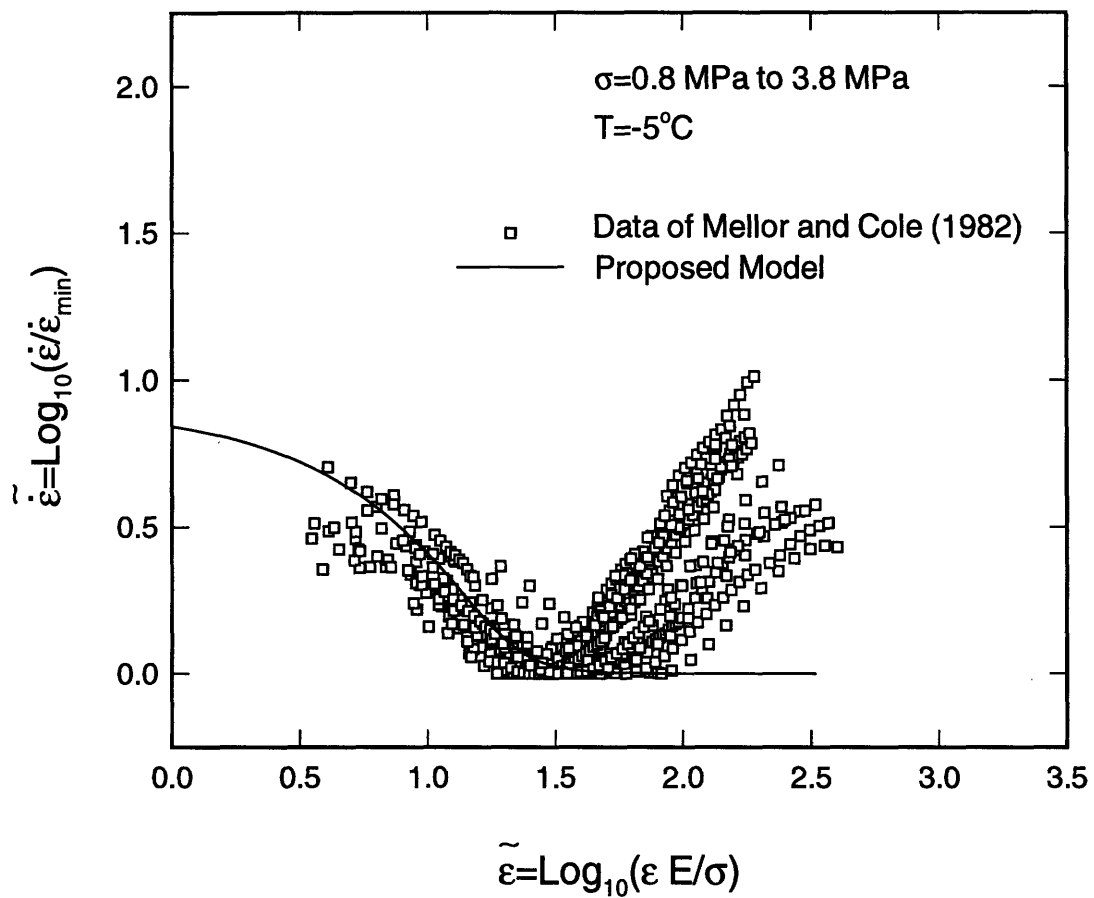


Figure 5-9: Dimensionless strain rate versus dimensionless strain. Model response is plotted with the data of Mellor and Cole (1982) under constant stress.

Chapter 6

A MULTIAXIAL CREEP MODEL, PART II: DAMAGE-ENHANCED CREEP

Abstract

A multiaxial constitutive damage-enhanced creep model for orthotropic polycrystalline ice is presented within the framework of the thermodynamic theory of irreversible processes. This Chapter formulates material anisotropy and damage anisotropy to describe the importance of the directional nature of material behavior. Many deformation mechanisms operate at the microstructural scale to induce flow and damage due to microcracking, and depend highly on loading rate, temperature and crystalline structure. Flow is attributed to the motion and production of dislocations and an interaction between the basal and non-basal systems of a constituent single crystal ice. The local internal stresses cause many stable microcracks under far field compression. Several mechanisms are involved in microcracking. These include dislocation pile-up, grain boundary sliding and elastic anisotropy; the dominant mechanism depends on loading conditions. Experimental results under various loadings show the occurrence of microcracking, which enhances the inelastic deformation of polycrystalline ice during the damage process. A multiaxial dissipation potential for the inelastic deformation is proposed for kinematic hardening, isotropic hardening and damage due to microcracks. Finally, comparison of the model with available experimental data shows good agreement and demonstrates the effectiveness of the model.

6.1 Introduction

Polycrystalline ice exists in nature at very high homologous temperatures ($> 0.9 T_M$). Consequently, the mechanical behavior of ice is highly non-linear and depends on loading rate and temperature, as well as on the granular microstructure. Typical compressive stress-strain curves of polycrystalline ice subjected to constant strain rates at $-10^\circ C$ are shown in Figure 6-1. At slow loading rates (strain rate $\leq 10^{-6} s^{-1}$), the deformation of ice depends mainly on the motion and production of dislocations, and their interactions with obstacles such as dislocations themselves and grain boundaries. As a result, ice exhibits ductile and viscoplastic behavior. At fast loading rates (strain rate $\geq 10^{-3} s^{-1}$), the dislocation movements is retarded and hence the inelastic strain is reduced. As a result, behavior of ice becomes brittle; the stress increases in an almost linear fashion with strain, up to the point of failure, as is the case for linear elastic materials. However, at intermediate loading rates, damage accumulation due to microcracks combined with dislocation activity has a significant influence on the deformation of ice. Moreover, at a loading rate corresponding to the ductile-to-brittle transition, the stress increases to a maximum and then decreases with increasing strain, resulting in strain-softening behavior. This behavioral transition is an important phenomenon in engineering applications involving ice loads on structures and the bearing capacity of ice.

In general, the ductile-to-brittle transition involves multiple modes of deformation, including elastic and creep deformations, damage due to distributed microcracking and the extension of localized macrocracks. The development of rational constitutive equations requires characterizing many of these complex deformation processes. The strategy used here to develop constitutive equations is to identify the dominant energy-dissipating mechanisms. In this study, energy is dissipated by the motion and production of dislocations and by the formation and growth of microcracks both inside and along grains.

This paper presents a multi-axial model for damage-enhanced creep for orthotropic polycrystalline ice. Problems in applied ice mechanics involve multi-axial states of stress and various loading rates. The most significant aspect of the proposed model in this paper is the formulation of kinetic equations which are based on actual physical processes. This physical understanding offers a model combining simultaneously-occurring processes that reflect salient micromechanical aspects. The derivation of the constitutive equations utilizes inter-

nal state variables and formulates their evolution equations; these internal state variables represent an average description of microstructural changes.

This chapter is organized as follows. In Section 6-2, a brief discussion is offered on the deformation mechanisms of ice and other materials. Section 6-3 develops mathematical formulations for a constitutive theory regarding anisotropic and isotropic polycrystalline ice based on the underlying mechanisms and material anisotropy of single crystal ice for inelastic behavior. In Section 6-3, average effective stress, inelastic dissipation potential and damage process are discussed. In particular, the average effective stress for polycrystalline ice is obtained by averaging the effective stresses for all single crystals in a representative volume. The inelastic strain rate is obtained based on the existence of the dissipation potential. In addition, in order to incorporate the effect of microcracks, a specific form of dissipation potential for inelastic flow is proposed to account for the enhancement of creep due to progressive damage, but before the initiation of macrocracking. Damage accumulation is accounted for by microcrack evolution. The equation for microcrack formation is proposed here for the first time as a result of a careful study of this phenomenon. A summary of model equations is given in Tables 6.1 and 6.2. Section 6-4 contains the model's parameters and predictions. Section 6-5 reports in summary form the findings and conclusions of this study.

6.2 Background

As described above, a variety of distinctly different mechanisms exists as a result of the deformation process of the microstructure of polycrystalline ice. Some of these mechanisms are intergranular effects (e.g., sliding and interlocking of grain boundaries), the distribution of the crystallographic orientation of single crystals, alterations of dislocation densities within grains and damage accumulation due to the formation and growth of microcracks. The relative significance of a particular mechanism varies with the levels of stress and with strain rate, temperature and crystalline structure (e.g., grain size, impurity). Intergranular effects, dislocation pile-up and the different creep resistance on slip systems induce internal stress, which causes microcracks and hardening behavior. Generally, the formation of microcracks will influence the mechanical behavior of materials mainly by reducing elastic constants,

enhancing the inelastic strain and producing localized macrocracks.

Microcracks have been found in many brittle materials, including both natural materials such as rock and ice and man-made materials such as concrete and ceramic. Both the tensile and compressive failures of these materials are generally controlled by the formation and propagation of microcracks. In particular, under tension, the first few microcracks lead to unstable crack growth and tensile failure. Under compression, the progressive formation of microcracks leads to widely distributed microcracking and damage accumulation. As the applied stress increases, microcracks lengthen, interact and coalesce into macrocracks, which lead to the final failure of the material.

Since a fracture mechanics approach for every single microcrack and for its influence on the deformation of material is difficult to implement in a model, a continuum damage mechanics approach is often applied with a macroscopic averaging procedure. Using various methods, such as self-consistent method, a differential scheme and pseudo-traction method, the effect of microcracks on the elastic properties of brittle materials, such as Young's modulus and Poisson's ratio, has been studied extensively by many researchers (e.g., Budiansky and O'Connell, 1976; Horii and Nemat-Nasser, 1983; Krajcinovic, 1989; Nemat-Nasser and Hori, 1993; Kachanov, 1994). Many of these methods have assumed that all microcracks are open or active, and they estimate elastic properties in terms of a parameter (the so-called crack density) by applying volume averaging or some other homogenization method. Horii and Nemat-Nasser (1983) have incorporated the effect of friction on crack faces and the crack closure criterion. Wu and Niu (1995) studied the interaction between microcracks and external boundary of the ice specimen in his numerical analysis.

In the study of metals, continuum damage mechanics approaches have been developed in order to describe the effect of microcracks on inelastic behavior, with an effective stress concept first introduced by Kachanov (1958) and Rabotnov (1969), and further developed by Leckie and Hayhurst (1974), Lemaitre and Chaboche (1978) and Murakami and Ohno (1981). Most of these studies focus on damage accumulation that cause ductile failure mechanism of void formation (nucleation), growth and coalescence. Void nucleation occurs due to brittle cracking or interfacial decohesion at grain boundaries. Damage models based on metallurgical studies are developed primarily for the increase of initial porosity at grain boundaries (e.g., Ashby and Raj, 1975; Dyson and McLean, 1977; Cocks and Ashby, 1982;

Argon, 1982). Based on a Gurson-type model (Gurson, 1977), numerous studies have characterized plastic flow in progressively-cavitating porous materials and developed constitutive models for plastic flow localization and fracture due to void coalescence (e.g., Needleman and Rice, 1978; Chu and Needleman, 1980; Pan et al., 1983; Needleman and Tvergaard, 1984; among many others).

Turning to the study of ice, many constitutive equations have been developed in the past two decades to model complex non-linear behavior (e.g., Sinha, 1978; Michel, 1978; LeGac and Duval, 1980; Ting and Shyam Sunder, 1985; Ashby and Duval, 1985; Szyszkowski and Glockner, 1985; Sinha, 1988; Choi and Karr, 1989; Jordaan and McKenna, 1988; Shyam Sunder and Wu, 1989a,b; Schapery, 1991; Zhan et al., 1994). In many of these models, little attention is paid to the micromechanisms which really dictate the behavior of polycrystalline ice.

Michel (1978) suggests a model based on easy slips on the basal plane and the corresponding grain boundary sliding accommodation. Sinha (1978) describes a phenomenological viscoelastic model based on the mechanism of grain boundary sliding, which he claims is responsible for transient creep. In Sinha's model, the exponent in relaxation time is used to account implicitly for the distribution of relaxation time. Constitutive models based on internal state variables are developed for inelastic deformation at the microstructural level by LeGac and Duval (1980), Ashby and Duval (1985), and Sunder and Wu(1989a,b). However, these models are proposed primarily to describe strain-hardening behavior in transient creep, without consideration of the effect of microcracks. In order to incorporate the effect of microcracks, a phenomenological approach based on continuum damage mechanics has been applied by Sjöling (1987), Sinha (1988), Jordaan and McKenna (1988), Choi and Karr (1989) and Zhan et al. (1994).

To quantify the effect of elastic damage due to microcracks, Wu and Shyam Sunder (1992) and Wu and Niu (1995) performed a theoretical analysis of crack nucleation in polycrystalline ice due to elastic anisotropy of the constituent single crystals. Wu and Shyam Sunder (1992) assumed a pseudo coupling exists between the underlying creep mechanism and distributed microcracking. Their approach, a simple addition of the creep strain to the elastic strain accounting for microcracking, has failed to show the strain-softening behavior of ice undergoing the damage process. Although elastic constants due to microcracks

are reduced, the effect of microcracks on elastic deformation is insignificant (Sinha, 1988). However, experimental data show the significant effect of damage due to microcracking on the enhancement of creep (Stone et al., 1989; Meyssonier and Duval, 1989; Jordaan et al., 1990; Xiao et al., 1991).

6.3 Formulation of Constitutive Model

Following the contracted Voigt notation, vector notation is used instead of tensor notation. Polycrystalline ice is a rate-dependent material, the total strain rate vector $\dot{\epsilon}$ is decomposed as follows

$$\dot{\epsilon} = \dot{\epsilon}^e + \dot{\epsilon}^c \quad (6.1)$$

where $\dot{\epsilon}^e$ and $\dot{\epsilon}^c$ are the elastic and inelastic strain rate vectors, respectively. The elastic strain rate vector is written as

$$\dot{\epsilon}^e = \mathbf{S} \dot{\sigma} \quad (6.2)$$

where σ is the applied stress and \mathbf{S} is the elastic compliance matrix of polycrystalline ice (see Appendix B of Chapter 5). The vector form of the strain and stress components are written respectively as $\epsilon = [\epsilon_{11} \ \epsilon_{22} \ \epsilon_{33} \ \epsilon_{23} \ \epsilon_{13} \ \epsilon_{12}]^T$ and $\sigma = [\sigma_{11} \ \sigma_{22} \ \sigma_{33} \ \sigma_{23} \ \sigma_{13} \ \sigma_{12}]^T$, where superscript T denotes the transpose operation.

The inelastic mechanical properties of single crystal ice and polycrystalline ice have been reviewed by Weertman (1973), Hobbs (1974), and Duval et al. (1983). In the following sections, a mathematical formulation for highly rate-dependent anisotropic polycrystalline ice based on the underlying mechanisms is presented for its inelastic behavior.

6.3.1 Inelastic Flow

We consider two forms of freshwater polycrystalline ice. First, we study a columnar-grained polycrystalline ice for which the c-axis orientation of the single crystals is randomly distributed in the x1-x2 plane normal to the x3 axis of the column, as shown in Fig. 6-2. This ice is transversely isotropic ice. The second type of ice is an equiaxed-granular polycrystalline ice in which the c-axis orientation of the constituent single crystals is randomly distributed

in all three directions (x1-x2-x3), as shown in Fig. 6-3. This ice is isotropic ice.

To derive the relationship between the inelastic strain-rate $\dot{\epsilon}^c$ and the stress σ , the averaged equivalent stress which is generalized for pressure-insensitive transversely isotropic materials with the same behavior in compression and tension is used. In this formulation, isotropic and kinematic hardening are incorporated by the internal variables, \mathbf{X} and B .

The reduced equivalent stress may be expressed as

$$\sigma_{d,eq}^2 = \frac{3}{\beta} \sigma_d^T \mathbf{G} \sigma_d \quad (6.3)$$

where the reduced stress vector is defined in terms of a back stress vector \mathbf{X} :

$$\sigma_d = \sigma - \mathbf{X} \quad (6.4)$$

The stress-transformation matrix \mathbf{G} is given by

$$\mathbf{G} = \begin{bmatrix} \frac{(a_1 + a_2)}{3} & -\frac{a_1}{3} & -\frac{a_2}{3} & 0 & 0 & 0 \\ -\frac{a_1}{3} & \frac{(a_1 + a_2)}{3} & -\frac{a_2}{3} & 0 & 0 & 0 \\ -\frac{a_2}{3} & -\frac{a_2}{3} & \frac{2a_2}{3} & 0 & 0 & 0 \\ 0 & 0 & 0 & 2a_4 & 0 & 0 \\ 0 & 0 & 0 & 0 & 2a_4 & 0 \\ 0 & 0 & 0 & 0 & 0 & 2a_6 \end{bmatrix}. \quad (6.5)$$

for columnar-grained polycrystalline ice and

$$\mathbf{G} = \begin{bmatrix} \frac{2}{3} & -\frac{1}{3} & -\frac{1}{3} & 0 & 0 & 0 \\ -\frac{1}{3} & \frac{2}{3} & -\frac{1}{3} & 0 & 0 & 0 \\ -\frac{1}{3} & -\frac{1}{3} & \frac{2}{3} & 0 & 0 & 0 \\ 0 & 0 & 0 & 2 & 0 & 0 \\ 0 & 0 & 0 & 0 & 2 & 0 \\ 0 & 0 & 0 & 0 & 0 & 2 \end{bmatrix}. \quad (6.6)$$

for equiaxed-granular polycrystalline ice.

In the rate-dependent context, there is no yield/failure surface and an inelastic dissipa-

tion function serves in deriving constitutive relations. If inelastic flow in polycrystalline ice *without microcracks* is taken to follow Glen's power law, a scalar-valued dissipation potential of the Norton-Hoff type can be defined and expressed as

$$\Phi_o = \frac{\dot{\epsilon}_o B}{n+1} \left(\frac{\sigma_{d,eq}}{B} \right)^n \quad (6.7)$$

where n is the stress exponent, usually taken as 3 in the experimental literature, the internal variable B represents the isotropic drag stress, and $\dot{\epsilon}_o$ is a temperature-dependent reference strain rate. The effect of temperature on the reference strain rate is represented well by an Arrhenius relationship

$$\dot{\epsilon}_o = A_o \exp\left(-\frac{Q}{RT}\right) \quad (6.8)$$

where A_o is a temperature-independent constant, Q is the activation energy, R is the universal gas constant, and T is the absolute temperature in degrees Kelvin.

The inelastic strain rate is determined as

$$\dot{\epsilon}^c = \frac{\partial \Phi_o}{\partial \sigma_d} = \dot{\epsilon}_o \frac{3}{\beta} \left(\frac{\sigma_{d,eq}}{B} \right)^n \frac{\mathbf{G}\sigma_d}{\sigma_{d,eq}}. \quad (6.9)$$

It is worth noting that for pressure-insensitive isotropic materials with the same behavior in compression and tension and no kinematic hardening, the inelastic strain rate are obtained from Eq. (6.9) as

$$\dot{\epsilon}^c = \dot{\epsilon}_o \frac{3}{2} \left(\frac{\sigma_{eq}}{B} \right)^n \frac{\boldsymbol{\sigma}'}{\sigma_{eq}} \quad (6.10)$$

where the equivalent stress is defined as

$$\sigma_{eq} = \left(\frac{3}{2} \boldsymbol{\sigma}' \cdot \boldsymbol{\sigma}' \right)^{1/2} \quad (6.11)$$

and $\boldsymbol{\sigma}'$ is the deviatoric stress.

6.3.2 Damage-enhanced Inelastic Flow

In metals, microcracks have some influence on inelastic strain rate, but this influence is generally weaker than the influence of microcracks on the elastic properties of the material

(Murakami and Ohno, 1981). Unlike the case of metals, however, the effect of microcracks in polycrystalline ice on inelastic creep can be too large to ignore. This influence is taken into account in the ensuing discussion of the formulation of a dissipation potential function.

6.3.2.1 Effect of Microcracks on Creep

Under constant stress loading, the shape of transient creep curve is the result of changes in the dislocation density, while tertiary creep may be the result of the growth of internal damage (e.g., microcracking and recrystallization). As constant stress increases, the internal damage becomes more dominant than the evolution of dislocation density; both transient and tertiary creep are enhanced significantly by microcracking. In this range, primary concern lies with damage growth due to microcracking and its effect on creep rate. The transition between the primary and tertiary part of creep is an external manifestation of the dominance of a particular microstructural change (e.g., the relative contribution of dislocation activities and microcracking).

With increasing microcrack activity, the inelastic strain rate increases. Weertman (1969) derived the effect of cracks on viscous creep rate, considering a crack as an array of dislocations for polycrystalline materials. The creep rate for non-intersecting, dilute cracks was written as

$$\dot{\epsilon}^c = \dot{\epsilon}_o^c \left(1 + 2\pi\sqrt{n}Na^2 \right) \quad (6.12)$$

where $\dot{\epsilon}_o^c$ is the creep rate of the undamaged ice, N is the number of cracks per unit area, a is the crack half-length and n is the stress exponent for power-law creep. However, the effects of microcracks appear to be more pronounced than the linear enhancement, as expressed in Eq. (6.12), and underestimate for materials with high crack density (Stone et al., 1989; Kalifa et al., 1989). For columnar-grained polycrystalline ice, Sinha (1988) applied Weertman's equation to consider the effect of the dilute crack enhancement on the viscous strain rate in his non-linear viscoelastic creep model. Jordaan and McKenna (1991) modified the crack enhancement factor in their model to include the crack interaction by using an exponential function. As mentioned by Duval et al. (1991), a detailed analysis is necessary to determine how microcracking really affects creep rate.

Meyssonier and Duval (1989) studied the influence of damage on the creep rate of

granular ice. The main results of this study were that damage notably enhances the creep rate and the stress exponent remains the same ($n = 3$). From constant stress tests on both intact and predamaged ice, Xiao et al. (1991) showed clear evidence of the influence of microcracks and damage on creep properties. Damage due to the formation and growth of microcracks leads to a small reduction in elastic stiffness. As shown from experiments of Xiao et al. (1991), elastic properties is little changed due to microcracks. Wu and Shyam Sunder (1992) also showed a small dependence of microcracks on the overall stress-strain curve in their numerical simulations of a micromechanical damage model by applying the mechanism of elastic anisotropy in polycrystalline ice. In this study, therefore, the effect of microcracks on elastic properties is not taken into consideration.

6.3.2.2 Formulation of Damage-enhanced Inelastic Flow

In the following formulation, the kinematic and isotropic hardening as well as the damage due to microcracks are taken into account. In order to incorporate damage due to microcracks into inelastic flow, the following form of dissipation potential for damage-enhanced inelastic flow is considered:

$$\Phi = \Phi_o F = \frac{\dot{\epsilon}_o B}{n+1} \left(\frac{\sigma_{d,eq}}{B} \right)^n F(n, D, Y) \quad (6.13)$$

where Φ_o is the dissipation potential for inelastic flow without microcracks, n is the stress exponent, the scalar function F is described below, D is a measure of damage, and Y is a measure of stress states. The reduced equivalent stress $\sigma_{d,e}$ is expressed as

$$\sigma_{d,eq}^2 = \frac{3}{\beta} \boldsymbol{\sigma}_d^T \mathbf{G} \boldsymbol{\sigma}_d \quad (6.14)$$

where the reduced stress $\boldsymbol{\sigma}_d$ and the stress-transformation matrix \mathbf{G} are defined by Eqs (6.4) and (6.5), respectively.

Rodin and Parks (1988) suggested a similar form of dissipation potential for inelastic flow in which hardening effects due to dislocations are ignored. The description of the material includes the construction of a scalar function $F(n, D, Y)$ of three dimensionless variables: the first variable describes the matrix response, the second is the averaged characteristic of the microstructure, and the last identifies a measure of stress state. For the dissipation

potential to be convex, F must satisfy the condition (Rodin and Parks, 1988)

$$FF'' - \frac{n}{n+1}F'^2 > 0 \quad (6.15)$$

where a prime denotes partial derivative of F with respect to Y . The later symbol is defined in Eq. (6.16). A variety of forms for F have been proposed for isotropic porous metals experiencing void growth (e.g., Haghi and Anand, 1992) and for isotropic material with cavitating grain-boundary facets (Hutchinson, 1983; Argon et al., 1985; Rodin and Parks, 1988).

Previously published experimental results (Sinha, 1988; Nixon and Wasif, 1992) in ice indicate that microcracks occur mainly in the direction of the maximum principal compressive stress. Considering material damage due to a population of aligned microcracks, it can be argued (Hutchinson, 1983; Rodin and Parks, 1988) that under proportional load histories the material preserve isotropy. We consider microcracks by specifying a scalar microcrack density ($D = w$). The damage anisotropy, however, can be implicitly taken into account by the introduction of the maximum principal stress σ_1 into the dissipation potential with the following relation:

$$Y = \frac{\sigma_1}{\sigma_{d,eq}}. \quad (6.16)$$

For the enhancement of creep due to microcracks in polycrystalline ice, the following function F is considered, according to Rodin and Parks (1988):

$$F = \left(1 + \alpha(n, \omega) Y^2\right)^{(n+1)/2}. \quad (6.17)$$

The function $\alpha(n, \omega)$ reflects material behavior and is independent of stresses at a point. The following forms, which satisfy convexity of the potential Eq. (6.15), are given as

$$\alpha(n, \omega) = 2\pi n^{1/2}\omega \quad (6.18)$$

for slit microcracks in columnar-grained S2 ice and

$$\alpha(n, \omega) = 8 \left(\frac{n}{n+3}\right)^{1/2} \omega \quad (6.19)$$

for penny-shaped microcracks in equiaxed-granular ice. The theoretical basis for these forms

is discussed for slit microcracks by Weertman (1969) and He and Hutchinson (1981), and for penny-shaped microcracks by He and Hutchinson (1981) and Rodin and Parks (1988).

The inelastic strain rate is obtained by

$$\dot{\epsilon}^c = \frac{\partial \Phi}{\partial \sigma_d}. \quad (6.20)$$

For the given dissipation potential in Eq. (6.13), the inelastic strain rate is determined as

$$\dot{\epsilon}^c = \dot{\epsilon}_o \left(\frac{\sigma_{d,eq}}{B} \right)^n \left(1 + \alpha(n, \omega) Y^2 \right)^{(n-1)/2} \left\{ \frac{3}{\beta} \frac{\mathbf{G}\sigma_d}{\sigma_{d,eq}} + \alpha(n, \omega) Y \frac{\partial \sigma_1}{\partial \sigma} \right\}. \quad (6.21)$$

For the case of isotropic polycrystalline ice under uniaxial stress σ , Eq. (6.21) reduces to

$$\dot{\epsilon}^c = \dot{\epsilon}_o \left(\frac{\sigma - X}{B} \right)^n \left(1 + \alpha(n, \omega) \right)^{(n+1)/2}. \quad (6.22)$$

And for the case of isotropic polycrystalline ice where there is no damage (i.e., $F(n, w = 0, Y) = 1$), Eq (6.21) reduces further to the well-known relation

$$\dot{\epsilon}^c = \dot{\epsilon}_o \frac{3}{2} \left(\frac{\sigma_{eq}}{B} \right)^n \frac{\sigma'}{\sigma_{eq}}. \quad (6.23)$$

It is worth noting that a wide variety of specific microstructural damage process for different materials can be described by similar mathematical expressions of the material damage.

6.3.2.3 Microcrack Density

We characterize the microcracks only by specification of their density ω defined as (Budiansky and O'Connell, 1976)

$$\omega = \frac{2N}{\pi} \left\langle \frac{A^2}{P} \right\rangle \quad (6.24)$$

where N is the number of microcracks per unit volume, A is the area of the microcrack, P is the perimeter, and the angle brackets denote an average. Experimental results indicate that the size of microcracks are of the order of the grain size (Cole, 1986; Sinha, 1988).

Columnar-grained S2 Ice

Consider columnar-grained S2 polycrystalline ice containing a population of aligned slit cracks of width $2c$ and length l , with a constant aspect ratio $l/2c \gg 1$, under compressive loading. Noting that A is $2cl$ and P is approximately $2l$, Eq. (6.24) results in

$$\omega = \frac{4}{\pi} N \langle c^2 l \rangle. \quad (6.25)$$

Assuming the average microcrack size, $2c$, to be equal to the length of the average grain facet and assuming the cross-sectional geometry of the grain to be hexagonal, it can be calculated by equating the area of a circle of the average grain diameter d with the area of the hexagon:

$$c \approx 0.275d. \quad (6.26)$$

Substituting Eq. (6.26) into Eq. (6.25) results in

$$\omega = \frac{N}{10.39} \langle d^2 l \rangle. \quad (6.27)$$

Equiaxed-granular Ice

We now consider equiaxed-granular ice and a population of aligned penny-shaped cracks of diameter $2c$ under compressive loading. Noting that A is πc^2 and P is $2\pi c$, Eq. (6.24) results in

$$\omega = N \langle c^3 \rangle. \quad (6.28)$$

Assuming the volume geometry of the grain to be dodecahedron, and assuming the average diameter of microcracks, $2c$, to be equal to the diameter of a circle inclosed by the pentagon surface of a dodecahedron, it can be shown that

$$c \approx 0.354d \quad (6.29)$$

where d is the average grain diameter, having the same volume $(4/3)\pi(d/2)^3$ as that of the

dodecahedron. Substituting Eq. (6.29) into Eq. (6.28) results in

$$\omega = \frac{N}{22.54} \langle d^3 \rangle. \quad (6.30)$$

6.3.2.4 Microcrack Evolution

Microcrack activity in ice has been monitored both visually and acoustically. Visual examination of microcrack formation during uniaxial compression has been performed in both columnar-grained freshwater ice (Sinha, 1988; Nixon and Wasif, 1992) and equiaxed-granular freshwater ice (Hallam et al., 1987; Kalifa et al., 1989). These experimental results show that the majority of microcracks are oriented parallel to the maximum principal loading axis (Gold, 1972; Sinha, 1982,1988).

Gold (1960) first monitored acoustic emissions for microcracking in columnar-grained freshwater ice under constant compressive stresses at -10°C . Gold's results showed that the rate of microcrack formation is dependent on duration time and on the magnitude of applied stress. Later, extensive studies on acoustic emissions were conducted in both columnar-grained freshwater ice (Gold, 1972; Sinha, 1982) and equiaxed-granular freshwater ice (Zaretsky et al., 1979; Cole, 1986) under a range of temperatures, stress levels and grain sizes. These studies showed that when the applied stress is greater than the critical stress, microcracks form. Plotting the strain dependence of microcracking density shows that microcrack density increases with applied stress. According to the results of these acoustic emissions for constant strain rate loading, the rate of microcracking is highest when the stress reaches its peak, and then diminishes significantly. These results demonstrate that microcracking is highly rate-sensitive and depends strongly on grain size.

In order to describe the microcracking dependence on stress and time, the following equation for the number of microcracks is proposed as a result of a study of the literature:

$$N = \begin{cases} N_o \left[1 - \exp \left(- \left(\frac{\sigma - \sigma_c}{\sigma_o} \right)^2 (\epsilon^c)^m \right) \right] & \text{when } \sigma \geq \sigma_c \\ 0 & \text{when } \sigma < \sigma_c \end{cases} \quad (6.31)$$

where N_o is a reference constant, σ_c is the critical stress for microcrack nucleation defined in Eq. (6.33), and σ_o is the reference stress, defining the sharpness of the transition.

6.3.2.5 Microcrack Nucleation

Microcrack nucleation is a fundamental phenomenon in the failure process of polycrystalline ice, since it occurs in both the ductile and brittle domains of deformation.

Stress concentrations at grain boundaries lead to the nucleation of microcracks. Various mechanisms, such as the grain boundary sliding mechanism (Sinha, 1984), the dislocation pile-up mechanism (Gold, 1972; Schulson, 1979; Cole, 1986), and elastic anisotropy mechanism (Cole, 1988), have been reported to predict microcrack nucleation and its dependence on parameters such as grain size and strain rate. It is generally believed that the elastic anisotropy is dominant in the brittle domain (i.e., strain rate $> 10^{-3} \text{ s}^{-1}$), while the other mechanisms are dominant in the ductile domain (i.e., strain rate $< 10^{-3} \text{ s}^{-1}$). However, Gupta et al. (1993) and Elvin and Shyam Sunder (1995) report that the mismatch in elastic moduli between neighboring grains in polycrystalline ice, under plane strain condition, is not high enough to form precursor cracks. Instead, they conclude that grain boundary sliding is the cause of microcracking in the brittle domain.

Grain boundary sliding driven by shear stresses along the inclined grain boundaries increases the wedging effect and tends to increase stress concentration at the triple grain junction (Elvin and Shyam Sunder, 1995). After the stress intensity factor exceeds the threshold value, a microcrack nucleates and grows unstably until it gets arrested at the neighboring triple point.

The critical stress required for crack nucleation is generally a function of temperature T , grain size d , fracture toughness K_{IC} and friction coefficient μ (Ketcham and Hobbs, 1969; Ashby and Hallam, 1986; Hallam, 1986; Schulson, 1990):

$$\sigma_c = \hat{\sigma}_c(T, d, K_{IC}, \mu) . \quad (6.32)$$

The experiments of Gold (1960, 1972), Cole (1986), and Schulson (1990) suggest a form for microcrack nucleation as:

$$\sigma_c = \sigma_{c1} + \sigma_{c2} \exp\left(-\frac{Q}{RT}\right) \frac{K_{IC} d^{-1/2}}{(1-\mu)} \quad (6.33)$$

where σ_{c1} , σ_{c2} , K_{IC} , μ , are material constants depending on the type of ice (equiaxed-granular

or columnar-grained). For a range of grain sizes ($d = 1 \sim 8 \text{ mm}$) and temperatures ($T = -2 \sim -40^\circ\text{C}$), the measured microcrack nucleation stress lies between 0.5 and 1.5 MPa .

6.3.3 Summary of Damage-enhanced Creep Model

A summary of the multiaxial damage-enhanced creep model is given in Table 6.1. Also a summary of an isotropic one-dimensional model is given in Table 6.2. The governing equations of the model are summarized here for isotropic polycrystalline ice under uniaxial stress σ .

Table 6.1: Summary of the multiaxial damage-enhanced creep model

- Total strain rate

$$\dot{\epsilon} = \dot{\epsilon}^e + \dot{\epsilon}^c \quad (6.34)$$

- Elastic strain rate

$$\dot{\epsilon}^e = \mathbf{S} \dot{\sigma} \quad (6.35)$$

- Damage-enhanced inelastic strain rate

$$\dot{\epsilon}^c = \dot{\epsilon}_o \left(\frac{\sigma_{d,eq}}{B} \right)^n \left(1 + \alpha(n, \omega) Y^2 \right)^{(n-1)/2} \left\{ \frac{3}{\beta} \frac{\mathbf{G} \sigma_d}{\sigma_{d,eq}} + \alpha(n, \omega) Y \frac{\partial \sigma_1}{\partial \sigma} \right\} \quad (6.36)$$

where $\dot{\epsilon}_o = A_o \exp\left(-\frac{Q}{RT}\right)$; $Y = \frac{\sigma_1}{\sigma_{d,eq}}$; $\sigma_d = \sigma - \mathbf{X}$; $\sigma_{d,eq}^2 = \frac{3}{\beta} \sigma_d^T \mathbf{G} \sigma_d$; $\beta = a_1 + a_2$

$$(6.37)$$

- Kinematic back stress

$$\dot{\mathbf{X}} = h_1 E (\dot{\epsilon}^c - r_1 \mathbf{X}^n) \quad \text{where} \quad r_1 = \dot{\epsilon}_o \left(\frac{1 - k_1}{k_1 k_2 B_o} \right)^n \quad (6.38)$$

- Isotropic drag stress

$$\dot{B} = \frac{h_2 E}{\sigma_{d,eq}} (B_{sat} - B) |\dot{\epsilon}_{eq}^c| \quad \text{where} \quad B_{sat} = k_2 B_o \quad (6.39)$$

- Creep enhancement factor and microcrack density

$$\alpha(n, \omega) = 2\pi n^{1/2} \omega; \quad \omega = \frac{N}{10.39} \langle d^2 l \rangle \quad \text{for columnar-grained S2 ice} \quad (6.40)$$

$$\alpha(n, \omega) = 8 \left(\frac{n}{n+3} \right)^{1/2} \omega; \quad \omega = \frac{N}{22.54} \langle d^3 \rangle \quad \text{for equiaxed-granular ice} \quad (6.41)$$

- Number of microcracks per unit volume

$$N = \begin{cases} N_o \left[1 - \exp\left(-\langle \frac{\sigma - \sigma_c}{\sigma_o} \rangle^2 (\epsilon_{eq}^c)^m \right) \right] & \text{when } \sigma \geq \sigma_c \\ 0 & \text{when } \sigma < \sigma_c \end{cases} \quad (6.42)$$

Table 6.2: Summary of the isotropic one-dimensional damage-enhanced creep model

- Total strain rate

$$\dot{\epsilon} = \dot{\epsilon}^e + \dot{\epsilon}^c \quad (6.43)$$

- Elastic strain rate

$$\dot{\epsilon}^e = \frac{\dot{\sigma}}{E} \quad (6.44)$$

- Damage-enhanced inelastic strain rate

$$\dot{\epsilon}^c = \dot{\epsilon}_o \left(\frac{\sigma - X}{B} \right)^n (1 + \alpha(n, \omega))^{(n+1)/2} \quad \text{where} \quad \dot{\epsilon}_o = A_o \exp \left(-\frac{Q}{RT} \right) \quad (6.45)$$

- Kinematic back stress

$$\dot{X} = h_1 E (\dot{\epsilon}^c - r_1 X^n) \quad \text{where} \quad r_1 = \dot{\epsilon}_o \left(\frac{1 - k_1}{k_1 k_2 B_o} \right)^n \quad (6.46)$$

- Isotropic drag stress

$$\dot{B} = \frac{h_2 E}{\sigma - X} (B_{sat} - B) |\dot{\epsilon}^c| \quad \text{where} \quad B_{sat} = k_2 B_o \quad (6.47)$$

- Creep enhancement factor and microcrack density

$$\alpha(n, \omega) = 2\pi n^{1/2} \omega; \quad \omega = \frac{N}{10.39} \langle d^2 l \rangle \quad \text{for columnar-grained S2 ice} \quad (6.48)$$

$$\alpha(n, \omega) = 8 \left(\frac{n}{n+3} \right)^{1/2} \omega; \quad \omega = \frac{N}{22.54} \langle d^3 \rangle \quad \text{for equiaxed-granular ice} \quad (6.49)$$

- Number of microcracks per unit volume

$$N = \begin{cases} N_o \left[1 - \exp \left(-\left(\frac{\sigma - \sigma_c}{\sigma_o} \right)^2 (\epsilon^c)^m \right) \right] & \text{when } \sigma \geq \sigma_c \\ 0 & \text{when } \sigma < \sigma_c \end{cases} \quad (6.50)$$

6.4 Model Parameters and Predictions

6.4.1 Parameters

Elastic Parameters

The elastic constants of polycrystalline ice are given in Appendix B of Chapter 5. The dynamic elastic constants of single crystal ice were determined at $T = -16^{\circ}\text{C}$ using the method of Brillouin spectroscopy, by Gammon et al. (1983). The theoretical effective elastic constants of polycrystalline ice can be computed by using various homogenization methods, such as the Ruess and Voigt assumptions (Sinha, 1989; Nanthikesan and Shyam Sunder, 1994), the self-consistent method (Wang and Schapery, 1995), and using a computational model (Elvin, 1996).

Creep Parameters

The values of material parameters n , A , Q , B_o , k_1 , k_2 , h_1 , h_2 and r_1 for any given material may be determined from isothermal constant stress tests. The procedures for determining creep parameters are described in Section 5.5.1 of Chapter 5.

The model parameters c_1 , c_2 , and c_6 are used to represent the creep anisotropy of ice single crystals. Without loss of any generality, c_2 can be taken as 1. Thus only two parameters need to be determined from constant stress tests on single crystal ice.

Damage Parameters

The damage parameters N_o , σ_c , σ_o and m may be estimated from experimental measurements. However, due to a lack of data for ice, the parameters are determined by fitting the model response to data.

In Table 6.3, a summary of the damage-enhanced model parameters is given for the different ice examined by Jordaan and McKenna (1991), Mellor and Cole (1982).

Table 6.3: Summary of model parameters

Parameters	Jordaan and McKenna (1991)	Mellor and Cole (1982)
E (MPa)	9000	9000
n	3	3.43
Q (kJ mol ⁻¹)	67	67
A (MPa ⁻³ s ⁻¹)	3.57×10^6	2.23×10^6
A_o (s ⁻¹)	1	1
B_o (MPa)	1.73×10^{-3}	7.92×10^{-3}
k_1	0.15	0.27
k_2	3.2	1.30
h_1	1/10	1/70
h_2	1/1.5	1/10
r_1 (MPa ⁻³ s ⁻¹)	5.21×10^{-5}	1.73×10^{-5}
N_o (m ⁻³)	2500	400
σ_c (MPa)	0.5	0.5
σ_o (MPa)	1.0	3.0
m	2.0	2.0

6.4.2 Model Comparisons

Jordaan and McKenna (1991) measured the stress strain curve of granular polycrystalline ice in compression at -10°C under an applied strain rate of 10^{-4} s^{-1} . The strain softening response due to microcracks without strain hardening is observed at this high strain rate. Figure 6-4 compares the prediction of the model with the data of Jordaan and McKenna (1991). The model prediction is in excellent agreement with the data, when the parameters in Table 6.3 are used.

Figure 6-5 shows the comparison of the model predictions and experimental data of Mellor and Cole (1982) under applied strain rate tests. The model predictions using the parameters in Table 6.3. show quite good agreement with the data. The stress-strain curves exhibit strain hardening as well as strain softening behavior. It is worth noting that the model response slightly overpredicts the data at the strain rate of $5.30 \times 10^{-7} \text{ s}^{-1}$. This might be due to recrystallization at very low loading rates, which is not modeled.

6.5 Conclusions

A comprehensive damage-enhanced creep model for orthotropic polycrystalline ice is formulated within the framework of thermodynamics theory of irreversible process. In this model, highly rate- and temperature-dependent mechanical behavior is described by the changing microstructures due to the movement and production of dislocations and microcracking. The proposed damage-enhanced model can simulate the distributed damage process due to microcracking under compressive loading. Constitutive equations are proposed to help bridge the physical processes within the material and the macroscopic behavior observed in experiments. The evolution functions of internal stresses are formulated with hardening and recovery functions due to the production and annihilation of dislocations, respectively. The damage effects due to microcracking are taken into account mainly for the enhancement of creep properties. The information obtained from experiments for the cracking activities during the deformation are used in this damage-enhanced creep formulation. The response of the model captures the experimentally measured stress-strain and strain-time curves.

As mentioned by Duval et al. (1991), a detailed analysis is necessary to determine how microcracking really affects the creep rate. Much work remains to be done to develop fully anisotropic damage evolution equation which account for microcrack growth, coalescence, and brittle fracture at high strain rates. The proposed orthotropic model, however, is useful for simulation of creep deflection of ice sheets under static loading and slow fracturing processes in ice-structure indentation.

Notations

A	temperature-independent constant in the minimum strain rate ($MPa^{-n}s^{-1}$)
A_o	temperature-independent constant in the reference strain rate (s^{-1})
a	material creep constant of isotropic polycrystalline ice
a_i	material creep constants of polycrystalline ice
B	isotropic hardening variable scalar (MPa)
B_{sat}	saturated value of isotropic hardening variable B (MPa)
C	undamaged elastic stiffness matrix of polycrystalline ice (MPa)
C_g	undamaged elastic stiffness matrix of single crystal ice (MPa)
$C'_{g,ij}$	undamaged elastic stiffness components of single crystal ice (MPa)
c	microcrack size
c_i	material creep constants of single crystal ice
d	grain size
D	measure of damage
E	isotropic Young's modulus (MPa)
F	damage enhancement function to dissipation function
G	stress-transformation tensor
H	kinematic transformation tensor
h_1, h_2	hardening constants of internal stresses X and B
K_{IC}	fracture toughness
k_1, k_2	dimensionless constants used in X_{sat} and B_{sat}
l	microcrack length along the column axis of columnar-grained S2 ice
m	strain rate exponent in N
N	Number of microcracks
N_o	reference constant
n	stress exponent in power law
Q	activation energy ($kJmol^{-1}$)
R	universal gas constant ($Jmol^{-1}K^{-1}$)
r	average microcrack radius
r_1	recovery constant in kinematic hardening variable X
S	undamaged elastic compliance matrix of polycrystalline ice (MPa^{-1})
\bar{S}	damaged elastic compliance matrix of single crystal ice (MPa^{-1})
S_g	undamaged elastic compliance matrix of single crystal ice (MPa^{-1})
$S'_{g,ij}$	undamaged elastic compliance components of single crystal ice (MPa^{-1})
T	temperature in degrees Kelvin (K)
T	transformation matrix
w	crack density
X, \mathbf{X}	kinematic back stress and tensor (vector) (MPa)
X_{sat}	saturated value of kinematic back stress X (MPa)
Y	measure of stress triaxility
x_1, x_2, x_3	reference global axes
x_1', x_2', x_3'	local axes

α	constant
β	material constant
$\epsilon, \dot{\epsilon}$	total strain and total strain rate (s^{-1})
$\epsilon^e, \dot{\epsilon}^e$	elastic strain and elastic strain rate (s^{-1})
$\epsilon^c, \dot{\epsilon}^c$	inelastic strain and inelastic strain rate (s^{-1})
$\dot{\epsilon}_o$	temperature-dependent reference strain rate (s^{-1})
$\boldsymbol{\epsilon}, \dot{\boldsymbol{\epsilon}}$	total strain and total strain rate tensor (vector) (s^{-1})
$\boldsymbol{\epsilon}^e, \dot{\boldsymbol{\epsilon}}^e$	elastic strain and elastic strain rate tensor (vector) (s^{-1})
$\boldsymbol{\epsilon}^c, \dot{\boldsymbol{\epsilon}}^c$	inelastic strain and inelastic strain rate tensor (vector) (s^{-1})
μ	shear modulus (MPa)
ν	average velocity of mobile dislocations
σ	stress (MPa)
σ_1	maximum principal tensile stress (MPa)
σ_c	microcrack nucleation stress (MPa)
$\sigma_{d,eq}$	reduced equivalent stress scalar for polycrystalline ice (MPa)
$\hat{\sigma}_e$	equivalent stress scalar for single crystal ice (MPa)
σ_{eq}	equivalent stress scalar for polycrystalline ice (MPa)
$\bar{\sigma}$	effective stress (MPa)
σ_i	internal stress (MPa)
σ_{ij}	stresses in the global frame (MPa)
σ'_{ij}	stresses in the local frame (MPa)
σ_o	reference stress to microcrack nucleation stress (MPa)
$\boldsymbol{\sigma}$	stress tensor (vector) (MPa)
$\boldsymbol{\sigma}_d$	reduced stress tensor (vector) defined as $\boldsymbol{\sigma} - \mathbf{X}$ (MPa)
ϕ	geometrical constant
Φ	dissipation potential for damaged polycrystalline ice
Φ_o	dissipation potential for undamaged polycrystalline ice
Θ	probability density function of c-axis orientation
θ, φ	c-axis orientation of single crystal ice in the global frame

References

- [1] Argon, A.S. (1982). Mechanisms and mechanics of fracture in creeping alloys. *Recent Advances in Creep and Fracture of Engineering Materials and Structures*, B. Wilshire and D.R.J. Owen (Ed.), pp. 1-52.
- [2] Argon, A.S., Lau, C.W., Ozmat, B., and Parks, D.M. (1985). Creep crack growth in ductile alloys. *Fundamentals of Deformation and Fracture*, K.J. Miller et al. (Ed.), Cambridge University Press, Cambridge, p. 189.
- [3] Ashby, M.F. and Duval, P. (1985). The creep polycrystalline ice. *Cold Regions Science and Technology*, Vol. 11, No.3, pp. 285-300.
- [4] Ashby, M.F. and Hallam, S.D. (1986). The failure of brittle solids containing small cracks under compressive stress states. *Acta Metallurgica*, Vol. 34, pp. 497-510.
- [5] Ashby, M.F. and Raj, R. (1975). Creep rupture. *The Mechanics and Physics of Fracture*, The Metals Society, London, pp. 148-158.
- [6] Budiansky, B. and O'Connell, R.J. (1976). Elastic moduli of a cracked solid. *International Journal of Solids and Structures*, Vol. 12, pp. 81-97.
- [7] Choi, K. and Karr, D.G. (1989). A damage mechanics model for uniaxial creep and cyclic loading of polycrystalline ice. *Proc. 8th Int. Conf. Offshore Mech. and Arctic Eng.*, ASME, Vol. 4, pp. 75-82.
- [8] Chu, C.C. and Needleman, A. (1980). Void nucleation effects in biaxially stretched sheets. *J. Eng. Materials Technology*, Vol. 102, pp. 249-256.
- [9] Cocks, A.C.F. and Ashby, M.F. (1982). On creep fracture by void growth. *Prog. Mat. Sci.*, Vol. 27, pp. 189-244.
- [10] Cole, D.M. (1986). Effect of grain size on the internal fracturing of polycrystalline ice. U.S. Army Corps of Eng., Cold Reg. Res. Eng. Lab., Report 86-5.
- [11] Cole, D.M. (1988). Crack nucleation in polycrystalline ice. *Cold Regions Science and Technology*, Vol. 15, pp. 79-87.
- [12] Duval, P., Ashby, M.F. and Anderman, I. (1983). Rate-controlling processes in the creep of polycrystalline ice. *The Journal of Physical Chemistry*, Vol. 87, No. 21, pp. 4066-4074.
- [13] Duval, P., Kalifa, P. and Meyssonier, J. (1991). Creep constitutive equations for polycrystalline ice and effect of microcracking. *Proc. IUTAM/IAHR Symp. on Ice-Structure Interaction*, Jones, S.J., McKenna, R.F., Tillotson, J. and Jordaan, I.J. (Ed.), Springer-Verlag, pp. 55-67.
- [14] Dyson, B.F. and McLean, D. (1977). Creep of Nimonic 80A in torsion and tension. *Metal Sci.*, Vol. 11, pp. 37-45.

- [15] Elvin, A.A. (1996). Number of grains required to homogenize elastic properties of polycrystalline ice. *Mechanics of Materials*, Vol. 22, pp. 51-64.
- [16] Elvin, A.A. and Shyam Sunder, S. (1995). Microcracking due to grain boundary sliding in S2 ice under uniaxial compression. *Ice Mechanics*, ASME, AMD, Vol. 207, pp. 21-32.
- [17] Gammon, P.H., Kieft, H., Clouter, M.J. and Denner, W.W. (1983). Elastic constants of artificial and natural ice samples by Brillouin spectroscopy. *Journal of Glaciology*, Vol. 29, pp. 433-459.
- [18] Gold, L.W. (1960). The cracking activity in ice during creep. *Canadian J. Phys.*, Vol. 38, No. 9, pp. 1137-1148.
- [19] Gold, L.W. (1972). The process of failure of columnar-grained ice. *Philosophical Magazine A*, Vol. 26, No. 2, pp. 311-328.
- [20] Gold, L.W. (1973). Activation energy for creep of columnar-grained ice. In: *Physics and chemistry of ice*, Eds. E. Whalley, S.J. Jones and L.W. Gold, Ottawa, Royal Society of Canada, pp. 362-364.
- [21] Gupta, V., Picu, R.C., and Frost, H.J. (1993). Crack nucleation mechanism in saline ice. *Ice Mechanics*, ASME, AMD, Vol. 163, pp. 199-216.
- [22] Gurson, A.L. (1977). Continuum theory of ductile rupture by void nucleation and growth: Part I - Yield criteria and flow rules for porous ductile media. *Trans. ASME J. Eng. Mater. Technol.*, Vol. 99, pp. 2-15.
- [23] Haghi, M. and Anand, L. (1992). A constitutive model for isotropic, porous, elastic-viscoplastic metals. *Mechanics of Materials*, Vol. 13, pp. 37-53.
- [24] Hallam, S.D. (1986). The role of fracture in limiting ice forces. *Proceedings of the IAHR Ice Symposium*, Iowa City, Iowa, pp. 287-319.
- [25] Hallam, S.D., Duval, P. and Ashby, M.F. (1987). A study of cracks in polycrystalline ice under uniaxial compression. *Journal de Physique*, Vol. 48, pp. C1-303- C1-311.
- [26] He, M.Y. and Hutchinson, J.W. (1981). The penny-shaped crack and the plane strain crack in an infinite body of power law material. *J. Appl. Mech.*, Vol. 48, pp. 830-840.
- [27] Hobbs, P.V. (1974). *Ice Physics*. Clarendon Press, Oxford.
- [28] Horii, H. and Nemat-Nasser, S. (1983). Overall moduli of solids with microcracks: loads-induced anisotropy. *Journal of the Mechanics and Physics of Solids*, Vol. 31, pp. 155-171.
- [29] Hutchinson, J.W. (1983). Constitutive behavior and crack tip fields for materials undergoing creep-constrained grain boundary cavitation. *Acta metall.*, Vol. 31, pp. 1079-1088.
- [30] Jordaan, I.J. and McKenna, R.F. (1988). Modelling of progressive damage in ice. *Proceedings IAHR Symposium on Ice*, Sapporo, Vol. 2, pp. 585-624.

- [31] Jordaan, I.J. and McKenna, R.F. (1991). Processes of deformation and fracture of ice in compression. *Proc. IUTAM/IAHR Symp. on Ice-Structure Interaction*, Jones, S.J., McKenna, R.F., Tillotson, J. and Jordaan, I.J. (Ed.), Springer-Verlag, pp. 283-309.
- [32] Jordaan, I.J., Stone, B.M., McKenna, R.F. and Fuglem, M. K. (1990). Effect of microcracking on the deformation of ice, *Proceedings of the 43rd Canadian Geotechnical Conference*, Quebec, Vol. 1, pp. 387-393.
- [33] Kachanov, L.M. (1958). Time of the fracture process under creep conditions. *Izv. Akad. Nauk SSR O.T.N., Tekh. Nauk*, Vol. 8, pp. 26-31.
- [34] Kachanov, M. (1994). Elastic solids with many cracks and related problems. *Advances in Applied Mechanics*, Vol. 30, pp. 259-445.
- [35] Kalifa, P., Duval, P. and Richard, M. (1989). Crack nucleation in polycrystalline ice under compressive stress states. *Proc. 8th Int. Conf. on Offshore Mechanics and Arctic Engineering*, The Hague, The Netherlands, Vol. 4, pp. 13-21.
- [36] Ketcham, W.M and Hobbs, P.V. (1969). An experimental determination of the surface energies of ice. *Philosophical Magazine A*, Vol. 19, pp. 1161-1173.
- [37] Krajcinovic, D. (1989). Damage mechanics. *Mechanics of Materials*, Vol. 8, pp. 117-197.
- [38] Le Gac, H. and Duval, P. (1980). Constitutive relations for the nonelastic deformation of polycrystalline ice. *Proceedings of the IUTAM Symposium on the Physics and Mechanics of Ice*, Edited by P. Tryde, Springer, pp. 51-59.
- [39] Leckie, F.A. and Hayhurst, D.R. (1974). Creep rupture of structures. *Proc. R. Soc. Lond. A*, Vol. 340, pp. 323-347.
- [40] Lemaitre, J. and Chaboche, J.L. (1978). Aspect Phénoménologique de la Rupture par Endommagement. *Journal de Mécanique Appliquée*, Vol. 2, pp. 317-365.
- [41] Mellor M. and Cole, D. (1982). Deformation and failure of ice under constant stress or constant strain rate. *Cold Regions Science and Technology*, Vol. 5, pp. 201-219.
- [42] Meyssonier, J. and Duval, P. (1989). Creep behavior of damaged ice under uniaxial compression: a preliminary study. *Proceedings of the 10th Int. Conf. on Port and Ocean Eng. under Arctic Conditions*, Lula, Sweden, Vol. 1, pp. 225-234.
- [43] Michel, B. (1978). The strength of polycrystalline ice. *Canadian Journal of Civil Engineering*, Vol. 5, No. 3, pp. 285-300.
- [44] Michel, B. and R.O. Ramseier (1971). Classification of river and lake ice. *Can. Geotech. J.*, Vol. 8, pp. 36-45.
- [45] Murakami, S. and Ohno, N. (1981). A continuum theory of creep and creep damage. *Creep in Structures*, A.R.S. Ponter and D.R. Hayhurst (Ed.), pp. 422-444, Springer, Berlin.

- [46] Nanthikesan, S. and Shyam Sunder, S. (1994). Anisotropic elasticity of polycrystalline ice I_h . *Cold Reg. sci. Technol.*, Vol. 22, pp. 149-169.
- [47] Needleman, A. and Rice, J.R. (1978). Limits to ductility set by plastic flow localization. *Mechanics of Sheet Metal Forming*, D.P. Koistinen et al. (Ed.), Plenum Publishing, pp. 237-267.
- [48] Needleman, A. and Tvergaard, V. (1984). An analysis of ductile rupture in notched bars. *J. Mech. Phys. Solids*, Vol. 32, pp. 461-490.
- [49] Nemat-Nasser, S. and Hori, M. (1993). *Micromechanics: Overall Properties of Heterogeneous Materials*, North-Holland, New York.
- [50] Nixon, W.A. and Wasif, M.A. (1992). Development of cracks in S2 freshwater ice under constant strain rate loading. *IAHR 92 Proceedings of the 11th International Symposium on ice*, Vol. 2, pp. 1167-1175.
- [51] Pan, J., Saje, M., and Needleman, A. (1983). Localization of deformation in rate sensitive porous plastic solids. *Int. J. Fracture*, Vol. 21, pp. 261-278.
- [52] Rabotnov, Y.N. (1969). *Creep problems in structural members*. North-Holland, Amsterdam.
- [53] Rodin, G.J. and Parks, D.M. (1988). A self-consistent analysis of a creeping matrix with aligned cracks. *J. Mech. Phys. Solids*, Vol. 36, pp. 237-249.
- [54] Schapery, R.A. (1991). Models for the deformation behavior of viscoelastic media with distributed damage and their applicability to ice. *Proc. IUTAM/IAHR Symp. on Ice-Structure Interaction*, Jones, S.J., McKenna, R.F., Tillotson, J. and Jordaan, I.J. (Ed.), Springer-Verlag, pp. 191-230.
- [55] Schulson, E.M. (1979). An analysis of the brittle to ductile transition in polycrystalline ice under tension. *Cold Regions Science and Technology*, Vol. 1, pp. 87-91.
- [56] Schulson, E.M. (1990). The brittle compressive fracture of ice. *Acta metall.*, Vol. 38, pp. 1963-1976.
- [57] Shyam Sunder, S. and Wu, M.S. (1989a). A differential flow model for polycrystalline ice. *Cold Regions Science and Technology*, Vol. 16, No. 1, pp. 45-62.
- [58] Shyam Sunder, S. and Wu, M.S. (1989b). A multi-axial differential model of flow in orthotropic polycrystalline ice. *Cold Regions Science and Technology*, Vol. 16, No. 2, pp. 223-235.
- [59] Sinha, N.K. (1978). Rheology of columnar-grained ice. *Experimental Mechanics*, Vol. 18, No. 12, pp. 464-470.
- [60] Sinha, N.K. (1982). Acoustic emission and microcracking in ice. *Proceedings of the 1982 Joint Conference on Experimental Mechanics*, Hawaii, May 23-28, 1982, Part II, pp. 767-772.

- [61] Sinha, N.K. (1984). Intercrystalline cracking, grain-boundary sliding, and delayed elasticity at high temperatures. *Journal of Materials science*, Vol. 19, pp. 359-376.
- [62] Sinha, N.K. (1988). Crack enhanced creep in polycrystalline material strain rate sensitive strength and deformation of ice. *Journal of Material Science*, Vol. 23, pp. 4415-4428.
- [63] Sinha, N.K. (1989). Elasticity of natural types of polycrystalline ice, *Cold Reg. Sci. Technol.*, Vol. 17, pp. 127-135.
- [64] Sjölin, S-G. (1987). A constitutive model for ice as a damaging visco-elastic material. *Cold Regions Science and Technology*, Vol. 14, pp. 247-262.
- [65] Stone, B.M., Jordaan, I.J., Jones, S.J. and McKenna, R.F. (1989). Damage of isotropic polycrystalline ice under moderate confining pressures. *Proceedings of the 10th Int. Conf. on Port and Ocean Eng. under Arctic Conditions*, Lula, Sweden, Vol. 1, pp. 408-419.
- [66] Szyszkowski, W. and Glockner, P.G. (1985). Modeling the time-dependent behaviour of ice. *Cold Regions Science and Technology*, Vol. 11, pp. 3-21.
- [67] Ting, S.-K. and Shyam Sunder, S. (1985). Constitutive modeling of sea ice with applications to indentation problems. *CSEOE Res. Rep. 3*, Dept. Civil Eng., Massachusetts Inst. Technol., 255 pp.
- [68] Wang, L. and Schapery, R.A. (1995). Prediction of elastic and viscoelastic properties of anisotropic columnar ice. *Ice Mechanics*, ASME, AMD, Vol. 207, pp. 33-47.
- [69] Weertman, J. (1969). Effects of cracks on creep rate. *Transactions Quarterly, Transactions of the ASM*, Vol. 62, No. 2, pp. 502-511.
- [70] Weertman, J. (1973). Creep of Ice. *Physics and Chemistry of Ice*, Whalley, E., Jones, S.J. and Gold, L.W. (Editors), pp. 320-337.
- [71] Wu, M.S. and Niu, J. (1995). Micromechanical prediction of the compressive failure of ice, Part I: Model development. *Mechanics of Materials*, Vol. 20, pp. 9-32.
- [72] Wu, M.S. and Shyam Sunder, S. (1992). Elastic anisotropy and micro-damage processes in polycrystalline ice, Part I: Theoretical formulation. *Int. J. Fracture*, Vol. 55, pp. 223-243.
- [73] Xiao, J., Jordaan, I.J., McKenna, R.F. and Frederking, R.M.W. (1991). Finite element modeling of spherical indentation tests on ice. *The 11th Int. Conf. on Port and Ocean Eng. under Arctic Conditions*, September 24-28, St. John's, Canada, Vol. 1, pp. 471-485.
- [74] Zaretsky, Y.K., Chumiehev, B.D., and Solomatin, V.I. (1979). Ice behavior under load. *Engineering Geology*, Vol. 13, pp. 299-309.
- [75] Zhan, C., Evgin, E. and Sinha, N.K. (1994). A three dimensional anisotropic constitutive model for ductile behavior of columnar grained ice. *Cold Regions Science and Technology*, Vol. 22, pp. 269-284.

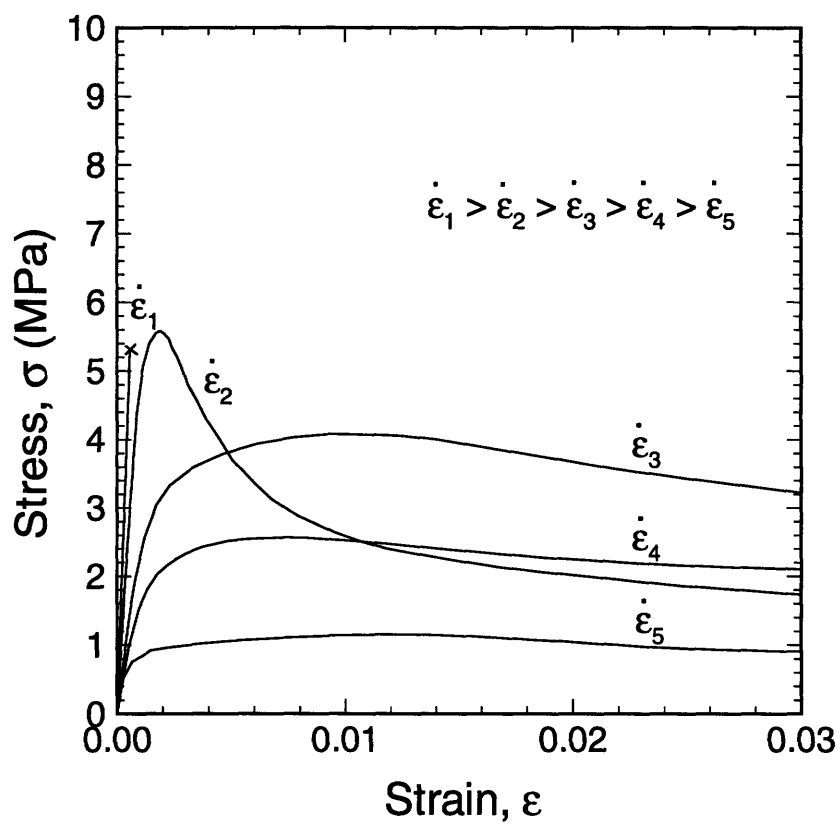


Figure 6-1: Typical stress-strain curves of polycrystalline ice under various levels of constant strain rate.

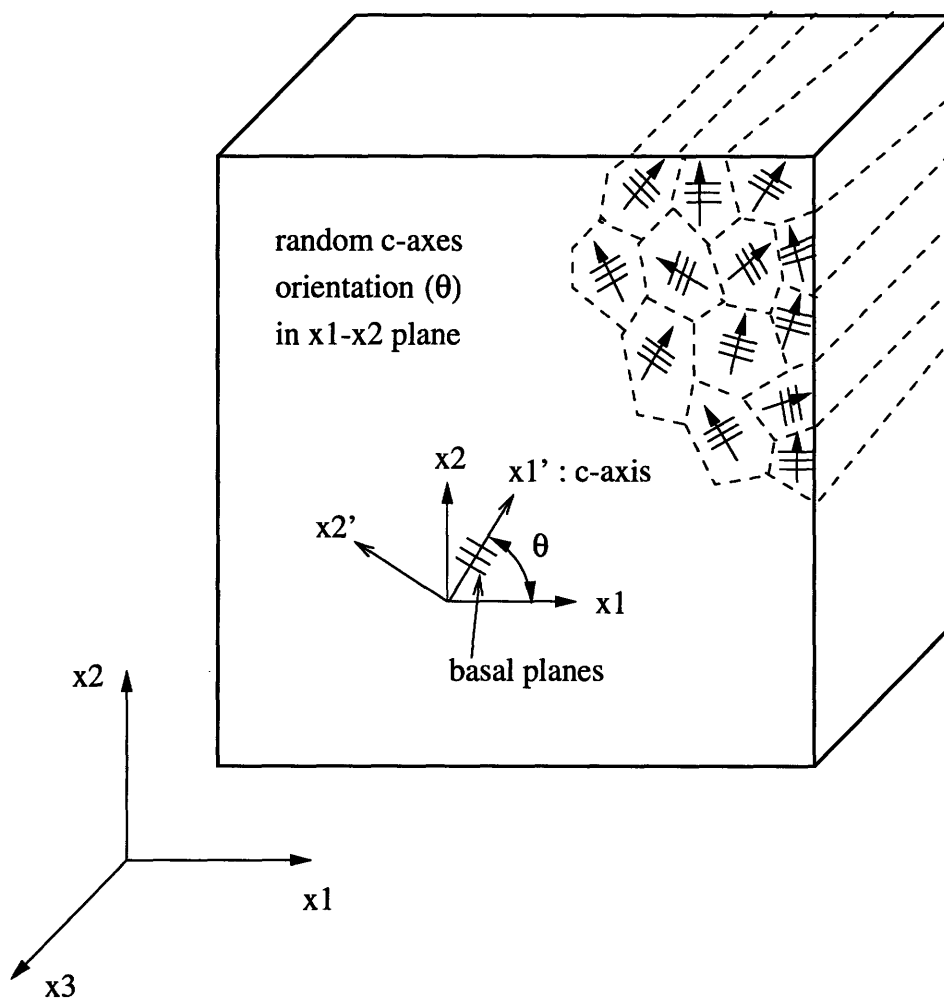


Figure 6-2: S2 polycrystalline ice containing crystals with random in-plane c-axes.

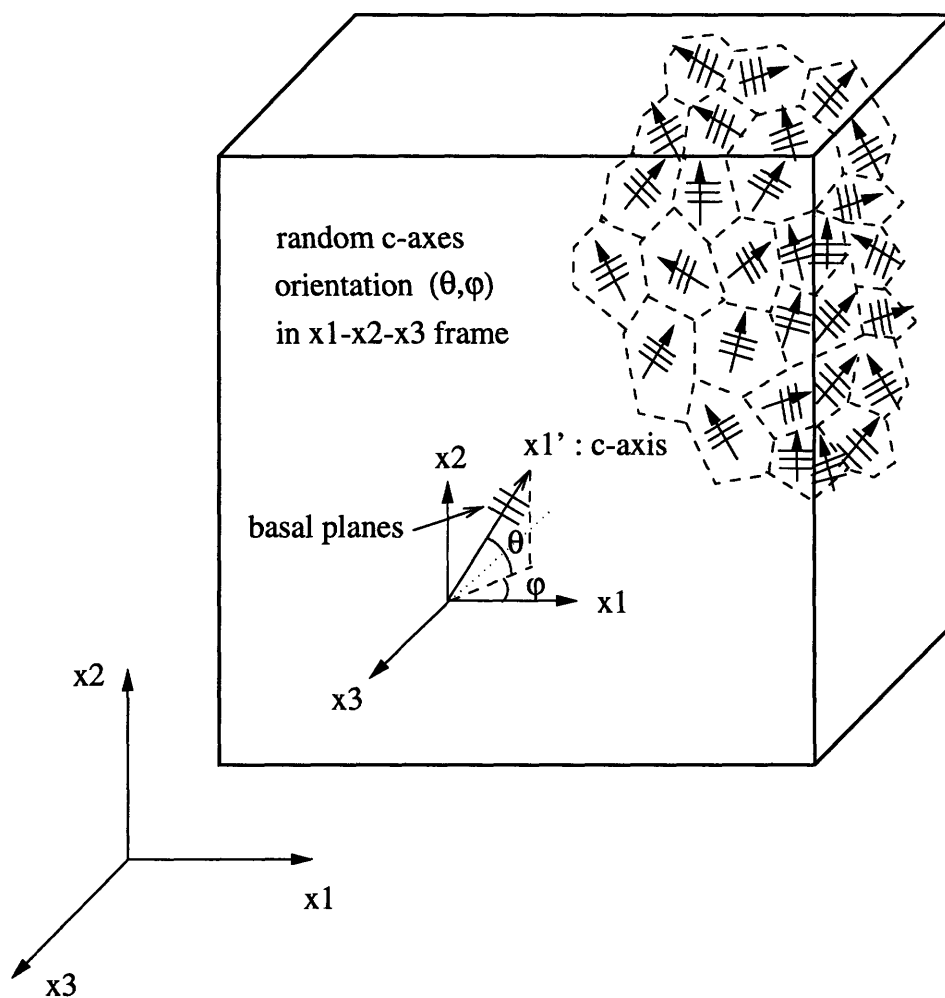


Figure 6-3: Equiaxed-granular polycrystalline ice containing crystals with random c-axes.

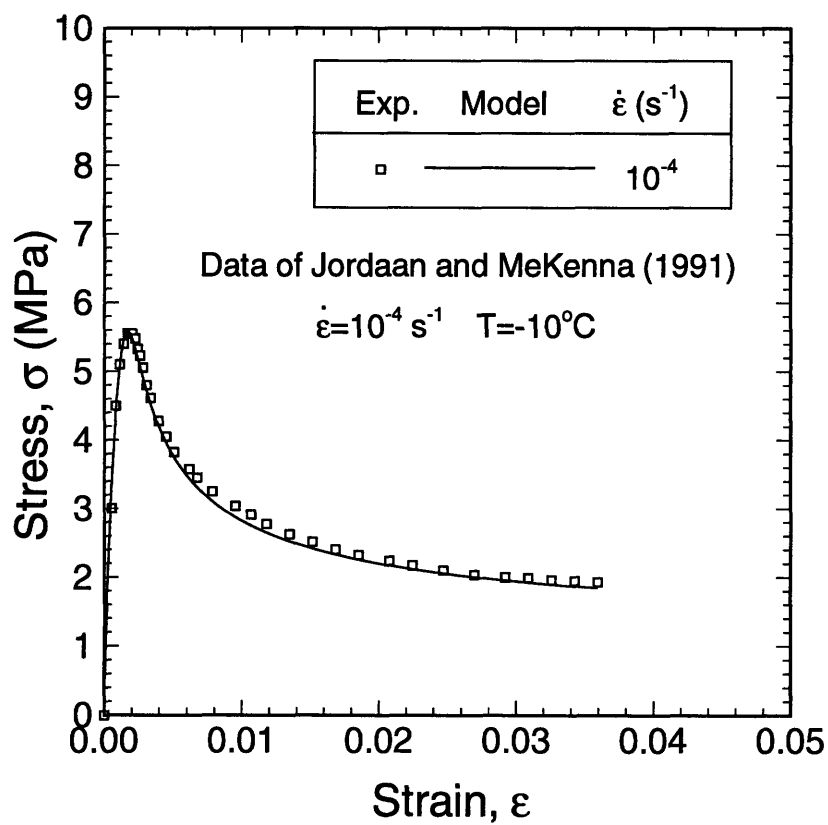


Figure 6-4: Stress-strain curve under constant strain-rate: the model prediction is compared with the data of Jordaan and MeKenna (1991).

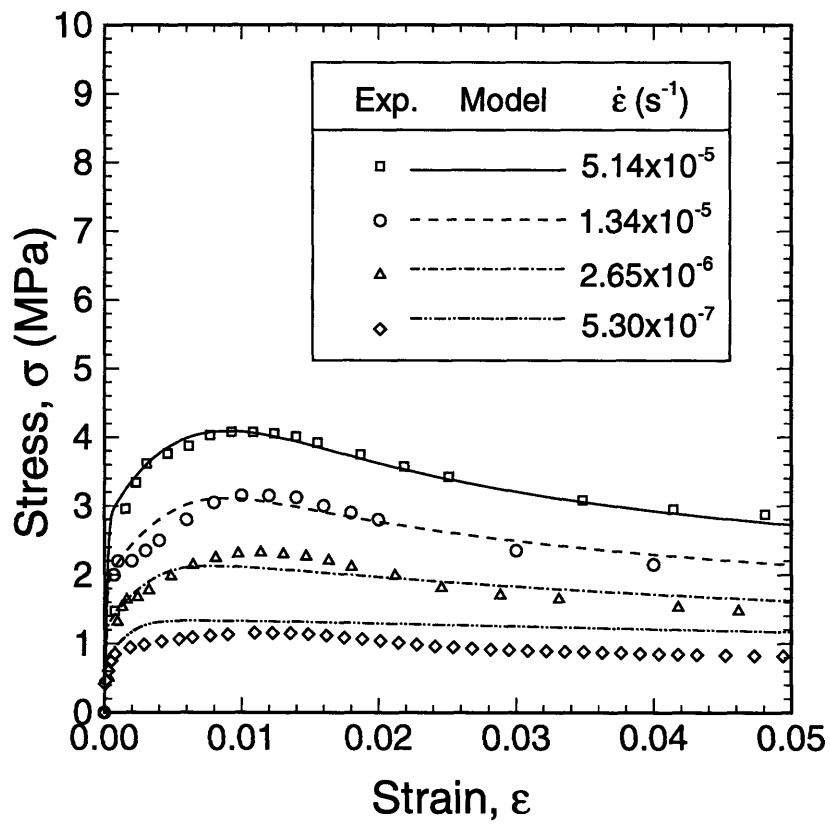


Figure 6-5: Stress-strain curves under constant strain-rates. The model prediction is compared with the data of Mellor and Cole (1982).

Chapter 7

CONCLUSIONS AND FUTURE RESEARCH

7.1 Summary of Present Work

This chapter summarizes the results of this thesis and proposes possible future research. The objective of this study has been to develop physically-based constitutive creep models for highly rate-dependent polycrystalline solids, such as polycrystalline ice. The constitutive models are based on physical mechanisms and microstructural properties.

Since polycrystalline ice is made up of a collection of individual crystals, its behavior is affected by the properties of the individual crystals. It is reported, however, that there are significant differences between the properties of single crystals and those of polycrystalline ice (Duval et al., 1983; Weertman, 1973). These differences may be due to such processes as intergranular effects (e.g., sliding and interlocking along grain boundaries), the distribution of the crystallographic orientation of single crystals, alterations of dislocation densities within grains, interactions of dislocations between slip systems, and damage accumulation due to microcracking.

In particular, the following models have been developed: (1) a constitutive creep model for single crystal ice; (2) relaxation process of polycrystalline ice under cyclic loading; (3) the viscoplastic behavior of polycrystalline ice; and (4) damage-enhanced viscoplastic behavior of polycrystalline ice. The salient results of each of these topics are summarized below.

A Creep Model for Single Crystal Ice

A constitutive creep model for single crystal ice has been formulated based on experimental results and the mechanism of the multiplication process of mobile dislocations. The model responses are in good agreement with available experimental data of single crystal ice, which is highly sensitive to changes in strain rate, stress, and temperature. Based on the assumption that the dislocation motion on the basal plane is the dominant mechanism for single crystal ice due to strong creep anisotropy, this chapter studied the effect of dislocation densities within crystals on the macroscopic response. Material properties used in the proposed model were the dislocation velocity and the changing dislocation density of single crystal ice based on experimental data. The model incorporates crystallographic basal orientation of single crystal ice. The uniaxial creep model was extended to biaxial loading. Parametric studies were performed to understand better the dependence of microstructural parameters on the macroscopic stress-strain curves. The model results are highly dependent on the loading rate, temperature, and orientation of the basal plane relative to the direction of the applied loading. Predicted stress-strain curve for the applied strain rate shows an upper and lower yielding. The strain-time response for the applied stress shows an accelerating strain.

Relaxation Process in Polycrystalline Ice

A constitutive model for polycrystalline ice subjected to cyclic loading applicable for relatively low anelastic strains, less than 10^{-3} , has been developed. The model is developed on the basis of the linear relationship between anelastic strain and stress, and the distribution of relaxation times which can be measured from internal friction. The relaxation process has a physical origin from internal stresses associated with intracrystalline processes of dislocations, and their distribution in grains due to the variation in basal plane orientation. The model predictions are then compared with cyclic experimental data that span a range of stress amplitudes ($0.6 - 1.4 \text{ MPa}$), and frequencies ($1 - 10^{-3} \text{ Hz}$) at -10°C . The proposed model is capable of describing the transient creep deformation behavior of polycrystalline ice under cyclic loading conditions. This study explains time-dependent elastic modulus of polycrystalline ice.

Viscoplastic Behavior

The proposed multi-axial, viscoplastic model for orthotropic polycrystalline ice is developed based on a physical process that governs rate- and temperature-dependent inelastic deformation as a result of the movement and production of the thermally-activated dislocations and an interactions of dislocations between the basal and non-basal systems of a constituent single crystal ice. The mathematical formulation is based on the theory of internal state variables. Two internal state variables, kinematic back stress and isotropic drag stress, are used to describe the various states of the microstructure. These internal stresses are responsible for strain hardening and transient creep. A specific form of dissipation potential, which incorporates internal stresses, is proposed for inelastic flow. Major features of the model include the hardening and recovery processes within the evolution equations of the internal stresses. The evolution function of isotropic drag stress is formulated with hardening and recovery functions due to the production and annihilation of dislocations. The evolution function of kinematic back stress is proposed based on an interaction of the basal and non-basal systems of single crystal ice. The proposed model satisfies the non-dimensional requirement of Ashby and Duval (1985) for strain, strain rate and time, and predicts the experimentally observed relationship between them with fixed material parameters. By using internal state variables and their evolution equations, transient creep of polycrystalline ice has been modeled successfully.

Damage-enhanced Viscoplastic Behavior

A multi-axial, damage-enhanced creep model for orthotropic polycrystalline ice is formulated within the framework of thermodynamics theory of irreversible process. In this model, highly rate- and temperature-dependent mechanical behavior is described by the changing microstructures such as the movement and production of dislocations and microcracking. The constitutive equations are proposed to help bridge the physical processes within the material and the macroscopic behavior observed experimentally. The damage effects due to microcracking are taken into account mainly for the enhancement of creep properties. The information obtained from experiments for the cracking activities during deformation are used in the present damage-enhanced creep formulation. A multi-axial dissipation potential for the inelastic deformation is proposed for kinematic hardening, isotropic hardening and damage due to microcracks. Finally, comparison of the model with available experimental data shows good agreement and demonstrates the effectiveness of the model.

7.2 Future Work

In this thesis, physically-based constitutive models for highly rate-dependent materials have been proposed. The models describe the viscoplastic and damage behavior of polycrystalline ice. Several improvements can be made in the following. First, the relaxation of internal stresses caused by microcracking needs to be better understood and modeled. Secondly, the anisotropy caused by anisotropic micro damage orientations need to be better described. Thirdly, the specific growth and coalescence mechanisms must be defined in order to describe the failure process.

All polycrystalline ice is made up of a collection of individual ice crystals, its behavior is affected by the properties of these individual crystals. It is reported, however, that there are significant differences between the properties of single crystals and those of polycrystalline ice (Duval et al., 1983; Weertman, 1973). These differences may be due to such processes as intergranular effects (e.g., sliding and interlocking along grain boundaries), the distribution of the crystallographic orientation of single crystals, alterations of dislocation densities within grains, an interaction of dislocations between slip systems, and damage accumulation due to microcracking.

In following studies, the aim should be to capture the behavior of polycrystalline aggregates based on multiple processes operating at microstructural scale. In particular, the following is suggested.

Behavior of Polycrystalline Ice: Finite Element Simulation

The aim of this study should be to capture the viscoplastic behavior of polycrystalline ice based on microstructural variables, such as elastic and creep properties of the individual crystals. Low strain rate should be modeled where little microcracking activity is observed. In Chapter 3, a constitutive creep model for single crystal ice is proposed based on the assumption that the dislocation motion on the basal plane is the dominant mechanism of single crystal ice due to strong creep anisotropy. The model describes the effect of dislocation densities within crystals on the macroscopic responses. The elastic response of polycrystalline ice based on elastic properties of single crystals is simulated numerically in Elvin (1996). In the future, the proposed creep model can be utilized in a numerical approach similar to Elvin (1996).

First, finite element simulation for non-homogeneous, viscoplastic deformation in polycrystalline ice modeled as a collection of single crystals can be performed based on elastic and creep properties of the individual single crystals with different orientations of the basal planes.

Secondly, a more advanced model would account for internal stresses build up at local sites such as grain boundaries due to intergranular effects. As a result, simulations of microcracks can be performed. The effect of distributed microcracks on the viscoplastic behavior of polycrystalline ice can be studied by numerically-generated polycrystalline samples and a unit cell model as presented in Elvin and Shyam Sunder (1996). This study will not only investigate quantitatively the enhancement of creep due to microcracks but might also be used to improve the form of damage-enhanced creep equations presented in Chapter 6.

Confinement Effect on Compressive Strength

For ductile yielding of ice at low strain rate, confining pressure has little effect on shear strength, and thus the same behavior in compression and tension is observed as for incompressible materials. Ice undergoes creep and the stress-strain response is independent of the hydrostatic stress. Thus a ductile yield surface is approximated by von-Mises criterion. As strain rates increase and internal microcracks develop, the tendency of a material to fracture under confinement is suppressed. Confinement has the apparent effect of increasing the ductility of brittle solids. Since the growth of cavities and microcracks is very sensitive to hydrostatic stress, damage is equally sensitive to the shear energy and the volumetric deformation energy. Consequently, the strength of ice is expected to increase with increasing hydrostatic stress, which can be predicted by the Mohr-Coulomb criterion or the Drucker-Prager criterion. In other words, ice exhibit brittle behavior at low hydrostatic pressure and more ductile behavior at high hydrostatic pressure. Based on experiments of the confined compressive strength under moderately to high strain rates (Jones (1982), Jones and Chew (1983) for isotropic polycrystalline ice; Timco and Frederking (1984) for granular/columnar sea ice; and Häuser (1981) for saline ice), the shear strength increases with increasing confining pressure up to a certain limit, but then starts to decrease with further increase in pressure.

Several yield functions have been developed to describe different tensile and compressive strengths by incorporating hydrostatic pressure (Reinicke and Ralston, 1977; Reinicke and

Remer, 1978; Nadreau and Michel, 1986). Previously published experimental results indicate that microcracks occur mainly in the direction of the maximum principal compressive stress. Anisotropic damage due to preferred microcrack orientations should be investigated by considering the relative importance of the maximum principal stress, the hydrostatic stress, and effective stress.

Numerical Modeling and Simulation of Ice-Structure Interaction

Despite the vast literature available on the subject of ice mechanics and ice-structure interaction, extensive and realistic quantitative calculations of ice loads have not been reported. Instead, analyses frequently present purely analytic theories, and thus no direct methods for estimating the ice loads on structures are provided, and the calculations are not compared with real data (Sanderson, 1989). The fact that ice plates undergo so many complex deformation processes, which greatly depend on loading rates, temperatures, ice thickness and the shape and dimension of the structures, may be the reason why no direct correlation between studies and predictions exists.

The failure of polycrystalline ice specimens and ice-structure interaction can be simulated by defining a realistic fracture criterion and the nucleation, growth, and coalescence of individual microcracks. This simulation would involve the physical understanding of the fracture processes.

A physically-based constitutive creep theory has been formulated and compared to the behavior of laboratory-scale ice in this thesis. A computational algorithm should be developed for simulating the complex material behavior in a finite element framework. Finally the physically-based and computationally-elegant constitutive creep model, when it is combined with microstructural fracture mechanics, might be used to solve the ice-structure interaction problems such as sub-surface penetration and in-plane indentation of a floating ice plate.

References

- [1] Ashby, M.F. and Duval, P. (1985). The creep polycrystalline ice. *Cold Regions Science and Technology*, Vol. 11, No.3, pp. 285-300.
- [2] Duval, P., Ashby, M.F. and Anderman, I. (1983). Rate-controlling processes in the creep of polycrystalline ice. *The Journal of Physical Chemistry*, Vol. 87, No. 21, pp. 4066-4074.
- [3] Elvin, A.A. (1996). Number of grains required to homogenize elastic properties of polycrystalline ice. *Mechanics of Materials*, Vol. 22, pp. 51-64.
- [4] Elvin, A.A. and Shyam Sunder, S. (1996). Microcracking due to grain boundary sliding in polycrystalline ice under uniaxial compression. *Acta Metall.*, Vol. 44, pp. 43-56.
- [5] Häuser, F.U. (1981). Multiaxial compressive strength tests on saline ice with brush-type loading platens. *Proc. IAHR 1981*, Quebec City, Vol. 2, pp. 526-539.
- [6] Jones, S.J. (1982). The confined compressive strength of polycrystalline ice. *J. Glaciology*, Vol. 20, pp. 171-177.
- [7] Jones, S.J. and Chew, H.A.M. (1983). Creep of ice as a function of hydrostatic pressure. *J. Phys. Chem.*, Vol. 87, pp. 4064-4066.
- [8] Nadreau, J.P. and Michel, B. (1986). Yield and failure envelope for ice under multiaxial compressive stresses. *Cold Regions Science and Technology*, Vol. 13, pp. 75-82.
- [9] Reinicke, K.M. and Ralston, T.D. (1977). Plastic limit analysis with an anisotropic, parabolic yield function. *Int. J. Rock Mech., Mining Sci. and Geomech. Abstr.*, Vol. 14, pp. 147-154.
- [10] Reinicke, K.M. and Remer, R. (1978). A procedure for the determination of ice forces - illustrated for polycrystalline ice. *Proc. IAHR 1978*, Lulea, Sweden, Vol. 1, pp. 217-238.
- [11] Sanderson, T.J.O. (1989). The Ice Load Question: Some Answers. *4th State-of-the-Art Report, Working Group on Ice Forces, IAHR*, U.S. Army Cold Regions Research and Engineering Laboratory, Hanover, NH., February, pp. 377-385.
- [12] Timco, G.M. and Frederking, R.M.W. (1984). An investigation of the failure envelope of granular/discontinuous-columnar sea ice. *Cold Regions Science and Technology*, Vol. 9, pp. 17-27.
- [13] Weertman, J. (1973). Creep of Ice. Whalley, E., Jones, S.J. and Gold, L.W. (Editors), *Physics and Chemistry of Ice*, pp. 320-337.